DERIVATION OF REFRACTION STATICS SOLUTION FOR 3D SEISMIC DATA IN OML-23 SOKU, NIGER DELTA USING THE DELAY-TIME APPROACH

By

ADIZUA, OKECHUKWU FRANK

(B.Sc, M.Sc Applied Geophysics – University of Port Harcourt)

Registration Number: 2013507010F

A PhD DISSERTATION SUBMITTED TO THE SCHOOL OF POSTGRADUATE STUDIES NNAMDI AZIKIWE UNIVERSITY, AWKA IN PARTIAL FULFILLMENT OF THE REQUIREMENTS FOR THE AWARD OF DEGREE OF DOCTOR OF PHILOSOPHY (Ph.D) IN APPLIED GEOPHYSICS

11th JUNE, 2019.

APPROVAL

The Ph.D Dissertation written by Adizua, Okechukwu Frank has been examined and approved for the award of degree of Doctor of Philosophy from Nnamdi Azikiwe University, Awka.

_____	_____
Prof. A. G. Onwuemesi **Supervisor I**	**Date**
_____	_____
Dr. E. K. Anakwuba **Supervisor II**	**Date**
_____	_____
Dr. N. E. Ajaegwu **Head of Department**	**Date**
_____	_____
Prof. K. K. Ibe **External Examiner**	**Date**
_____	_____
Prof. S. O. Anigbogu **Dean, Faculty of Physical Sciences**	**Date**
_____	_____
Prof. (Mrs.) P. K. Igbokwe **Dean, School of Post Graduate Studies**	**Date**

DEDICATION

This PhD Dissertation is dedicated to God Almighty – The Author and Finisher of my Faith, from whom I draw strength daily in the journey of life and HIM who has continued to prove himself as GOD in all my affairs even in the “darkest of days”.

ACKNOWLEDGMENTS

My profound thanks first goes to my supervisors, Professor Onwuemesi, A. G. and Dr. Anakwuba, E. K., I am so grateful for your constant patience, guidance and the academic leadership which steered the dissertation assignment and for not giving up on me despite all the odds. I am so grateful to the immediate past Dean of Postgraduate School – Professor Odumegwu, I. H. and the current Dean, Prof. (Mrs.) Igbokwe, P. K., for their current reforms which made my graduate study at the Nnamdi Azikiwe University - UNIZIK very enjoyable. I thank the Head of Department – Dr. Ajaegwu, N. E. and the entire faculty of the Geological Sciences Department for their supports and positive criticisms which further strengthened the work. I appreciate in a special way Professor Okoro, A. U., the PG Coordinator for Geology, who equally served as my internal – external examiner during my seminars at the Departmental level, for all his incisive comments, corrections and contribution to the dissertation. Dr. Obiadi, I. I., is highly appreciated for his lines of thoughts and his thorough critique of the work; it went a long way in strengthening and deepening the dissertation. I thank the Dean, Faculty of Physical Sciences – Professor Anigbogu, S. O. and the entire team of examiners and assessors at the Departmental, Faculty and PG Board panels. The review and critique of Professor Ekpunobi, A. J., who served as my internal – external examiner at the Faculty seminar stage, to the dissertation was apt and is highly appreciated.

I thank my wonderful family for all their encouragements; my darling wife – Mrs. Adizua, Nwakausor Susan, who has always been instrumental to all my achievements in life. My angelic and beautiful daughter – Thecla Chukwufumnaya and my cute son – Shane Kainyechukwuekene are my greatest motivation. I thank my dear parents - Sir Adizua, Anthony Obiora and Lady Adizua, Francisca Anucha. My Dad has always been there for me and has instilled in me a great sense of purpose and responsibility right from my childhood. I thank my dear Mother who strongly believes in my dreams and aspiration and is prepared to go the extra miles to ensure the actualization of our dreams and purpose. You invested a great deal of resources in this dream and I am happy it has now yielded the fruits you have always longed for – God bless you. I appreciate and thank my wonderful siblings, Onyebuchi and Uchenna and their lovely families, Anumia and Peter. You guys are the best siblings ever. Onyebuchi – I call you “Agunnaya” – you are just too much. You are already a blessed man but there are still greater realms of blessings – this I wish and pray for you.

This work couldn't have been achieved without the incisive inputs and contribution of intelligent and resourceful Geophysicists and Geologists. In no particular order, I appreciate Oluwaseun Peter Olaleye, Victor Tobrise, Chidozie Opara and Mfon Akpan. I am also grateful to GEDCO Company of Canada for the license granted to use *VISTA*^{TM} for the research and Landmark Graphics Corporation (a Halliburton Company) of the USA for access to use *proMAX 3D* to perform and implement advanced seismic processing routines in the course of the dissertation. I acknowledge all the BIG Men (Industry based mentors) who operated from behind the scene to give this work the much needed Industry backing and support. Without them, this project wouldn't have been realized.

I wish to formally appreciate an erudite and accomplished foremost Geophysicist of our time – Professor Ebeniro, J. O. who has been a great source of inspiration, a mentor and a father. Prof. EJO, I am so proud to be one of your protégé. I appreciate and acknowledge my colleagues and research team associates – Dr(s) Ehirim, Sofolabo, Dagogo, Balogun, Okorie, Inichinbia, Emujakporue, Nwankwo and Nwosu. This acknowledgement would not be complete without thanking and appreciating my fathers in the Department of Physics – University of Port Harcourt; Professor(s) Ekine, A. S., Owate, I. O., Avwiri, G. O., Abumere, O. E., Abbey, T. M., Okujagu, C. U., and Chukwuocha, E. O. I appreciate my immediate past HOD – Dr. (Mrs.) Osarolube, E. and my current HOD Dr. Chad-Umoren, Y. E. I appreciate all my other colleagues and friends (whom unfortunately, I wouldn't be able to mention) in other research areas and options within the Department. I also acknowledge and thank all those who have at different times prayed and wished me well and contributed in one way or the other towards the realization of my noble quest to acquire the degree of Doctor of Philosophy (Ph.D) in Applied Geophysics.

Finally to my God and Father "Jehovah Elohim". I call you – The Announcer and Decorator – The All Sufficient God –. Lord you saw me through from the Beginning of the Programme and now to its END. That I achieved this academic feat is only by your GRACE and DIVINE ARRANGEMENT.

TABLE OF CONTENTS

LIST OF FIGURES

LIST OF TABLES

LIST OF APPENDICES

ABSTRACT

OML-23 SOKU is a prospect in the onshore Niger Delta Basin with huge hydrocarbon potential but is plagued with statics problem. This poses a serious challenge for the seismic imaging of the prospect which in turn, would result in erroneous interpretations. To avert these problems, it is imperative for a refraction statics solution to be derived and applied for OML-23, SOKU which has necessitated the study. The aim of the study is to derive a refraction statics solution for 3D seismic data from OML-23, SOKU using the delay time approach. The objectives are to: generate a near-surface model of the prospect in terms of weathering and sub-weathering layer thicknesses and velocities; adapt the near-surface model in deriving a refraction statics solution for the prospect; determine the effectiveness of the statics solution on shot gathers from the prospect; determine the effectiveness of the statics solution on stacked and migrated sections of dataset from the prospect. Seismic noise and amplitude compensation problems which were identified on the seismic dataset were resolved using appropriate processing strategies as their undesirable effects on data quality would hamper the successful actualization of the focal objective for the study. The methodology involved using an integrated (hybrid) approach of inversion of refracted arrivals and up-hole data using special plugins on PROMAX and VISTA software to build a reliable near-surface model of the area. The near-surface model formed the input for deriving the refraction statics solutions for the SOKU dataset. The solutions comprised field statics, refraction statics, 1^{st} and 2^{nd} residual statics which resolved the remnant, uncorrected long and short wavelength statics effect. These solutions were loaded on both software and applied to the dataset using appropriate flow commands to perform the statics correction for the dataset in order to resolve the identified statics problem of the prospect. The result obtained from the near-surface model showed a weathering layer and three consolidated sub-weathering layers. The thicknesses obtained for the weathering, first, second and third consolidated sub-weathering layers ranged from (3 - 18m), (14 – 124m), (62 – 322m) and (248 – 493m) respectively while the velocities ranged from (520m/s), (1614 – 1723m/s), (1708 – 1758m/s) and (1950 – 1976m/s) respectively. At the shot gather processing stage, better alignment of reflection events was achieved; reflection events were exhibiting better continuity and assumed a near-hyperbolic appearance. At the stacking stage, reflectors were properly aligned and continuous with no incidence of mis-ties of reflectors, jittery reflections were moved to their actual position on the common midpoint (CMP) panel. At the migration stage, imaging quality (spatial and temporal resolution) was tremendously enhanced. Reflection continuity across the migrated section was grossly improved and true amplitudes were restored from the post migration results. In conclusion, the derived and applied refraction statics solution had adequately resolved the statics problem of SOKU. This is evident from the enhanced quality of seismic subsurface imaging results achieved. The correct derivation and application of refraction statics for seismic datasets plays a crucial role in enhancing subsurface seismic imaging for accurate geophysical and geological interpretation in the quest to identifying potential and prolific hydrocarbon reservoirs.

CHAPTER ONE
INTRODUCTION

1.1 Background to the Study

The primary objective and ultimate goal in reflection seismic data processing is to obtain as accurately as possible the image of the subsurface, which is very vital for accurate interpretation during exploration for hydrocarbon resources and other geological targets. The typical target of seismic interpretation is identification of features which could reveal the oil and gas prospects of the region under investigation. The common ways to find potential hydrocarbon accumulation is to look for structural and stratigraphic traps by employing the means of modern sophisticated imaging and interpretation software tools. These images are obtained by using a sequence of processing steps, and therefore the interpretation can only be meaningful and reliable when all these processing steps are correct and sufficiently accurate.

One of the key steps of seismic data processing is the statics correction. The term statics denotes the highly variable travel times of reflected waves (ray path 2) (Figure 1.1)

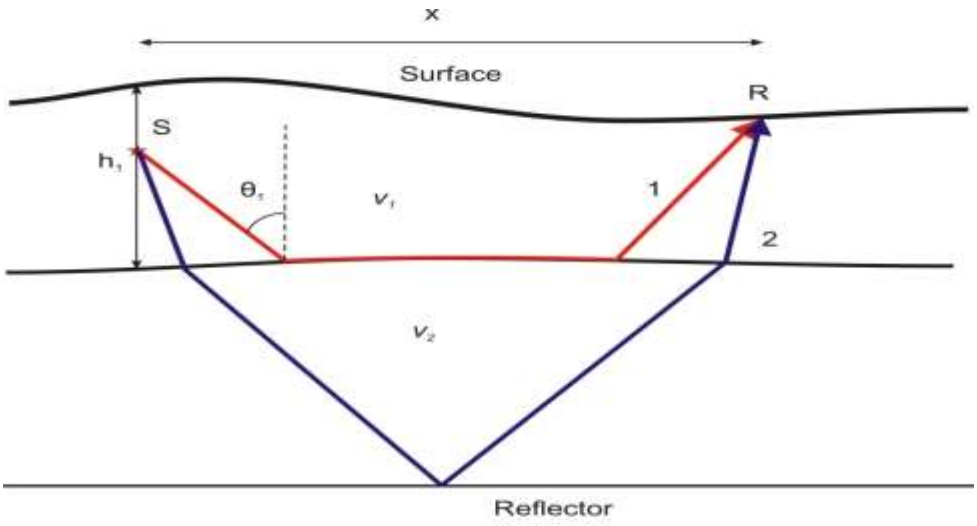

Figure 1.1: Schematics of a 2D reflection survey subsurface. The source is at position S and the receiver is positioned at R. The ray path "1" represents a head wave and ray path "2" is a reflected wave. (Atul, 2009)

accumulated during their propagation within the shallow subsurface (Telford *et al.*, 1990). The near-surface layer (weathered zone) is unconsolidated and significantly more non-uniform than the deeper layers. The uneven thickness of the near- surface layers and low velocities lead to large (often up to ~50 ms or more), strongly variable time shifts of the reflected waves recorded from the deeper layers (Figure 1.1). Because reflected rays propagate nearly vertically within the low-velocity weathered zone, such time shifts are practically independent of the depth of reflections, and they are consequently called statics.

If not properly reduced or mitigated, static shifts are capable of completely disrupting the coherence of reflections during common midpoint stacking. Spurious reflection patterns on shot gathers and loss of depth resolution could equally be a consequence of incorrect or inaccurate statics. Images obtained from such spurious reflection patterns would most certainly lead to erroneous interpretations which is not desirable and money and time would have been wasted. The process for compensating statics is referred to as statics correction; this is one of the most critical and time consuming steps in reflection data processing and forms the fulcrum for this dissertation, as a refraction statics solution would be derived and applied to 3D seismic field datasets from OML-23 SOKU, in the Niger Delta Basin, to resolve the statics problem, so that an accurate subsurface image could be obtained for interpretation and exploitation purposes.

1.2 Statement of the Problem

The recognition of the effect of the near surface layer and its velocity distribution plays a vital role in the estimation of static corrections especially for onshore seismic datasets. The accuracy of static corrections estimation has essential effects on results of many processing procedures. The important ones are velocity analysis, stacking and migration. The errors in static correction estimation are the sources of serious structural and stratigraphic interpretation errors. Also, seismic inversion,

and AVO procedures are adversely affected by poor static corrections. Before statics correction can be well derived and implemented to seismic records, it is pertinent to first estimate the model of the near surface in terms of weathering and sub-weathering layer thicknesses and velocities. The weathered layer lies just below the ground surface and consists of unconsolidated sediments overlying the bed rocks. It varies in thickness and the velocity of the weathered layer is generally less than the sub-weathered layers below it. It is heterogeneous in composition with a wide range of velocities and large energy distribution as a result of frictional losses in unconsolidated sediment, which causes variable delay in travel times of the seismic waves (Cox, 1999). This delay in travel times causes or gives rise to inaccurate near-surface velocity estimation which when not properly accounted or corrected for eventually introduces structural anomalies in deeper seismic reflection events when observed on seismic records.

The problem of derivation of a reliable refraction statics solution for 3D onshore seismic data in OML-23, SOKU is thus the focal problem which this dissertation is seeking to address, to mitigate as much as possible, its undesirable effects for further processing of the seismic dataset. The motivation for this research direction/path was anchored on our resolve to providing a solution to the statics problem of SOKU (OML-23). The research target therefore, is to derive and implement refraction statics for the SOKU 3D seismic datasets and to determine the effectiveness of the derived and implemented refraction statics solution on shot gathers, a stacked and migrated sections of the seismic data over the investigated prospect.

1.3 Aim and Objectives of the Study

The research aim is to derive a refraction statics solution for 3D seismic data in OML-23 (SOKU) Niger Delta using the delay - time approach.

The objectives of the study are,

i) Generation of a near-surface model of the earth over OML-23 (SOKU) in terms of weathering and sub-weathering layer thicknesses and seismic velocities.

ii) The generated near-surface model of the earth would then be adapted into deriving a refraction statics solution that would be incorporated into the processing workflow for the dataset.

iii) Determining the effectiveness of the derived refraction statics solution on shot gathers from the investigated prospect in Field File Identification (FFID) configuration.

iv) Determining the effectiveness of the derived statics solution on a stacked section of the data over the investigated prospect.

v) Determining the effectiveness of the derived statics solution on a migrated section of the dataset over the investigated prospect.

1.4 Scope of the Study

The scope of the research would entail estimation of a near surface velocity and depth model over the prospect using the Delay-Time approach. Distortions due to near-surface velocity variations would be removed after identifying the Low Velocity Layer (LVL) from the estimated near surface model. Subsequently, a reliable refraction statics solution (statics correction) for OML-23 (SOKU) would be derived and applied to the seismic field datasets from the estimated near-surface model. The effectiveness or success of the derived and applied refraction statics solution would thereafter be determined on shot gathers, a stacked section and finally, a migrated section of the dataset.

1.5 Limitation of the Study

A minor limitation for the present study is the unavailability of a special tool called “Tomostatics” which is a recent tomographic or imaging modeling tool that could have been deployed to image the near-surface. The “Tomostatics” application is not running on the current

software tools (Vista^{TM} , 2012 edition and Promax^{TM}) being deployed for the study. Efforts to get the "Tomostatics" application have been unsuccessful in the past several months, which is the reason a hybrid approach, of combining refraction arrival inversion and uphole survey measurements, (with the aid of special processing plugins) is deployed in the near-surface imaging for the present study.

1.6 Significance of the Study

Errors in static correction induce errors in procedures such as velocity analysis, stacking and migration. Inaccuracy in these procedures will result in spurious structural and stratigraphic anomalies which are not true representation of the subsurface and eventually leads to misinterpretation of potential geologic and geophysical targets.

The research therefore is very important and would benefit the following;

A) Industry based 2D/3D seismic data processors:

The refraction statics solution to be derived and implemented on the 3D seismic datasets for the present study would grossly enhance the accuracy and reliability of the following key seismic processing procedures;

i) Velocity analysis
ii) Inversion
iii) AVO applications
iv) Stacking
v) Migration

B) The Academic/Research communities:

The academic/research community would be presented with processing strategies and steps which would be documented as journal papers to demonstrate how the methods adopted were applied in solving the processing challenge at hand. They in turn could adopt these documented processing strategies to solve future related seismic processing challenges.

1.7 Location, Geometry and Geologic settings of the Study Area

The prospect (OML-23, SOKU) lies within the onshore part of the Niger-Delta Basin, Nigeria (Figure 1.2). The prospect is situated in the south-eastern part of the onshore Niger Delta and is a few kilometers away from Port Harcourt in Rivers State of Nigeria. The prospect covers areas and towns in parts of present day Rivers and Bayelsa States of Nigeria. The land surface within the prospect area is characterized by low-lying plains typical of the modern Niger Delta. These plains have swamps that are commonly flooded during the peak of rainy season. The prospect area is also characterized by sediments which are predominantly aerated, unconsolidated and undulating sands with variable thicknesses. The geographical grids of the prospect is 5°11' - 5°40'N and 6°42' - 7°11'E. The area slopes imperceptibly in the southern direction towards the Atlantic Ocean and is drained by a network of rivers and their adjoining creeks.

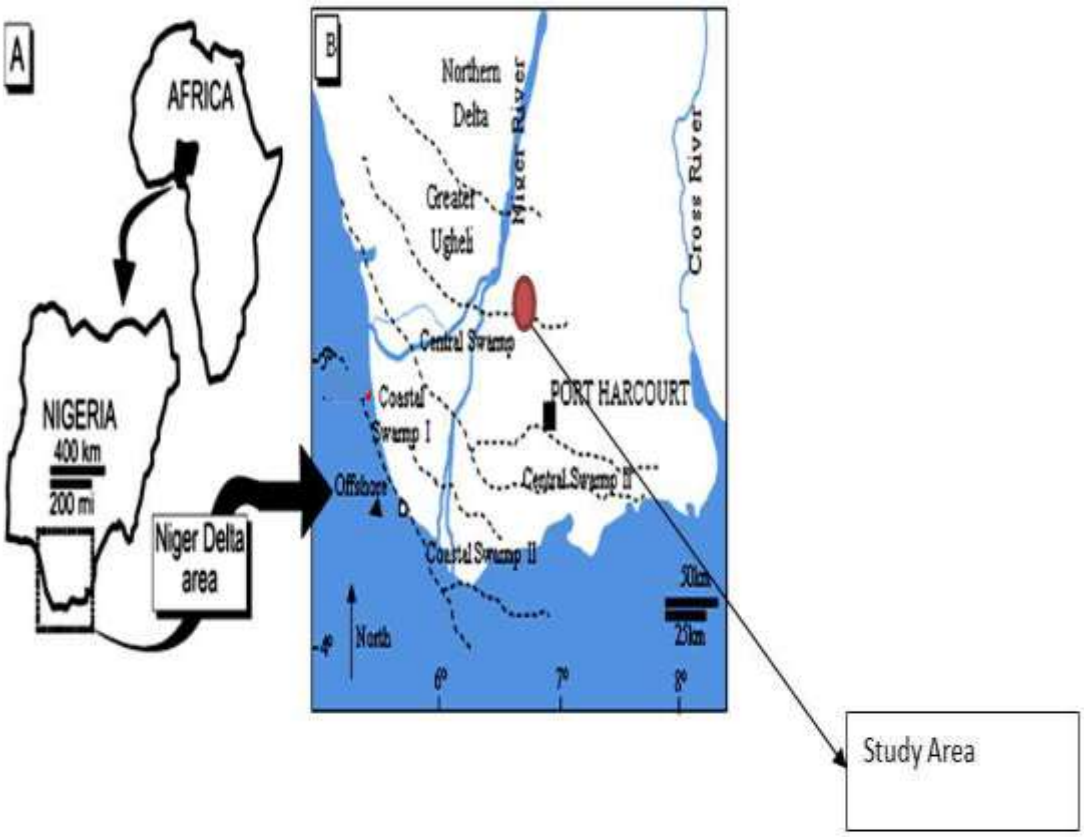

Figure 1.2: Map of the Niger Delta showing location of the study area

The prospect covers an extensive area of over 151.3 square km., the geometry of the prospect is as shown in Figure 1.3 with its boundaries clearly defined in terms of their respective coordinates.

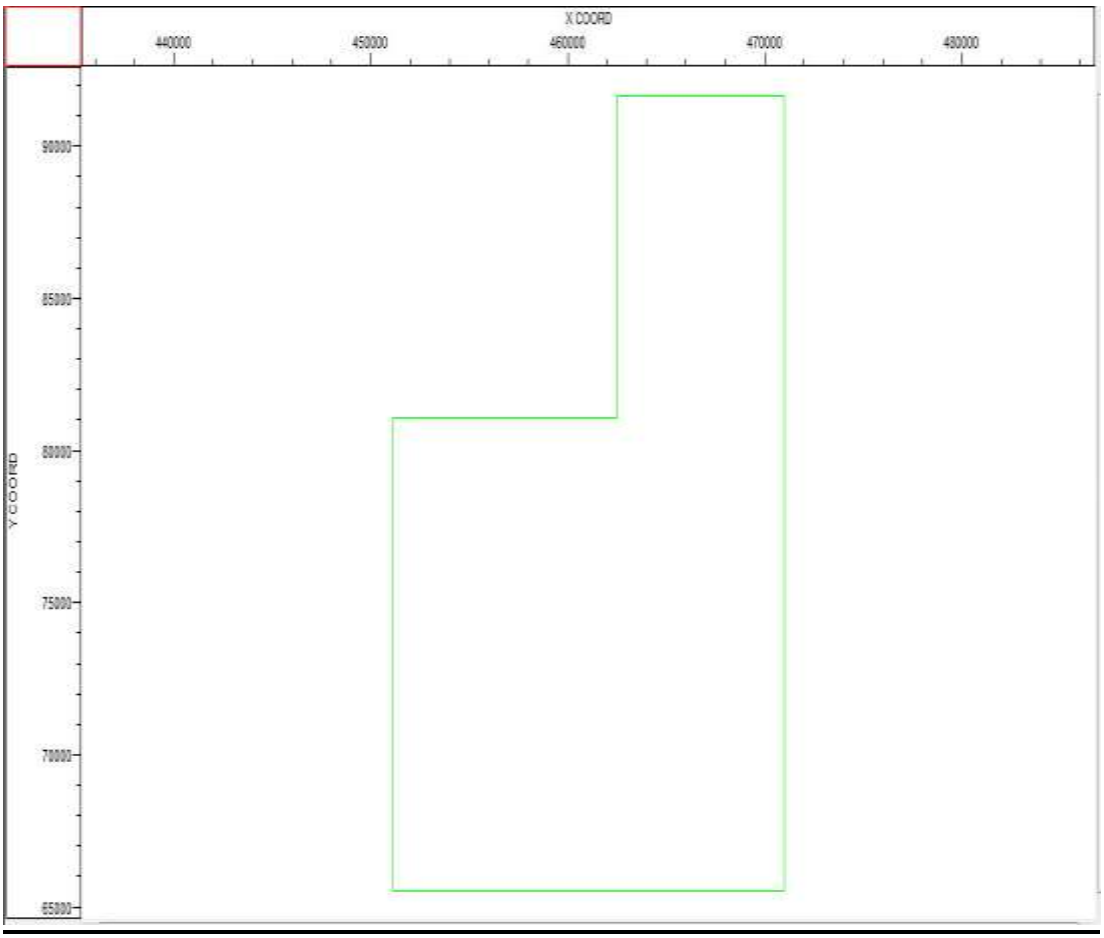

Figure 1.3: Geometry of the prospect field showing its boundaries and coordinates.

The vegetation around the prospect is mainly mangrove which posed a serious challenge of easy access for the seismic crew during the acquisition program. The 3D seismic acquisition for the prospect was executed in three (3) phases. Each acquisition phase covered approximately 13 swaths. The entire acquisition was prosecuted with well over 27,500 shots using a Sercel 428 recording instrument. The shooting geometry was a symmetric split spread configuration with an offset range from 25-6500m. Prior to the 3D seismic data acquisition program, a total of about 50 uphole location points were established for uphole shooting across the entire prospect. The prospect (OML-23, SOKU) is currently being evaluated for its hydrocarbon potential.

CHAPTER TWO

LITERATURE REVIEW

2.1 Previous works on Refraction Methods, Near-surface Imaging and Refraction Statics

The refraction method was the first seismic technique to be used in petroleum exploration, and in the 1920's, it achieved spectacular success in Iran and the Gulf Coast of the USA. The 1950's represent a significant period in the development of refraction techniques. Almost all of the major issues had been identified and many advances had been achieved. They include the mapping of irregular refractors, complex wave-speed functions in the layers above the target refractor, undetected layers, wave-speed reversals, anisotropy, and refraction migration (Feroci *et al*., 2000 and Stark, 2008). In the last fifty years, most research has focused on the various methods for inverting travel-time data to map targets in the near surface region for geotechnical, groundwater and environmental applications, and for statics corrections for seismic reflection surveys (Stone, 1995).

Refraction data can be acquired either by a separate refraction survey in the field, or by using the first arrivals recorded as part of a seismic reflection survey. The latter approach is now more appropriate than it was a few years ago because the group interval, and hence array lengths, are much smaller, thereby minimizing the attenuation of the refracted arrival. To obtain good estimates of refraction arrival times, the source and receiver should be as broadband as possible with minimal filtering applied to the data recording (Hagedoorn, 1959). During seismic reflection acquisition, the arrival times of refracted waves, often referred to as the 'first breaks', are also recorded and usually used to calculate near surface velocity structure for statics correction. Some advantages of using seismic reflection records for an analysis of refraction data are as follows:

i) There are no additional acquisition costs.

ii) A large amount of redundancy for acquisition crew or field personnel is achievable.

iii) The source and receiver locations are those used in the reflection survey.

iv) Refractors can usually be mapped well below the weathered layer and on a continuous basis.

Several authors have described and documented procedures for calculating near surface layer characteristics and statics correction from high resolution seismic surveys. Some of their findings are hereby presented;

Chun and Jacewitz (1981) discussed the content of the first arrivals and presented a surface consistent solution of refraction statics by the formation of time surfaces. They also indicated that large error distributions often remained after solutions have been obtained. Steeples *et al.,* (1990) described pitfalls and key point in calculating statics correction for shallow seismic reflection surveys. Brouwer and Helbig (1998) developed 'ray tracing statics correction' method that gives better results for shallow structures in high resolution seismic surveys.

Pugin and Pullan (2000) presented a new technique 'first arrival alignments static correction' which they applied on shallow high resolution reflection data. This technique calculates and takes care of short, medium and long wavelength statics. It is an iterative process in which the velocity model of the near surface is known and some kind of comparison of ray traced results and a known model is carried out to get the final statics correction.

Lawton (1989) used differences in first-arrival travel-times between adjacent records in multifold reflection surveys to compute the depth and velocity structure of near-surface layers. The travel-time differences as a function of source-receiver offset provide a direct indication of the number of refractors present, with each refractor being defined by an offset range with a constant time difference. For each refractor, the time-difference value at a common receiver from two shot points is used to partition the intercept time into the delay time at each shot-point. This

procedure is repeated until the delay times at all shot points and for all refractors have been computed. Refractor depths and velocities are evaluated from this suite of delay times.

Zanzi and Carlini (1991) proposed a new method for refraction statics reducing the computational time without reducing accuracy. The first arrivals, common-offset organized, formed the data space. The method involved Fourier transformation of any common-offset data vector with respect to the common mid-point. As a result, the data are decomposed in a number of subspaces, associated with the wave-numbers, which can be independently inverted to obtain any wavelength of the near-surface model.

Docherty (1992) investigated the feasibility of computing the weathering model from travel-times of refracted first arrivals. The problem was formulated in terms of the difference in arrival time of adjacent receivers, resulting in a much sparser matrix for inversion. Lateral variations in both the weathering thickness and velocity were sought. In most cases, it was necessary to include a small number of constraints to obtain the true weathering model. Any roughness in the solution that was not required to fit the data was most effectively removed using a second difference smoothing technique. Two layers make up the mode: a laterally inhomogeneous weathering layer and a uniform high speed refractor. The weathering layers were divided into cells of constant velocity. Each cell was bounded by the observation surface and below by the refractor. Boundaries between adjacent cells were vertical. In the study a constant refractor velocity was assumed.

Bohm *et al.*, (2006) used a joint inversion of both first and refracted arrivals in order to obtain a well-resolved velocity field for the computation of statics correction. After the analysis of the diving waves, they inverted the travel-times associated with the refracted events by using the velocity model obtained from the diving waves as the initial model. Also after inverting the two refracted arrivals separately they used the resulting output velocity field as a new initial model

for jointly inverting again the direct arrivals and the travel-times with the first and second refracted waves, in order to obtain a more accurate velocity field in depth.

Zhu *et al*., (1992) demonstrated that turning ray tomography could image near-surface velocities more accurately than refraction statics methods. In their study, the medium to be imaged was discretized into grids of small rectangular cells, each of which contains a single velocity. Sources and receivers were both located on the surface. The updated velocities were slightly smoothened (damped) after every iteration. This was an approach they termed the Constrained Damped Simultaneous Iterative Reconstruction Technique (CDSIRT). Their study confirmed that tomostatics is noticeably closer to the true statics where velocity inversions are significant. Generally, long spatial wavelength statics appeared to be estimated better using tomostatics, although a tomostatics bias exists with increasing depth due to damping and smoothing in the tomography algorithm. The output image of their linear inversion was remarkably robust to a wide range of reasonable initial models.

Stefani (1995) used turning ray tomography for estimating near-surface velocity structure in areas where conventional refraction statics techniques failed because of poor data or lack of smooth refractor/velocity structure. The method comprised nonlinear iterations of forward ray tracing through triangular cells linear in slowness squared, coupled with the LSQR linear inversion algorithm.

Rajasekaran and McMechan (1996) performed the tomography on prestack time picks using the Simultaneous Iterative Reconstruction Technique (SIRT) algorithm with modifications to include reflected as well as turned rays. Travel times of head waves were well approximated by rays turned in a small velocity gradient below a high contrast reflector, and so were included automatically as a special case of turned rays. The reflections, which correspond to predominantly near vertical propagation, define horizontal changes in the model, but not the vertical changes. Conversely, the

turned transmissions were better able to define the vertical changes. Increasing the effective aperture by combining reflection and transmission data and performing tomography on this composite data set produced a better image of the 2D velocity distribution.

Opara *et al.*, (2017, 2018) implemented first and refracted arrival inversion to build a near-surface model and compute a preliminary (partial) statics correction for 3D seismic field datasets from an onshore Niger Delta prospect field.

Lanz *et al*., (1998) investigated the applicability of surface based 2D refraction tomography (turning ray tomography) for delineating the geometry of a landfill. The depth of the near-surface model did not exceed 100m. The velocity in the layers encountered rapidly increased from 1000m/s to 1500m/s. geophone and source spacing were set to 2 and 8m respectively. Sampling interval of 0, 25m was used. The result achieved from the study demonstrated that the tomographic refraction scheme may be an efficient means of studying the very shallow subsurface but complementary geological and other geophysical data are required to make interpretation more reliable.

Zhang and Toksoz (1998) presented a nonlinear refraction travel time tomography method that consisted of a new version of the shortest path ray – tracing approach, a regularized nonlinear inversion method that inverts "travel time curves" rather than travel times alone, and Monte Carlo method for nonlinear uncertainty analysis of the final solution. Seismic ray paths were defined by calculating the shortest travel time paths through a network consisting of nodes and representing the earth. They solved an inverse problem that explicitly minimizes data misfit as well as model roughness.

Ditmar *et al*., (1999) developed an algorithm for tomographic inversion of travel times of reflected and refracted seismic waves. In the case of a very inexact initial model, a layer by layer inversion strategy was recommended as a first inversion step. They assumed that the model consisted of several layers separated by interfaces represented by a set of points connected by

straight segments. Velocity distribution in each layer was described by means of its own velocity grid, the layer being completed inside the grid. The velocity values were specified at grid-nodes and bilinear interpolations were used in between nodes.

Bridle and Aramco (2009) analyzed the applications of refraction statics and Tomostatics on test lines. For longer deeper anomalies with irregular ray-paths, refraction statics and Tomostatics were expected to provide major improvements; however, only marginal improvements were observed. In the test line considered the refraction statics provided the best section visually in terms of signal strength, sharpness and continuity, with a structure that seems geologically reasonable.

Kolawole *et al.*, (2012) analyzed a refraction seismic survey in the Niger Delta Basin where a 3–layer earth model was analyzed. The correlation and interpretation of the observed lithological successions with velocities and depths of boundaries across the two refraction points with 3-layer models suggest an irregularity along the true base of the weathering layer, probably caused by faulting. The true depths of base of weathering layer, as well as velocities of weathering layer and consolidated layers for the two refraction points with 3-layer models were calculated.

Ajani *et al.*, (2013) used the low velocity layer (LVL) method to determine the depth of the weathered layer and velocities of near-surface layers over the Omerelu Area in River State, Nigeria. In the test conducted, the depth of weathered layer in the study area varies between 12m - 13m. The velocities of the weathered layer and the consolidated layer varied between 500 m/s – 550 m/s and 1790 m/s – 1875 m/s respectively.

Zhu *et al.*, (2014) applied several different approaches to obtaining statics solutions for the processing of deep reflection seismic data in the South China province. Each approach they applied yielded an output which they compared in order to find the most appropriate statics solution. They observed that statics solutions based on tomographic principle or combining the low-

frequency components of field statics with the high-frequency ones of refraction statics could provide reasonable statics solutions for deep reflection seismic data in the province which is characterized by a very rugged surface topography. They equally observed that the two statics solutions could correct the statics anomalies of both long spatial wavelengths and short ones. The surface-consistent residual static corrections served as an extra quality control measure to compensate or tackle the remaining statics effects prevalent on the data after the implementation of the first statics solutions. Their conclusion was that statics solutions based on tomographic principles could provide proper solutions for the statics problem in their terrain that was marked by very uneven and rugged topography. Their opinion was that combining the low-frequency components of field statics solutions with the high-frequency ones of refraction statics solutions could equally provide reasonable solutions for the deep reflection seismic data in the province. Their surface-consistent residual static corrections were also good compensations to the procedures of the first statics solutions in their investigation and left the deep reflection seismic data free of statics anomalies. They final conclusion was that proper statics solution can improve both qualities and resolutions of seismic sections.

Statics problems are big challenges for the processing of deep reflection seismic data and it is very important to accurately calculate the statics at the time of processing of land seismic data. This subsequently improves the quality of other processing stages which in turn impacts positively on the overall integrity, quality and resolution of the imaged section. This process which seems straightforward is quite delicate and could be made more complicated if the survey area is overlain by irregular topography such as sand dunes of varying heights which introduces a low velocity layer (LVL) challenge into the mix. To adequately remove the effect of rapid velocity changes in the near-surface specially that of the LVL or weathering layer, correct estimation of statics due to the presence of weathering zones, (sand dunes in this instance)

becomes very imperative. Roy *et al.,* (2008 and 2010) while processing 3D vibroseis data acquired in the sand dune area of Western Rajasthan, India, observed that gathers were not aligned properly even after application of field statics. The field statics calculation was based on shallow refraction data. The stacked output of the gathers gave rise to "patchy reflections" in the zones of interest as well as at shallower and deeper level. To overcome this processing problem, first break refraction picking on 3D vibroseis data was utilized to estimate the near–surface model. First breaks were picked swath wise on the 3D data and the near-surface model computed to calculate statics. This method has a minor limitation owing from the fact that different statics values were observed for common shots/receivers in adjoining swaths over the entire survey area. They now proposed a method of employing entire 3D data volume as a single input to build near-surface model. The new resulting stack outputs showed remarkable improvements as those patchy reflections were reduced and subsequent processing stages were enhanced.

Correcting near-surface velocity and elevation variations with statics is an essential stage in the implementation of statics correction which is a very key step in the processing of land seismic data. The correct implementation of statics correction improves the qualities of subsequent processing steps and are key determinants to the quality and resolution of the final imaged section (Li *et al*., 2011; Deere, 2009; Laak and Zaghloul, 2009; Li *et al.*, 2009a; Raef, 2009; Stein *et al.*, 2009; Han *et al*., 2008; Vossen and Trampert, 2007; Yan *et al*., 2006; Criss and Cunningham, 2001). Static corrections as defined by (Cox, 1999; Sheriff, 1991) are corrections applied to seismic data to compensate for the effects of variations in elevation, weathering thickness, weathering velocity, or reference to a datum. The objective therefore, is to determine the reflection arrival times which would have been observed if all measurements had been made on a (usually) flat plane with no weathering or low-velocity material present. Hence it leads to the concept of surface-consistent

corrections, which are dependent on the location of the source (or receiver) but are independent of the source to receiver offset or time of the recorded data (Deere, 2009; Cox, 1999).

There are many issues which are associated with the near surface and related with the variation of velocity and thickness in the near-surface layers. Field statics can compensate the data for the common datum problem which have been carefully investigated and documented by (Luo *et al.*, 2010; Li *et al*., 2009b and Huang *et al*., 2008). There are lots of statics correction methods based on the seismic refraction principle, which can be used to resolve velocities of shallow layers using head waves, such as slope (or intercept) method (Knox, 1967), delay time method (as demonstrated by Coppens, 1985), reciprocal method (Palmer, 1980), least square method (Chang *et al.*, 2002; Simmons and Backus, 1992) and turn-rays method (Henley, 2009; Criss and Cunningham, 2001). Tomographic static correction methods have been investigated and applied by many researchers (Liu *et al.*, 2010; Li *et al*., 2009b; Yordkayhun *et al*., 2009; Zhu *et al*., 2008; Taner *et al*., 1998) to obtain static corrections using the tomographic velocity models based on the first-arrival information. These statics methods require a large number of rays going through the model areas evenly with different ray angles. Ray tomography methods have been used to build near-surface velocity models using first-arrival information and to estimate the statics correction (Zhang *et al*., 2009; Ke *et al*., 2007). Many residual statics correction methods have been developed in order to compensate for the time delays in the past few decades, such as the travel time inversion based method (Hatherly *et al*., 1994), stack-power maximization method (Ronen and Claerbout, 1985), non-stationary residual statics method (Henley, 2012) and sparsity maximization method (Gholami, 2013).

In reality, many factors pose serious limitations to the correct and appropriate implementation of static corrections thereby making statics correction a difficult processing step to handle. These factors include rugged surface acquisition topography, non-planar refractors, near-surface low-

velocity layers, lateral variant velocities of weathering layers and variations of underground water tables (Li *et al*., 2009b; Wang, 1999). Errors in static corrections lead to the loss of seismic resolutions, both temporal and spatial, and these poses serious difficulties and confusions during the interpretations of such seismic sections.

Near-surface seismic imaging techniques have been widely demonstrated and used in an increasing number of applications (Steeples and Miller, 1990; Buker *et al.*, 1998; Juhlin *et al*., 2002). One of the difficult challenges in reflection seismic processing is that poor images are generally obtained in the upper part of the sections due to shot- associated noise, surface waves and direct arrivals that obscure the reflected energy (Miller *et al.*, 1998). In most situations or instances, the shallowest reflections are removed prior to normal moveout (NMO) corrections and stacking. The resultant effect being that details from the upper part of the section is lost. In addition, heterogeneities or the non-uniform geologic conditions in the near-surface lead to statics correction problems. Therefore, a joint interpretation of refraction and reflection seismic data from the near-surface can have many benefits. Several approaches, some simple while others very sophisticated and complex have been deployed in interpretation of refraction seismic data and tomographic inversion schemes on how to better image the near-surface have been extensively discussed in the diverse literatures (Hampson and Russell, 1984; Lines and Treitel, 1984; Marsden, 1993; Macrides and Dennis, 1994; Belfer and Landa, 1996; Lanz *et al.*, 1998; Taner *et al.*, 1998; Marti *et al.*, 2002 and Bergman *et al.*, 2004).

Yordkayhun *et al.*, (2007), in a bid to understand the near-surface structure over a CO_2SINK (carbon dioxide storage and monitoring) project in the Ketzin area in Germany used first arrival travel times to image the near-surface structure and to provide an improved velocity function for the interpretation of seismic reflection data. In order to obtain additional structural information and to improve the velocity function estimates, travel time inversion based on the generalized linear inversion (GLI) method proposed by Hampson and Russell (1984), based on iterative least-squares

inversion (Lines and Treitel, 1984; Menke, 1984) was adapted by them in building the velocity–depth model of the near-surface. The successfully obtained the velocity-depth profiles of the upper most 400 m over the investigated area which was basically overlain by sedimentary sequences. The sedimentary rocks were characterized by a gradual increase in the velocity field with depth without strong contrasts and nearly insignificant lateral velocity variations. First arrivals represent refracted energy that has propagated along the fastest path in the sub-surface before arriving at the surface. Processing and interpretation techniques that involve analysis of these travel- times are well known and a number of popular methods are in use. Recent advances in inversion of seismic refraction data have made it possible to image heterogeneous media, as well as solving statics correction problems (Olsen, 1989; Boschetti *et al*., 1996; Bergman *et al*., 2004).

There are different approaches in the application of refraction statics corrections for 3D seismic data processing such as the generalized linear inversion (GLI-3D) approach by Hampson and Russell (1984). In this method, an initial subsurface model is input by the user, consisting simply of a number of flat, constant velocity layers. The model is then iteratively updated, by using a generalized linear inversion (GLI) algorithm, in such a way as to reduce the difference between the observed breaks and those calculated from the model. The advantage of the GLI algorithm is full redundancy of observed breaks reducing the sensitivity of the solution to picking errors and the final model of the subsurface is nearly close to the input geological model. The drawback of the GLI is that the reliability of the inversion schemes depends primarily on the sophistication of the modeling programme and the constraints imposed upon the possible solutions. This limitation is now remedied by a method which is a spin-off of the reciprocal method by Hawkins (1961). This method is called the delay time analysis (Gardner, 1967) which was initially tested and applied by (Barry, 1967) and has been recently fully developed by Lawton (1989). In the delay time analysis

or approach, the underlying principle involves using differences in first arrival travel times between adjacent records in reflection surveys to compute the depth and velocity structure of the near-surface layers. The travel time differences as a function of source – receiver offset provide a direct indication of the number of refractors present, with each refractor being defined by an offset range with a constant time difference. For each refractor, the time difference value at a common receiver from two shot points is used to partition the intercept time into the delay time at each shot point.

This procedure is repeated until the delay times at all shot points and for all refractors have been computed. Refractor depths and velocities are evaluated from the suite of delay times. A surface – consistent statics correction to a selected datum level is then calculated at each surface station, using a replacement velocity equal to that of the deepest refractor. Statics correction is one of the most important steps in onshore seismic data processing and is generally calculated with thickness and velocity parameters of a near-surface weathering layer. The methods that invert the near surface structures using the first break-time of seismic data include refraction and tomographic methods.

The advantage of the refraction method is that it can obtain a relative accurate delay time, but it relies on other near-surface investigations to obtain the velocity of the weathering layer. The advantage of using the tomography method is that it is capable of obtaining the weathering layer velocity, although it still relies on the other near-surface investigations to determine the thickness of the weathering layer.

At present, the statics correction methods commonly used includes the refraction statics correction and the tomographic inversion statics correction. Another advantage of the refraction statics correction method over the tomographic method is its capability to obtain good quality and high frequency statics by inverting the given surface velocity. By contrast, the surface structure model cannot be inverted unless it relies on other near- surface investigation means to determine the velocity of the weathering layer as the restriction. Due to under-sampling of near-

surface data or the difference between the investigated beds of interest, it is likely that some error in the surface velocity will occur (Cox, 2004). The incorrect surface velocity may lead to an incorrect reflector depth, and result in a long wavelength statics residue (Lin *et al*., 2006). Therefore, understanding how to determine a rational surface velocity is a key way to improve the effect of the refraction statics correction. The tomographic method extracts the distributions of velocity and reflection coefficients using the comprehensive observation results from a large amount of shot points and geophone points. It can typically obtain a relatively accurate velocity trend; hence, its long wavelength statics correction component is good, while its high-frequency component is generally poor. Meanwhile, differences in selecting the top interface of a high velocity layer may also lead to some differences in statics. Hence, these two static methods complement each other, and they are both commonly applied together when dealing with statics correction computation for complex areas. In general, there are two ways to combine the tomographic and refraction methods;

i) Perform the tomographic inversion using the model obtained through the inversion of the reflection computation as the initial model, which achieves the surface structure mode of the tomographic inversion features.

ii) Calculate the refraction and the tomographic statics respectively, using a specified separation radius to separate the long-wavelength component of the tomographic statics correction and the short-wavelength component of the refraction statics correction, and integrating them together as a final statics correction.

The latter method has worked in some areas, but there are several factors that lead to uncertainties. The first one is the inaccuracy of the weathering layer velocity for the refraction statics correction, which had impacted both the long-wavelength and the short-wavelength statics. The uncertain bottom boundary of the tomographic inversion model may

influence the long-wavelength component; In addition, the different separation radius may also differ in the final statics. (Kong *et al.*, 2013) proposed a method to extract the surface velocity from the tomographic inversion model, such that the surface velocity can be used in the refraction inversion. They were able to achieve a stable and unique solution. Their approach combined both the tomographic inversion and the refraction static correction in what they termed "Joint inversion of tomography and refraction".

Tomographic statics are commonly used during the processing of seismic data, especially in the areas with rapid lateral velocity variations (Hao *et al*., 2011; Luo *et al*., 2010; Han *et al*., 2008; Wang, 2005; Yang *et al.*, 2005). Tomography is defined by (Sheriff, 1991) as a method for finding the velocity and reflectivity distribution from a multitude of observations using combinations of source and receiver locations. The tomographic inversion approaches use the first arrival information of the recorded wave-front to inverse the velocity distribution of the near-surface without the assumption of layer structure in order to produce a near-surface velocity model which best fits the observed minimum arrival times. Space is divided into cells and the data are expressed as line integrals along ray paths through the cells. Adjustment and updating of the near-surface velocity model is done iteratively until the differences between arrival times of model and those of the observed data reach acceptable levels or are unchanged between iterations (Becerra *et al*., 2009; Henley, 2009; Li *et al*., 2009b; Vossen and Trampert, 2007; Chang *et al*., 2002). Tomographic methods include the Algebraic Reconstruction Technique - ART (Henley, 2009), the Simultaneous Reconstruction Technique - SIRT (Aster *et al*., 2005; Emily and Bradford, 2002) and the Gauss-Seidel Method (Taner *et al*., 1998).

The statics solutions based on tomography principle need a large number of different ray paths to go through each of the cells with a wide-angle coverage and constrains of indirect regularization during the inversion are mitigated. The methods provide proper corrections for long

and middle spatial wavelength components of statics correction in situations where the field is characterized by rugged surface topography and rapidly changing velocities in the near-surface layers. However, there are still some shortcomings of statics correction based on tomographic techniques and the uncertainties in tomographic velocity models have also been investigated using a 2D seismic line acquired in Colombia through a variety of numerical techniques (Becerra *et al*., 2009).

Refraction methods allow one to derive estimates of the thicknesses and velocities of the near-surface layers by analyzing the first-breaks of the seismic records (Luo *et al*., 2010; Wu *et al*., 2009; Duan, 2006; Lin *et al*., 2006; Pan *et al*., 2003). According to the Huygens' Principle, every point on an advancing wave-front could be regarded as the source of a secondary wave and that a later wave-front is the envelope tangent to all the secondary waves (Cox, 1999). The important concept in seismic refraction is that when a seismic ray crosses a boundary between two formations of different velocities, then the ray is bent according to Snell's law which defines that the sine of refracted angle is equal to the ratio of the velocities of the two formations. Therefore, the statics correction based on refraction survey acquires the information of the first-arrival time of the wave-field from refractor and the refractor velocity. Hence, there are two basic conditions for refraction survey, that is, a relative stable refraction interface between the two formations and the acknowledged near-surface velocity distribution (Bridle and Aramco, 2009; Liu, 1998). Applying the statics correction based on refraction survey can ensure structural integrity in the processed section. Refraction statics are effective for correcting long spatial wavelength anomalies and compensating for the weathering layers. Actually, refraction statics are also effective against short spatial wavelength anomalies (Liu, 1998).

The weathered zone due to its variable and non-uniform composition induces irregular time shifts (statics) for both reflected and refracted waves; statics correction therefore is a procedure

that seeks to compensate for these irregular time shifts. Several types of statics have been differentiated (Telford *et al.*, 1990). The statics due to the differences in surface elevations which affect both sources and receivers are regarded as elevation statics. These statics can be corrected relatively easily if the elevations and the near-surface seismic velocities are known. Sources typically have additional negative statics due to their being buried at variable depth below the surface; such statics can be compensated by using the "uphole" times measured by the wave propagation from the sources to the nearest receivers. Additional static shifts are also associated with velocity variations within the weathered zone itself, such as caused by layering or variations of its depth. By their relation to the source or receiver position, statics are also subdivided to source and receiver statics, and the "total" statics of a seismic trace is the sum of all three statics at the corresponding source and at receiver locations. Finally, statics are called "surface-consistent" if they are only related to the surface locations of the source and receivers and not to their individual properties.

All of the statics above can be incorporated in the concept of "refraction statics" (Yilmaz, 2001). Refraction statics represent a group of methods based on constructing a realistic model of the shallow subsurface by inverting the refracted arrivals (ray path 1) (Figure 2.1). This model should incorporate the complete topography, depths of buried sources, as well as the variations in the structure of the weathered zone. This is the most complete and advanced approach to developing refraction statics solution, and it is the approach employed in the present dissertation. Refraction statics calculations are based on the use of refracted head waves to model

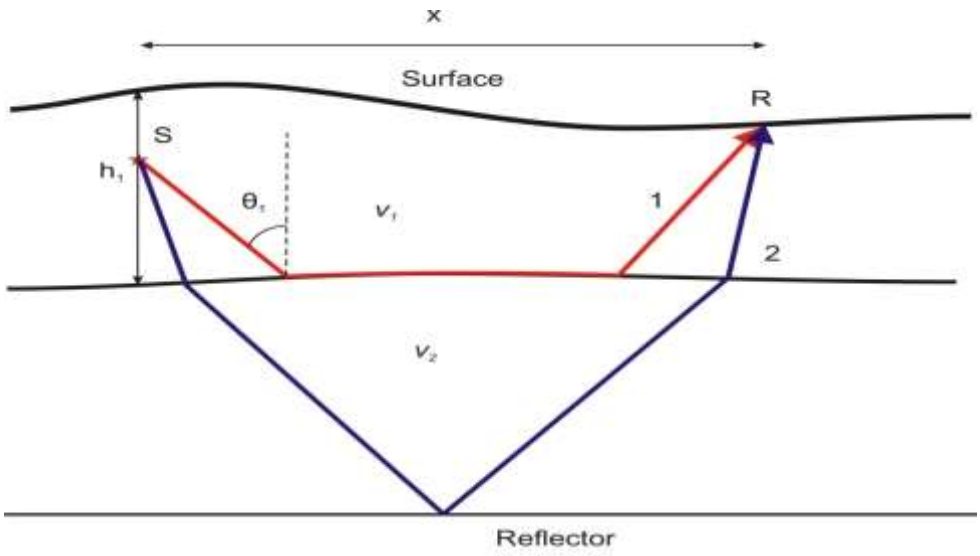

Figure 2.1: Schematics of a 2D reflection survey subsurface. The source is at position S and the receiver is positioned at R. The ray path "1" represents a head wave and ray path "2" is a reflected wave. (Atul, 2009)

the first-arrival travel times. Several refraction statics methods are in broad use today; these methods take the first-arrival times as input and use different kinds of travel-time modeling to derive estimates of the depths and/or subsurface velocities. Most of these travel time models are based on the following dependence equation of Atul (2009), of the head-wave travel time on the source-receiver distance x in a horizontal one-layer case (Figure 2.1):

$$t(x) = \frac{2h_1}{v_1} cos\theta_1 + px \qquad (2.1)$$

where, h_1 is the thickness of the layer 1 in (Figure 2.1) v_1 – its velocity, v_2 is the velocity of bottom layer, and p ($\sin\theta_1/v_1 = 1/v_2$) is the ray parameter.

This equation relates the observed property (time) to the physical properties (depth and velocity) of the layers beneath the source receiver locations. By analyzing the dependence of t on x, model parameters v_1, and h_1 in this equation can be estimated. In practice, spatially-variable layer velocities and thicknesses are used, and multiple layers may be needed for accurate modeling of the subsurface structure (Figure 2.1). These differences in the models determine the differences between the various methods.

In order to derive statics from a layered model, consider a nearly-vertically propagating ray shown in Figure 2.2. As shown, for modeling and inversion, it is convenient to use models with multiple constant-velocity layers. For a single such layer, if the datum is located within the "base" layer beneath it (Figure 2.2),

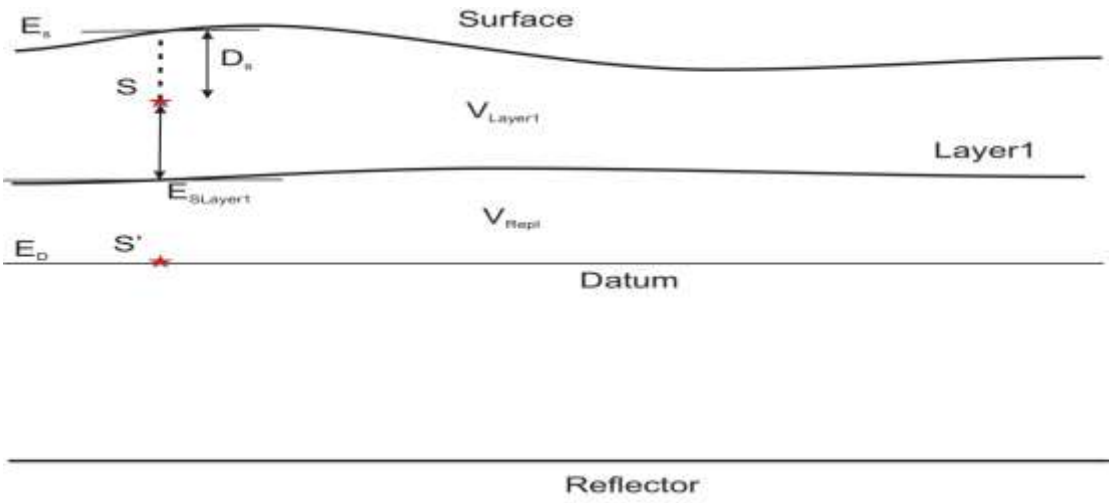

Figure 2.2: Schematics for calculating source statics for a single-layer weathered zone. E_S, E_D, $E_{SLayer1}$ are the elevations at respective positions. V_{Layer1} is the velocity of layer 1. (Atul, 2009)

The total source static is calculated using the equation by Atul as:

$$t_s = \frac{E_s - D_s - E_{sLayer1}}{V_{Layer-1}} + \frac{E_{sLayer1} - E_D}{V_{Replacement}} \qquad (2.2)$$

where E_S is the elevation at the surface directly above the source location, D_S is the source depth, $E_{Slayer1}$ is the elevation at the base of layer directly below the source location, E_D is the elevation of the datum, and $V_{\text{Replacement}}$ is the replacement velocity. Subtraction of this static value from travel times would effectively move the source (point S) to the datum (point S'; Figure 2.2). The static at the receiver location can be calculated in the same way (without the D_S term), and the total trace static would be the sum of the source and receiver statics. This decomposition of the total refraction statics could as well be naturally extended to a multi-layer case.

From the foregoing, we could summarize that the application of refracted arrivals to imaging near surface heterogeneities and to estimate statics correction is and would remain a subject of many research investigations. A new integrated (hybrid) approach to near-surface imaging is implemented for the present study that incorporates the fusion of both refracted arrival inversion and uphole survey measurements. This approach would yield a more robust and reliable near surface model which would in turn make the refraction statics solution to be derived and applied to the seismic datasets more ideal. From this literature survey, a complete refraction statics solution for processing onshore seismic datasets within the Niger Delta Basin has not been derived with its efficiency demonstrated on shot gathers, stacked or migrated sections. This is now the focus of the present dissertation as the complete refraction statics solution to be derived and applied would be the first documented for 3D seismic reflection data acquired within the onshore Niger Delta Basin, Nigeria using the proposed near-surface modeling approach.

2.2 Introduction to the Seismic Methods

Seismic waves are elastic waves generated by sudden release of energy in the ground or in the water. These seismic waves are further classified as;

1) Body waves, which are of two types;

a) Compressional (P) waves and

b) Shear (S) waves.

2) Surface waves, which are of two types;

a) Love waves and

b) Rayleigh waves.

Surface waves travel along the surface of the earth and are responsible for losses and damages during earthquakes whereas Body waves as the name suggest are the waves that traverse through the subsurface and are critical for imaging the earth subsurface (Pritchett, 1990).

These waves are classified based on their particle motion. Particle motions of P-waves are in the direction of wave propagation whereas the particle motions of S-waves are perpendicular to the direction of wave propagation. It is pertinent to note that P-waves travel faster than S-waves. The particle motion of surface waves is more complex. At the surface, the particle motion in a Rayleigh wave is elliptical and retrograde to the direction of wave propagation and in Love waves; particle motion is horizontal with no vertical motion. A more detailed discussion of these waves and the different terminologies associated with exploration seismology could be found in Sheriff (2002).

P-wave seismology is mainly used in exploration work. P-waves are the only modes that are employed to provide information about the subsurface in the current study. With the advancement of seismic instruments and energy sources S-wave seismology is also increasingly used in exploration work. P-wave exploration seismic methods further fall into two broad categories of;

i) Reflection seismology; and

ii) Refraction seismology.

The former essentially relies on the detection of echoes from the contacts between differing types of rock in the earth with the final goal of imaging the subsurface structure (Evans, 1997). Making a reflection profile image requires that a series of corrections be applied to the data in order to increase the signal to noise ratio. The latter, refraction method does not provide an image but does attempt to describe the geology in terms of the seismic wave speeds and thicknesses of layers. The basic input to this method is the travel times of the first arriving seismic waves from the source. Three P-waves are of interest in refraction seismology (Figure 2.3).

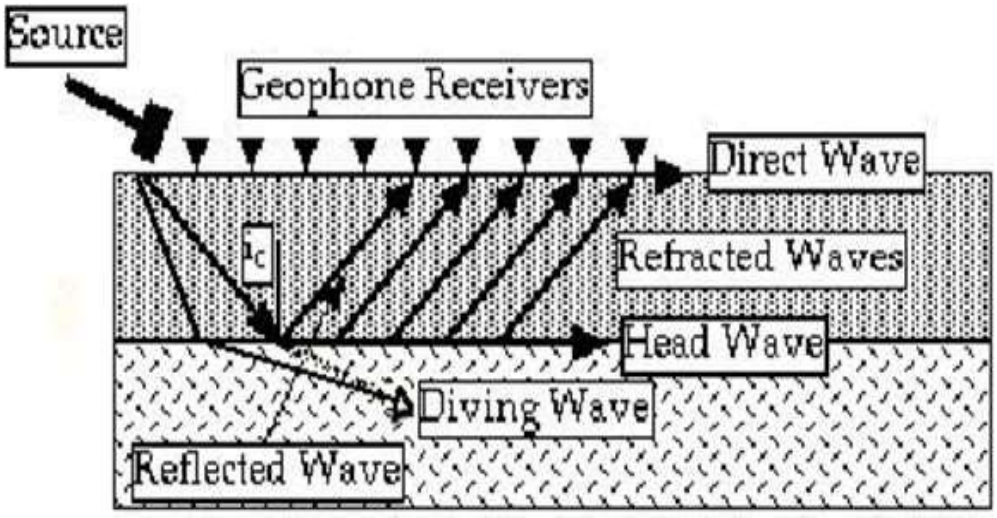

Figure 2.3: Sketch illustration showing the reflected, refracted, head, and direct waves (Source: Global Geophysics, UCL, 2009).

These three P-waves which are of interest in refraction seismology are;

1. Direct waves
2. Head waves
3. Refracted waves

The direct wave propagates along the upper surface layer (layer1) boundary. If the incident wave hits at the critical angle, the critically refracted head wave travels along the layer 1 - layer 2 interface. Refracted waves propagate from the interface as the head wave progresses, with exit angles equal to the critical angle. Seismic wave created by an explosive source emanate outward from the shot point in a 3D sense. Huygen's principle is commonly used to explain the response of the wave. Every point on an expanding wave front can be considered as the source point of a secondary wave front. The envelope of the secondary wave fronts produces the primary wave fronts after a small time increment. The trajectories of a point moving outward are known in optics as a ray, and hence in seismic exploration are referred to as a ray path.

Brief explanations of the characteristics of some key seismic events are presented below;

2.2.1 Reflections: The phenomenon in which the energy or wave from a seismic source has been returned from an interface having acoustic impedance contrast (reflector) or series of

contrasts within the earth are called reflection. This phenomenon is pictorially represented in Figure 2.4.

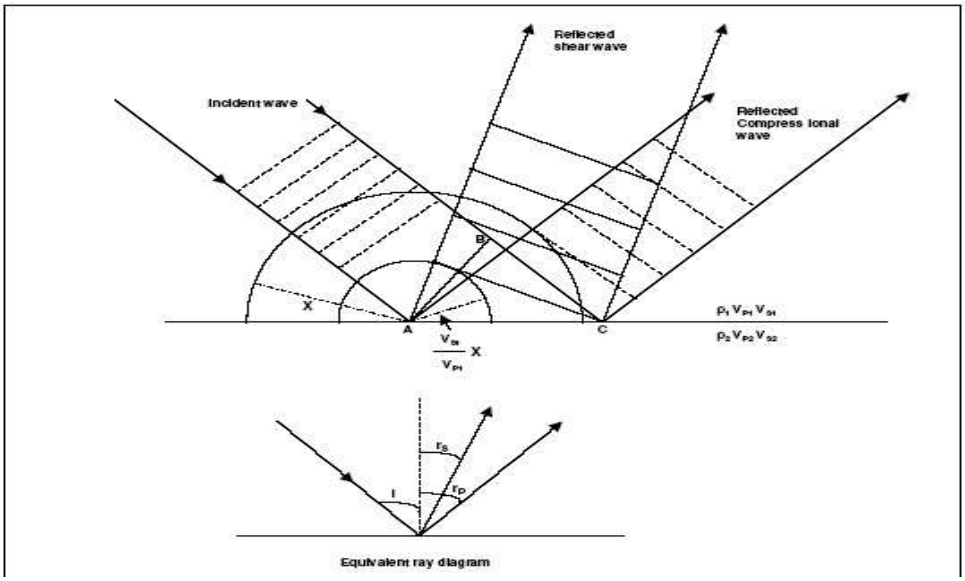

Figure 2.4: Reflection of a plane compressional wave at an interface (Kumar, 2005)

The amplitude and polarity of reflections depend on the acoustic properties of the material on both sides of the discontinuity. Acoustic impedance is the product of density and velocity. The relationship among incident amplitude A_i, reflected amplitude A_r, and reflection coefficient R_C, is given by the expression of Sheriff and Geldart, (1999):

$$A_r = R_C \times A_i \qquad (2.3)$$

where,

$$R_C = \frac{(\rho_2 V_2 - \rho_1 V_1)}{(\rho_2 V_2 + \rho_1 V_1)} \qquad (2.4)$$

Where velocity is constant, a density contrast will cause a reflection and vice versa. In other words, any abrupt change in acoustic impedance causes a reflection to occur. Energy not reflected is transmitted. With a large R_C, less transmission occurs and hence signal-to-noise ratio reduces below such an interface (Kumar, 2005).

2.2.2 Critical Reflection: When an impinging wave arrives at such an angle of incidence that energy travels horizontally along the interface at the velocity of the second medium, then critical reflection occurs. The incident angle i_C, at which critical reflection occurs can be found using Snell's Law.

$$\text{Sin } i_c = \left(\frac{V_1}{V_2}\right) \text{ Sin } 90° = \left(\frac{V_1}{V_2}\right) \qquad (2.5)$$

2.2.3 Refractions: The change in direction of a seismic ray upon passing into a medium with a different velocity is called refraction. Snell's law describes how waves refract. It states that the sine of the incident angle of a ray, (sin i), divided by the initial medium velocity V_1 equals the sine of the refracted angle of a ray (sin r), divided by the lower medium velocity V_2, that is:

$$\text{Sin } \left(\frac{i}{V_1}\right) = \text{Sin } \left(\frac{r}{V_2}\right) \qquad (2.6)$$

When a wave encounters an abrupt change in elastic properties, part of the energy is reflected, and part is transmitted or refracted (Figure 2.5) with a change in the direction of propagation occurring at the interface.

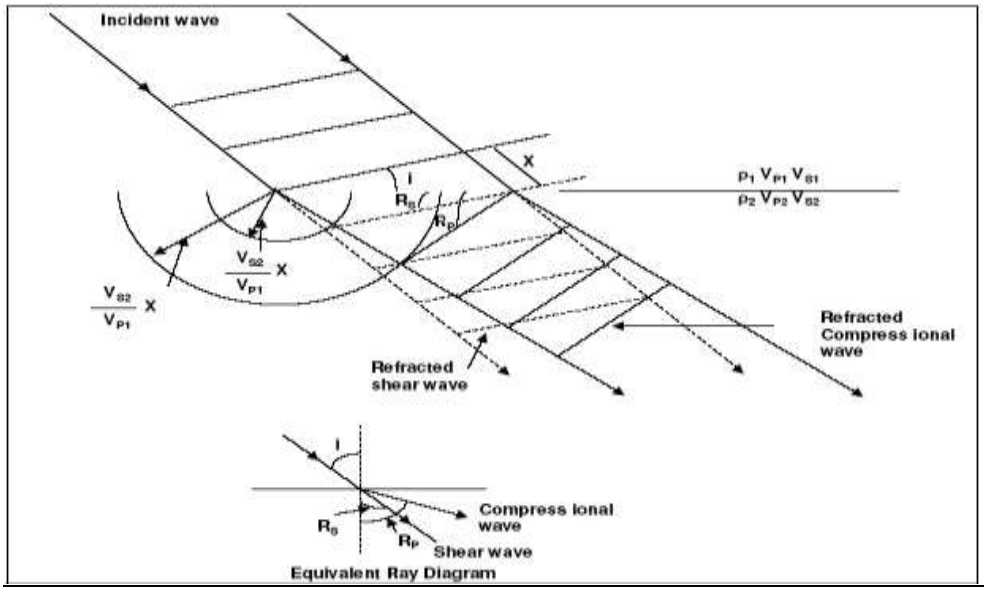

Figure 2.5: Refraction of plane compressional wave across interface (Kumar, 2005)

2.2.4 Diffractions: Diffractions (Figure 2.6) occur at sharp discontinuities, such as at the edge of a bed, fault, or geologic pillow. When the wave front arrives at the edge, a portion of the energy travels through into the higher velocity region, but much of it is reflected. The reflected wave front arrives at the receivers and gets aligned along the trajectory of a parabola on the seismic record.

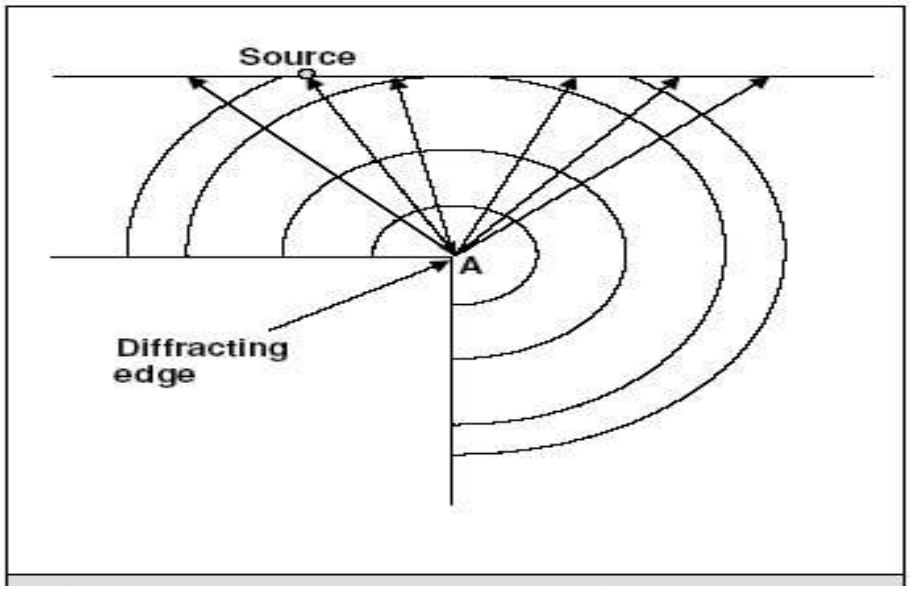

Figure 2.6: Diffraction from the edge. The source of a diffracted radiation has been set into oscillation by waves generated on the surface. Radial lines with arrows are ray paths; circular arcs are wave fronts (Dobrin and Savit, 1988).

In conventional in-line recording, diffractions may arrive from out of the plane of the seismic line/profile. Such diffractions are considered as noise and reduce the signal-to-noise ratio. However, in 3D recording, in which specialized data processing techniques are used (i.e., the 3D seismic migration), the diffractions are considered as useful scattered energy because the data-processing routines transfer the diffracted energy back to the point from which is generated, thereby enhancing the subsurface image. Hence in 3D surveys, out-of-the plane diffractions events are considered part of the signal (Yilmaz, 1987).

2.2.5 Multiples: Seismic energies that have been reflected more than once are called multiples. Virtually all seismic energy contains some forms of multiples. They could be grouped into long-path and short-path multiples. The important distinction between long-path and short-path multiples is that a long-path multiple arrives as a distinct event whereas a short-path multiple arrives soon after the primary and changes the wave shape.

2.2.6 Seismic Noise: The reliability of seismic mapping is strongly dependent on the quality of the records/data. The term "signal" is often used to denote any event on the seismic record from which we wish to obtain information from whereas everything else is termed "noise", including coherent events that interfere with the observation and measurement of signals (Gadallah and Fisher, 2005). The signal-to-noise ratio (SNR) is the ratio of the signal energy in a specified portion of the record to the total noise energy in the same portion. Poor records result whenever the signal-to-noise ratio is small. Seismic noise may be either

a) Coherent or

b) Incoherent

Coherent noise includes surface waves, reflections or reflected refractions from near-surface structures such as fault planes or buried stream channels, refractions carried by high-velocity stringers, noise caused by vehicular traffic or farm tractors, multiples and so forth. All the preceding except multiples travel essentially horizontally and all except vehicular noise are repeatable on successive shots (Sadi, 1980). Coherent noise is sometimes subdivided into:

i) Energy that travels essentially horizontally and

ii) Energy that reaches the spread more or less vertically

Incoherent noise on the other hand is often referred to as random noise (spatially random), which implies not only non-predictability but also, that they possess certain statistical properties.

Incoherent noise is due to scattering from near-surface irregularities and inhomogeneity such as boulders and small-scale faulting. Non repeatable random noise may be due to wind shaking a geophone or causing the roots of trees to move, which generates seismic waves, stones ejected by the shot and falling back on the earth near a geophone, ocean waves beating on a seashore, distant earthquakes, a person walking near a geophone, and so on (Kearey and Brooks, 1991).

2.3 Overview of 2D/3D Reflection Seismic Data Acquisition

In seismic reflection, different seismic acquisition geometries can be adapted but the basic concept remains the same for all. Essentially, in 2D active source seismology, the acquisition geometry consists of a line of receivers (Figure 2.7) along which the seismic source is activated. The receivers will in most cases, at least for land surveys, be geophones which provide a voltage proportional to the amplitude of the particle velocity of the ground motion as the wave passes (Knodel *et al.*, 2007). 3D reflection techniques in which a 3D volume (x,y,z) of crust is sampled and monitored using a planar, rather than a linear array of shots and receivers. In practice, this is accomplished by laying out thousands of geophones along parallel lines of receiver groups and then shooting into the entire array (receivers) from each shot point along a series of orthogonal shot lines (Sheriff and Geldart, 1999).

On land, 3D data are normally collected using the crossed spread array and therefore samples a volume of the subsurface rather than an area contained in a vertical plane. The positions of all the shots (source) and detectors (geophones) must be accurately surveyed so that eventually corrections are made for elevation and weathering variations (Cox, 1999). Although complicated by the fact that a typical 3D survey (Figure 2.7) contains orders of magnitude (enormous data) to be processed, the actual processing steps are fairly similar to those for 2D surveys. The end result, however, is a data cube that can be sliced to produce synthetic 2D profiles in any arbitrary direction through the data, horizontal slices at arbitrary depths (time slices), horizon slices showing

reflectivity variations in map-plan for picked marker horizons, and 3D tomographic images that can be viewed from any perspective. In the parlance of such exploration, the 'offset' refers to the distance of a given receiver from the seismic source along the surface of the earth. In seismic reflection, seismic energy is reflected back to the surface from underlying layer of higher density and velocity. Whereas in seismic refraction the wave is refracted back to the surface and recorded (Stone, 1995).

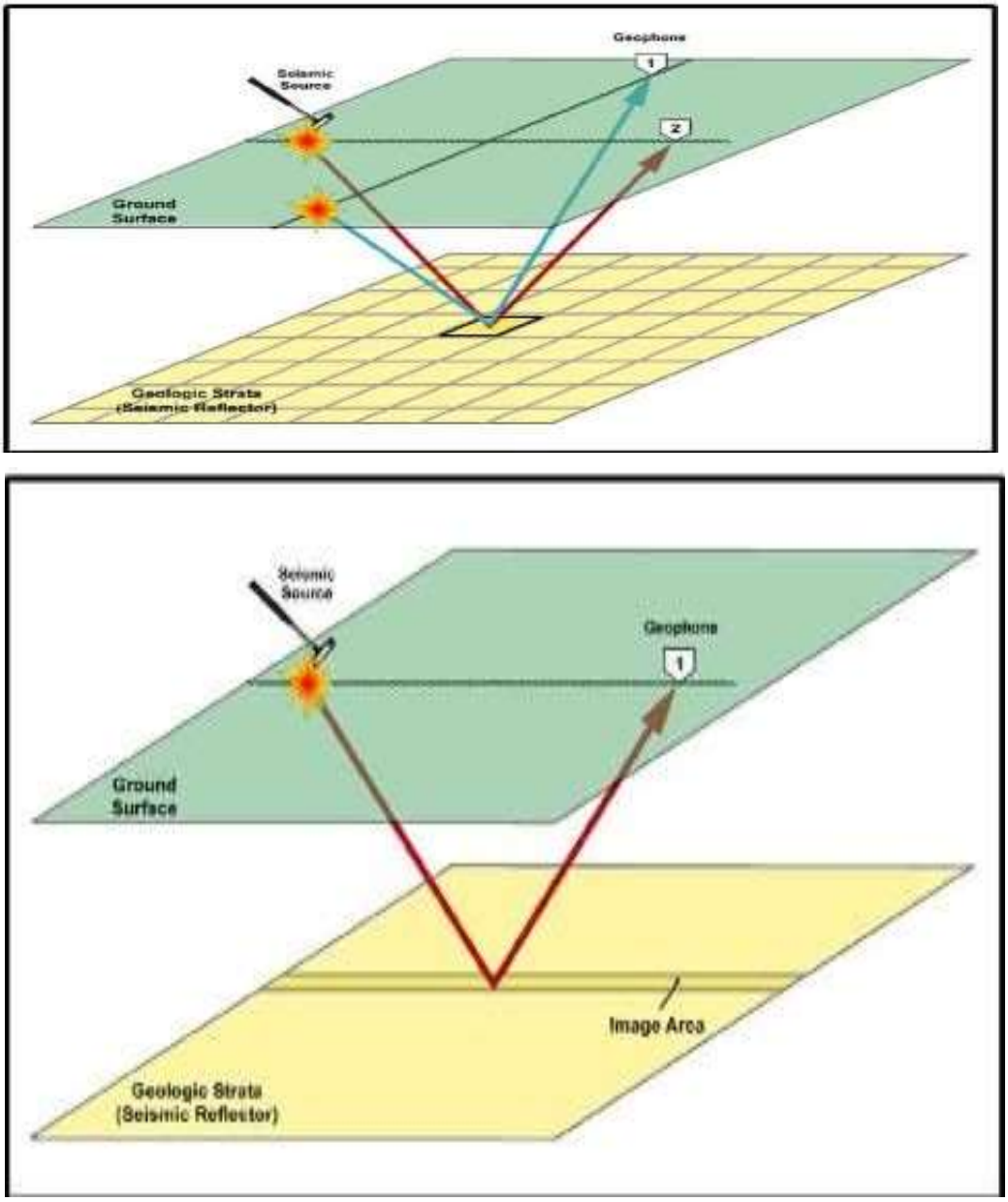

Figure 2.7: Schematic diagram of a 3D (top) and 2D (bottom) survey.

For a typical seismic reflection acquisition, refractions are also unavoidably recorded (Figure 2.8).

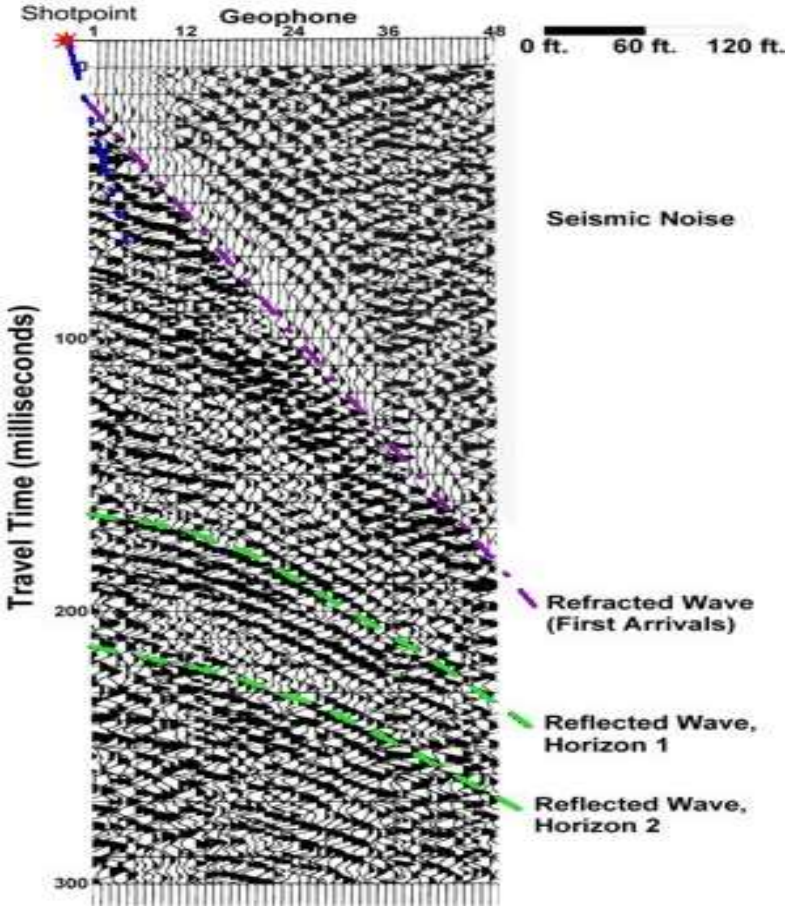

Figure 2.8: A refracted wave as it appears on a raw seismic shot record (Enviroscan, 2009).

Hence, the refraction analysis essentially comes for free in the acquisition of high resolution seismic profiling, although their utility can be diminished by the use of geophone groups which average the response sometimes over many tens of meters. Energy sources for generating seismic waves are of different types and most commonly used land energy sources are dynamite and seismic vibrators. The former gives a sharp and high energy pulse but for a variety of reasons including cost, environmental impact, and safety it is often avoided. The dataset for the present study was acquired from a 3-D seismic reflection survey using dynamite sources. As seismic waves travel from the source to the

receiver their travel time is recorded. The distance between the source and the receiver is known and this travel time is used to calculate velocity of the subsurface material. The seismic velocity is an important physical property that can reveal a great deal about the compressibility of the rock and its fluid content (Figure 2.9).

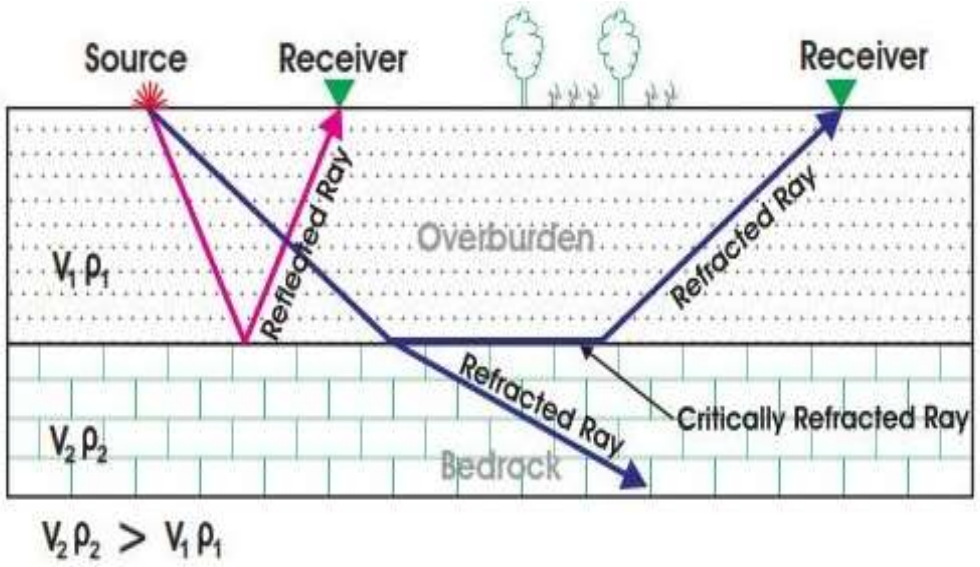

Figure 2.9: Sketch showing seismic reflected and refracted wave with simple two layer case. Velocity (V_1) and density (ρ) of first layer (Overburden) is lower than the velocity (V_2) and density (ρ_2) of second layer (Bedrock) (Ahmad, 2006)

The seismic reflection method is mainly used to produce images of the subsurface structure. Seismic refraction analysis, are used to obtain the subsurface velocity information. Together, these methods provide meaningful complementary information and are useful for geological interpretation (Sjogren *et al.*, 1979 and El-Behairy *et al.*, 1997).

2.4 Overview of 2D/3D Seismic Data Processing

The seismic exploration method has greatly improved over time in both the areas of data acquisition and processing. Digital recording along with the CMP multifold coverage was introduced during the early 60's. Data acquired from the field are usually prepared for processing by the field party or acquisition team themselves and then sent to the data

processing centre. Processing is required because the data collected from the field is not a true representation of the subsurface and hence nothing of importance can be inferred from it. With the advent of high end computing systems modern day processing has become a lot easier than it really used to be. Turnaround times have therefore come down with lot of processing taking place in-field or onboard (Beckett *et al*., 1995).

Field records which are obtained after 2D/3D seismic data acquisition is usually a superposition or combination of the following;

2.4.1) Reflections,
2.4.2) Coherent noise, and
2.4.3) Random ambient noise.

2.4.1 Reflections: Reflections are recognized by their hyperbolic travel times. If the reflection interface is horizontally flat, the reflection hyperbola is symmetric with respect to zero offset. On the other hand if it is dipping interface, then the reflection hyperbola is skewed in the up dip direction.

2.4.2 Coherent noise: Coherent noise could further be subdivided into several categories.

i) Ground roll is recognized by its low frequency, strong amplitude and low group velocity. It is the vertical component of dispersive surface waves i.e. Raleigh waves. Typically we try to eliminate ground roll in the field itself by array forming of receivers.

ii) Guided waves are persistent, especially in shallow marine records in areas with hard water bottom. Guided waves also are found in the land records. These waves are largely attenuated by CMP stacking (Yilmaz, 1987). Because of their prominently linear move-out, in principle they also can be suppressed by dip filtering techniques. One such filtering technique is based on 2D Fourier transformation of the shot record.

iii) Side scattered noise commonly occurs at the water bottom, where there is no flat, smooth

topography.

iv) Cable noise is another form of coherent noise which is linear and low in amplitude and frequency. It appears on shot records as late arrivals.

v) Another form of coherent noise is the air wave which has a velocity of 300 m/s. It can be a serious problem when shooting with surface charges. Notch muting is the only way of removing them. Power lines also give rise to noisy traces in the form of a mono frequency wave of about (50 or 60 Hz).

vi) Multiples are another type of coherent noise. They are secondary reflections having inter- or intra- bed ray paths. They propagate both in sub and super- critical regions.

vii) Power lines also cause noisy traces in the form of a mono-frequency wave. A mono-frequency way may be 50 or 60 Hz, depending on where the field survey was conducted. Notch filters are often used in the field to suppress such energy.

2.4.3 Random noise: Random noise could result from various sources during seismic acquisition, such as poor planting of geophones, wind effects, transient movements in and around the vicinity where a survey is being carried out, wave motion in the water (for marine surveys) and possibly from faulty recording instruments – what is termed electrical noise.

One important and very crucial aspect of seismic data processing is to uncover genuine reflections by suppressing all unwanted energies (noise of various types) so that meaningful interpretations can be made. The objective of seismic data processing is therefore to convert the information recorded in the field to a form that can be used for geological interpretation. Through processing we are enhancing the signal to noise ratio, removing the seismic impulse from the trace (inverse filtering) and repositioning the reflectors to its true location (NMO,

DMO and migration), thereby making it a true representation of the actual subsurface structure (Yilmaz, 2001).

Seismic data processing is composed of basically five types of corrections and adjustments:

a) Time,
b) Amplitude,
c) Frequency-phase content,
d) Data compressing (stacking), and
e) Data positioning (migration)

These adjustments increase the signal-to-noise ratio, correct the data for various physical processes that obscure the desired (geologic) information of the seismic data, and reduce the volume of data that the geophysicist must analyze. The geologic information desired from seismic data is the shape and relative position of the geologic features of interest.

a) Time adjustments: Time adjustments fall into two categories:

i) Static and
ii) Dynamic

Static time corrections are a function of both time and offset and convert the times of the reflections into coincidence with those that would have been recorded at zero offset, that is, to what would have been recorded if source and receiver were located at the same point (Cox, 1999).

b) Amplitude adjustments: Amplitude adjustments correct the amplitude decay with time due to spherical divergence and energy dissipation in the earth. There are two broad types of amplitude gain programs:

i) Structural amplitude gaining or automatic gain control (AGC), and
ii) Relative true amplitude gain correction

The first scales amplitudes to a nearly alike amplitude and is generally chosen for structural mapping purposes. The second attempts to keep the relative amplitude information so that the amplitude anomalies associated with facies changes, porosity variations, and gaseous hydrocarbons are preserved.

c) Frequency-phase content: The frequency-phase content of the data is manipulated to enhance signal and attenuate noise. Appropriate band-pass filters (one-channel filtering) can be selected by reference to frequency scans of the data which aid in determining the frequency content of the signals. De-convolution is the inverse filtering technique used to compress an oscillatory (long) source waveform, often seen in marine data, into as near a spike (unit-impulse function) as possible. Ghosts, seafloor multiples, and near-surface reverberations can often be attenuated through de-convolution approaches. Many de-convolution techniques use the autocorrelation of the trace to design an inverse operator that removes undesirable, predictable energy.

d) Data compressing (Stacking): The data compression technique generally used is the common midpoint (CMP) stack. It sums all offsets of a CMP gather into one trace. 48-fold to 96-fold stacks are commonly used today. Conventional 2D seismic data initially exist in a 3D space: the three axes are time, offset and a coordinate x along the line of survey. 3D data consist initially of a 4D data set; the coordinates being time, offset and two horizontal spatial coordinates, x and y, which lies on the midpoint axis.

e) Data Positioning (Migration): The data positioning adjustment is also known as migration. Migration basically seeks to move energy from its CMP position to its proper spatial location. In the presence of dip, the CMP location is not the true subsurface location of the reflection. Migration collapses diffractions to foci, increases the visual spatial resolution,

and corrects amplitudes for geometric focusing effects and spatial smearing. Migration techniques have been developed for application to pre-stack datasets, post-stack datasets, or a combination of both (Yilmaz, 2001).

The overall objectives for seismic data processing could therefore be summarized as;

i) To enhance the signal to noise ratio (S/N).

ii) To produce seismic cross section representative of geology.

iii) To meet the exploration objectives of the client.

2.5 Overview of Routine 2D/3D Seismic Data Processing Sequences

Since the introduction of digital recording, a routine sequence in seismic data processing has evolved. There are three primary steps in processing seismic data

i) De-convolution,

ii) Stacking, and

iii) Migration,

Figure 2.10 is a schematic showing the dimension and order of application of these processing sequences. The block represents the seismic data volume in processing coordinates – midpoint, offset and time.

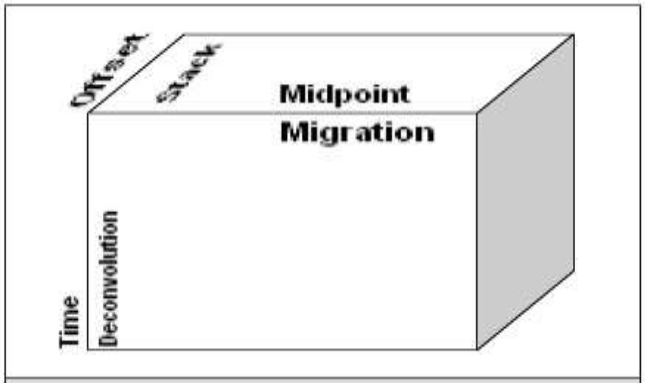

Figure 2.10: Seismic data volume represented in processing coordinates – midpoint – offset – time. Deconvolution acts on the data along the time axis and increases temporal resolution. Stacking compresses the data volume in the offset direction and yields the plane of stacked section (the frontal face of the block). Migration then moves the dipping events to their true subsurface positions and collapses all diffractions, and thus increases lateral resolution (Kumar, 2005).

All other processing techniques may be considered secondary in that they help improve the effectiveness of the primary processes. The secondary processing steps include corrections (statics, geometric, NMO, DMO, velocity analysis, filtering etc.). Many of the secondary processes are designed to make data compatible with the assumptions of the three primary processes. Deconvolution assumes a stationary, vertically incident, minimum-phase, source wavelet and white reflectivity series that is free of noise. Stacking assumes hyperbolic move-out while migration is based on a zero-offset (primaries only) wave field assumption. Conventional processing of reflection seismic data yields an earth image represented by a seismic section usually displayed in time. A conventional processing flow (Yilmaz, 2001) is presented below highlighting relevant procedures that are carried out in the cause of seismic data processing.

1. Pre-Processing
   a. Demultiplexing
   b. Reformatting
   c. Resampling
   c. Editing
   d. Geometry Merging (Labeling)
   e. Static Corrections
   f. True Amplitude Recovery
      i. Spherical Divergence Correction
      ii. Absorption/Attenuation Correction
   g. Muting
2. Time Invariant Filtering
3. CMP Sorting
4. Deconvolution
5. Velocity Analysis
6. Residual Static Corrections
7. Velocity Analysis
8. NMO Corrections

9. DMO Correction
10. Inverse NMO Correction
11. Velocity Analysis
12. NMO Correction, Muting and Stacking
13. Deconvolution
14. Time Variant Spectral Whitening
15. Time Variant Filtering
16. Migration
17. Gain Application

2.6 Statics Correction

Statics correction which most often is shortened to as statics generally refers to "corrections applied to seismic data to compensate for the effects of variations in elevation, weathering thickness, weathering velocity, or reference to a datum" (Sheriff, 1991). Statics are time shifts applied to seismic data to compensate for:

i) Variations in elevations on land,
ii) Variations in source and receiver depths (marine gun/cable, land source),
iii) Tidal effects (in marine and transitional zones seismic data acquisition and processing),
iv) Variations in velocity/thickness of near surface layers,
v) Change in data reference times.

The objective is to determine the reflection arrival times which would have been observed if all measurements had been made on a (usually) flat plane with no weathering or low-velocity material present. These corrections are based on uphole data, refraction first-breaks, and/or event shooting. Uphole-based statics involve the direct measurement of vertical travel-times from a buried source. This is usually the best statics correction method where feasible. First-break based statics are the most common method of making field (or first estimate) statics corrections (Hatherly *et al*., 1994). The approach adopted for the present study was an

integrated approach of iteratively fusing both methods, that is, refraction arrival inversion with uphole measurements to build a better, robust and more reliable refraction statics solution for data acquired from OML-23, SOKU that is currently being processed.

The term 'statics' is used to denote constant time shift of whole data traces, as opposed to variable time shifts as applied by NMO corrections which are dynamic (Hampson and Russell, 1984). The elevation needed for shot/receiver time correction is obtained from labeling records. The velocity needed for calculating the time shift is obtained from shot uphole times. The elevation corrections (also called datum correction) may be used to bring all times in a seismic record to a fixed level in the subsurface which now becomes the final processing datum (FPD). The FPD could be any arbitrary level (depending on the client requirement or the choice of the processor) or mean sea level. Statics corrections in a nutshell is simply a time shift given to the traces in order to compensate for effects of the lateral variations in elevation, weathering layer thickness, and velocity; Sheriff' (2002) Encyclopedic Dictionary of Exploration Geophysics. During seismic wave propagation from the seismic source to the receivers the waves must pass through low velocity near surface materials. Seismic waves travel slower in the low velocity material and their travel times are increased. Because the velocities of the near surface materials can be substantially lower than the underlying bedrock, the time of a reflection from depth will also vary due to these lateral variations in travel times. Correct statics correction is a key factor in shallow seismic data processing. If not properly tackled, static shifts are capable of completely disrupting the coherence of reflections during common midpoint stacking. Spurious reflection patterns and loss of depth resolution can also arise from incorrect or inaccurate statics (Cox, 1999).

Within the general irregular time shifts related to the weathered zone, several types of statics are differentiated (Telford *et al.*, 1976). The statics due to the differences in surface elevations which affect both sources and receivers, called elevation statics. By their relation to the source or receiver position, statics are also subdivided to source and receiver statics, and the "total" statics of a seismic trace is the sum of all three statics at the corresponding source and at receiver locations. Finally, statics are called "surface consistent" if they are only related to the surface locations of the source and receivers and not to their individual properties. All of the statics above can be incorporated in the concept of "refraction statics" (Yilmaz, 2001). Refraction statics calculations are based on the use of refracted head waves to model the first-arrival travel times. Several refraction-statics methods are in use, such as the Plus-Minus method, Generalized Reciprocal method, and the Generalized Linear Inverse method. These methods take the first-arrival times as input and use different kinds of travel-time modeling to derive estimates of the depths and/or subsurface velocities (Russell, 1990). Data-smoothing statics methods assume that patterns of irregularity that most events have in common result from near-surface variations and hence statics correction trace shifts should be such as to minimize such irregularities. Most automatic statics determination programs employ statistical methods to achieve the minimization.

One way to think about these shifts is if one were to essentially strip off the top parts of the earth making the surface of the earth now on bedrock and with no topography. This 'new' surface of the earth is called the datum elevation to which all of the seismic traces are corrected. Then statics correction is applied and data is shifted to that reference datum. Figure 2.11 schematically shows the statics correction procedure. After calculating weathering layer

thickness and velocity, statics correction i.e., time shifts to source and receiver, is calculated. Statics correction is applied by moving 'source' to the datum (source) as well as receiver to the datum (receiver).

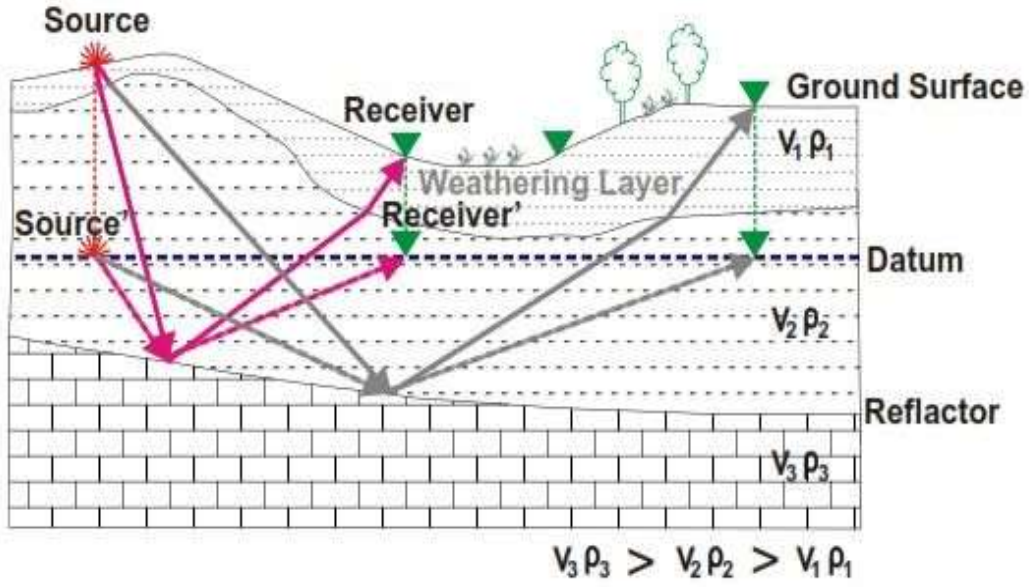

Figure 2.11: Sketch showing statics correction procedure. Statics correction is applied by moving 'source' to the datum (source) as well as receiver to the datum (receiver). (Ahmad, 2006)

The major focus for the present study is to derive a comprehensive and complete statics solution which would consist of field or datum statics, refraction statics and residual (1st and 2nd) statics for addressing the already identified statics problem of OML-23 SOKU. The impact of the derived and implemented or applied statics would subsequently be determined on several shot gathers from the field in Field File Identification (FFID) configuration and on stacked and migrated sections of the dataset from the prospect.

An attempt is made in this section to describe the underlying principles and give background theories of the approaches we intend using in obtaining the complete set of statics solutions to be derived and implemented for the SOKU seismic datasets to tackle its statics problem.

2.6.1 Field Statics

The concept of field statics which is also referred to as datum statics or at times – elevation statics involves the computation and removal of the effect of different source and receiver elevations by introducing a new horizontal plane (reference datum) below the low velocity layer, in order to place or simulate all sources and receivers on this reference plane (Figure 2.12) which is usually in most cases below the elevation of the lowest source or receiver.

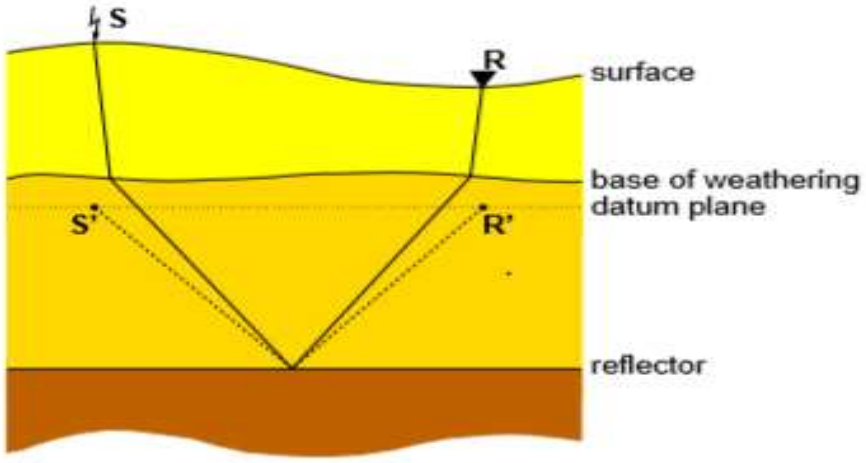

Figure 2.12: Schematic of a pseudo - source and receiver location (S' and R') on a reference datum from the actual source (S) and receiver (R) positions on the earth's surface in the build up to field statics.

A replacement velocity ($\boldsymbol{V_r}$) for the materials between the datum and the source or receiver is needed. This parameter is either assumed from prior knowledge of replacement velocity within an area or by its estimation using either uphole times or direct arrival information.

The field (datum or elevation) statics $\boldsymbol{t_D}$ is given by the expression;

$$t_D = \frac{[(E_S - Z_S - E_D) + (E_R - Z_R - E_D)]}{V_r} \qquad (2.7)$$

For the scenario depicted or described by Figure 2.13

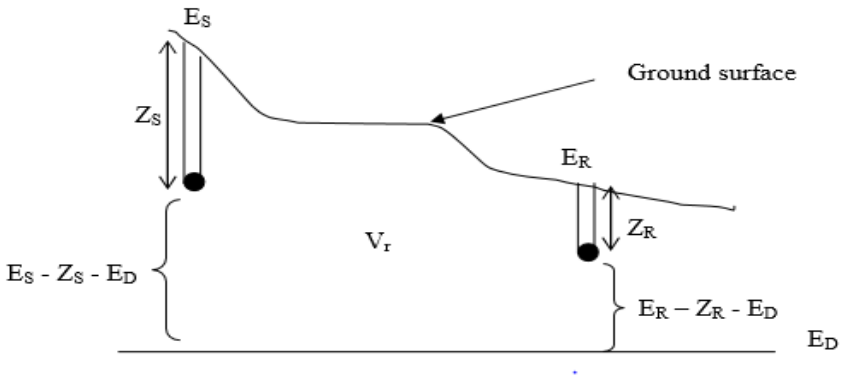

Figure 2.13: Schematic illustration of the procedure for the computation of field statics.

Where;

E_S: Ground elevation at the shot location

Z_S: Depth of shot

E_R: Ground elevation at receiver location

Z_R: Depth of receiver

E_D: Datum elevation

V_r: Replacement velocity

When $\boldsymbol{t_D}$ is computed, it is then subtracted from the two –way travel time of the trace belonging to that particular source – receiver pair for the implementation of the field statics. The procedure described above, gives a basic view of what field statics entails. However, it is insightful to state that the procedure could in some instances be some-what more complex than as described above. Field statics have been successfully implemented to seismic datasets (Huang *et al*., 2008; Li *et al*., 2009; Luo *et al*., 2010 and Ponnam *et al*., 2013).

2.6.2 Refraction Statics

Static anomalies whose spatial wave-lengths are longer than a spread-length are not uncommon and if not corrected could produce false structures in seismic sections (Marsden, 1993). Applying refraction statics are an effective means for correcting for these long spatial

wavelength anomalies and they could also correct for shorter spatial wavelength anomalies (Liu, 1998). The wavelength of statics being describe here refers to the width of the lateral (velocity or thickness) change in the weathering layer relative to the spread length (maximum offset). Refraction statics is also a means by which the seismic data is compensated for the effect of the low velocity layer (or weathering layer) (Zhu *et al*., 2014).

For the later objective to be achieved, a model of the weathering layer characteristics (thickness and velocity) must be estimated before refraction statics calculation can be performed. A couple of methods have evolved for the computation of refraction statics, ranging from the pioneering approaches of the Plus Minus method (Hagedoorn, 1959) to the Slope/Intercept method (Knox, 1967), both based on the delay – time approximation of refracted travel times to solve for the statics (Yilmaz, 2001). More recent approaches includes the Generalized Reciprocal methods (Palmer, 1981), the Generalized Linear Inversion – GLI (Hampson and Russell, 1984), the Delay Time method which has now been fully developed by Lawton (1989, 1990) based on Gardner's idea. The Delay Time approach has successfully been adapted in recent times to perform refraction statics (Baker, 1999; Butler, 2005; Duan, 2006; Bridle and Aramco, 2009 and Opara *et al.*, 2018). This approach was adopted in the build up to the refraction statics component of the overall statics solution being sought for the currently investigated prospect.

2.6.3 Residual Statics (1st and 2nd)

The derivation and application of field statics (also called datum or elevation statics) and the subsequent application of refraction statics does not completely resolve statics anomalies from seismic data (Marsden, 1993; Jing, 2003 and Yin *et al.*, 2014). These remnant or residual static anomalies are due to discrepancies in the low velocity layer. No matter how well the approaches deployed to derive velocity and thicknesses of the near-surface may be, it is still very key to state

that such models in actual sense is some-what a simplification of the actual geology because the earth structure is complex and is nearly impossible to model accurately. The discrepancies between the derived model and the actual earth model results in errors in the statics correction estimation. The residual statics anomalies are tackled by the implementation of residual statics (1^{st} and 2^{nd}) corrections. The residual statics corrections are time shifts applied to traces in order to compensate for time delays and the statics model as a function of time and space (Sheriff, 1991; Li *et al.*, 2011 and Henley, 2012).

The residual statics corrections are actually a subset of the statics correction (Cox, 1999). A combination of field statics, refraction statics and residual statics corrections forms ideally a comprehensive and complete statics solution to adequately address the statics problem of seismic field dataset. Residual statics programs are anchored on either linear-surface consistent methods or non-linear surface consistent methods (Russell, 1990). The former method is more widely in use and was the approach used in the study. This approach assumes that the static shifts are time delays that only depend on the source and receiver locations on the surface, not on ray paths in the subsurface. This assumption is valid only if all ray paths, regardless of source-receiver offset, are vertical in the near surface. The surface-consistent assumption is generally good because the weathered layer usually has a low velocity and refraction towards the normal at its base tends to make ray paths vertical.

The total residual time shift, t_{ijk}, could be expressed as:

$$t_{ijk} = r_i + s_j + G_k + M_k x_{ij}^2, \qquad (2.8)$$

where,

r_i: is the residual static time shift associated with the i^{th} receiver,

s_j: is the residual static time shift associated with the j^{th} source,

G_k: is the difference in two-way travel time at a reference CMP and the travel time at the k^{th} CMP, and

$M_k\ x_{ij}^2$: is the residual move out that accounts for the imperfect NMO correction.
G_k is a structural term, while M_k is a hyperbolic term.

The ultimate objective of the residual statics correction procedure is to determine the unknown variables (r_i, s_j, G_k, and M_k) from the known variables (t_{ijk} and x_{ij}). Usually, there are more equations than unknowns; hence, a least-squares approach to minimize the error energy is adopted;

$$E = \sum_{ijk} [(r_i + s_j + G_k + M_k\ x_{ij}^2) - t_{ijk}]^2 \qquad (2.9)$$

Residual statics correction in standard processing practice, involves three progressive phases as detailed in Figure 2.14:

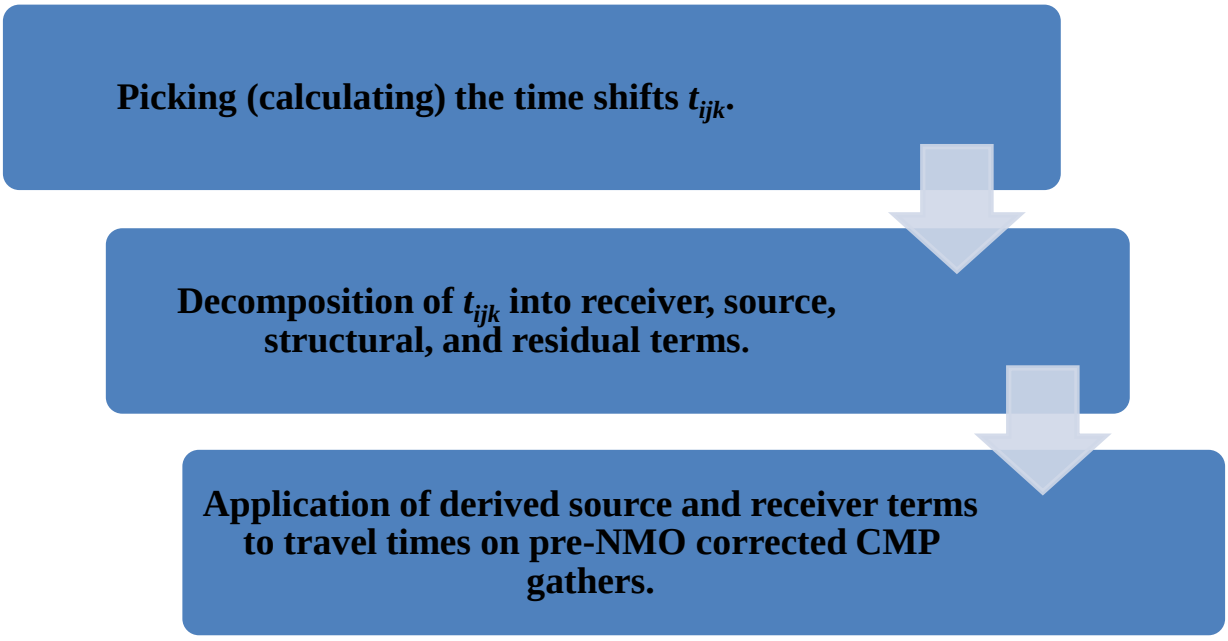

Figure 2.14: Processing sequences entailed in the implementation of the residual statics correction.

2.7 Weathering Layer

In many land data acquisition areas, the ground is covered with a relatively thin layer of low seismic velocity materials. Geophysicists call this layer the weathering layer. The seismic

weathering layer is a near-surface low velocity layer in which the portion of air filled pore space of rocks is usually more than of water filled (Cox, 1999). The 'geological' weathering layer is the result of rock decomposition. In general, the thickness of the seismic weathering layer is between a few centimeters and 50 meters or more, but the thickness of this layer can be extremely irregular. Also, the velocity can vary rapidly in the lateral and vertical direction. In most cases, the seismic weathering layer is thicker than the geological one. The base of the seismic weathering layer is defined as the depth where a change to a significant higher velocity occurs or where the velocity stabilizes. It coincides sometimes with the water table and/or with the base of the geological weathering layer. The term low velocity layer (LVL) is often used for the seismic weathering layer. The typical velocity for the weathering layer is between 500 m/s and 800 m/s compared to sub-weathering velocities of 1500 m/s and up.

These weathered layers are mostly related to aerated materials above the water table or to geologically recent unconsolidated sediments on a substratum of harder consolidated rocks. This seismic layer, despite the geophysicist's terminology, appears to have very little to do with the geologic weathered layer. However, variations in the physical properties of this upper layer can cause a dramatic deterioration in the quality of land seismic data if they are not acknowledged as a problem and appropriate measures or actions taken during data acquisition and processing to mitigate this effect. This degradation of the quality of land seismic data by these variations is illustrated in Figure 2.15 (a) and (b) (Wiggins *et al*., 1976 and Marsden, 1993).

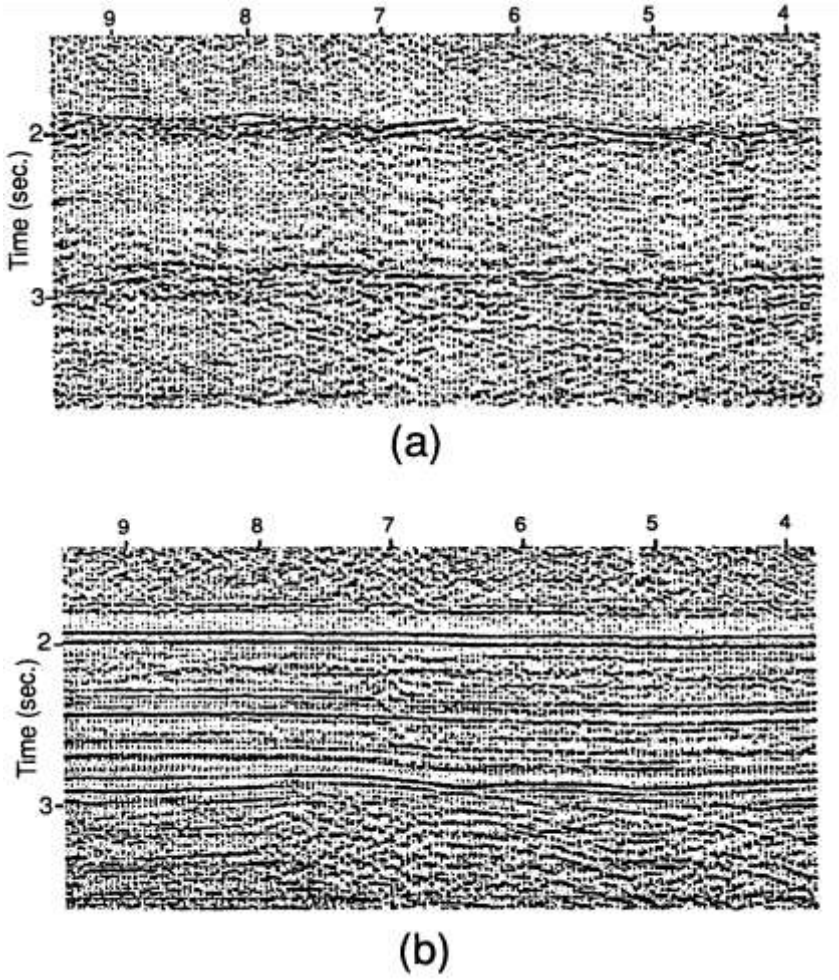

Figure 2.15 (a) Part of a seismic line processed without static corrections. (b) Same data processed with statics correction. It is observed that the resolution and continuity of events are improved in (b) than in (a) (Wiggins *et al.*, 1976 and Marsden, 1993).

Usually, the thickness of such a seismic weathering layer is determined by refraction seismic or Uphole-surveys. If an Uphole survey is used, the information is obtained only at discrete points along the seismic line. The weathered layer has the same effect as a low-pass filter, as it shows a high rate of energy absorption which mostly affects high frequencies. Due to its loose and highly variable structure, it may not just delay the seismic energy, but also scatter it. In most petroleum exploration surveys on land, where targets may lie at a couple of kilometers depth, the

uppermost few hundred meters are dealt with in statics while any deeper structures are regarded as velocity anomalies and treated during velocity analysis.

Problems caused by the near-surface low-velocity layer have been known for over half a century. Some of the earliest research papers in geophysical prospecting were concerned with attempts to determine their thickness and velocity, or compensate those early seismic records for the time delays caused by the low-velocity layer. In pre-digital days, field statics and refraction statics were thought to be the complete statics solution; then, in the wave of the success of residual statics programs (first developed in the 1970s), it was felt that statistical methods alone were the answer. However, the consensus today within the exploration industry is that each method has its own place in adding to the complete statics solution (Marsden, 1993). Despite the many technologies that deal with different aspects of the near surface, problems or issues related with these technologies still abound as of today. Two of the most difficult, and most often cited, problems are:

i) Need for more accurate near-surface velocity models

ii) Need for models of the near surface to allow adequate acquisition design

The need for higher resolution data is increasing remarkably in recent times and this makes it imperative for better statics corrections among other things. Statics corrections is perhaps the most important step in the processing of land data for their correct and successful implementation leads to improved quality in subsequent processing steps, which in turn, impacts positively on the overall integrity, quality, and resolution of the imaged section. Errors in the statics correction lead to a loss of seismic resolution, both temporal and spatial, and a less-than-optimum interpretation of the seismic dataset. Also, if statics corrections are not properly derived, then a myriad of problems could beset the interpreter, such as, lines with variable

datum, seismic events which mis-tie at intersections, false structural anomalies remaining in the data, false events being created out of noise, and eventually the data quality in most instances would not be optimized (Marsden, 1993).

Therefore, a good statics solution is desirable for two reasons: to obtain the correct structural interpretation and to obtain a high-resolution section which can be used for stratigraphic interpretation. It should be noted that either of these criteria can be met without satisfying the other by application of one or another of the different statics technologies that are available; however, it is most desirable to satisfy both criteria (Marsden, 1993a, 1993b and 1993c).

2.8 Near-surface Conditions and Near-surface Velocities

In many exploration terrains, the surface is covered with a relatively thin and uniform low-velocity layer, but frequently we know that this is not always the case. Some of the near-surface conditions which are frequently encountered are all illustrated in Figure 2.16. They include, but are not limited to, elevation changes, sand dunes and other eolian deposits, buried river channels, buried glacial scours, permafrost, evaporites, variable water table, leached zones, volcanics, peat deposits, and coal seams.

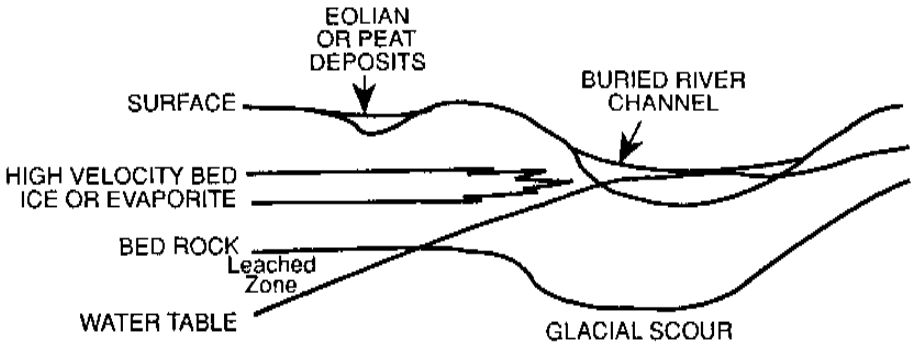

Figure 2.16: Some of the frequently encountered near-surface conditions, which if not adequately modeled, result in errors in the computed statics corrections and a degraded seismic image (Marsden, 1993).

The simplified near-surface earth model shown in Figure 2.17 (Marsden, 1993), illustrates the impact of the near-surface problem. The depth model has a variable overburden thickness due to elevation changes and other effects and its interval velocity is assumed constant. The attitude of the seismic reflections clearly does not represent the structural attitude of the reflectors in the depth model. Similar effects could be produced by holding the overburden thickness constant and varying its interval velocity. Where the overburden is thicker (or of lower interval velocity), a seismic wavelet takes longer to travel through the layer and conversely where it is thinner (or of higher interval velocity), a seismic wavelet requires less time to traverse the layer.

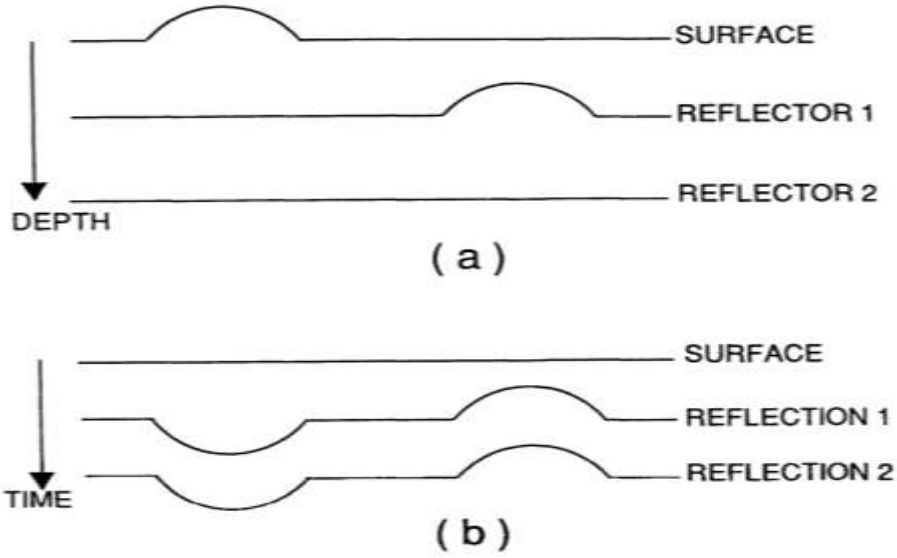

Figure 2.17: (a) A depth model. (b) The model's seismic time response, illustrating the fundamental issues of the statics problem. Changes in the elevation and thickness of the near-surface low-velocity layer produce time structures on reflections from flat reflectors. Lateral variations in the interval velocity of the near surface have similar effects (Marsden, 1993).

Seismic recording involves a source and receiver, usually many receivers, separated by some offset distance. The ray path for a single reflection on a seismic recording is shown in Figure 2.18.

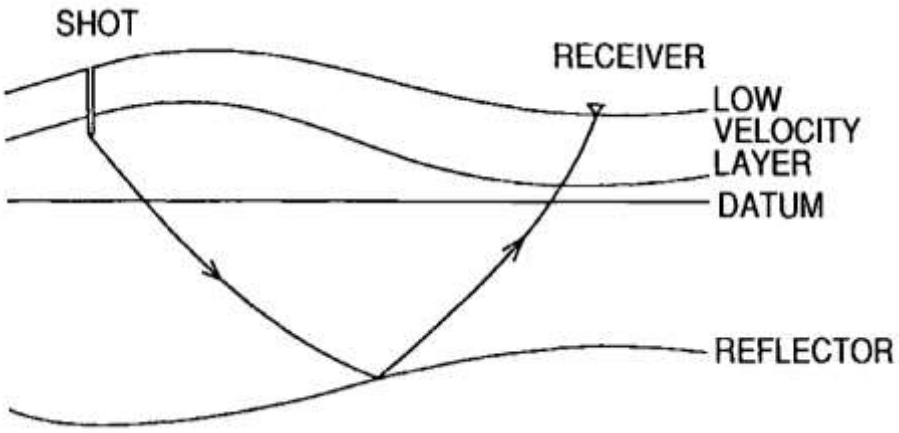

Figure 2.18: Near-surface model with a seismic ray path shown between source and receiver

From Figure 2.17 and Figure 2.18, it can easily be seen that the travel time of a wavelet along the ray path is influenced by the surface elevations of the geophone and shot point, by the velocity and thickness of the near-surface layers above the datum, by the depth and dip of the reflector itself, the distance separating the source and receiver, and lastly by the average velocity between the datum and the reflector. During processing, each of the above effects usually undergoes one or two corrections at a time, until the seismic data provide a quality image of the subsurface. With conventional multifold data, a number of traces are added together in such a way that the summing, or stacking, enhances primary reflections at the expense of noise or unwanted signal. Corrections applied to the seismic traces so that the data can be properly stacked are of two types, static and dynamic. Statics corrections involve a constant time shift to the data traces whereas dynamic corrections involve time variable shifts. Corrections made to each seismic trace for elevation effects (elevation statics) and near-surface low-velocity effects (weathering statics) by conceptually moving the shots (shot statics) and receivers (the receiver statics) to a common reference surface (the datum plane) are greatly simplified if it is assumed that energy travels vertically in the interval above the datum plane (Marsden, 1993).

Computation of datum statics correction requires a near-surface model that includes the thicknesses and velocities of the layers present. Near-surface velocities as well as those below the weathered layer are needed. The range of velocities this encompasses is large, from about 100 to 7000 m/s. The velocity of the weathered layer is generally less than the sub-weathered layers below it. Ricker, (1977), suggested an even lower velocity in the Low Velocity Layer, noting that it may drop to as low as 30m/s. Several researchers have published information on velocities of rocks, most of them, indicating a considerable range of velocities associated with the near surface and weathering layer. Press, (1986), produced a compilation (from many sources) of compressional and shear wave velocity ranges for common rocks. The velocity ranges are listed in Table 2.1 for several igneous, sedimentary, and metamorphic rocks.

Table 2.1: Seismic velocities in Igneous, Sedimentary, and Metamorphic rocks (Cox, 1999).

Material	**Velocity V_p (km/s)**	**Velocity V_S (km/s)**
Anhydrite	**4.1 – 5.0**	**2.67 – 2.99**
Basalt	**5.06 – 6.4**	**2.72 – 3.21**
Chalk	**2.1 – 4.2**	
Dolomite	**3.5 – 6.9**	
Gneiss	**3.5 – 7.5**	
Granite	**4.8 – 6.0**	**2.87 – 3.23**
Gypsum	**2.0 – 3.5**	
Limestone	**1.7 – 7.0**	
Marble	**3.75 – 6.94**	**2.02 – 3.86**
Salt	**4.4 – 6.5**	
Sandstone	**1.4 – 4.3**	
Sandstone–shale	**2.1 – 4.5**	
Shale and slate	**2.3 – 4.7**	

Velocity is a vector and not a scalar quantity, and therefore its direction should be strictly specified whenever a velocity value is given (Cordier, 1985). As with any physical parameter (velocity in this instance), anisotropy exists within the subsurface. Anisotropy in its most basic definition is simply when a value (like velocity) varies with the direction in which it is measured. Elevation statics correction are computed with a vertical velocity which, aside from in a few complex or highly folded areas, will be approximately perpendicular to the bedding planes. Under most geologic conditions, this is the velocity that is estimated by an Uphole survey. In contrast, the refraction statics method which is often used to obtain information about the near surface, estimates the velocity parallel to the bedding plane. The compressional velocity parallel to the bedding plane is typically 10–15% faster than the velocity perpendicular to it (Sheriff, 2002). In some circumstances, however, it is possible for the velocity perpendicular to the bedding plane to be greater than that parallel to it (Postma, 1955). Thus, if only the refraction velocity is available, a suitable factor must be applied to convert the value to an equivalent vertical velocity for any subsequent computations of datum statics correction. This ratio can be estimated from velocities computed from refraction and uphole surveys for specific formations within an area.

Seismic P- or S-waves propagate according to the wave equation, which is a partial differential equation. By integrating it we can predict the wave-field at any point and time from the initial solution, providing the medium is isotropic and homogeneous. The velocity with which P-waves (longitudinal) propagate through the ground, V_p, is associated with the density and elasticity of the rocks concerned as presented by Telford *et al.*, (1976).

$$\nu_p = \sqrt{\frac{\lambda+2\mu}{\rho}} \qquad (2.10)$$

Where $\mu(\rho)$ is known as the shear modulus and $\lambda(\rho)$ is the elastic modulus.

2.9 Uphole Surveys

The uphole survey is a viable means of determining the thickness of the near-surface layers and the time for seismic energy to travel through these layers, and hence their velocities (Cox, 1999). The information obtained from uphole surveys provide complementary details that aids in the interpretation of conventional seismic refraction/reflection data. The uphole survey locations serve as control points and when tied to seismic data extends the well location (uphole survey point) information away from the hole or to interpolate between two or more holes across the seismic volume.

Sheriff (1991) defined an uphole survey as; "successive sources at varying depths in a borehole in order to determine the velocities of the near-surface formations, the weathering thickness, and (sometimes) the variations of record quality with source depth". In continuation, he stated further that "sometimes a string of geophones is placed in a hole of the order of 200ft (approximately 60m) deep to measure the vertical travel times from a nearby shallow source".

Uphole surveys are not used universally, and their expensive cost of deployment is a critical factor that limits its wide range of application. Uphole survey information (models) were iteratively integrated with refraction arrival inversion models to build a more robust and reliable near-surface model in a hybrid approach in this dissertation. Two common techniques or configurations exist for data acquisition during uphole surveys, they are;

i) Source in borehole and receivers at the surface
ii) Receivers in borehole and source at the surface

Both configurations are illustrated in Figures 2.19 and 2.20 respectively.

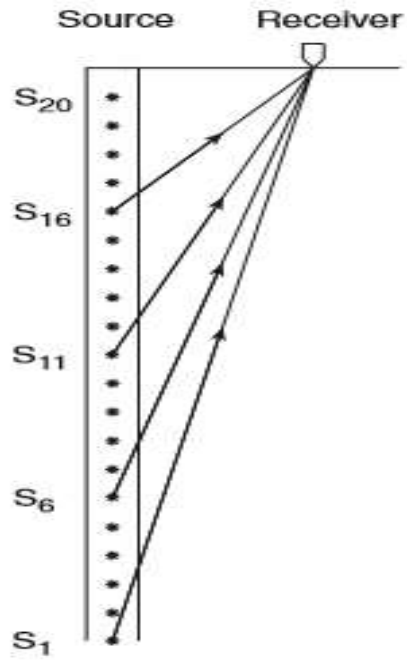

Figure 2.19: Uphole survey configuration for Sources in borehole, Receiver at the surface. (After Cox, 1999)

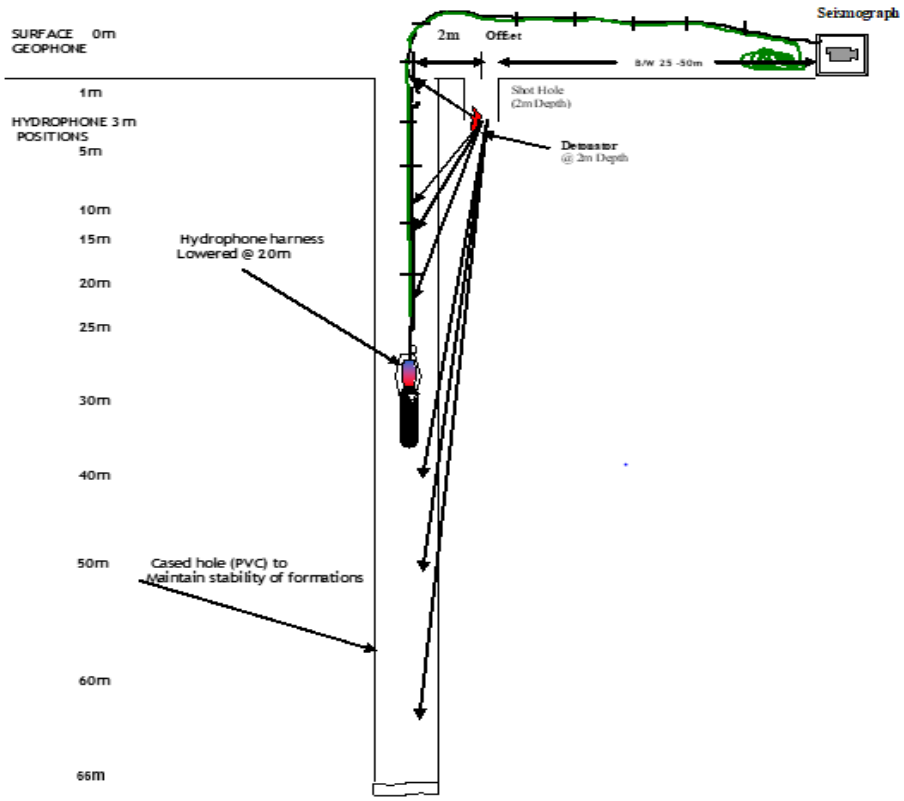

Figure 2.20: Uphole survey configuration for Receivers in borehole, Source at the surface. (Source: CNPC/BGP Technical Report, 2014)

Regardless of the method or configuration adopted to acquire the data, with either sources (uphole recording) or receivers (downhole recording) in the borehole, the basic procedure is the same. Once the uphole data is acquired, the interpretation essentially entails;

i) Picking the first arrivals from each depth level
ii) Applying any necessary corrections to these times
iii) Plotting the data and estimating the velocities and thicknesses of the various layers identified.

In so doing, a near-surface model would have been obtained. Details on the underlying principles, methods of implementation of uphole surveys, data collection, reduction/conversion and correction as well as interpretational approaches to uphole survey models can be found in Franklin (1981), Wong *et al*. (1987), Hunter and Burns (1990), Whiteley *et al*. (1990a and 1990b) and Cox (1999).

2.10 Replacement Velocity

Datum statics correction require that the weathered layer be removed and the times adjusted from the base of the weathered layer up to, or down to, the reference datum. The velocity used for this correction is normally called the replacement velocity, or sometimes the datum velocity, elevation velocity, or sub-weathering velocity. If the reference datum is below the base of the weathered layer, the replacement velocity is normally computed from the velocity profile at this depth, that is, the velocity within the sub-weathered layer. If datum is above the base of the weathered layer, material with a velocity close to that at the base of the weathered layer is used to infill the layer. The replacement velocity may be constant for a line or, more typically, may change slowly along the line. Where major lateral changes in geology, and hence velocity occur at or just below the base of the weathered layer, the replacement velocity profile generally reflects these changes. The necessary velocity

information may not be available at the time that the datum statics corrections are computed due to insufficient areal information.

Beck and Steinberg (1986) however, have suggested that the replacement velocity can be computed later in the processing sequence. This approach requires all initial processes to be referenced to the floating datum plane, using a provisional replacement velocity to derive the datum statics corrections. The final replacement velocity is then generated from all available information, such as velocity analyses and borehole data, and used to convert the data from the floating datum to the final datum. The replacement velocity is used to correct times of almost vertical ray paths (the datum statics correction definition assumes vertical ray paths). The value used for the replacement velocity is also likely to be used in the interpretation of velocity analyses and as part of the velocity–depth model for subsequent time to-depth conversion, or other processes such as depth migration. A factor that should be noted is that an error in the replacement velocity (for computing the elevation correction) leads to incorrect statics corrections.

2.11 Refraction Seismic in relation to the Near Surface

A seismic ray which crosses a boundary between two formations of different velocities is refracted according to Snell's law (Figure 2.21). This law states that the ratio of the sine of the incident angle Θ_1 and refracted angle Θ_2 is equal to the ratio of the velocities of the two formations v_1 and v_2:

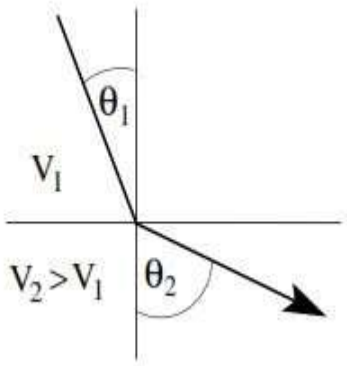

$$\frac{\sin\theta_1}{\sin\theta_2} = \frac{v_1}{v_2}.$$

Figure 2.21: A seismic ray which crosses a boundary. The ratio between the sine of the incident angle Θ_1 and refracted angle Θ_2 is equal to the ratio of the velocities of the two formations V_1 and V_2 (Snell's law).

As long as the velocity increases with depth, the ray is refracted away from the normal. For the so called critical angle, $\Theta_1 = \Theta_c$, and the refracted angle $\Theta_2 = 90°$.

The critical angle Θ_c follows from first principle (Dobrin and Savit, 1988), as

$$\text{Sin } \theta_C = \frac{v_1}{v_2} \qquad (2.11)$$

If a wave-front reaches the interface under the critical angle, it propagates along the boundary with the velocity of the lower medium. At every point of the ray-path along the boundary, there exists a ray from the boundary to the surface. The angle between all this rays and the normal to the boundary is the incident angle Θ_c.

The most convenient way to represent refraction data is to plot the first-arrival time, ***t*** vs. the source-receiver distance, ***x*** (Figure 2.22a). In the following, the time-distance relations for the case of two layers with velocities V_1 and V_2 separated by a horizontal discontinuity at depth Z_0 is derived from basic trigonometric identities and the fact that velocity is simply distance divided by time. The total time along the refraction path ABCD in Figure 2.22(b) is

$$t_x = t_{AB} + t_{BC} + t_{CD} = 2t_{AB} + t_{BC}$$

$$= 2\frac{Z_0}{v_1 Cos\,\theta_C} + \frac{x - 2Z_0 \tan\theta_C}{v_2}$$

$$= 2\frac{Z_0}{v_1 \,\mathrm{Cos}\,\theta_C} - \frac{2Z_0 \,\mathrm{Sin}\,\theta_C}{v_2 \,\mathrm{Cos}\,\theta_C} + \frac{x}{v_2} \qquad (2.12)$$

If it is required to express t_x in terms of velocities only, then (2.12) can be re-expressed as,

$$t_x = \frac{x}{v_2} + \frac{2Z_0\sqrt{v_2^2 - v_1^2}}{v_1\, v_2} \qquad (2.13)$$

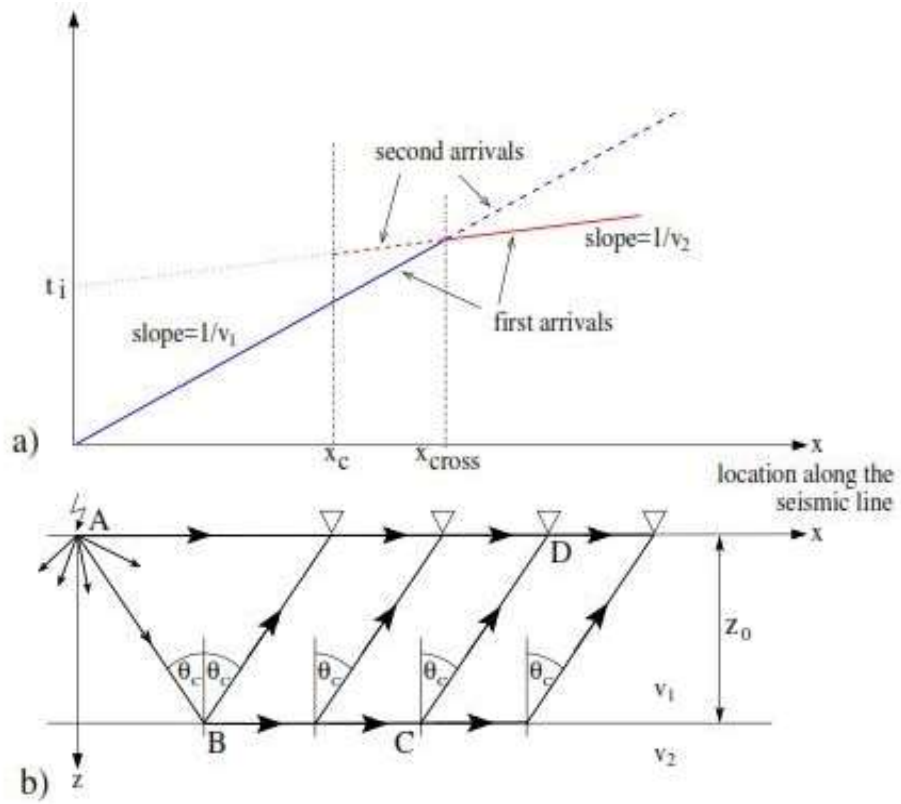

Figure 2.22 (a) Travel-time curves of the refracted and the direct wave.
(b) Refracted and direct rays in the corresponding model with two layers separated by a horizontal interface (Kearey and Brooks, 1991).

On a t_X versus x plot, equation (2.13) is that of a straight line which has a slope of $1/V_2$ and which intersects the t_X axis ($x = 0$) at the so-called intercept time.

$$t_i = \frac{2Z_0\sqrt{v_2^2 - v_1^2}}{v_1\, v_2} \qquad (2.14)$$

The direct arrival is simply given by a straight line with a slope of $1/V_1$ that, in a t_X versus x *plot,* intersects the t_X axis (x = 0) at t = 0. In the time-distance plot, the travel- time curves of the direct and refracted wave intersects each other at the crossover distance

$$x_{cross} = 2Z_0 \sqrt{\frac{v_2 + v_1}{v_2 - v_1}} \qquad (2.15)$$

The depth Z_0 of the interface can be calculated by means of equation (2.14). In terms of t_i and the velocities V_1 and V_2, equation (2.14) can be solved for Z_0 to obtain

$$Z_0 = \frac{t_i}{2} \frac{v_1 v_2}{\sqrt{v_2^2 - v_1^2}} \qquad (2.16)$$

It can be seen from Figure 2.22 that the first refracted ray intersects the surface at the critical distance x_c. This corresponds to the source-receiver offset where the length of the ray along the refractor is zero, i.e., the case of critical reflection. The critical distance can as well be expressed as

$$x_c = \frac{2Z_0 v_1}{\sqrt{v_2^2 - v_1^2}} \qquad (2.17)$$

The theory explained above has illustrated the basic idea behind refraction seismic for planar reflectors, only. A detailed description of a 3-layer, dipping layer, and multi-layer cases could be found in Cox (1999).

2.12 Refraction-based methods and existing approaches to obtain a Near-surface Model

Refraction based methods that can be used to obtain a near-surface model are group into;

i) Intercept-time methods,
ii) Reciprocal/Delay-time methods, and
iii) Ray tracing/Tomographic methods.

Each technique has its advantages over the other and can be used in different geological situations. The choice of the type of interpretation technique is a function of the complexity of the subsurface geology.

The intercept-time method is the simplest method of seismic refraction interpretation. This method assumes flat layers and does not incorporate geological dip. In this method slope and intercept time are used to calculate velocity and depth of refractors. However there can be problems with such a simple method as it does not readily account for lateral variations. To understand how refraction techniques acquire information for the near- surface model, it is best to look at a hypothetical time-distance curve (Figure 2.23).

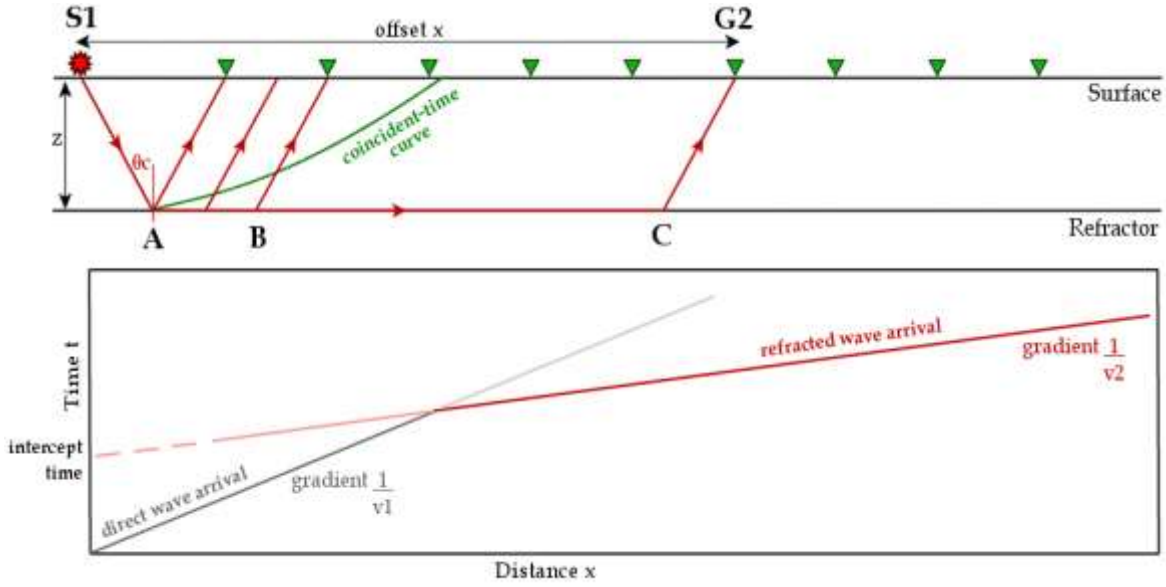

Figure 2.23: Time-distance plot for horizontal two-layer case, showing first arrivals from direct and refracted wave and extrapolation to read off the intercept time (Alten, 2009)

This scenario represents a plane, horizontal interfaces of constant velocity, representing a 1D case where only one shot would be necessary to obtain all the information, as there are no dipping surfaces. Above the time-distance curve in Figure 2.23, there is a simplified model of the spread layout. It shows that the boundary between the two parallel layers is at depth z and the emergent point of the first refracted wave on the interface is at point A. It can equally be seen

that in close proximity to the shot point, the first arrival is the direct wave and it is apparent that the slope of the time-distance curve in this area is a direct measure of the velocity in the first layer v_1. The refracted rays may be visible in the form of second arrivals. Rays emergent at point B arrive simultaneously with the direct arrivals, so the two travel-time curves intersect (at the crossover distance which is the offset at the surface, not along the refractor). At distances beyond B, refracted arrivals reach the receivers ahead of the direct wave and produce a slope with gradient $\frac{1}{v_2}$ on the time-distance plot.

To show that the velocity of the second layer can be directly deduced from these recordings, the following equations are set up (Alten, 2009):

If the time taken to travel horizontally from S_1 to G_2 via A and C is

$$t = \frac{S_1A}{V_1} + \frac{AC}{V_2} + \frac{CG_2}{V_1} \qquad (2.18)$$

and we know the line S_1A hits the interface at the critical angle θ_C at depth z, we can rewrite the equation (2.18) as

$$t = \frac{z}{V_1 cos\theta_c} + \frac{x-2z\ tan\theta_c}{V_2} + \frac{z}{V_1 cos\theta_c} \qquad (2.19)$$

Using Snell's law, this is equivalent to

$$t = \frac{x}{V_2} + \frac{2z\cos\theta_c}{V_1} \qquad (2.20)$$

Equation (2.20) has the form of a straight line equation with $\frac{1}{V_2}$ being the gradient. In order to be able to solve this equation with three unknowns (z, V_1, V_2), we determine V_1 from the slope of the direct arrival, V_2 from the slope of the refracted arrival and z is worked out by assuming the offset x to be zero and reading the intercept time off the extrapolated time-distance plot to obtain a value for the term $\frac{2z\cos\theta_c}{V_1}$, in which the refractor depth is now the only unknown. The

crucial point worthy of note here is that this method is limited to a simple case of parallel bedding planes. The velocity is presumed to be constant within the two media and the structures are horizontal. None of these conditions is usually fulfilled in reality and hence is a serious limitation to this refraction interpretation method. A scenario of multi-layered geologies and the possibility of dipping refractors, as well as a gradual velocity increase with depth is the ideal situation encountered in the subsurface. Figure 2.23 shows that a correct determination of near-surface information requires, a recording of the head wave over any receiver, so that a precise gradient can be read off the time-distance plot. Shortening the distance over which the slope is measured is likely to result in errors of judgment on the part of the interpreter, giving inappropriate results for V_1, V_2 and z. This problem becomes even more recognizable in multi-layer cases (Figure 2.24), where the number of refractors that can be mapped is dependent on structural factors and spread layouts; this is still a case of a 1D situation with no dips.

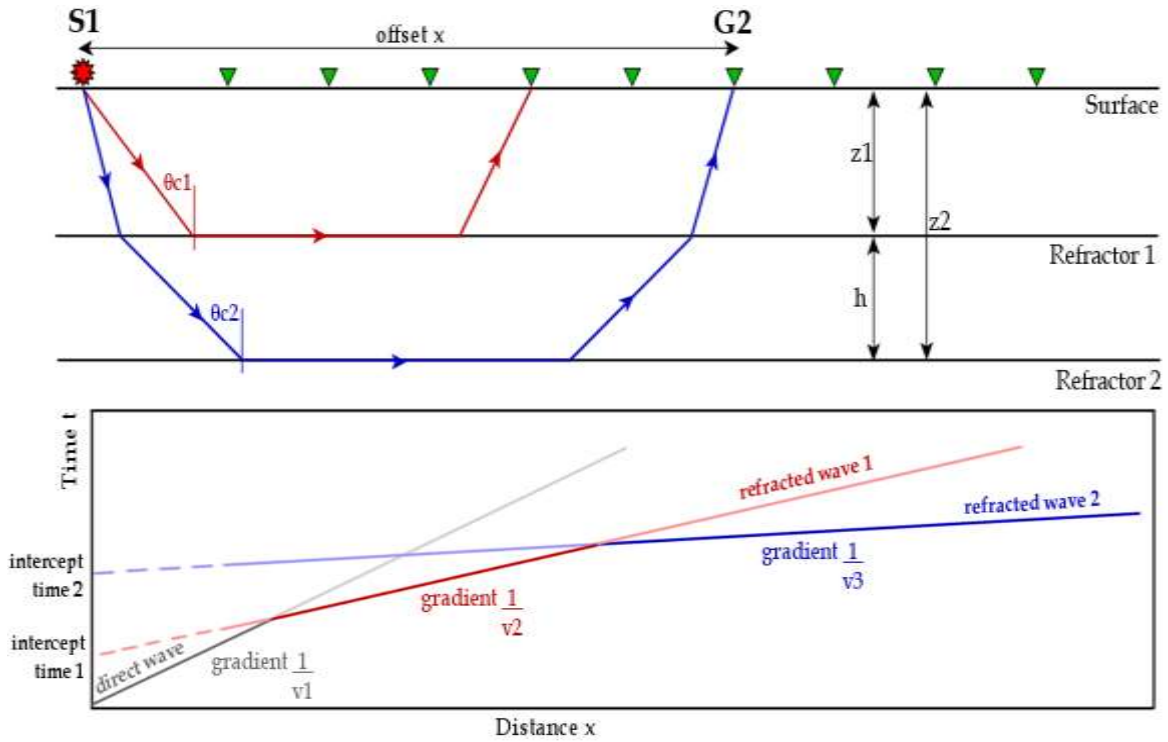

Figure 2.24: Time-distance plot for horizontal three-layer case, where two bends in the first arrival curve at the crossover distances mark increases in velocity (Alten, 2009)

Figure 2.24 shows the time-distance curve of first arrivals in a three-layer case. The equations for the two top layers are the same as in a simple two-layer case, and the third layer can be computed by applying the same concept but with a few modifications. The slope of the third refractor is equivalent to $\frac{1}{V_3}$, on the assumption of a parallel horizontal layering scenario. In order to calculate the depth of this layer (z_2), the same theory above applies, working with the depth of the refractor relative to the layer above (h) and using its intercept time (intercept time 2). Whereas the depth of the shallow refractor is equal to its thickness, the depth of the deeper refractor is the sum of its thickness and the depth of the layer above.

Theoretically, this method could be extended indefinitely to any number of layers, building up a system of equations to satisfy even more refractors. Practical limitations, however, such as the need for very long offsets to record first arrivals from deep refractors and the problem of differentiating clearly between the layers, particularly if the velocity changes are small, reduce the standard model to a maximum of 2 to 3 layers. The geology of the survey area greatly affects the resolution of the model. The bend in the travel-time curves mark the onset of a new layer and indicates where the crossover distance along the surface is found, that is, where the refracted wave overtakes the direct wave, or in multi-layer cases, where the waves from a deeper refractor overtake those from the shallower refractor. A reasonably strong velocity contrast between two layers manifests itself as a clear bend and hence an easier velocity determination. Too strong velocity contrasts between thin layers, however, might result in hidden layers, as they are not obviously separate refractors on the time-distance plots and lead to erroneous depth estimations. Layers of very small thickness compared to the surrounding ones might only appear as a second arrival and not as a first, which makes them impractical for refraction analysis. Another situation which can give rise to hidden layers is velocity inversions

(Cox, 1999). This, common in permafrost regions, causes seismic waves to be refracted towards the normal when they hit the interface between the fast layer and the underlying slower layer. Incident waves will not strike the lower layer at the critical angle in order to produce the refracted wave that runs along the interface and eventually produces the measurable head wave. This shows that the concept of refraction surveys to provide near-surface information is only valid if the velocity increases with depth. This is true even when dealing with non-horizontal layering situations, leading to 2D/3D scenarios, that is, where one shot does not suffice to acquire subsurface information. Dipping refractors, be it just one or multiple dipping interfaces, can be resolved adequately as long as reciprocal shots are employed. Reciprocal shots require shot-receiver locations to be interchangeable to give a forward and reverse shot for the same underground profile. That way, an up-dip and down-dip velocity, along with an up-dip and down-dip thickness could be determined, from which the true values can be deduced. The reciprocity of this method refers to the travel-time of the wave, which should be the same if the shot and the receiver station are reversed.

If the stratigraphy consists of very thin layers, the resolution (governed by the geophone spacing of the refraction profile) might not be sufficient to distinguish them as individual layers and, instead, the curved travel-time plots appear to give a velocity gradient. However, if the subsurface beds are dipping, as is usually the case, the effective and frequently used methods are the reciprocal and delay time methods. The term ‘reciprocal time’ is the travel time along the refractor from one end shot of the receiver for ‘forward profile’ and vice versa for the ‘reverse profile. In this method both forward and reverse spread data should be recorded. This type of acquisition geometry is typical for seismic refraction surveys. But in the case of seismic reflection surveys where refractions are also recorded, this forward and reverse shot scheme might not

exist. But an algorithm designed to solve these kinds of cases can sort data and create pseudo forward and reverse shot schemes. Forward and reverse shots are usually required to calculate subsurface dip of the refractors. Theoretically, both forward and reverse times should be equal if reciprocity exists. Both times are not equal because of dipping bed, undulating layers, and change in refractor velocity. In this situation, the common refraction interpretation methods are the Plus-Minus method (Hagedoorn, 1959), the ABC method (Edge and Laby, 1931), the Gardner method (Gardner, 1967), which has evolved over time and has now been fully developed by Lawton (1990) as the Delay-Time method and the Generalized Reciprocal Method (GRM) (Palmer, 1981).

In 'Ray tracing' methods, seismic ray paths are traced through the input geological-velocity model; the theoretical travel times are calculated and matched against the actual first breaks. Inversion is carried out to calculate the travel time differences between actual and theoretical first breaks and the input model is updated with travel time residuals for the next iteration. Iterations continue until a predetermined stopping criterion is matched. In this method two different inversion approaches exist,

i) A layer based inversion, and

ii) A full cell/block based tomographic inversion.

Among layer based inversion methods, the Generalized Linear Inversion (GLI) method is common (Hampson and Russell, 1984). In this method the near surface geological model is proposed and rays are traced through this model. In the full tomographic inversion approach, the velocities are allowed to vary in both the horizontal and vertical directions. The subsurface geological model is divided into blocks/cells of equal slowness which are inverted for such as in the GLI method. In the areas of severe velocity variations this method gives acceptable results.

There are other methods of interpreting data acquired from refraction surveys; many are based on similar principles to the ones already mentioned, while others take a wholly different approach, such as wave front methods. The Plus-Minus method proposed by Hagedoorn (1959), is worthy of mention here, it requires a reversed refraction profile with receivers at common surface locations for a forward and reverse shot. The so-called plus time – the sum of the two travel times from the sources to the common surface location, minus the reciprocal time between the two sources – gives information about the travel time from the surface to the refractor and is thus a measure of the delay time. The minus time leads to a straight line equation with a gradient corresponding to the refractor velocity.

A generalization of this approach is Palmer's idea of the generalized reciprocal method (GRM), which can be applied to a common surface, as well as common subsurface locations. Likewise, it relies on reciprocal times on a reversed refraction profile, but while the Plus-Minus approach works on parallel horizontal layering, the GRM is insensitive to dips up to 20^{o} and can handle velocity gradients. The drawback of Plus-Minus and GRM approaches is that they are limited to in-line applications, or 2D layouts, while the Delay-Time method (Lawton, 1990) can be extended to a 3D configuration which is more desirable. These techniques are exhaustively discussed in Cox, 1999. For refraction arrivals recorded as part of a reflection survey, the most widely used and accepted interpretation methods are the Delay-Time approach or tomographic technique. The Delay-Time approach is the method used in interpreting the refraction data which was used to build a near-surface model for an appropriate refraction statics solution to be derived for the seismic dataset from the investigated prospect (OML-23, SOKU), to resolve its statics problem. This choice was guided by the flexibility of the method to be

adaptable for a multi-layer, dipping case as is the case in the Niger Delta Basin where the prospect is situated.

2.13 The Refraction Delay-Time Approach

The refraction delay-time method or approach is a recent refraction statics correction technique that uses the travel-times of critically refracted seismic energy to compute the depth and velocity structure of near-surface layers. It was actually developed and applied by Lawton, (1990) based on Gardner's delay – time analysis (Gardner, 1967). It assumes the near-surface structure is simple and layer based. It neither has severe topography variations nor has rapid lateral velocity variation in layers beneath the near-surface weathering layer. It resolves intermediate and long-wavelength weathering statics anomalies that may not be handled by residual statics corrections.

The delay time method is basically a continuation of the two-layer intercept method. Equation (2.20) for the travel-time t at any offset x was said to be $t = \frac{x}{V_2} + \frac{2z\cos\theta_c}{V_1}$, this can be rewritten as an expression of the intercept time t_0

(where x = 0) to give the depth z as $z = \frac{t_0}{2}\frac{V_1}{cos\theta_c}$, rewriting this expression of z to get rid of θ_c term, we get,

$$z = \frac{t_0}{2}\frac{V_1V_2}{\sqrt{(V_2^2 - V_1^2)}} \qquad (2.21)$$

The delay-time concept now splits this intercept time t_0 into a shot and receiver component and posits that, if the true refractor velocity is known, the intercept time at offset x corresponds to the time difference between the actual arrival time t and the time travelled along the interface vertically below shot and receiver,

$$t_0 = t - \frac{x}{v_{refractor}} \qquad (2.22)$$

The ray paths in Figure 2.25, show which travel paths and travel times this concept corresponds to. The delay-time as defined by Gardner (1967), is composed of the receiver delay time $t_{R/delay}$ at one end of the profile and the source delay time $t_{S/delay}$ at the other, so that in the special case of horizontal parallel layers, these two delay times are equal. If this is the case, each delay time is half the intercept time and Equation (2.20)

can be re-expressed as

$$z_R = t_{R/delay} \frac{V_1 V_2}{\sqrt{(V_2^2 - V_1^1)}} \qquad (2.23)$$

$$\text{or } z_s = t_{S/delay} \frac{V_1 V_2}{\sqrt{(V_2^2 - V_1^2)}}, \qquad (2.24)$$

giving the refractor depths at receiver and shot stations, respectively.

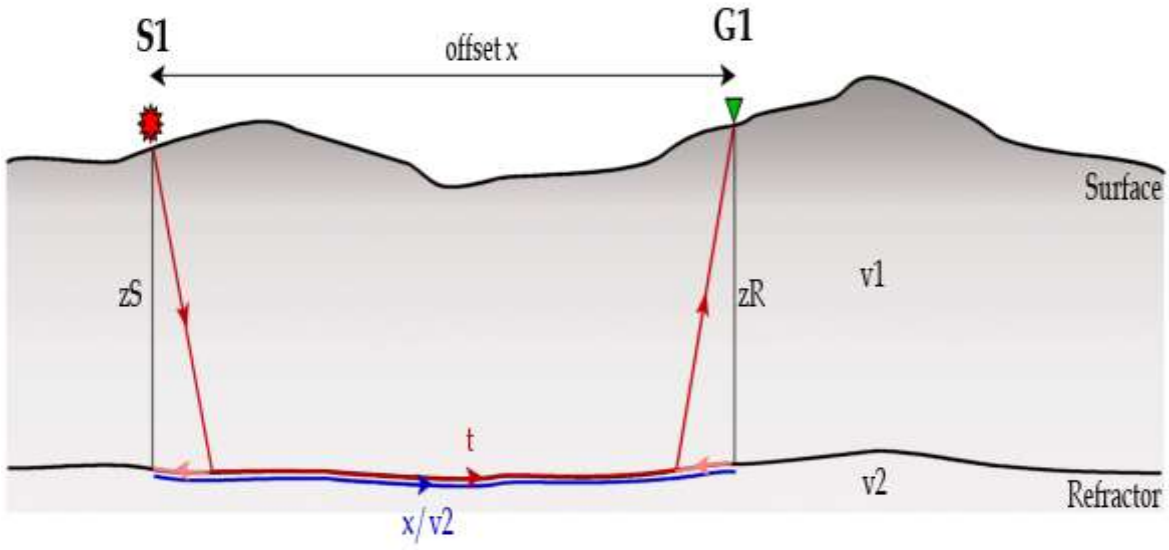

Figure 2.25: Blue ray path corresponds to distance between vertical downward projections of S_1 and G_1, waves taking time $\frac{x}{V_2}$; red ray path corresponds to actual travel time t; delay time is the difference between the two and can be decomposed to give depths z_S and z_R at either end of the profile (Alten, 2009).

Further use of the delay-time concept is sometimes made directly in datum statics, where the delay times are taken to be weathering corrections when the layering is sufficiently flat or only has limited dip, and the critical angle is small enough to assume the incident rays to

be close to vertical. The overall workflow to derive the correction statics is as follows: first, the first-arrival energy (first break) needs to be picked. Normally, only the first 2 to 3 layers are picked. The picked first breaks are then examined for correctness by performing geometry quality control QC and repositioning them if and where necessary adjustments are required. Furthermore, a velocity model is derived, and finally the statics is calculated after defining intermediate datum and final datum. The method used to interpret the refraction data used for the current study (the Delay-time approach), as previously stated was first fully developed by Lawton (1989) based on Gardner' idea, it has evolved (Lawton, 1990) and has been revised in recent times (Baker, 1999; Butler, 2005; Duan, 2006 and Bridle and Aramco, 2009). This method can indirectly estimate intercept time and bedrock velocity using the first breaks. It uses the multiplicity of first-break data available in multi-fold reflection surveys to determine the number of refractors present and to calculate statistically robust delayed times and refractor velocities. It mitigates the ambiguity in the interpretation of travel time-distance graphs caused by the presence of topography or structure on the refractor. Figure 2.26 is a two-layer model with one layer over half a space.

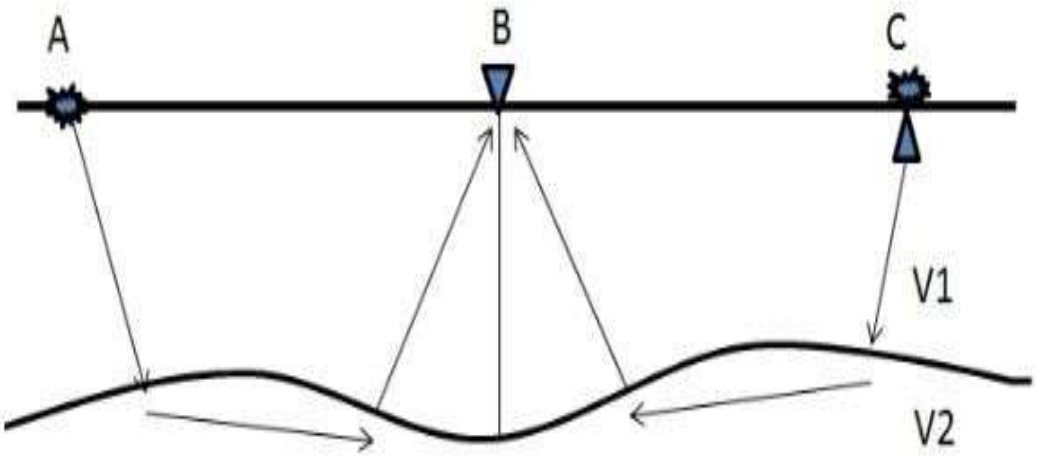

Figure 2.26: Two layer refraction delay-time model (Cox, 1999)

The first layer could be considered as the weathering layer with an undulating base. It shows three ray paths associated with shot-receiver pairs AB, BC, and AC. Assuming that the delay times for a shot point and receiver at a common location are equal; the following equations could easily be derived (Cox, 1999 after Lawton, 1989) as follows:

$$T_{AB} = T_A + \frac{AB}{V_2} + T_B \quad (2.25)$$

$$T_{BC} = T_C + \frac{BC}{V_2} + T_B \quad (2.26)$$

$$T_{AC} = T_A + \frac{AC}{V_2} + T_C \quad (2.27)$$

$$T_{AC} - T_{BC} = T_A - T_B + \frac{AB}{V_2} \quad (2.28)$$

$$T_{AB} - (T_{AC} - T_{BC}) = 2T_B \quad (2.29)$$

$$T_B = \frac{1}{2}(T_{AB} + T_{BC} - T_{AC}) \quad (2.30)$$

$$T_A = \frac{z_A \cos\theta}{V_1}$$

$$T_B = \frac{z_B \cos\theta}{V_1}$$

$$T_C = \frac{z_C \cos\theta}{V_1} \quad (2.31)$$

$$\theta_1 = \arcsin\frac{V_1}{V_2} \quad (2.32)$$

T_{AB}, T_{AC} and T_{BC} represent first-arrival travel times from source to receiver. T_A, T_B, T_C are delayed travel time for A, B, and C respectively. Θ is incident angle. Z_A, Z_B, and Z_C are the depth from shot/receiver to the refractor, and velocities in the two layers are V_1 and V_2. Delay

times for deeper refractors can be computed in an identical manner by using further offset from the shot points. In the general case for refractor n, the delayed time (Cox, 1999) is expressed as

$$T_{ABn} = T_{An} + \frac{AB}{V_{n+1}} + T_{Bn} \quad (2.33)$$

$$T_{An} = \sum_{i=1}^{n} \frac{Z_{Ai} \cos \theta_i}{V_1} \quad (2.34)$$

$$\theta_i = \arcsin \frac{V_i}{V_{i+1}} \quad (2.35)$$

This approach can be used to interpret refraction data from subsurface situations where there is a high vertical-velocity contrast and this is crucial in deriving a correct refraction statics solution in such situations.

2.14 Overview of the Geology of the Niger Delta Basin

The Niger Delta Basin is a large arcuate Tertiary prograding sedimentary complex deposited under transitional marine, deltaic and continental environments since Paleocene in the north to Recent in the south. It occupies an area lying between longitude 4°E- 9°E and latitude 4°N - 6°N. It is bounded in the east by the Calabar Flank and Abakaliki Trough, in the west by the Benin Flank, in the north by the Anambra Basin and in the south by the Atlantic Ocean. Both marine and mixed continental depositional environment characterize the Niger Delta Basin of Nigeria (Uko *et al.*, 1992). The Niger Delta covers an area of about 75,000 square km (28,957 mi^2) in southern Nigeria. Figure 2.27 shows the Niger Delta Area in southern Nigeria.

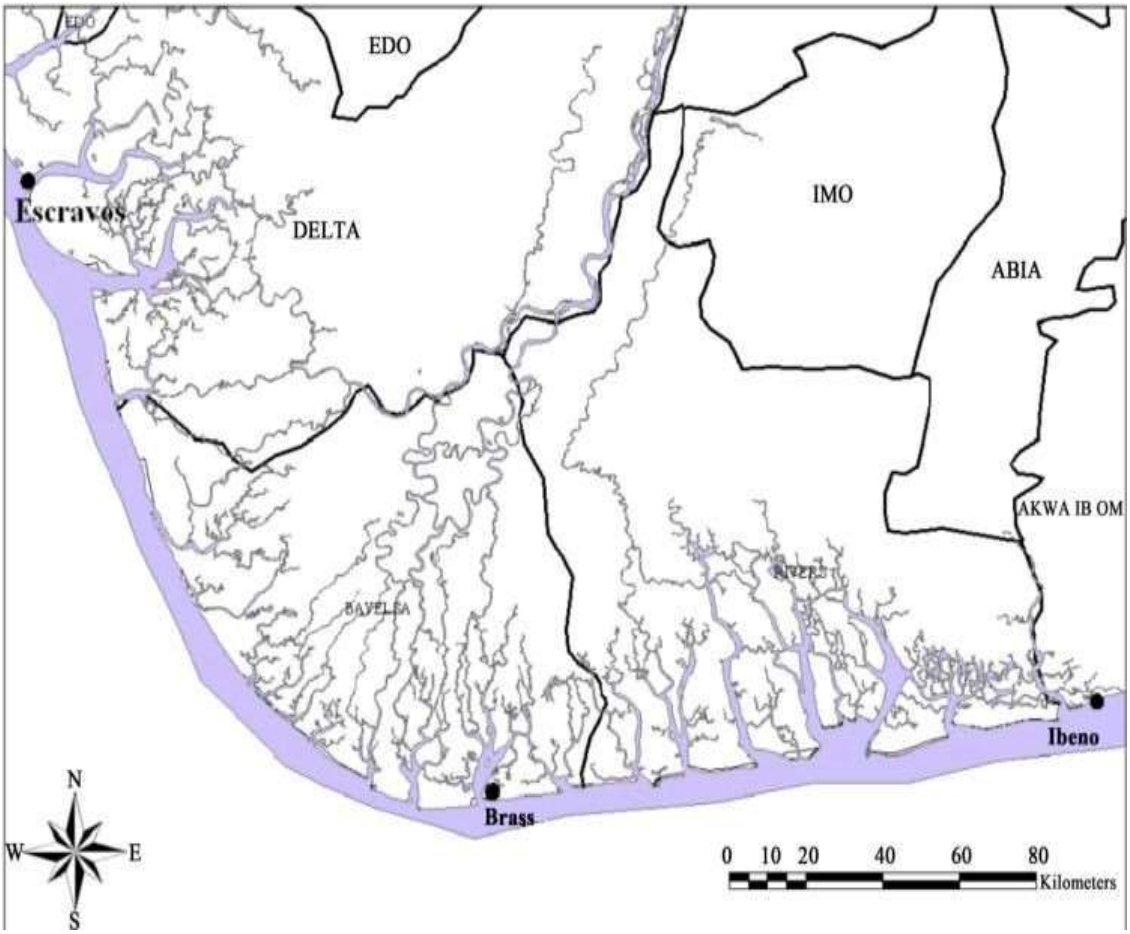

Figure 2.27: The Niger-Delta Area in southern Nigeria (Short and Stauble, 1967).

From the Eocene to the present, the Delta has prograded southwest ward, forming depobelts (Figure 2.28) that represent the most active portion of the Delta (Doust and Omatsola, 1990). These depobelts form one of the largest regressive deltas in the world with an area of some 300,000 km^2 (Kulke, 1995), a sediment volume of 500,000 km^3 and a sediment thickness of over 10km in the basin depo-center (Hospers, 1965).

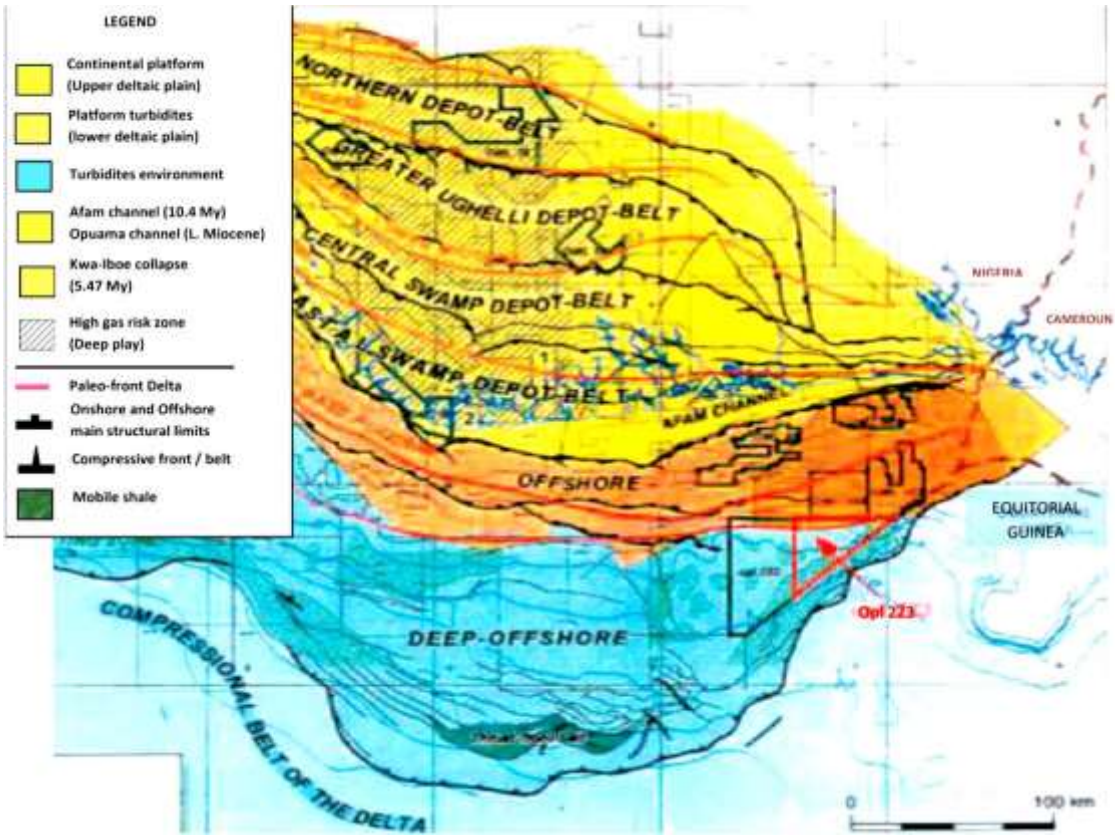

Figure 2.28: Map of Niger Delta showing the depobelts (Short and Stauble, 1967)

The Niger Delta Basin consists of three main tertiary stratigraphic units overlain by Quaternary deposits (Short and Stauble, 1967) (Table 2.2). These three subsurface stratigraphic units are the Benin, Agbada and Akata formations.

Table 2.2: Geologic units of the Niger Delta (Short and Stauble, 1967)

Geologic Unit	Lithology	Age
Alluvium (general)	Gravel, sand, clay, silt	Quaternary
Freshwater backswamp and meander belt	Sand, clay, some silt and gravel	
Mangrove and salt water/backswamps	Medium-fine sand, clay and some silt	
Sombreiro-warri deltaic plain	Sand, clay and some silt	
Benin formation (coastal plain sand)	Coarse to medium sand with subordinate silt and clay lenses	Miocene
Agbada formation	Mixture of sand, clay and silt	Eocene
Akata formation	Clay	Paleocene

The base is the Akata Formation comprising mainly of marine shale and sand beds. Its composition consists of primarily dark-grey sandy, silty-shale with plant remains towards the top of the Formation. It is over 1200m thick and thought to be the main hydrocarbon kitchen of the Niger Delta Basin (Kulke, 1995). The overlying Agbada Formation is a sequence of alternating sandstones and shales. It consists of an upper predominantly sandy section with minor shale intercalations and a lower shale unit which is thicker than the upper sandy section. The thickness is over 3000m. The Benin Formation is made up of predominantly massive, highly porous fresh water-bearing sandstone, with local inter-bed of shales. Quaternary deposits made up of top soil, red laterite, clay, fine sand, medium sand and coarse sand constitute alluvium of the Benin Formation. The thickness is variable but exceeds 1800m.

The Niger Delta is one of the most hydrocarbon-rich regions in the world. Exploration and exploitation of hydrocarbons have been going on in the region since 1956, when oil was discovered at Oloibiri in present day Bayelsa State, Nigeria. It is an excellent petroleum province, ranked by the U.S. Geological Survey World Energy Assessment as the twelfth richest in petroleum resources, with 2.2 % of the world's discovered oil and 1.4 % of the world's discovered gas (Klett *et al.*, 1997). By virtue of the size and volume of petroleum accumulation in the Niger Delta basin, various exploration strategies have been devised to recover the enormous oil and gas deposits locked therein. The delta formed at the site of a rift triple junction related to the opening of the southern Atlantic from the Late Jurassic to the Cretaceous. The Delta proper began progading in the Eocene, accumulating sediments that now are over 10 km thick. The Niger Delta Petroleum Province contains only one identified petroleum system, namely the Tertiary Niger Delta (Akata –Agbada) Petroleum System (Klett *et al.*, 1997). The western boundary is the Benin Flank - a west-north trending hinge line at the margin of the West Africa

basement Massif. The northeastern boundary is defined by outcrops of the Cretaceous on the Abakaliki High and further east-south by the Calabar Flank. The litho-stratigraphic cross section of the Niger Delta Basin is shown (Figure 2.29) with the three distinct – Benin, Agbada and the Akata Formations.

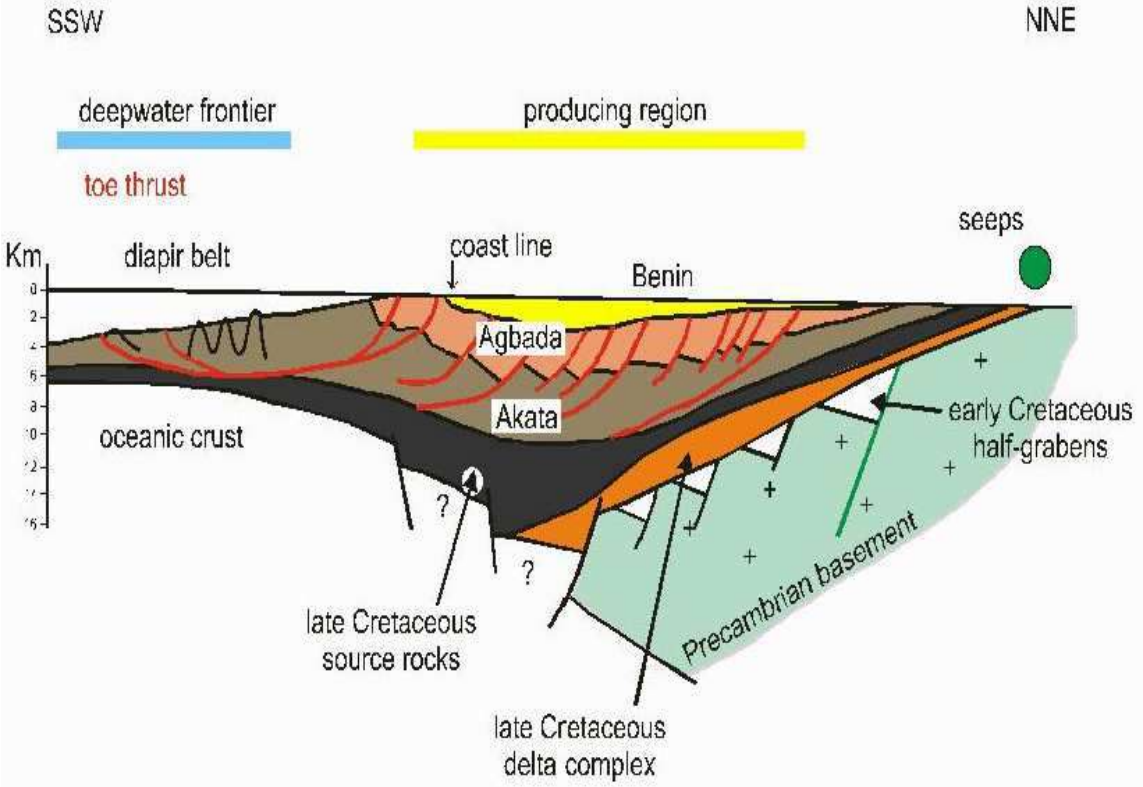

Figure 2.29: The Niger Delta litho-stratigraphic cross section showing the Benin, Agbada and Akata Formations (Allen, 1965)

The Niger Delta Basin is characterized by some fault configurations (structures), those identified include shale diapirs, roll-over anticlines, collapsed growth fault crests, and steeply dipping, closely spaced flank faults. Some of these identified fault configurations are shown in Figure 2.30. These faults mostly offset different parts of the Agbada Formation and flatten into detachment planes near the top of the Akata Formation (Merki, 1970).

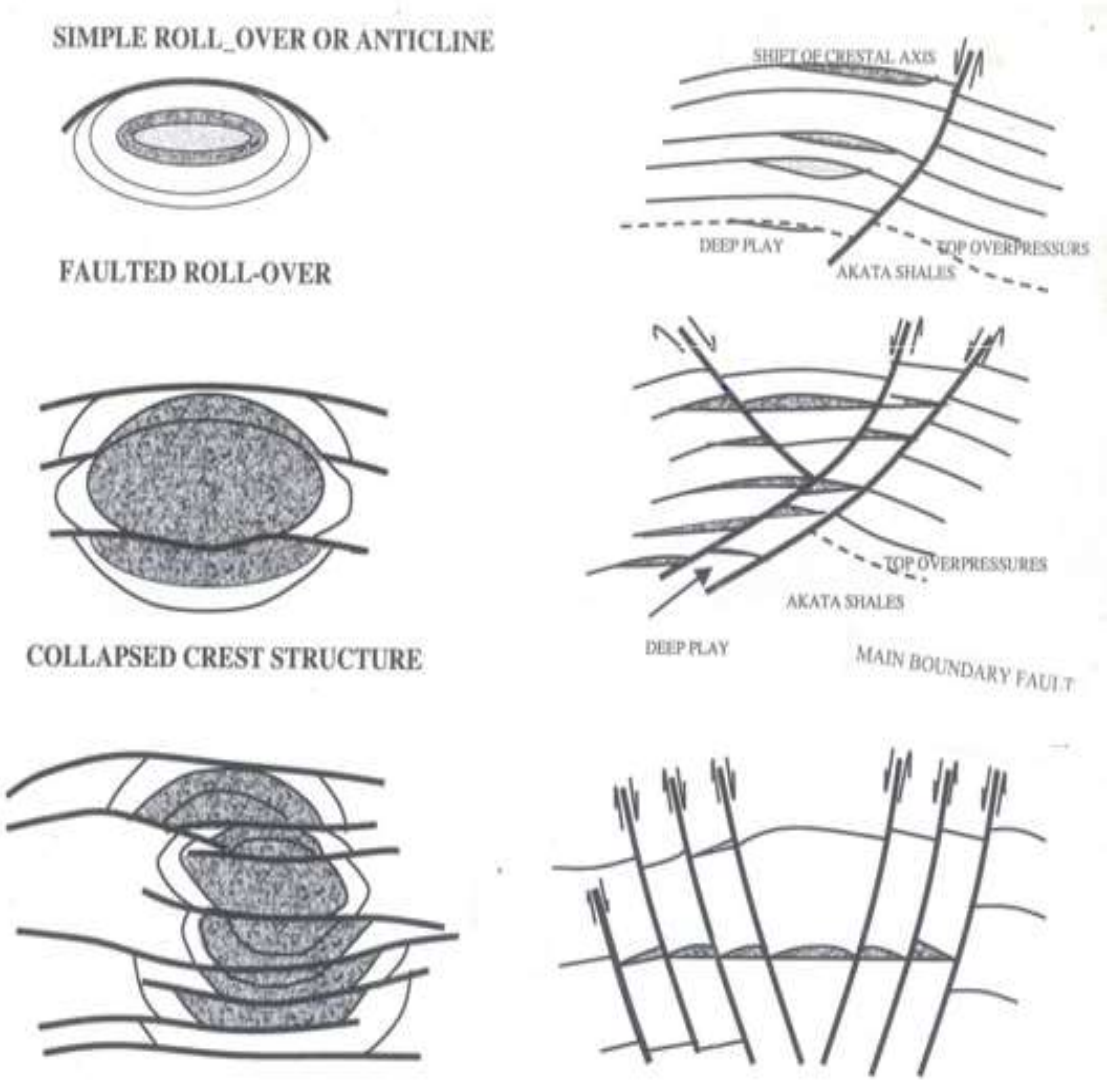

Figure 2.30: Conventional trapping configurations in the Niger Delta Basin (Merki, 1970).

Petroleum resources in the Niger Delta is produced from sandstone and unconsolidated sand reservoirs predominantly in the Agbada Formation. The major migration paths of hydrocarbon from the source rocks to these reservoirs are through the planes of growth faults (Merki, 1970). This is based on the assumption that permeability suitable for migration to take place is due to the presence of sand streak in the fault planes. Another possible migration path for the hydrocarbon could be from the over pressured shale sections. The characteristics of the reservoirs of the Agbada Formation are controlled by depositional environments and the depths

of burial. Known reservoir rocks are Eocene to Pliocene in age, and are often stacked, ranging in thicknesses from as little as 15m to as large as 45m. The primary source rock is the upper Akata Formation, the marine-shale facies of the delta, which possibly emanated from inter-bedded marine shale of the lowermost Agbada Formation. Oil is produced from sandstone facies within the Agbada Formation, however, turbidite sand in the upper Akata Formation is a potential target in deep water offshore and possibly beneath currently producing intervals in the onshore parts of the Basin. Most known traps in the Niger Delta Basin are structural although stratigraphic traps are not uncommon. The structural traps developed during synsedimentary deformation of the Agbada paralic sequence. A variety of structural trapping elements exists; including those associated with simple rollover structures, structures with multiple growth faults, structures with antithetic faults, and collapsed crest structures. The primary seal rock in the Niger Delta is the inter-bedded shale within the Agbada Formation. The shale provides three types of seals; clay smears along faults, inter-bedded sealing units against which reservoir sands are juxtaposed due to faulting and vertical seals (Merki, 1970).

Intensive exploration efforts over the last 35 years in and around the Niger Delta Basin has led to a succession of significant discoveries, notably are the Bonga, Agbami/Ekoli and Akpo discoveries in Nigeria. However, the full potential of the continental slope and the rise seaward of the shelf break is only recently becoming the focus of attention, with a number of exploration programs having resulted in major successes in recent years. Extensive regional 2D and 3D multi-client seismic data acquisition programs executed by a number of companies have provided high quality regional datasets that has enabled the unprecedented discoveries made lately in locating potential and prolific hydrocarbon fields.

CHAPTER THREE

MATERIALS AND METHODS

3.1 Materials (Data) and Software Tools Deployed

The materials and processing facilities deployed for the present study include;

i) Unprocessed seismic data in SEG-D format from prospect OML-23, SOKU in the onshore Niger Delta Basin (over 28GB size on hard disk).

ii) The accompanying Geometry/SPS (Source – Receiver) relation information files for the prospect OML-23, SOKU. (Selected SPS files from the prospect are shown in the appendix.)

iii) Uphole data/information acquired from the prospect OML-23, SOKU

iv) State of the Art High-end PC workstation with substantial Hard disk and Random Access Memory (RAM) size.

v) VISTA^{TM} interactive 2D/3D seismic data processing software for preliminary in-house seismic data processing.

vi) PROMAX^{TM} interactive 2D/3D seismic data processing software for the advanced seismic data processing stages.

vii) MESA Expert Version 10.04 which was used to load the coordinates of the study area. It was equally used to load and display the SPS files.

viii) Global Mapper 15 ^{TM}, which aided in viewing the geographical settings and terrain of the study area in terms of seismic objects (SO) and non-seismic objects (NSO).

ix) Processing support/facilities of the Geophysics Research Laboratory at the University of Port Harcourt and the Data Processing Centre of Excellence of Bureau for Geophysical Prospecting/China National Petroleum Corporation (BGP/CNPC) at Eleme, Port Harcourt.

3.2 Methodology

The methodology adopted at the different stages of the study, from the estimation of the near-surface velocity and thickness model over the investigated prospect from pre-stack seismic data, up to the refraction statics solution derivation stages for OML-23 SOKU, as well as the advanced processing stages where the success of the derived refraction statics solution was determined on shot gathers, and the data quality of both stacked and migrated sections of the datasets, is outlined in this section.

The starting point in deriving refraction statics solution entails preliminary pre-processing of the acquired data like loading the field geometry parameters, extensive quality control, removal of auxiliary channels and bad traces and possibly carrying out minor noise reduction processes to the data to increase the signal to noise ratio (SNR). Once geometry is loaded, the seismic data are sorted with source numbers as the primary keys, and line numbers and offsets as the secondary keys to enable for efficient travel-time picking. The next step is to pick the first breaks in this sorted order. Due to the large amplitudes of the first breaks, they are easily recognized from the shot displays. However, noisy portions of the data may be more difficult or ambiguous to pick because the noise imprints could smear the visibility of the first breaks. Generally, the seismic data processor selects the amplitude peaks, troughs, or zero crossings for travel-time picking, and tries maintaining its consistency throughout the entire dataset. In order to keep picking consistent, switching to other sort orders (e.g., by common receivers or midpoints, CMP) could be useful.

The entire processing methodology deployed is summarized with these three key stages:

i.) The data preparation and pre-processing stage which involved 3D binning and Fold calculation, generating the Linear move-out (LMO) plot, picking first breaks and performing

quality control (QC) of the picked first breaks.

ii.) The second stage involved generating a geometry database of control points for the seismic data from the prospect – OML-23, SOKU, and building a near-surface velocity and thickness model from the data using the proposed hybrid near-surface imaging approach. Then the derivation of the refraction statics solution which will then be applied to the seismic dataset, followed by the comparison of the results between the statics-corrected and uncorrected output for shot gathers in Field File Identification (FFID) configuration.

iii).The third and final stage is the advanced stage, where the data processing was extended to stacking and migration and the effectiveness of the derived refraction statics solution was equally determined for both the stacked and migrated outputs of the SOKU dataset.

3.2.1 Field Data Characteristics

This section describes the testing of parameters used during the acquisition of the dataset and the pre-processing steps taken in achieving the objectives of this study. The data acquired from the prospect OML-23 SOKU, had several receiver and source lines as expected. A very significant portion of the data (about 13 swaths) was used out of the full spread of over 30 swaths which were acquired in three (3) acquisition phases. Processing the entire dataset would have been near impossible because superior processing hardware such as PROLIAN Server PC parallel processing workstations and their likes are extremely expensive to acquire and deploy. The portion of the dataset used had the following field characteristics; the receiver lines were six (6) in number and were trending in the North-South direction. They include In-lines 48, 62, 76, 90, 104, 118. The cross-lines or source lines which were trending in the East-West direction included cross-lines 608, 624, 640, 656, 672, 688. Several shot positions were also offset to either the left or right of the cross-line to avoid obstacles which could not be removed

from the surveyed area. The inline and cross-line range of the source and receiver lines used for this study is shown in Figure 3.1.

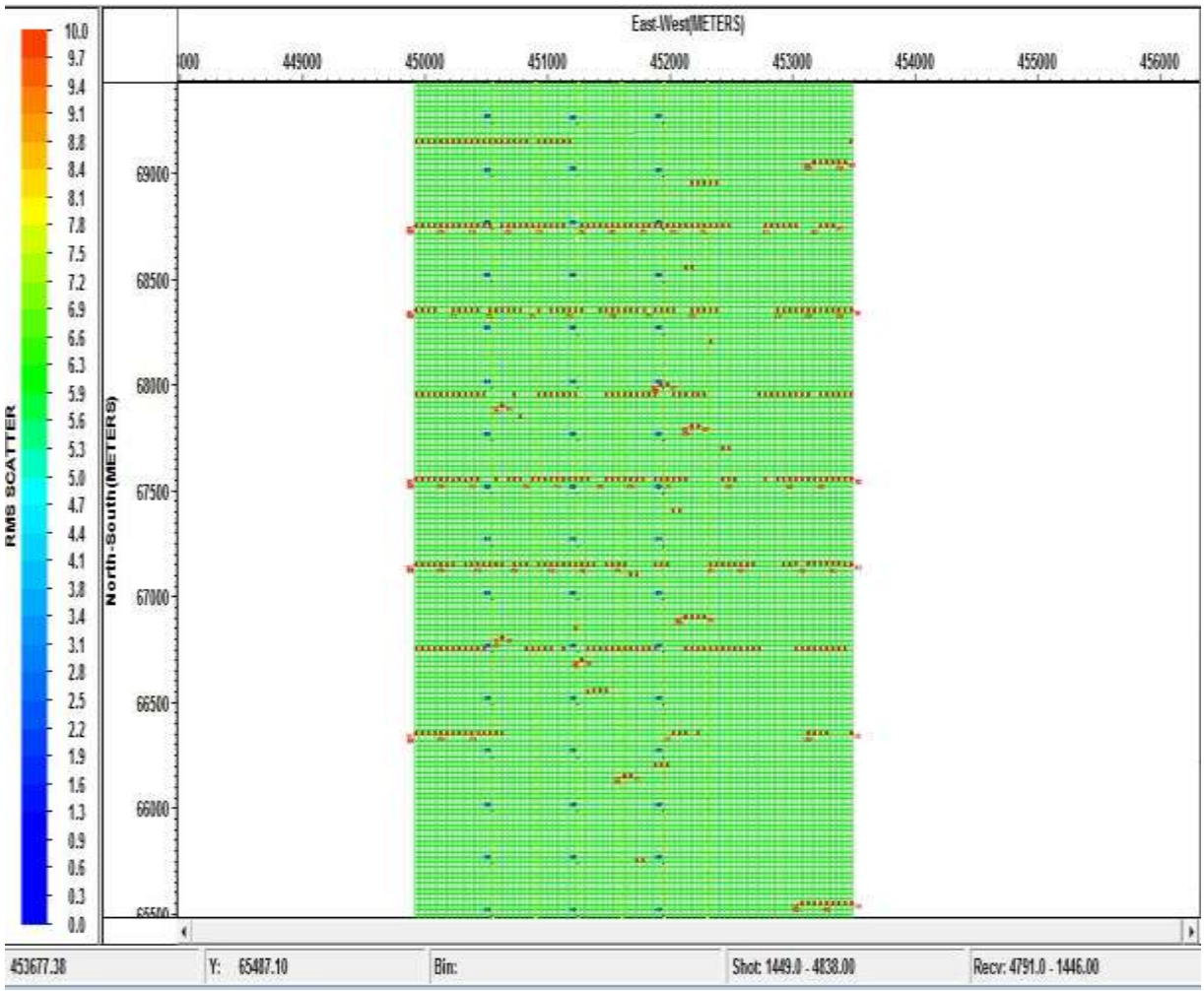

Figure 3.1: Inline and cross-line configuration over the surveyed area.

3.2.2 Data Acquisition Parameters

The seismic data used for the study was acquired from OML-23, SOKU. The acquisition was done in 3 acquisition phases with well over 27441 shots. The 3D shooting geometry was symmetric split spread. The 3D acquisition was done by IDSL (BGP/CNPC) using Sercel 428 recording instruments with nominal fold coverage of 56. The 3D seismic acquisition parameters are shown in Table 3.1.

Table 3.1: Data acquisition parameters for the 3D seismic survey in OML-23, SOKU

DESCRIPTION	DETAILS
GENERAL	
Recording format	SEG-D
SEISMIC SOURCE	
Energy source	Dynamite(2kg)
Shot Per Salvo	32
Depth	40m
Shot interval	50m
RECORDING SYSTEM	
Instrument:	SERCEL 428XL
Sample Interval:	2ms
Station Unit Type:	FDUI
Low cut filter:	3 Hz/6 dB
High cut filter:	200 Hz
Recording length	8sec
RECEIVER	
Channel per Patch:	1792
Number of Group:	18
Receiver Point Spacing:	50m
Receiver Line Spacing:	400m
Geophone Type	SM4
Processing Data Format	SEG-D DEMUX (IEEE Flt point)
Polarity	SEG
OTHERS	
Measurement System	Meters
Fold coverage	56
Offset Range	25-6000m
Re-sampling rate	4msec
Bin size	25 by 25m
Shot line interval	400m
Receiver line interval	400m
Hole type	Single deep hole

3.3 Identified Processing Problems

The major task of this research is to derive statics solution that would be used in processing 3D seismic data acquired from OML-23, SOKU. Hence the derivation and implementation of statics correction on the seismic datasets is the principal processing challenge the current study seeks to address. However, other minor challenges which could smear and (or) impede the success of the correct implementation of the statics solution to be derived and applied are amplitude compensation and noise challenges. These two challenges were equally resolved before initiating the process of determining the effectiveness and success of the derived statics solution on the shot gathers the stacked and then the migrated sections of the datasets.

3.4 Methods deployed to address the identified processing problems

The major processing challenges of the OML-23, SOKU seismic datasets are;

i) Statics Correction Problem.
ii) Amplitude Compensation Problem.
iii) Noise Removal Problem.

These problems were resolved using the processing strategies described in sections 3.4.1, 3.4.2 and 3.4.3.

3.4.1 Method of solution to the Statics Correction Problem.

The solution to the statics correction problem was solved using the delay time approach on both VISTA™ and PROMAX™ processing platforms. Four key progressive stages were involved in the actual derivation and implementation of the statics correction and these stages are;

i) Field Statics (Datum or Elevation) Correction
ii) 3D Refraction Statics Correction (Delay time Model)

iii) 1st Residual Statics Correction (Max. Power)

iv) 2nd Residual Statics Correction (Max. Power)

Before and after figures would be presented in the subsequent sections to demonstrate the effectiveness and success of the derived and applied refraction statics solution on the datasets.

3.4.2 Method of solution to Amplitude Compensation Problem.

For real seismic data, the amplitude of a reflection is influenced by several factors, including source and receiver, wave front divergence, stratum absorption, formation structure, reflectors, and interference waves. All of these factors make reflections vary in waveform and energy at different reflection positions (shallow, middle, and deep) as well as among different traces and shots. These differences result in obvious effects on the precision of deconvolution, normal move out, statics corrections, and velocity analysis. Consequently, it is very important to perform the amplitude compensation before stacking to compensate for lost amplitude due to the aforementioned factors. The amplitude compensation problem was solved by applying the following procedures.

i) True Amplitude Compensation (TAC)

ii) Surface Consistent Amplitude Compensation (SCAC)

iii) Q Compensation (Q.C)

iv) Residual Amplitude Compensation (RAC)

3.4.3 Method of solution to Noise Problems.

We faced a couple of processing dilemma in selecting appropriate parameters to either mute or attenuate the diversity of noises present on the acquired data from the current prospect. However, best considerations based on already established processing algorithms and previous processing experiences were used as the basis for selecting band pass and other filter types that

were used in tackling the diversity of noise problems identified on the datasets. The processing steps taken to solve the diversity of noise problems that pervaded the SOKU dataset include;

i) Design of Low Cut Filters.

ii) Ground Roll Wave Attenuation.

iii) Coherent Noise Attenuation.

iv) Wild Amplitude Attenuation.

v) Residual Noise Attenuation.

vi) 4D Random Noise Attenuation (RNA)

3.5 Processing steps and sequences adopted

The necessary and relevant processing steps and sequences adopted to enable realizing the processing objectives are itemized below:

1. Field Data Loading/Format Conversion (4ms) and Data Display
2. Geometry Definition/Merging/Binning/LMO
3. First Break Picking/First Break Quality Control Model
4. Analysis of First Breaks and Refraction Statics Calculations/Applications
5. PSTM Bad Shot/Trace Editing
6. Amplitude Recovery
7. Deconvolution (Pre-stack Noise removal)
8. Surface Consistent Amplitude Compensation
9. Q. Compensation (Phase only, optional)
10. Deconvolution (SCDC)
11. 1st Velocity Analysis
12. Residual Noise Attenuation

13. Residual Amplitude Scaling
14. 2nd Velocity Analysis (1km grid)
15. 1st Residual Statics
16. 3rd Velocity Analysis (1km grid)
17. 2nd Residual Statics
18. 4D RNA Applications
19. *Tau-P* Deconvolution
20. CDP to G Depth
21. F-X (Explicit) PSTM Velocity
22. 3D Volume F-X (Explicit) Migration
23. Migrated Stack Generation
24. Post Stack FXY
25. Zero Phase Conversion
26. Final Display (Filter/Scaling)

3.5.1 Field Data Loading / Format Conversion and Data Display

Field seismic data recorded on 3592 cartridge tape in SEG-D format was received, then loaded and converted to Geo-East Internal Format (on Promax™) and SEG-Y (on Vista™). The field seismic data was resampled from 2ms to 4ms after it was loaded. The acquired 3D seismic data from the prospect field were loaded using appropriate flow commands (Disk Data Input) on Promax™. In executing the Disk Data Input flow, all the header details like trace numbers, channel numbers, Field File Identification (FFID) were taken into account. After the loading procedure, the raw shots acquired from the prospect were displayed and inspected. Figure 3.2 shows a display of the raw shots from in-line 79 in FFID and channel number order.

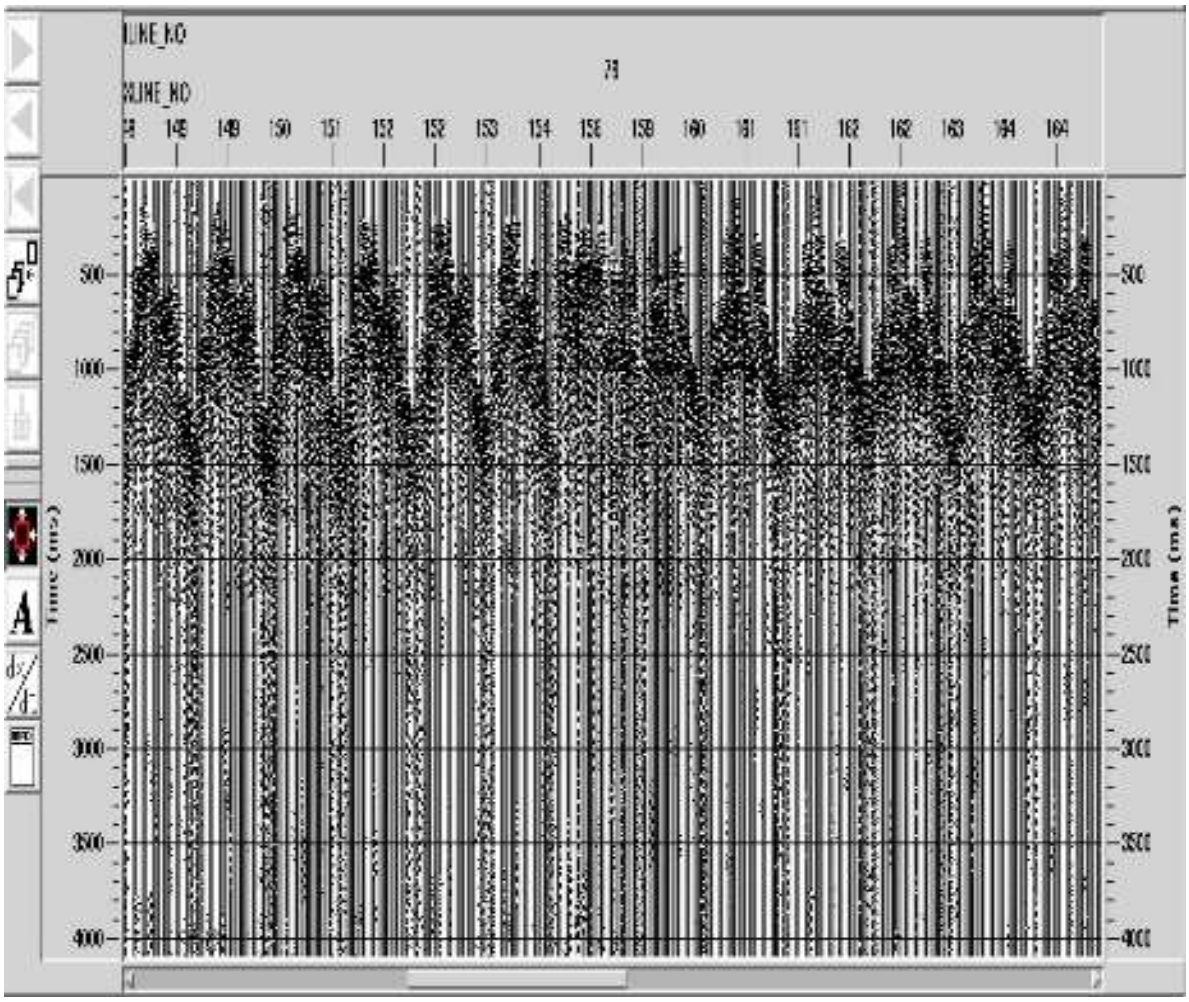

Figure 3.2: Display of raw shots from In-line 79 in FFID and channel number order

3.5.2 Geometry Definition/Merging/Binning/LMO

Graphical Geometry Quality Control (QC) is a special way to quickly find errors in the assignment of geometry. The process applies linear move-out to shots and slices multiple shots together in a vertical fashion based on receiver surface station. The geometry file for the prospect was equally loaded. All details that relates to receiver files, source files and relation files were all entered into a special spread sheet to load the geometry. Thereafter, QC was performed (Figure 3.3) for the loaded geometry to identify and correct possible errors associated with wrong loading of geometry. The QC check showed that geometry was properly loaded as evident from the control line (the green lines).

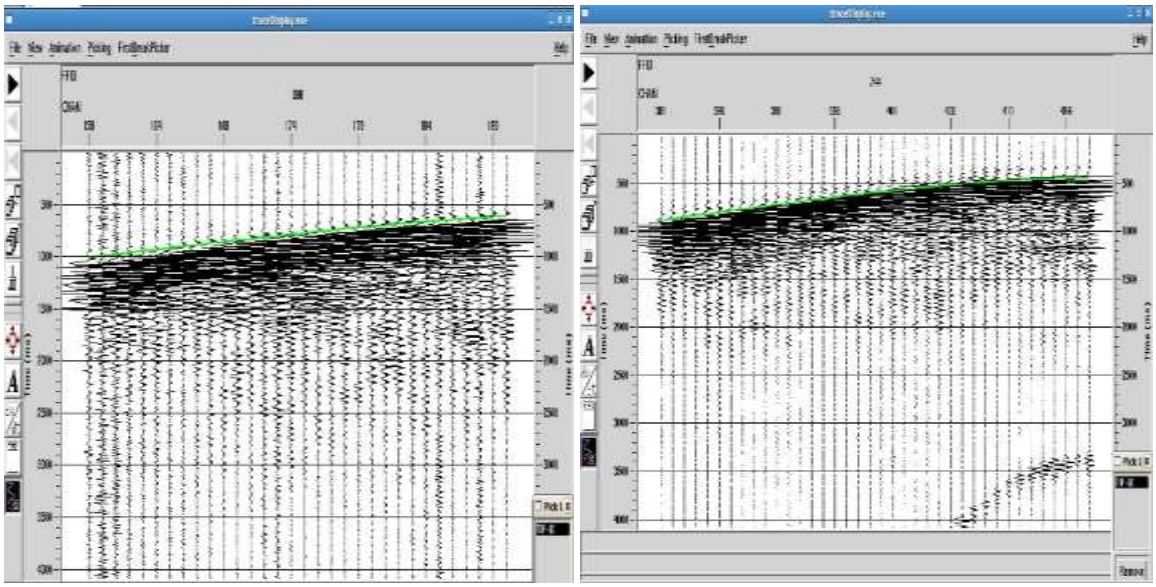

Figure 3.3: Quality Control (QC check) performed on loaded geometry from the field.

The merging of the loaded 3D seismic data file (raw shots) and the loaded geometry (source-receiver- relation, SPS files) was subsequently performed. Linear Moveout (LMO) and LMO QC were equally performed (Figure 3.4) and preliminary frequency spectral analysis of the data to ascertain the frequency and power/energy content of the data (Figure 3.5).

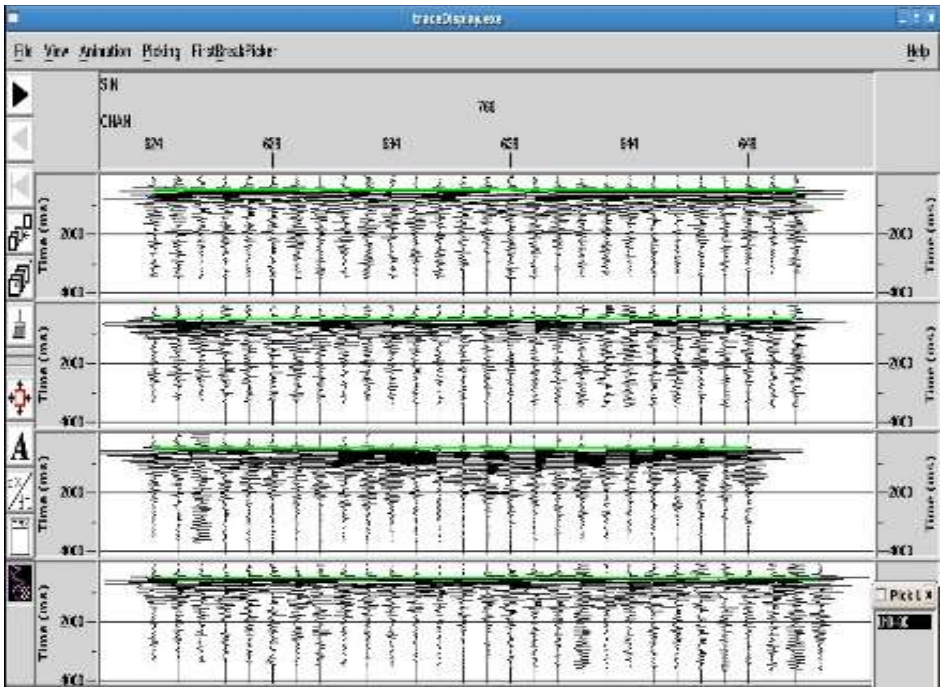

Figure 3.4: Linear Move out (LMO) – QC check performed was satisfactory

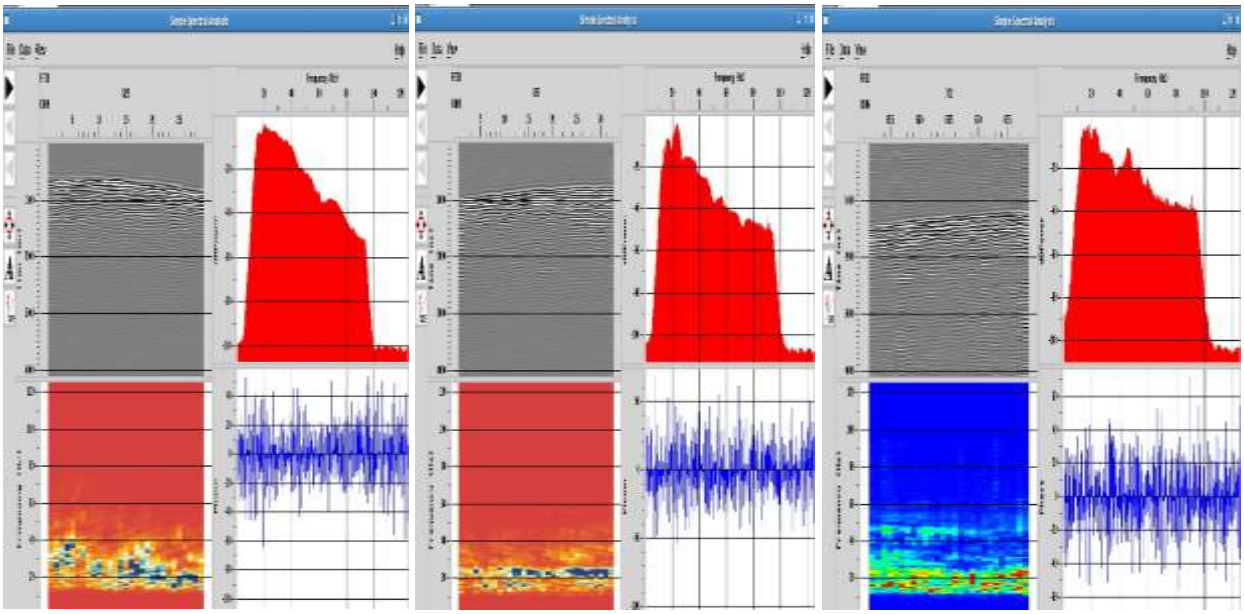

Figure 3.5: Frequency spectral analysis performed for different sections of the data showing the appreciable amount of energy embedded in the acquired data.

3.5.3 First break Picking / First break Quality Control Model

In seismic data processing, first break picking is the task of determining as accurately as possible, the onset of the first signal arrivals from a given set of seismic traces (Sabbione and Velis, 2010). Generally, these arrivals are associated with the energy of refracted waves at the base of the weathering layer or in other instances, the direct wave that travels directly from the source to the receiver. The correct determination of the onset of first arrivals (first break times) is the required and key input parameter for the inversion procedure to image or model the near-surface. The travel time of an arrival could be determined by identifying the point on the trace, when the effects of the seismic wave first appear, this procedure is called picking and the end result is known as a pick, and a wiggle trace is usually the best form of display to work with. Recognizing the onset of an arrival involves identifying a change or break as it were, in the character or appearance of the trace from its pre-arrival state, in terms of amplitude, and/or frequency, and/or phase (Lankston, 1990). The picking of the first breaks was done using an automatic routine after defining appropriate time gates (time gate functions) (Figure 3.6).

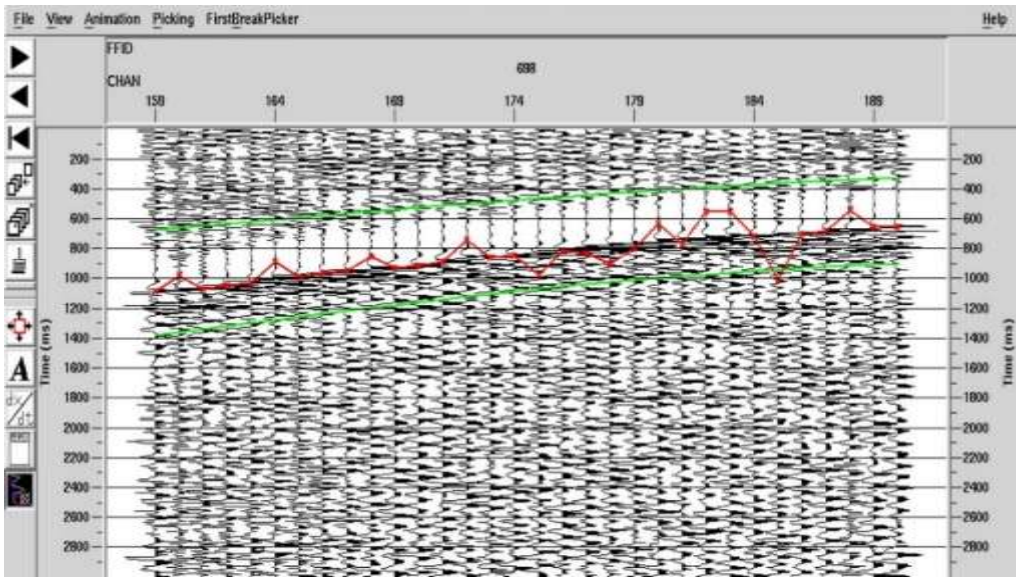

Figure 3.6: The automatic first break picker routine display for Channel 698. The red points are the point of picks by the routine whereas the green border lines represent the time gates defined.

The picks were later on manually edited with utmost care since time shifts due to travel time errors would ultimately lead to non-reliable models of the sub-surface (Bais *et al*., 2003). Figure 3.7 is the edited first break pick for the channel 698 within the defined time gates.

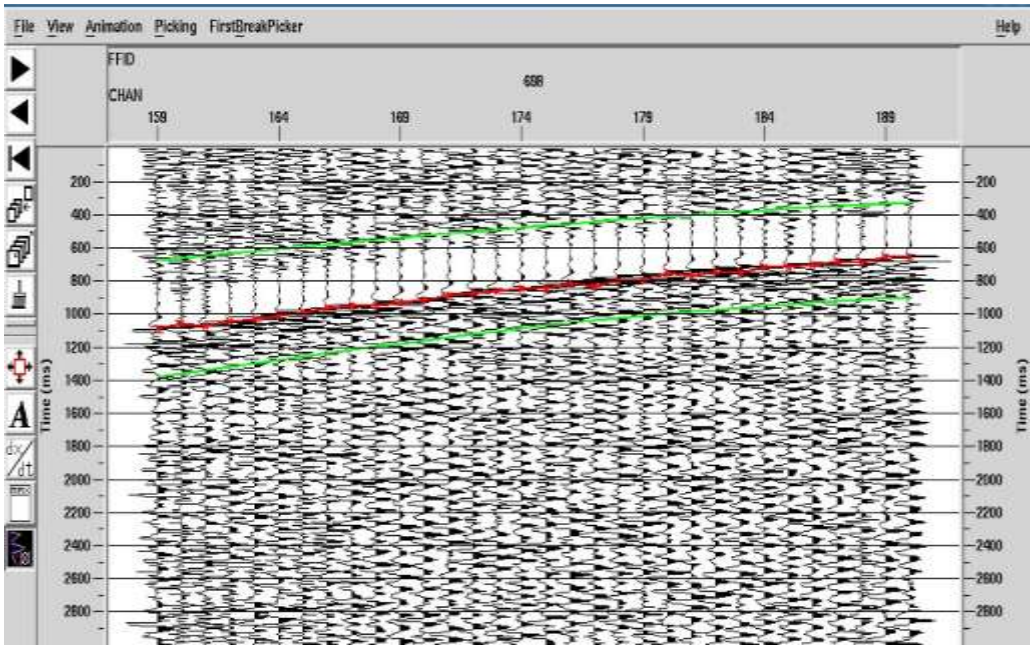

Figure 3.7: The edited automatic first break picker routine display for Channel 698. The red points are the point of picks, which have now been properly aligned to the onset of the first break for all the traces within this channel. The green border lines represent the time gates defined.

Standard quality control (QC) checks were performed for the picks over the prospect (Figure 3.8), showing that the travel times were sufficiently accurate and could be inverted appropriately to yield a reliable and close to accurate near-surface model, which is one of the key objective for the present study.

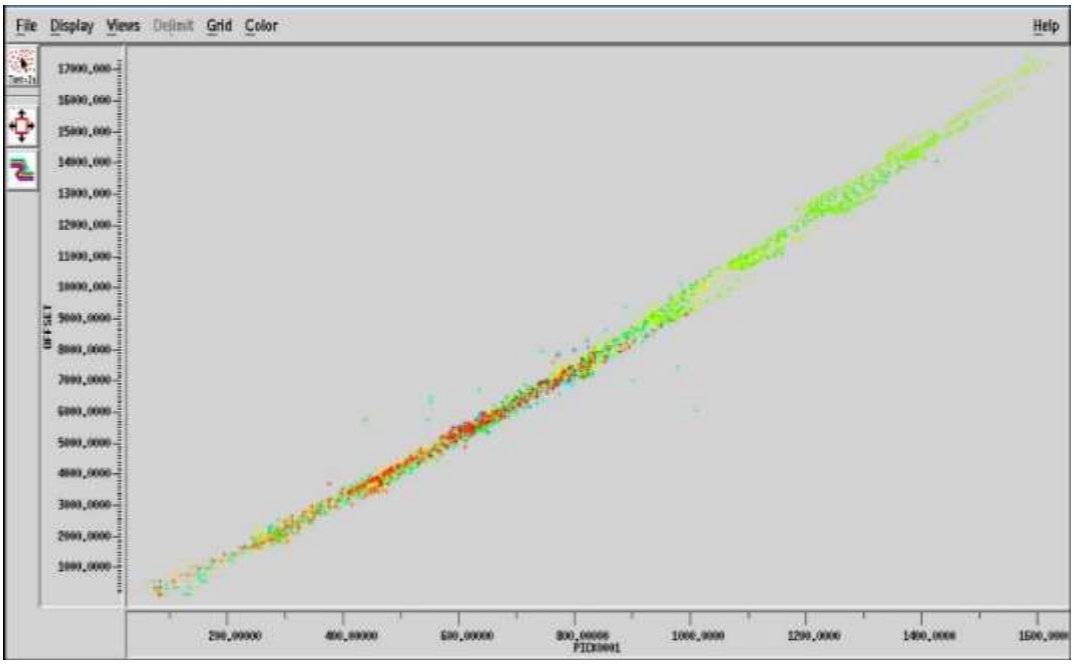

Figure 3.8: The first break pick QC model for the prospect. The near linear cluster of the picked points is a positive indicator that picks were accurately done and could be used as input parameter for a reliable inversion to model the near-surface.

First-break picks associated with the refracted arrival times were used in an inversion scheme to study the near-surface low-velocity zone and in subsequent determination of the statics corrections. Static correction is a correction applied to geophysical (seismic) data, to compensate for the effect of near-surface irregularities, differences in the elevation of shots and geophones, or any application to correct the positions of source and receivers. First breaks were initially picked automatically and then manually edited. The refraction arrival (first break) inversion was integrated with uphole measurements using special processing plugins (add-ons) to build a more reliable near-surface model which eventually would result to an accurate derivation of the refraction statics solution.

3.5.4 Refraction Statics Calculation/Application

Differences in first-arrival travel times between adjacent records in multifold reflection surveys can be used to compute the depth and velocity structure of near-surface layers. The procedure uses the redundancy of first-break data in multifold surveys to enable a statistically reliable refraction analysis to be undertaken for either end-on or split-spread recording geometries. The travel time differences as a function of source-receiver offset provides a direct indication of the number of refractors present, with each refractor being defined by an offset range with a constant time difference. These parameters were crucial to the proper estimation of the refraction statics correction.

3.5.5 Bad Shot Trace Edit

Every shot was checked and bad traces were edited and (or) muted off with the aid of Promax^{TM} and Vista^{TM} processing routines/modules.

3.5.6 Amplitude Recovery

The raw shot records showed how the amplitude (energy content) level of the raw data decayed rapidly with depth due to transmission losses and wave front divergence. To correct this, standard amplitude compensation routines were applied in order to optimize the processing objectives of the study and obtain the best results.

3.5.7 Pre-Stack Noise Removal

Based on the spectral analysis, the dominant frequency range and velocity of linear noise was identified. Based on the frequency and velocity differences, the linear noises were effectively attenuated. The noise classes that were attenuated from the datasets included coherent noise (predominantly ground rolls), wild noise with some patches of random noise imprints. This was performed to boost the signal to noise ratio (SNR). To achieve the noise attenuation objective,

the seismic data was transformed from time-space domain to frequency-space domain; the linear noises were then separated and effectively suppressed, while frequency component outside the defined range remained unaffected. After the noises were attenuated, we again transformed back the datasets to the conventional time – space domain and an appreciable noise attenuation result was achieved.

3.5.8 Surface Consistent Amplitude Compensation (SCAC)

SCAC is a pre-stack amplitude compensation module which removes the trace energy differences resulting from the source and/or receiver conditions. It first performs the geometric divergence and absorbing coefficients compensation and then the surface consistent amplitude equalization. The pre-stack single trace equalization is the only process or means by which relative amplitude preservation can be achieved. The geometric divergence and absorbing terms could not be accurately (100%) compensated due to inexact absorbing coefficients and velocity functions.

3.5.9 Q Compensation

Phase-Amplitude Q Compensation applies accurate, but slow, temporally and spatially variant Q compensation to seismic data. This compensation may be optionally limited to phase-only or amplitude-only corrections. No migration of the data is performed at this stage. This module employs modifications of the well-known F-K phase-shift and Stolt migration algorithms.

3.5.10 Surface Consistent Deconvolution

Deconvolution is a very important processing stage in seismic data processing. It is applied to attenuate (or remove) multiples and their attendant ringing effects on seismic data, compress wavelet and improve the vertical resolution of the obtained imaging output. In order to achieve optimum results, different deconvolution parameters were tested. The deconvolution gaps of

4ms, 8ms, 12ms, 16ms, 20ms, and 24ms were tested and eventually the 12ms gap was chosen as it gave the best vertical resolution. We equally tested operator lengths of 160ms, 200ms, 240ms, 280ms, and 320ms but also settled for 240ms. Additional white noise (0.01%) was also tested. Predictive deconvolution tests were also run but surface consistent deconvolution was implemented.

3.5.11 Horizon Consistent 1km by 1km Velocity Analysis

Stacking velocities were picked from velocity analysis run on selected in-lines across the investigated prospect. The lines were selected to form a 1km x 1km grid of velocities. The velocities were generally well behaved and had a consistent trend. When all the velocities were picked, a variety of quality control procedures were performed on the data. NMO (Normal Move out) was performed on the gathers for each of the lines using the picked velocities to check the resulting 'flatness". Stacking panels were displayed to adjust the velocity slightly. It was ensured that all the gathers were monitored and checked properly for enhanced imaging at their appropriate positions.

3.5.12 Residual Noise Attenuation

This module helped to remove residual dominant noise imprints on the datasets (both coherent and incoherent) remaining after the initial noise attenuation routine on the data. Frequency content of the data was carefully taken into account while applying this module to preserve the primary reflections.

3.5.13 Residual Amplitude Scaling

Residual amplitude scaling is a step in seismic data processing to compensate for amplitude attenuation, spherical divergence and other associated effects by adjusting the amplitude of the data. The end goal of this routine is to get the data to a state where the reflection amplitudes

relate directly to the change in rock properties giving rise to them. Two processes were involved here; Residual amplitude analysis, which used statistical methods to establish compensation functions in a large spatial range of offset and common midpoint (CMP), and then the Residual amplitude compensation, which applies the compensation function established from the residual amplitude analysis to the datasets.

3.5.14 2nd Velocity Analysis 1km x 1km Interval

Guided by the first velocity analysis, the second velocity analysis was performed. Stacking velocities were picked from velocity analysis run on selected inlines across the investigated prospect. The lines were selected to form a 1km x 1km grid of velocities. The velocities were generally well behaved and had a consistent trend. When all the velocities were picked, a variety of quality control procedures were again performed on the data. NMO was applied to gathers for each of the lines using the picked velocities to check the resulting 'flatness". Stacking panels were displayed to adjust the velocity slightly.

3.5.15 Residual Statics

Although datum statics corrections were applied to remove travel-time effects of elevation changes along the seismic line, it was still necessary to remove residual near-surface travel-time delays that are the result of varying velocity and/or varying depth of the weathering layer. Promax™ offered several residual statics applications and all were surface consistent solutions.

3.5.16 4D Random Noise Attenuation (RNA) Applications

This module on Promax™ performed 3D Pre-stack Random Noise Attenuation based on F-XYZ domain predictive noise removal in 3D frequency domain; it used the least square theory of multi-channel complex number to calculate a 3D predictive operator, and then, uses the calculated operator to perform predictive filtering on the 3D seismic data volume so as to

attenuate the random noise. Random Noise Attenuation operates and deals with noise in four domains, that is CMP, Offset, Trace and finally in the Time domain. The aim is to produce high resolution datasets and remove unwanted noise on the data as much as possible, to boost the signal to noise ratio (SNR).

3.5.17 Tau-P Deconvolution

Tau-P domain based deconvolution was carried out on the dataset. It was observed that Tau-P deconvolution with an operator length of 320ms and gap of 28ms produced the optimal result. The purpose for using this processing module on Promax^{TM}, was for the purpose of multiples suppression and to remove unwanted noise from meaningful reflection signals, to produce an unambiguous processed output that is most desirable for an accurate and reliable interpretation of the subsurface structures.

3.5.18 Pre-Stack Time Migration.

The CMP gathers for pre-stack migration required that the gathers be devoid of statics problems, have high signal-noise ratios (SNR) with good energy balance. After pre-stack signal processing, the CMP gathers were ready for pre-stack migration. For reflection imaging of different dip with different stacking velocity, pre-stack time migration became an ideal method to be implemented. At present, pre-stack time migration is rapidly developing and fast becoming the choice technology for seismic migration imaging. It plays important roles in imaging fine structural features which could be associated with traps in the search for potential hydrocarbon (oil and gas) reservoirs. The advantages of pre-stack time migration include;

i) The migration algorithm makes use of the root-mean square (RMS) velocity. This RMS velocity field is relatively easy to adjust.

ii) Pre-stack time migration is the good imaging tool for inhomogeneous media, such as the

currently investigated prospect OML-23, SOKU and it is about the most accurate imaging technique for time domain migration.

The processing sequences entailed in executing pre-stack time migration routines involve the following;

i) Generating an RMS velocity field using stacking velocity and then creating an RMS velocity volume.

ii) Pre-stack time migration using RMS velocity volume by ray-tracing method on the target lines.

iii) Analysing the updated velocity on the pre-stack time migrated gathers of target lines and then updating the velocity field.

iv) Re-generating the velocity volume using updated RMS velocity field.

v) Re-running Pre-stack Time Migration (PSTM) on target lines with new velocity volume;

vi) Repeating steps (i) – (iii) until events in CRP gathers are flattened.

vii) Running PSTM on the whole 3D dataset and outputting all CRP gathers.

viii) Final Mute and stack

3.5.18.1 Migration Velocity Field establishment and Optimization in Pre-stack Time Migration

The migration velocity field determines the diffraction path during the execution of the migration routine and ultimately determines the correctness and accuracy of subsurface imaging. Therefore, the correct basis for executing an optimal pre-stack time migration processing, is anchored on the establishment of an accurate migration velocity field. The migration velocity field optimization sequences involve;

i) Stacking velocity being converted to RMS velocity.

ii) Performing Pre-Stack Time Migration to output CRP gathers.

iii) Running updated velocity analysis with CRP gathers.

iv) Creating a new RMS velocity field and performing the next iteration of Pre-stack Time Migration.

v) Repeating steps (ii) – (iv) to obtain an accurate RMS field for Pre-stack Time Migration.

Migration velocities were picked and updated on selected target lines. The lines were selected to form a 500m x 500m grid of velocities.

3.5.19 PSTM Velocity Analysis

Residual velocity analysis, including second-order and fourth-order based approaches were implemented. This was to correct for residual move-out at large offsets, by estimating weak anisotropy to enable exploitation of the data at very large offsets, than is ordinarily feasible with second-order techniques.

3.5.20 3D F-X (Explicit) PSTM

Promax^{TM} possesses an amplitude-preserving F-X (Explicit) Pre-stack Time Migration (PSTM) routine that is ideal for imaging complex geologic conditions or velocity fields, and does not require employing pre-stack depth migration to meet imaging goals. This module is not limited to the straight ray approximation as is the case for most other PSTM processing tools that use the two-term double square root equation. The applied migration routine accounted for higher order terms in the travel time versus offset and NMO expansion by explicit ray tracing. The routine could also have been used to iteratively build the 3D RMS velocity field through target outputs in the form of in-lines, cross-lines, common receiver point (CRP) gathers and full 3D volumes.

3.5.21 Migrated Stack Generation

This processing module basically involved the generation of the final migrated stack.

3.5.22 Post Stack FXY Deconvolution

To further enhance the data quality F-XY Deconvolution was applied to the migrated gathers. The Mixing parameters for the F-XY Deconvolution with their time ranges (Table 3.2) was carefully tested and optimized. The Mixing parameter and the time ranges for which they were applied on the migrated gathers and with their associated mix percentages are shown below;

Table 3.2: Table of Mixing Parameters and Time ranges for F-XY Deconvolution

Parameter	Time (ms)	Mix (%)
Mixing	**500**	**70**
	900	**75**
	2400	**80**
	3000	**70**
	5200	**80**
	6000	**90**

3.5.23 Zero Phasing Conversion

The data for interpretation should be zero phase. In theory, zero phase data would normally have a higher resolution. After analysis and tests, the data was converted to zero phase with the aid of the zero phasing filter factor extracted from the dataset. This step was to transform the minimum phase wavelet of the seismic data into a zero phase wavelet that has the same amplitude spectrum.

3.5.24 Final Display Filter Scaling

A time variant scaling function was tested and applied to the seismic data to ensure that the amplitude of the data becomes reasonably balanced. To further suppress traces of undesirable noise and to increase the SNR, a Time Variant Filter (TVF) was tested using Band Pass Filtering. After test evaluations, the following TVF parameters (Table 3.3) were applied to the dataset.

Table 3.3: Table of Time Variant Filter Parameters applied during Time Variant Scaling

Application Time (ms)	Band Filter (Hz)
0 – 1200	**8 – 15 – 45 - 60**
1500 – 2700	**7 – 12 – 40 - 60**
3000 – 6000	**6 – 10 – 24 - 30**

3.5.25 Spectral Whitening

Spectral whitening which is also known as (broadening or balancing) is used to improve the resolution and appearance of seismic data and is a quick means of attempting to correct for possible frequency attenuations. This routine was carefully and thoroughly implemented on the dataset, to recover attenuated frequencies.

3.5.26 SEG-Y Out

This process offers the means of displaying or outputting a SEG-Y disk image file.

3.6 Data Preparation and Pre-processing (First Processing Stage)

In this first processing stage of the research, the data was binned using the geometry/SPS files, before picking the Linear Move Out (LMO) velocity, then picking the first breaks and finally, performing quality control analysis on the picked first breaks.

3.6.1 3D Seismic Data Binning

The process of binning 3D seismic data is simplified if one transforms from the survey's spatial coordinates to a binning coordinate system. For uniform rectangular bins, this transform along with an integer truncation which is all that is required to assign bins for a survey (Mark, 1994). When a multi-fold 3D seismic survey is acquired, a major step in its processing is the assignment of each seismic trace to an areal bin. Bins represent local areas on the earth's surface which are used to collect traces for stacking, processing or analysis. Due to the two dimensional nature of 3-D seismic survey geometries, locations of interest generally do not fall on a set of surface points, but tend to scatter throughout the survey area. Binning is the act of asserting that a group of traces contains a common geometrical property, usually that of being close to the same common mid-point (CMP) shot or receiver position. A binning system is defined by the boundaries of a uniform rectangular grid. All traces whose surface locations fall within the

same cell of this grid will share the same bin. Each Binned Grid had an approximate dimension of 25m × 25m with a lock spacing configuration (Figure 3.9a). The Binning information was subsequently saved to the file headers and used to generate the Binning grid (Figure 3.9b), when appropriate processing flows were executed on Vista™ and Promax™ platforms.

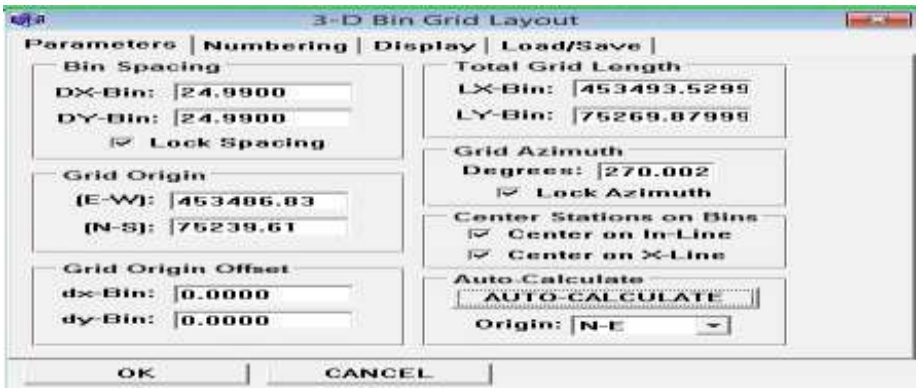

Figure 3.9a: Binning grid parameters

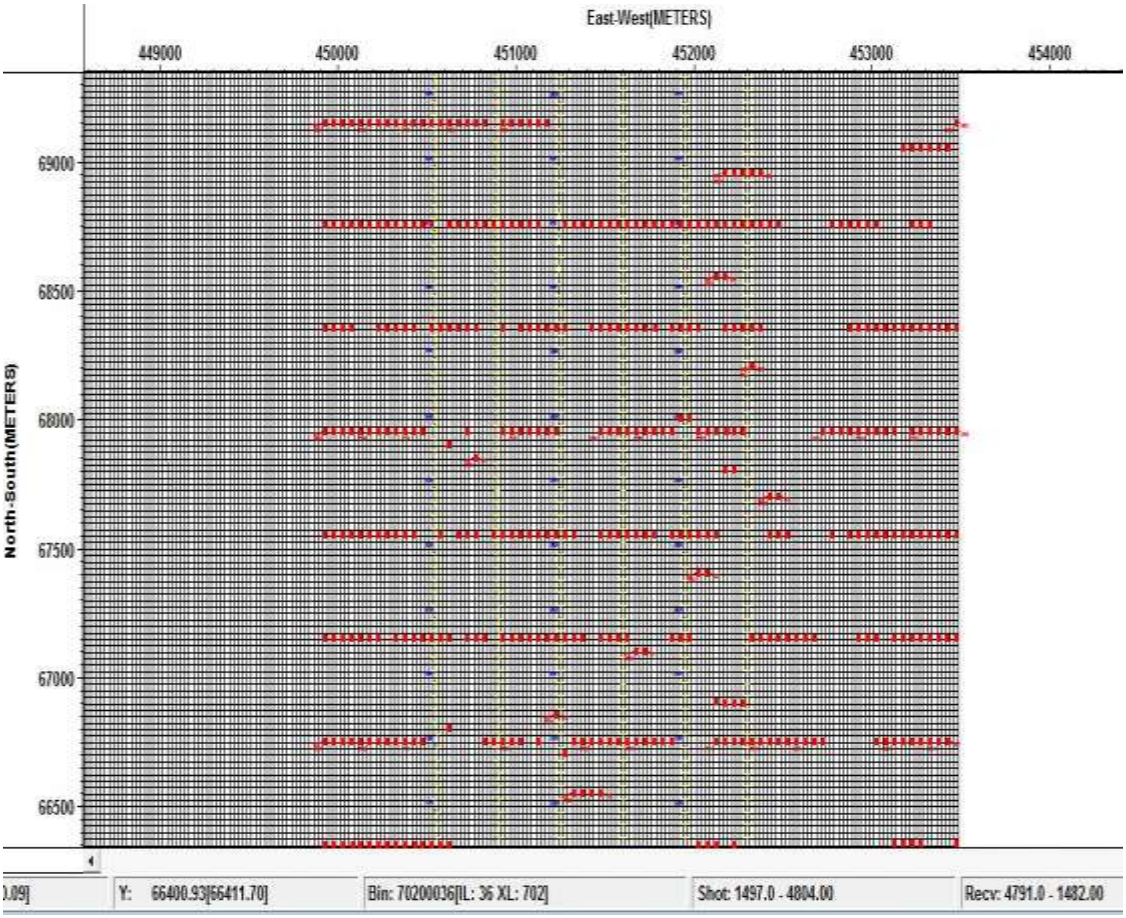

Figure 3.9b: Binning grid (black) defined by source lines (red) and receiver lines (blue)

3.6.2 Fold Calculation and Analysis

In addition to binning the data, the fold associated with a particular 3D stacking bin was equally computed. The fold which is also called multiplicity is simply, the number of times that the same midpoint is sampled by different shots and different receivers. It is a measure of the redundancy of common midpoint seismic data and is equivalent to the number of offset receivers that record a given data point or in a given bin that are added during stacking to produce a single trace. Typical values of fold for modern seismic data range from 60 to 240 for 2D seismic data, and 10 to 120 for 3D seismic data. For the SOKU dataset, a fold value of 42 was obtained which is within the recommended range for standard 3D seismic data processing. It was observed that the fold gradually increased from a minimum (at the edge of the Bin) to a maximum (at the centre of the Bin), which is the most desirable pattern or trend (Figure 3.10).

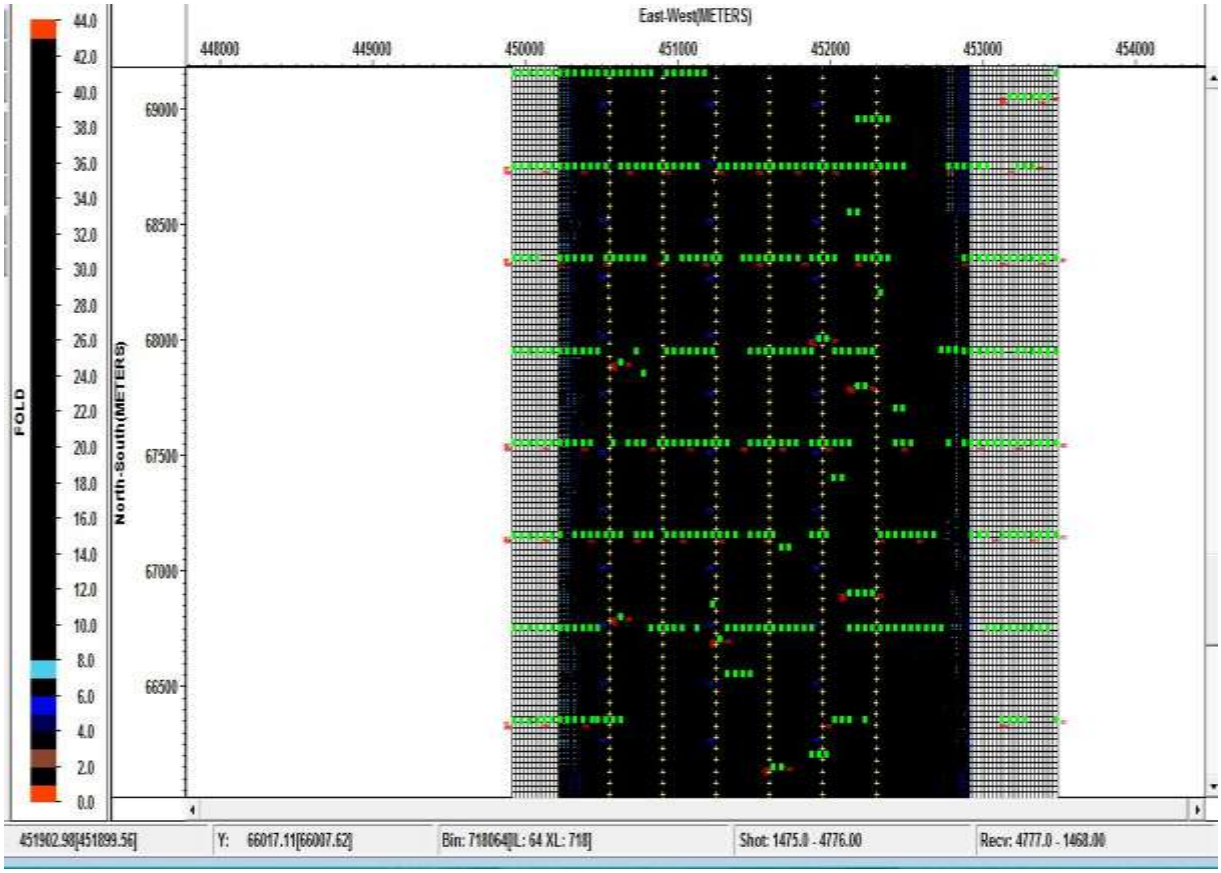

Figure 3.10: The fold computed for the OML-23 SOKU dataset had a fold value of 42.

3.6.3 Linear Move out (LMO)

One common error mostly encountered in the pre-processing stages is that of wrong identification of shot point location. It could also be possible that the wrong receivers are active (picked). The other possible error could be wrongly identified locations of the receivers. The Linear Move out (LMO) is a vital tool to identify these errors in the geometry. LMO compares arrival times recorded for the given source-receiver geometry to those calculated assuming a constant velocity surface. Pre-processing quality control should include these geometry checks; these were performed in the current study (After Burger *et al*., 1998) with the sole aim of enhancing seismic data quality in the pre-processing stages. Beckett *et al*., (1995) pointed out the use of LMO to identify geometry errors at the pre-processing stages to reduce the overall seismic data processing turnaround time. The generally adopted method is to apply LMO and check for the departures from the LMO. These departures signify the error in the location of the receivers or shot point. In this stage, the LMO pick icon was used to pick the LMO velocity from a single shot, after which it was saved to the file header, and used as input to run an LMO processing flow on the entire seismic dataset (Figures 3.11a and 3.11b) using appropriate LMO functions (Figure 3.12).

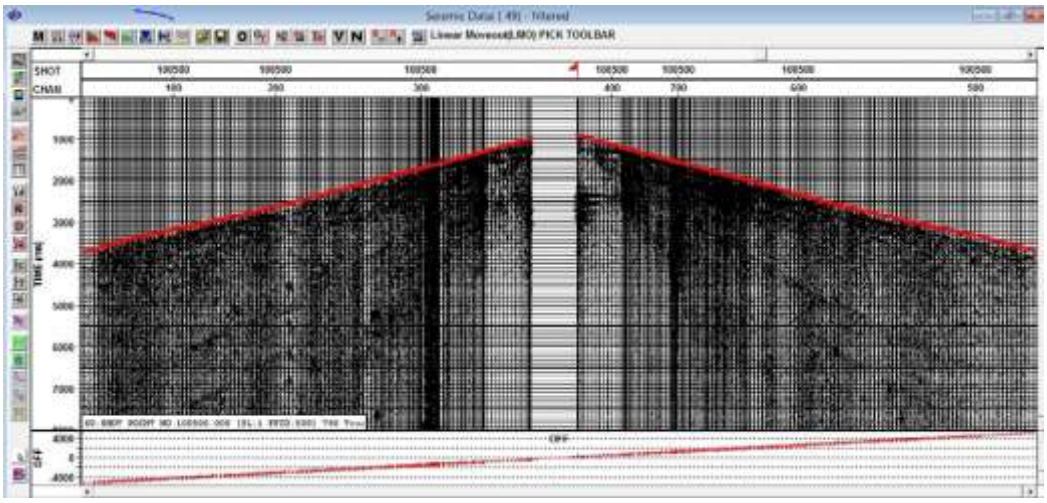

Figure 3.11a: LMO velocity (Red Lines) as picked on the data set

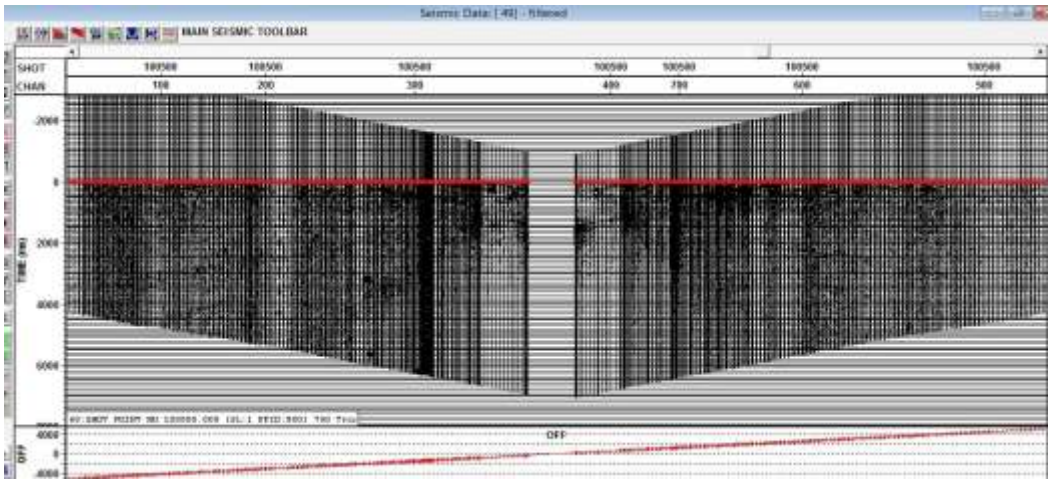

Figure 3.11b: Flattened LMO (velocity in red). The first breaks are parallel to the LMO.

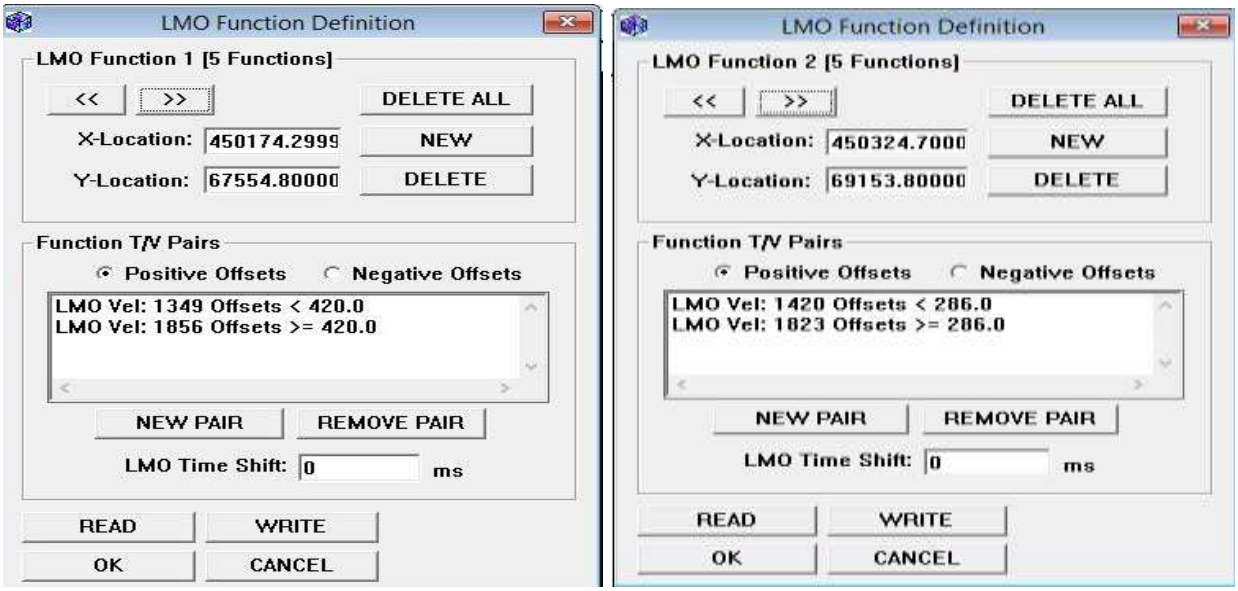

Figure 3.12: LMO velocity functions picked from the shot record.

3.6.4 First-Break Picking and Analysis

In seismic data processing, first-break picking is the act of accurately determining, given a set of seismic traces, the onsets of the first signal arrivals. In general, these arrivals are associated with the energy of refracted waves at the base of the weathering layer or to the direct wave that travels directly from the source to the receiver. The accurate determination of the first arrivals onset (first-break times) is a crucial requirement for calculating statics correction, which

is a fundamental and vital stage in the seismic data processing workflow. Clearly, the effectiveness of refraction-based methods of statics correction depends on the picking-process reliability (Yilmaz, 2001). Naturally their arrival time increases with increasing offset. The onshore SOKU dataset was acquired using dynamite sources, such impulsive sources tend to yield fairly clear signals. Using the first-break picking module of the processing software, the first-break picking was in the first instant performed manually for a few shots and then subsequently, using the automatic picker flow command with the LMO function (Figure 3.13) to pick the entire portion of the dataset for first-breaks and the results were corrected interactively via visual inspection.

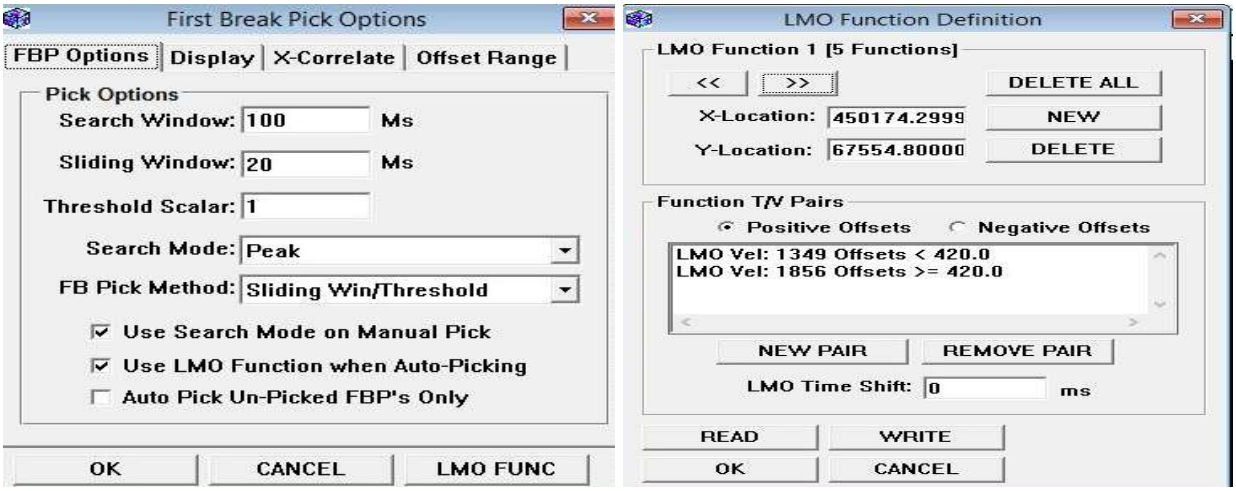

Figure 3.13: Parameterization of the First break picking module

The first-breaks of the shot records over the prospect was properly picked and with minimal errors. These errors are assumed not to be present when picks are scattered throughout the data (Figure 3.14a) and are not congested or clustered in a particular area. Congestion of first-breaks in a particular region in the first-break quality control X-T plot is an indication of poorly picked first-breaks. In general, the maximum standard deviation should be less than 20, and the average of the errors for all shots should be around 10. However, in practice, errors are often caused by

geometry or picking error. In this case, the utility indicates the deviation error range for all the first-breaks and how they are distributed (Figure 3.14a and 3.14b). The first-break pick (FBP) standard deviation color codes signify different errors and distributions in the picked geometry line, varying from a range of 0 (in blue) to 14 (in orange). Shots with larger reciprocal errors are distinct and this offers a seismic data processor an opportunity to refine the first break picks shot by shot at areas where the errors are observed. Figure 3.15 shows the picked first-breaks display on the seismic dataset.

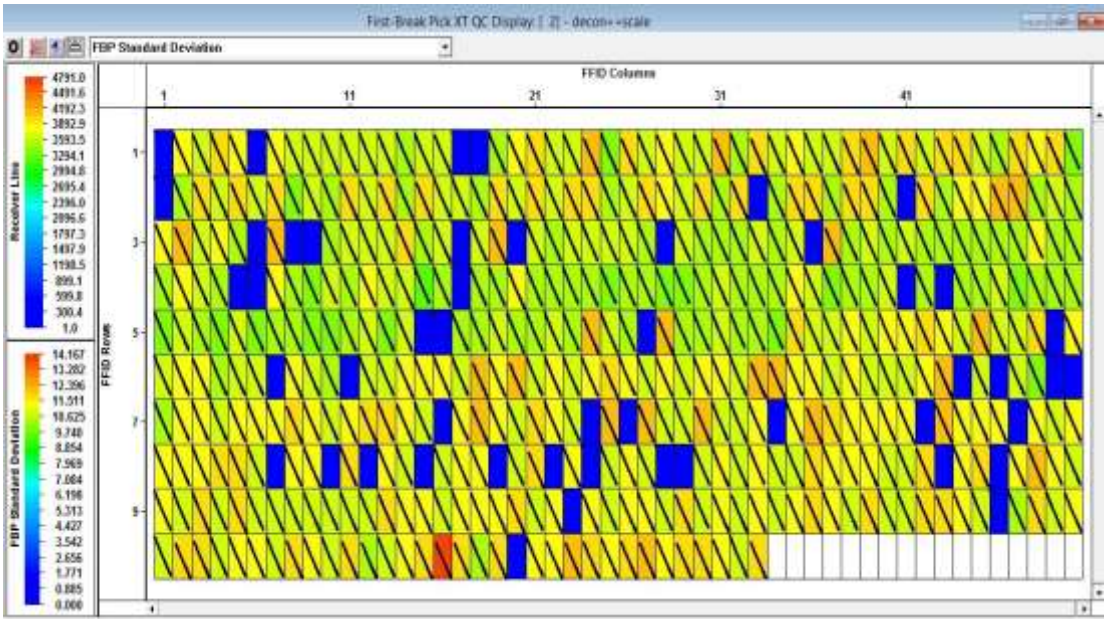

Figure 3.14a: First-breaks Quality Control X-T Plot

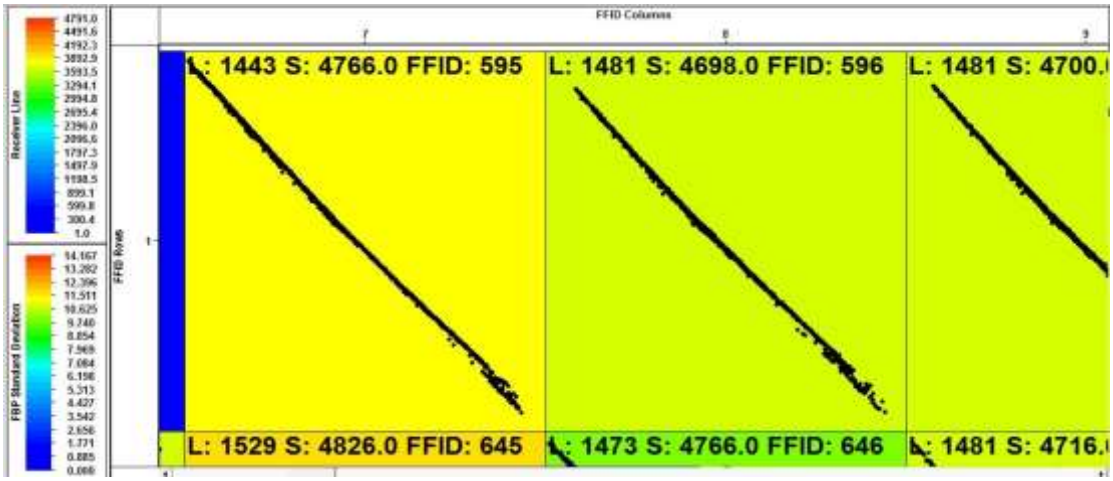

Figure 3.14b: First-breaks Quality Control X-T Plot.

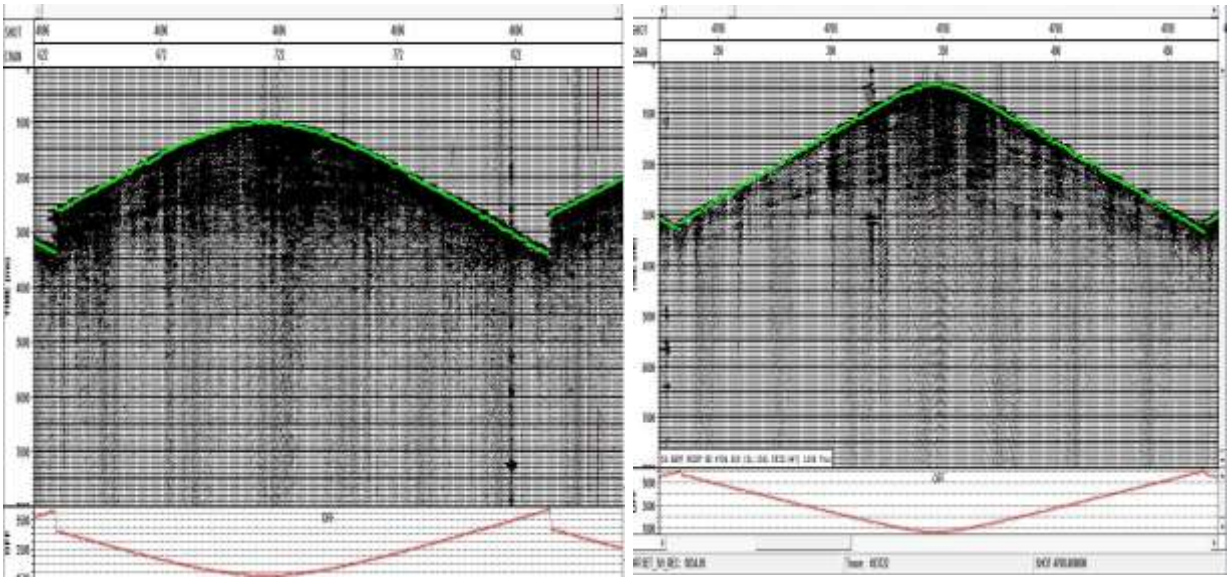

Figure 3.15: First break picks display on the pre-stack seismic dataset for OML-23 SOKU.

3.7 Refraction Data Processing (Second Processing Stage)

The refraction method is widely used in determining the thicknesses and velocities of the near-surface layers. It requires an accurate picking for the first arrival times. The Elevation/Refraction statics program analyses the relationship between the seismic data and first-break picks which have been saved to the file headers. It uses this relationship to estimate a velocity and depth model at all location within the survey area. The general refraction statics procedure consists of firstly, picking a control point (either source or receiver point) across the survey area, and visually checking the corresponding picks for any form of scattering and deviations from the gather, after which, the velocity of the layers are picked along the first breaks within the offset window. Secondly, control points were automatically generated all over the survey area, based on the initial manually picked control points. Having found the results desirable, we proceeded to generate the various velocity and depth profiles for the various layers within the investigated prospect with the aid of the processing tool. The 3D refraction statics parameters (Figures 3.16a and 3.16b) for a 3-layer sub-weathering case was

applied, using a weathering layer velocity of 520m/s obtained from the up-hole survey measurement for SOKU. A refractor replacement velocity of 1750 m/s was used. The desirable range of replacement velocities for onshore Niger Delta Basin datasets is within 1700 - 1850 m/s. A datum elevation of 0 m, a model time range of 350 ms (value was selected based on the width of first-breaks), and a minimum and maximum offset of 20m and 6800m respectively were used to derive the elevation and refraction statics. The shortest offsets (< 50m) were excluded from the calculation because they are most likely emanating from direct arrivals instead of refractions. Similarly, the longest offsets (> 6800m) were also excluded because the signal to noise ratio tends to decrease with increasing offsets and at some point might not be high enough to ensure accurate picks.

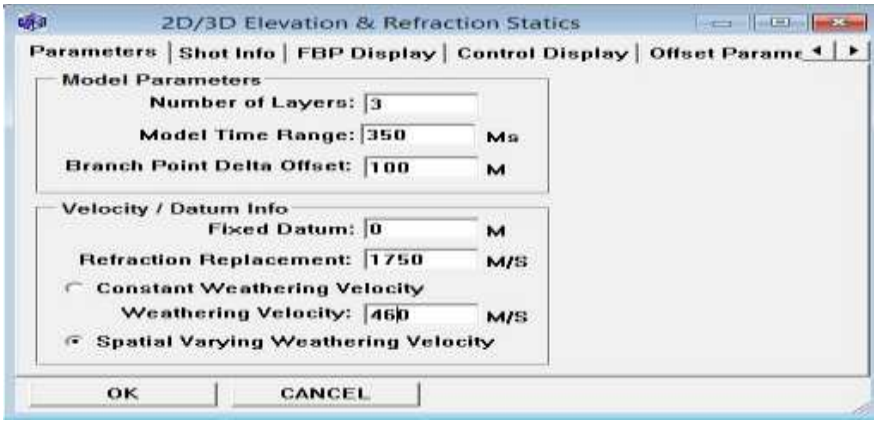

Figure 3.16a**:** 3-D elevation/refraction statics velocity parameters

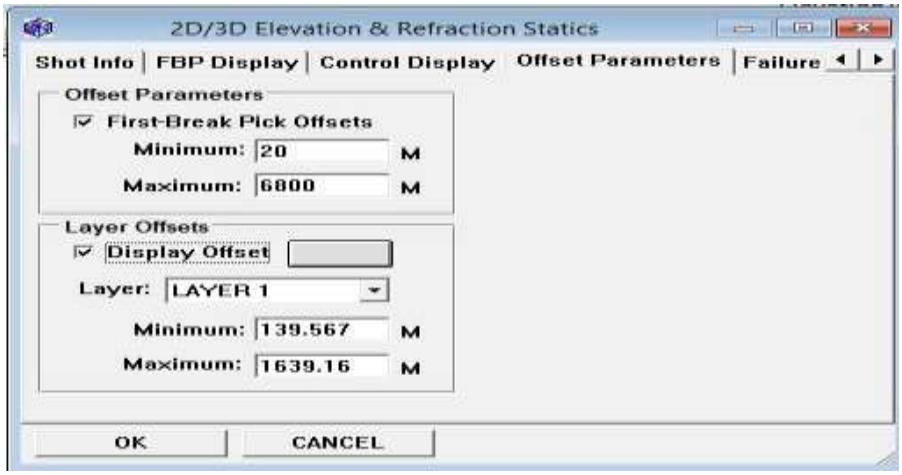

Figure 3.16b: 3-D elevation/refraction statics offset and layer parameter

3.7.1 Control Points and Model Building

In this procedure, one first defines a series of control points in the geometry window. Each control point is typically a collection of many shots (10 to 20) - or groups of receivers. The control points are spread around the survey area and attempts were made to get a reasonably accurate long wavelength picture of the near surface layers. An increment in the number of shots inside the circle will have a smoothing effect on the solution, once the circle has been drawn; an Offset-Time (X-T) plot of the first breaks for the shots inside the circle should be seen on the right panel (Figure 3.17). If the result is as desired and reasonably smooth, the layer velocities for the control point along the marked first breaks is then picked (Figure 3.18).

The number of layers depends on the number of the different slopes that can be observed in the first breaks. The radius for automatically generating the control points could be adjusted (Figure 3.19) to any desired length. A 100m radius was chosen taking into cognizance of the computing power of the processing hardware deployed for the present study. The width of the blue corridor (model time range) and the gap between layers (branch point delta offset) could be modified in the parameter tab as well (Figure 3.19). Subsequently, more control points were created automatically on the binned grid defined for the entire surveyed area of prospect SOKU and a total of over 1250 control points were created automatically in the geometry window (Figure 3.17).

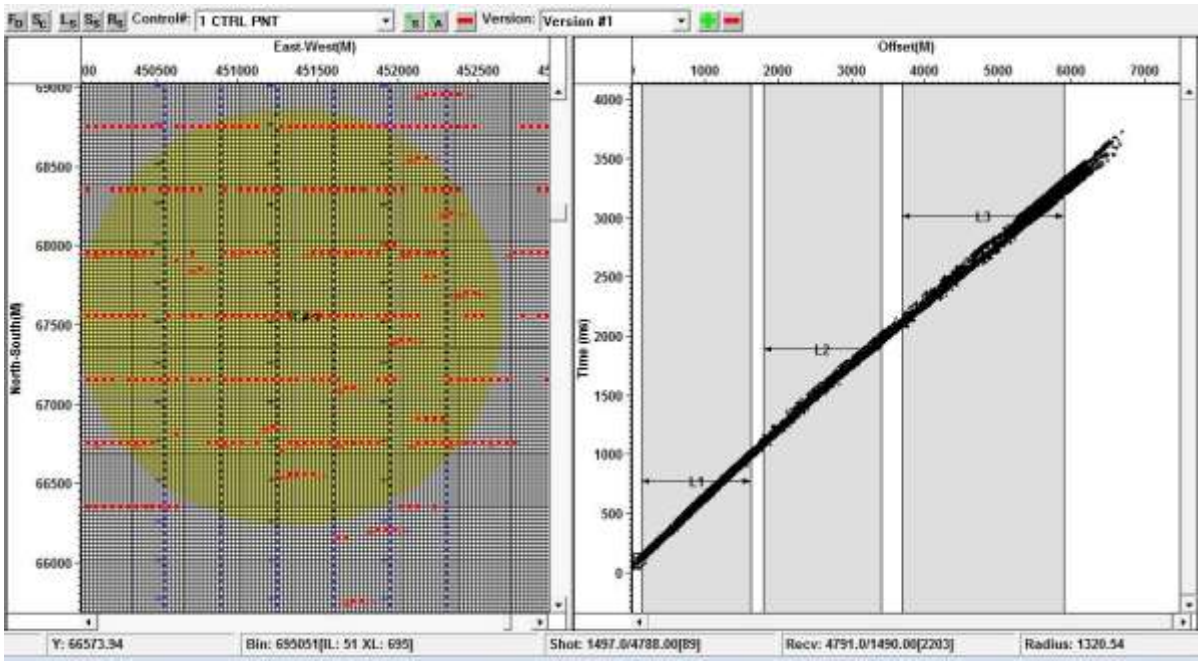

Figure 3.17: Picked control points in geometry window (left) and the corresponding first-break picks in offset window (right)

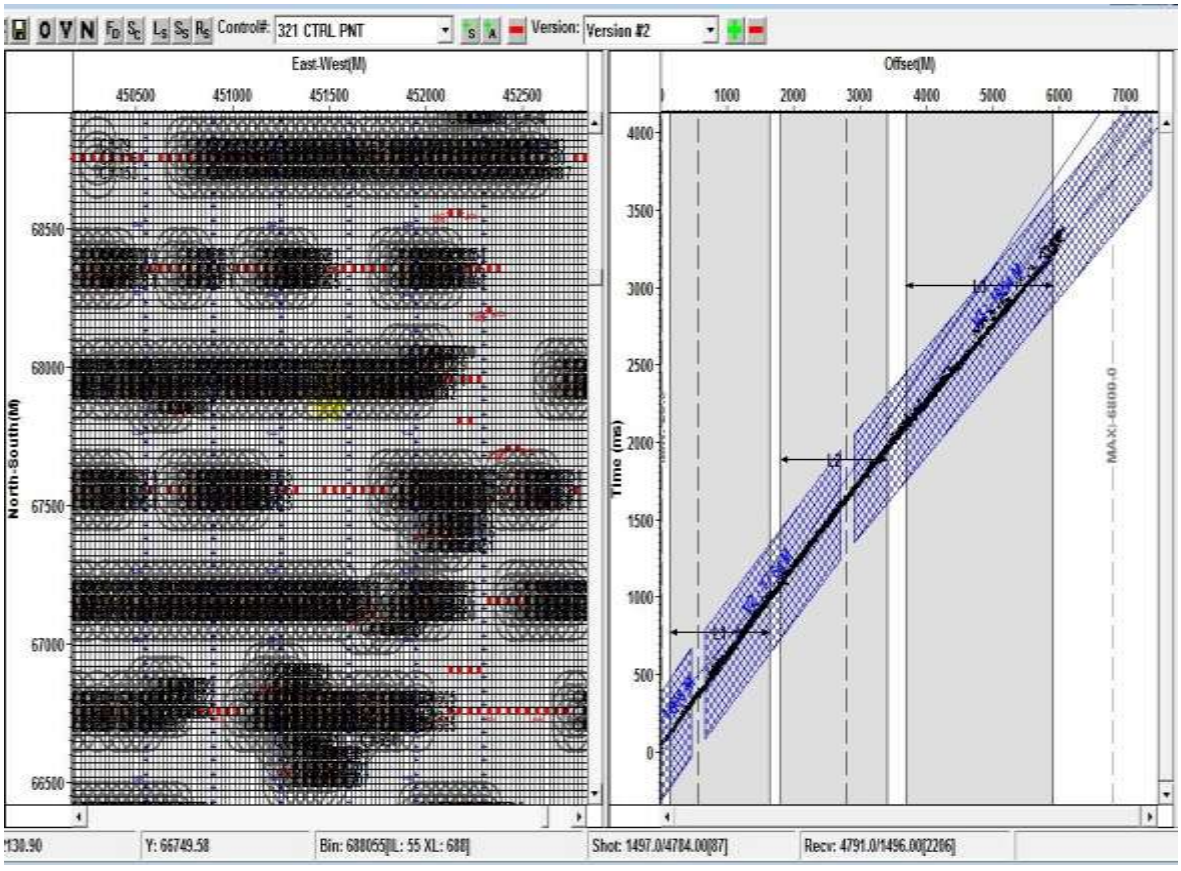

Figure 3.18: Picked velocities for layers 1, 2, and 3 (right hand) and interpolated control points for the survey (left hand).

Figure 3.19: Parameter for interpolating Automatic "fill-in" control points

3.7.2 Velocity Smoothening

In order to mitigate the edge-effect artifacts resulting in excessive perturbations along the eastern and southern edges of the models, the velocity model was smoothened. To achieve this, the near-surface velocity profile was adjusted so that it forms part of a consistent near-surface model. A smooth radius value of 100m was equally applied to the three consolidated or sub-weathering layers (Figure 3.20).

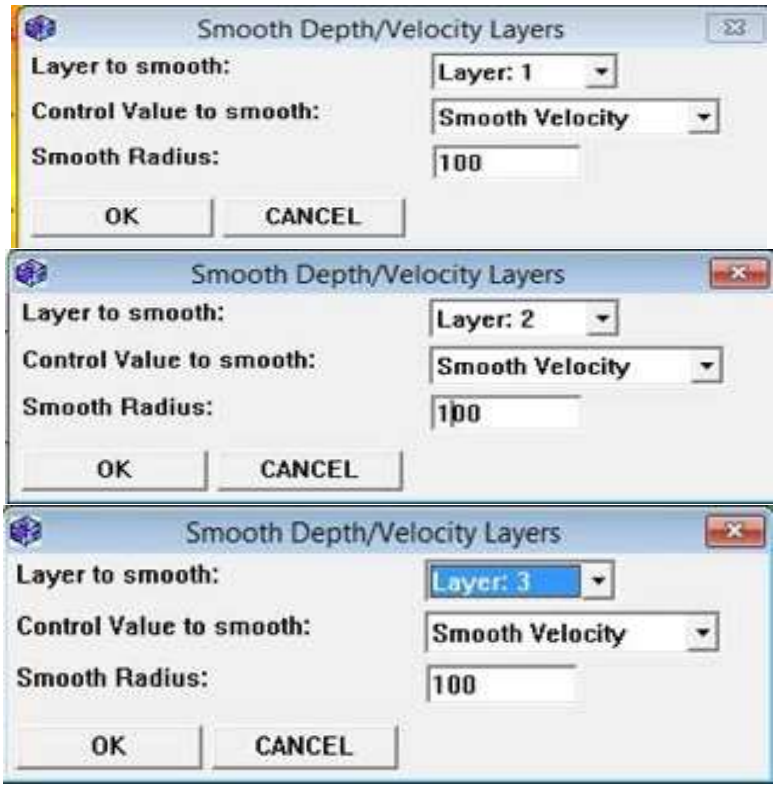

Figure 3.20: Parameters used to produce a smoothened near-surface model.

3.7.3 The Hybrid Near-surface Modeling Approach

The up-hole model of the near-surface, in terms of weathering and sub-weathering properties (thicknesses and seismic velocities), was obtained from the up-hole survey data acquired from the prospect using the UDISYS interpretation tool and guided by the surface (shot point) and shot offset corrections. The refracted arrivals harvested from the 3D seismic reflection survey were equally interpreted using inverse methods. The input parameters to the inversion were the travel times of selected arrivals and the locations of the detectors and the sources. In most of the commonly used refraction data interpretation methods, it is pertinent to group arrivals that have followed equivalent paths through the subsurface; this could be established through their ray-path trajectories. When this was achieved, the methods for inverting the travel time data became straightforward. If the grouping of arrivals was however inaccurate, the inversion will not produce the optimal result or model which best describes or approximates the actual local geology. Adequate care was taken to ensure that the grouping of arrivals was accurately done. Eventually, the two near-surface models were then passed through a special in-house algorithm (program) to adaptively merge both models into an integrated (hybrid) model which is more robust, reliable and a better approximation of the near-surface geology of the prospect. The algorithm leverages on the advantages of both models to build an optimal model.

3.7.4 Refraction Statics Computation

Refraction methods provides a vital means to derive estimates of the thicknesses and velocities of the near surface layers by analyzing the first-breaks of the seismic records (Luo *et al*., 2010; Wu *et al*., 2009; Duan, 2006; Lin *et al*., 2006; Pan *et al*., 2003). Statics correction based on refraction survey requires the information of the first-arrival time of wave field from refractor and the refractor velocity (Cox, 1999). Hence, there are two basic conditions required

for implementing statics correction from refraction surveys, these conditions include; a relative stable refraction interface between the two formations (that is the boundary between the weathered zone and the first sub-weathering layer) and the acknowledged near-surface velocity distribution (modified after Bridle and Aramco, 2009; Liu, 1998). Applying the refraction statics correction based on refraction survey enhances the structural integrity in the processed section; this is a focal and major objective of this dissertation. Refraction statics can be effective for correcting long spatial wavelength anomalies and compensating for the weathering layers, and are also effective against short spatial wavelength anomalies (Liu, 1998).

For the present study, a comprehensive statics solution was derived using the processing software, this solutions comprise of; field (elevation or datum) statics, long wave and short wave refraction statics, then 1st and 2nd residual statics. These statics solutions were adapted to a processing workflow which was eventually applied to the 3D SOKU seismic dataset. The long wave statics was calculated from the derived model whereas the short wave statics was calculated using surface-consistent residual times. The idea is that if the defined model is not very accurate or exact, then the short wave statics helps to compensate for the error inherent in the former. Finally, 1st and 2nd residual statics correction routines were equally applied to the SOKU dataset to ensure all unresolved statics effects on the data (after the initial application of the field statics and refraction statics) were corrected. Processing flows on Promax was used to achieve this latter objective. It is incisive to note that slight discrepancies exist in statics correction terminologies on both VISTA^{TM} and PROMAX^{TM} processing platforms, but the idea behind the concept of statics correction on both platforms is essentially the same.

The final derived comprehensive statics solution on the VISTA™ platform was a summation of the elevation statics, long wave statics, short wave statics and the residual (1st and 2nd) statics and is expressed by the relation;

Final Statics Solution = Elevation Statics + Long wave Statics + Short wave Statics + Residual (1st and 2nd) Statics

The equivalent expression for the final comprehensive statics solution on the PROMAX™ processing platform is simply a summation of the field statics, refraction statics and the residual (1st and 2nd) statics and is expressed as;

Final Statics Solution = Field Statics + Refraction Statics + Residual (1st and 2nd) Statics

3.7.4.1 Field (Elevation or Datum) Statics

The field (elevation or datum) statics computed was with reference to a fixed datum. Field statics involve the computation and removal of the effect of different source and receive elevations. This involves bringing the source and receiver to a common datum. For this to be achieved, a replacement velocity is usually required. The replacement velocity is either assumed from prior knowledge of replacement velocity within the area or it can be estimated from up-hole times or direct arrivals from an up-hole survey. For our study, we used a replacement velocity value of 1750 m/s which was computed from an up-hole acquisition survey that was carried out in the prospect prior to the full execution of the 3D seismic acquisition program.

3.7.4.2 Long wave Statics

Long wave statics primarily involves resolving a near-surface velocity model. This kind of statics are computed by least square fitting of the first breaks of the shots inside a circle called the Control Point (in the VISTA™ software parlance). The velocity of the layers is estimated from the slope of the breaks and the layer thicknesses from the intercepts with the time axis. Long wave statics corrects for relatively large near-surface structural effects and this improves the display of reflection events which ultimately enhances the imaging quality of the subsurface.

3.7.4.3 Short wave Statics

Errors made by the field statics correction are mainly due to the inaccuracies in the near-surface model, which in most instances is a simplification of the actual geology. This additional processing step is necessary to compensate for these errors. This processing step also serves as a means to eliminate small variations of reflection travel times caused by rapid changes in elevation, the base of weathering layer, and weathering velocity. This statics are a surface consistent solution. A theoretical first break is computed for each trace based on the velocity model built during the long wave refraction statics computation. The difference between the theoretical and the actual first break is then used to compute a surface consistent shot and receiver set of statics based on refractions. Short wave refraction statics corrects for small near-surface structural effects and also improves the quality of subsurface image.

3.7.4.4 1st and 2nd Residual Statics

To achieve surface consistency, 1st and 2nd residual statics correction procedures were performed on the seismic data being processed. This provided an additional and more reliable time shift for every source or receiver location. Residual statics correction is usually applied after datum correction but it is also possible to do residual statics correction without any preceding datum statics correction but this is not an ideal processing practice. Both long and short wavelength statics correction together with the elevation statics corrections, each play their special roles in the refraction statics solution mix to achieve surface consistency. The parameters for the residual statics correction were defined according to the range of values of the data (Figure 3.21) to apply residual statics correction to the pre-stack traces. The higher the number of iterations, the larger the computing time required by the two deployed processing software (Vista^{TM} and Promax^{TM}). Both processing software use a Gauss-Siedel approach to solve

for residual statics, and needs a minimum of three iterations for convergence. A total of at least five (5) iterations were implemented. The values were subsequently saved to the seismic data header file.

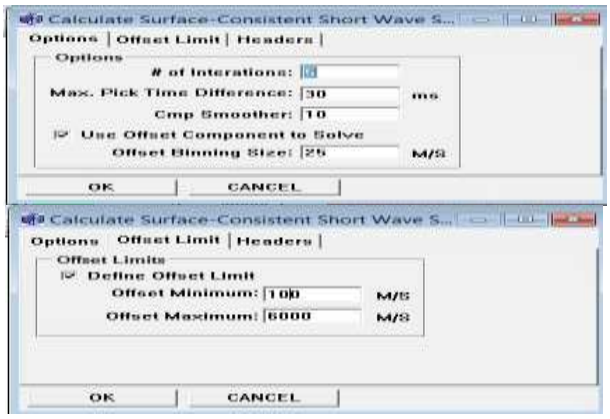

Figure 3.21: Residual statics correction parameters

3.8 The Refraction statics processing flow

After saving the refraction statics to the headers, a processing flow was used to apply the derived statics solution on the data. The statics applied included the elevation statics from the surface to the fixed datum, long-wave and short-wave statics and finally the 1st and 2nd residual statics. The first Apply Statics (StatShft) icon (Figure 3.22), applied the elevation statics while the second icon applied the long wave refraction statics, while the third icon applied the short wave refraction statics to the seismic data. The residual statics routines were executed with a separate flow command on Promax™.

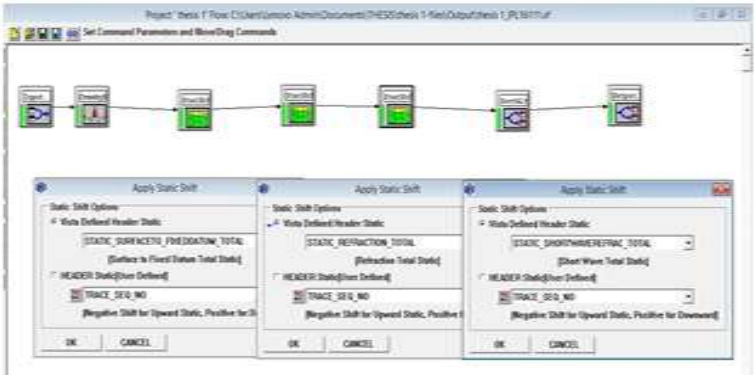

Figure 3.22: The final refraction statics execution flow

3.9 Final Processing Stage

This stage in the processing sequence basically involved velocity analysis, stacking and migration of the 3D seismic dataset from the prospect - SOKU, in a bid to determine the impact and effectiveness of the derived and applied refraction statics solution at these final processing stages.

3.9.1 Velocity Analysis

Velocity analysis is an interactive tool used to interpret stacking or Normal Move out (NMO) velocities on 2D and 3D pre-stack seismic data. Velocity analysis is usually done on common midpoint (CMP) gathers where the hyperbolic alignment is often reasonable. The procedure basically involves comparing a series of stacked traces in which a range of velocities were applied in NMO. Velocity analysis can be carried out through either the method of Velocity Spectrum Analysis (***VSA***) (which provides an interactive means to pick the velocity which is correct for applying NMO corrections) or Multi Velocity Function Stacks (***MVFS***) (which displays a series of side by side stacked traces for a set of common depth points (CDP). These traces are corrected for NMO with a series of different velocities. The velocities can be a series of time variant velocity functions. In standard processing practice, ***MVFS*** are used generally to fine tune the velocity field picked using ***VSA***.

3.9.2 Stacking of the Dataset

Stacking is a data compression procedure which primarily is aimed at summing up of all the traces which have a common reflection point. The common midpoint (CMP) stacking approach was adopted in the study. The CMP stacking equally increased the SNR as signals got enhanced at the expense of some category of noise. A brute stack was first generated by stacking the gathers before any form of deconvolution and detailed velocity analysis to have a rough idea about the

different horizons or reflecting interfaces and prevailing noises inherent in the data. This stack became the reference stack which was compared with the stack generated after the implementation of the full processing workflow with the complete refraction statics solution derived and applied.

3.9.3 Migration of the Dataset

Migration is an important and crucial procedure that attempts to correct the directions of geological structures inherent in the seismic section. Migration redistributes energy in the seismic section to enhance the imaging of the true subsurface geological structures. It is carried out to rearrange seismic data in a way that reflection events are displayed at their true subsurface positions. It collapses diffraction back to their point of origin. It improves temporal and lateral resolutions, thereby providing a more accurate time or depth section. A time migration algorithm (an Explicit Finite Difference 3D Time Method, FX (Explicit) type) was performed for the SOKU dataset.

These conclusions were arrived upon after implementing all the processing routines;

i) Different processing parameters were tested in order to achieve optimal results. The processing outputs improved step by step (progressively) as the parameters were iterated.

ii) The PSTM processing results was better than onboard processing result as is usually expected.

iii) The target zones of most inlines were of clear (spatial and temporal) resolution.

iv) The final processed output provided a remarkably good and clear subsurface seismic image for a reliable geophysical and geological interpretation of structures which could house potential hydrocarbon (oil and gas) traps.

CHAPTER FOUR

RESULTS AND DISCUSSION

The results are sequentially arranged in the order in which they were obtained. Presented first are the results obtained after modeling the near-surface (velocity and depth models) over the investigated prospect (OML-23 SOKU), from extracted parameters obtained from some preliminary pre-processing stages, inversion of the refraction arrivals, up-hole measurements and header file details. Subsequently the derived refraction statics solution, which was based on the modeled near-surface, would be shown. Quantitative field (source and receiver) statics results would be shown and eventually the derived refraction statics solution would then be applied to the SOKU dataset and its effectiveness would be determined on seismic shot gathers, on a stacked seismic section and finally on a migrated seismic section. The ultimate objective is to show how the derived refraction statics solution has solved the statics problem of SOKU and has enhanced the subsurface seismic imaging of the prospect.

4.1 Near-Surface Model (Velocity and Depth/Thickness of Near-Surface Layers)

The topography of the SOKU area was mapped to justify (in the first instance) the critical need for deriving a refraction statics solution for the seismic dataset from this prospect. Figure 4.1 (a), (b) and (c) are Plots of Offset (source – receiver distance) versus Source Index Number (SIN) over the study area to show the topography. Three different views are shown from different orientations and they clearly reveal a rugged and undulating terrain with non-uniform topography which requires that a reliable refraction statics solution be derived and applied on the dataset to address this uneven topography problem which would certainly induce non-uniform arrival times from the reflectors at different receiver locations.

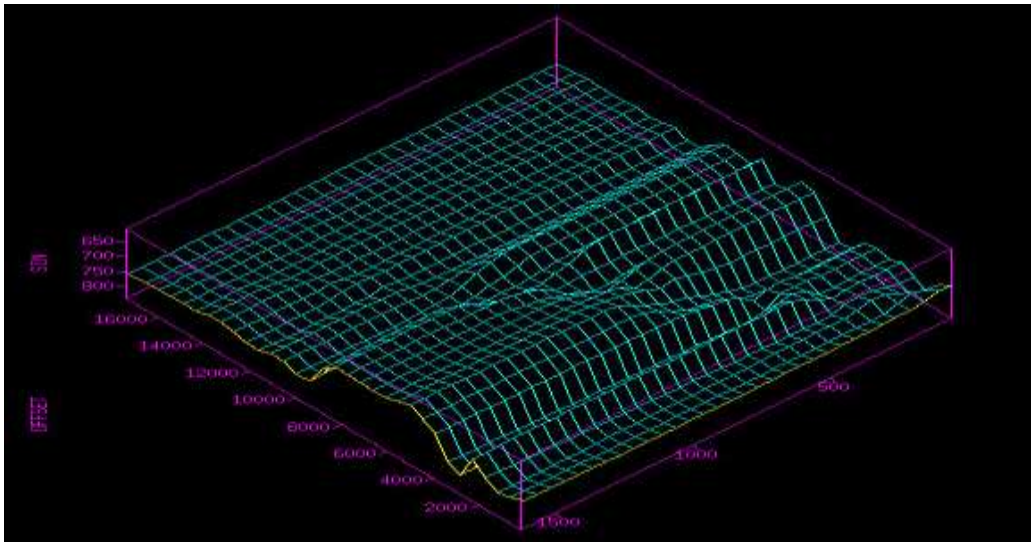

(a)

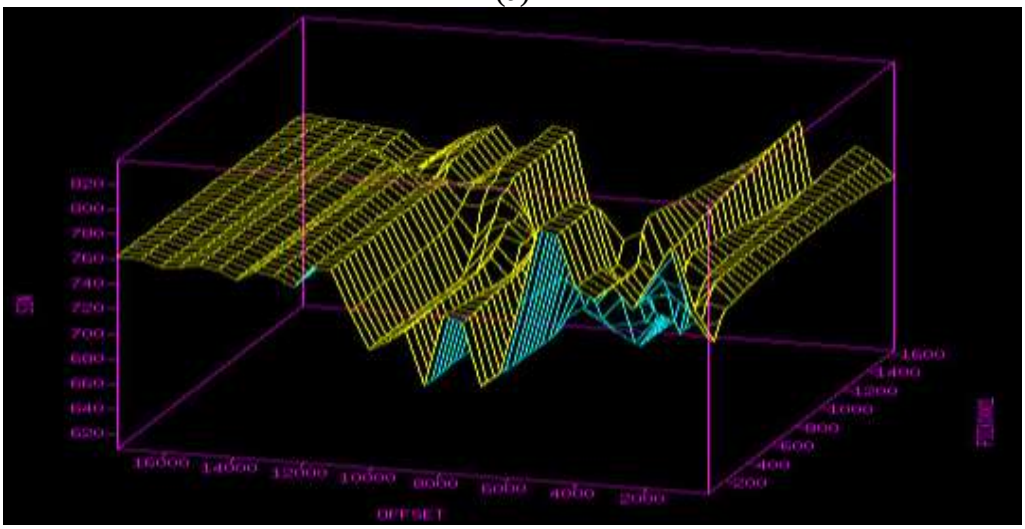

(b)

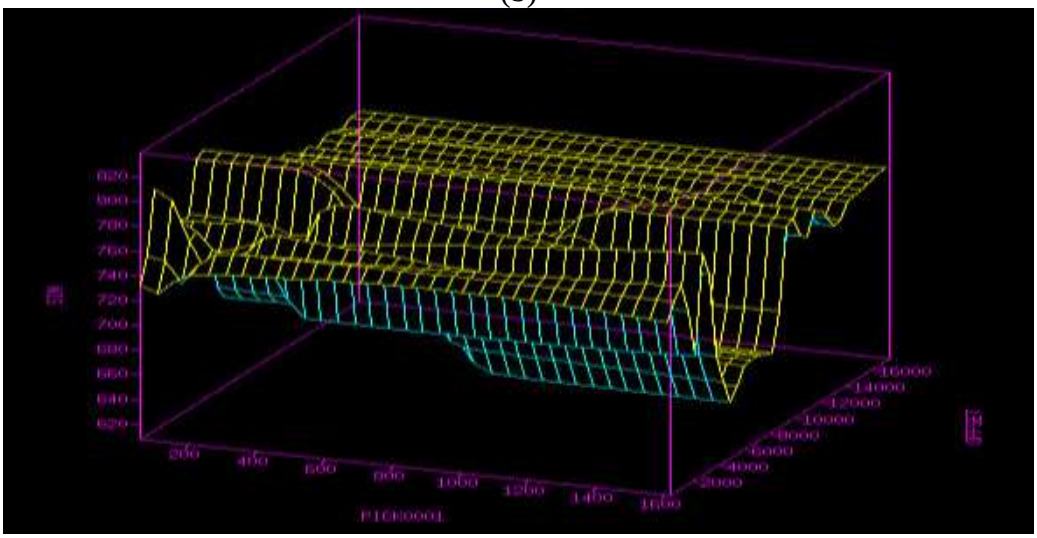

(c)

Figure 4.1: Offset Versus Source Index Number (SIN) Plot Showing Topography

Similarly, Figures 4.2 and 4.3 shows elevation (topography) in In-line and X-line directions respectively over a section of the prospect, and still, clearly reveals the un-even and non-uniform nature of the SOKU area. This further justifies the need for a comprehensive refraction statics solution to be derived and applied to the dataset.

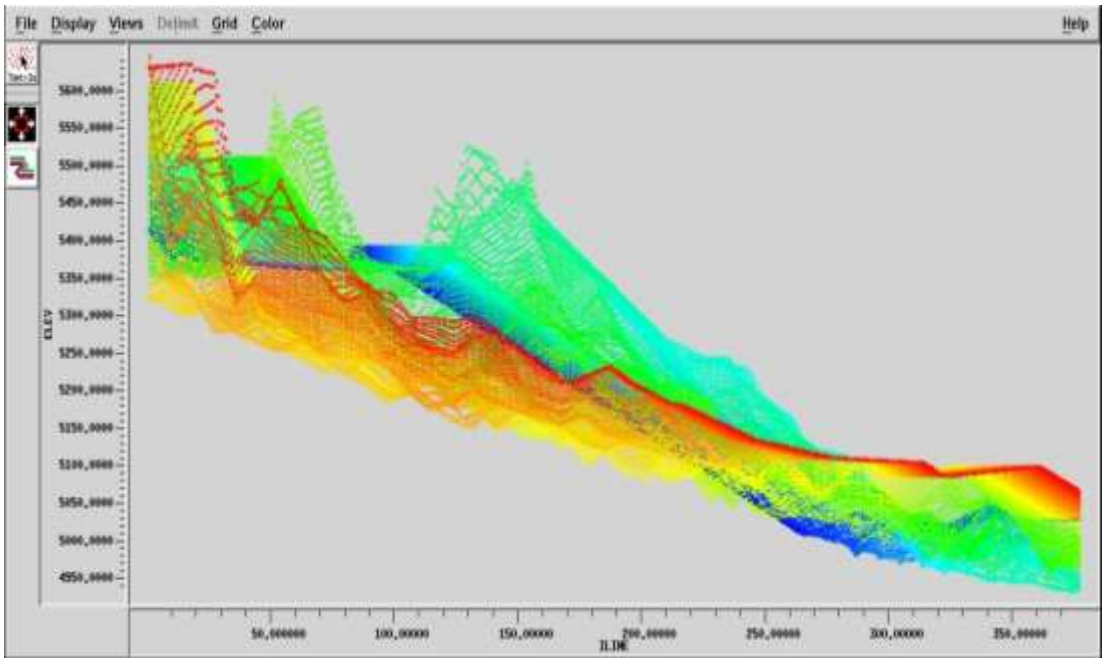

Figure 4.2: A Plot showing the elevation view over the survey area in the in-line direction

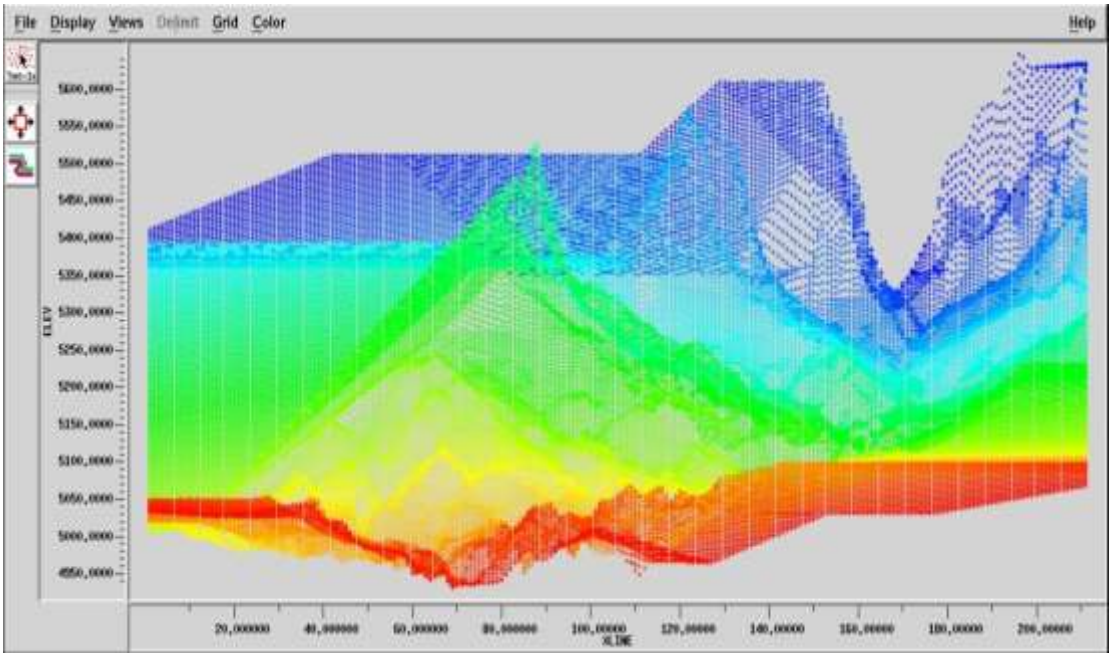

Figure 4.3: A Plot showing elevation view over the survey area in the cross-line (x-line) direction

Wireframe diagrams, Figure 4.4 (a), (b), (c) and (d) were equally generated for the investigated prospect (SOKU) to reveal the block elevation patterns and trend. As previously established, the elevation is un-even and non-uniform as seen from the wireframe diagrams from the respective positions.

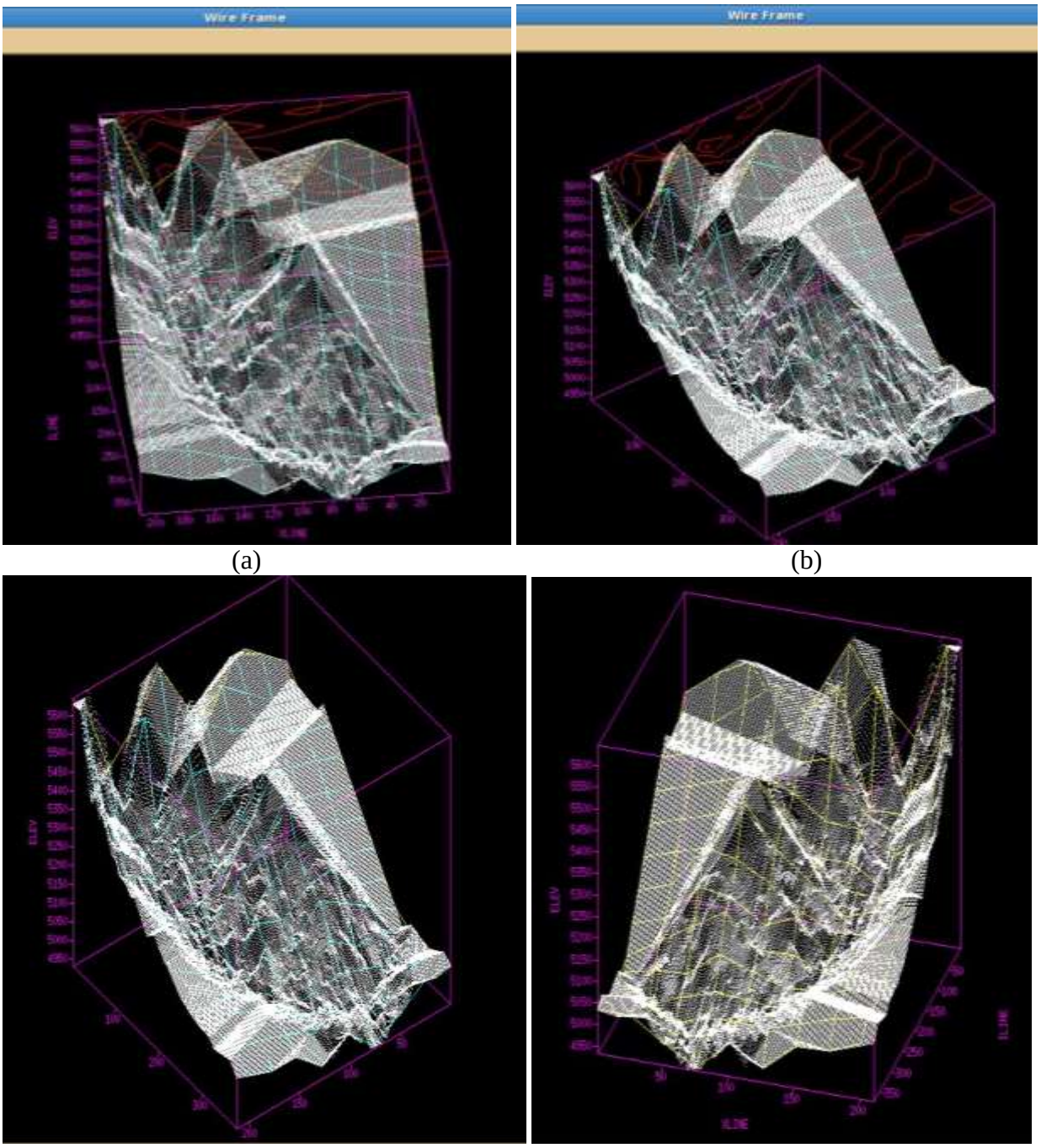

(a) (b)

(c) (d)

Figure 4.4: Wire Frame Diagrams Showing the Elevation over the Survey area.

The Refraction technique which provides a means for utilizing the travel-times of critically refracted seismic waves, to compute the depth and velocity structure of the near-surface layers over areas for which a survey is carried out was deployed. It indirectly estimated intercept time and bedrock velocity using the first-arrival times which were used to estimate a velocity and depth model over the survey area in conjunction with uphole derived models. Four (4) major layers were identified based on their velocity trends; a top most weathering layer and three underlying consolidated layers. Figure 4.5 shows an interactive velocity picking tool bar that was used during the 1st and 2nd velocity analysis in the processing sequence.

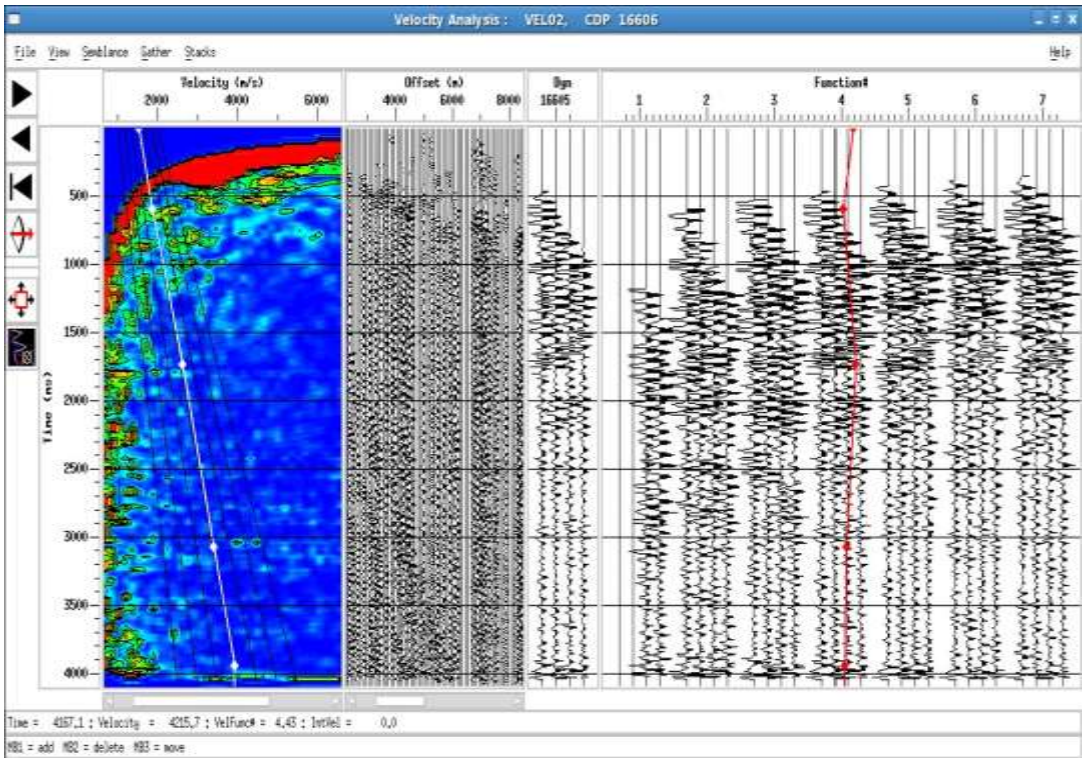

Figure 4.5: Velocity picking tool bar used during 1st and 2nd velocity analysis

Figure 4.6 and Figure 4.7 show the velocity field of the near-surface over the SOKU area after 1st and 2nd velocity analysis respectively. On close examination of both velocity fields, it is observed that there are sharp demarcations in the velocity field after the 1st velocity analysis. This sharp demarcation now blends better after slight adjustments were made to picked parameters during

the 2nd velocity analysis. The velocity field (profile) after 2nd velocity analysis became the optimal velocity field for the investigated prospect.

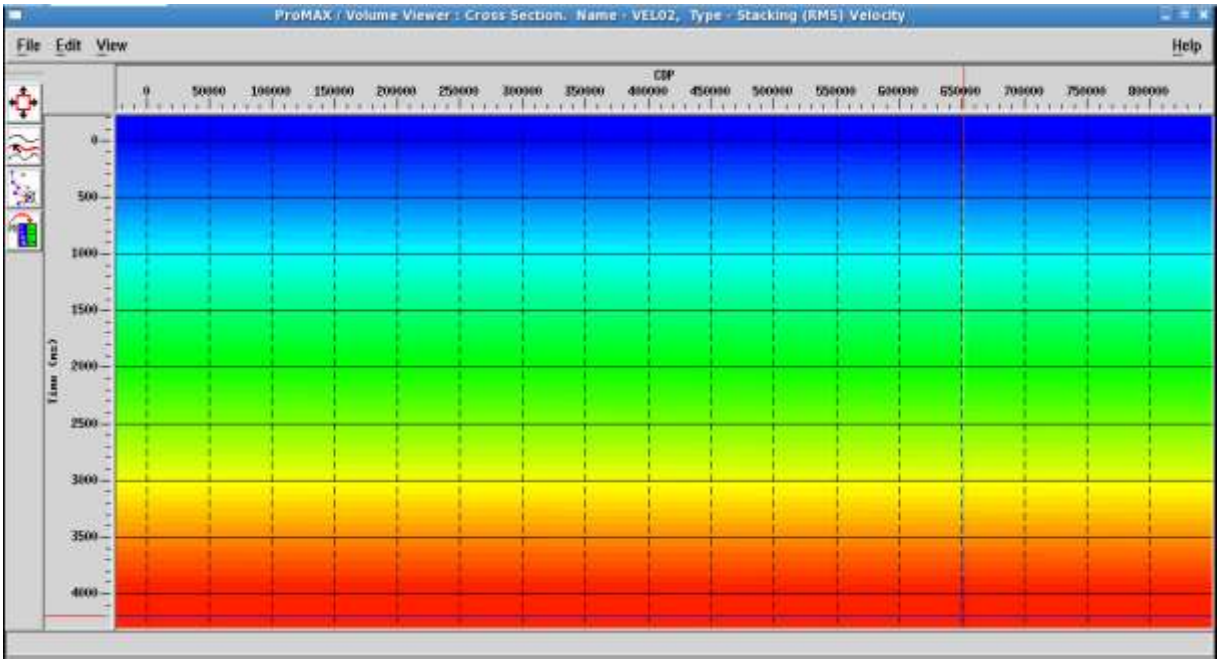

Figure 4.6: Velocity Field Obtained after 1st Velocity Analysis

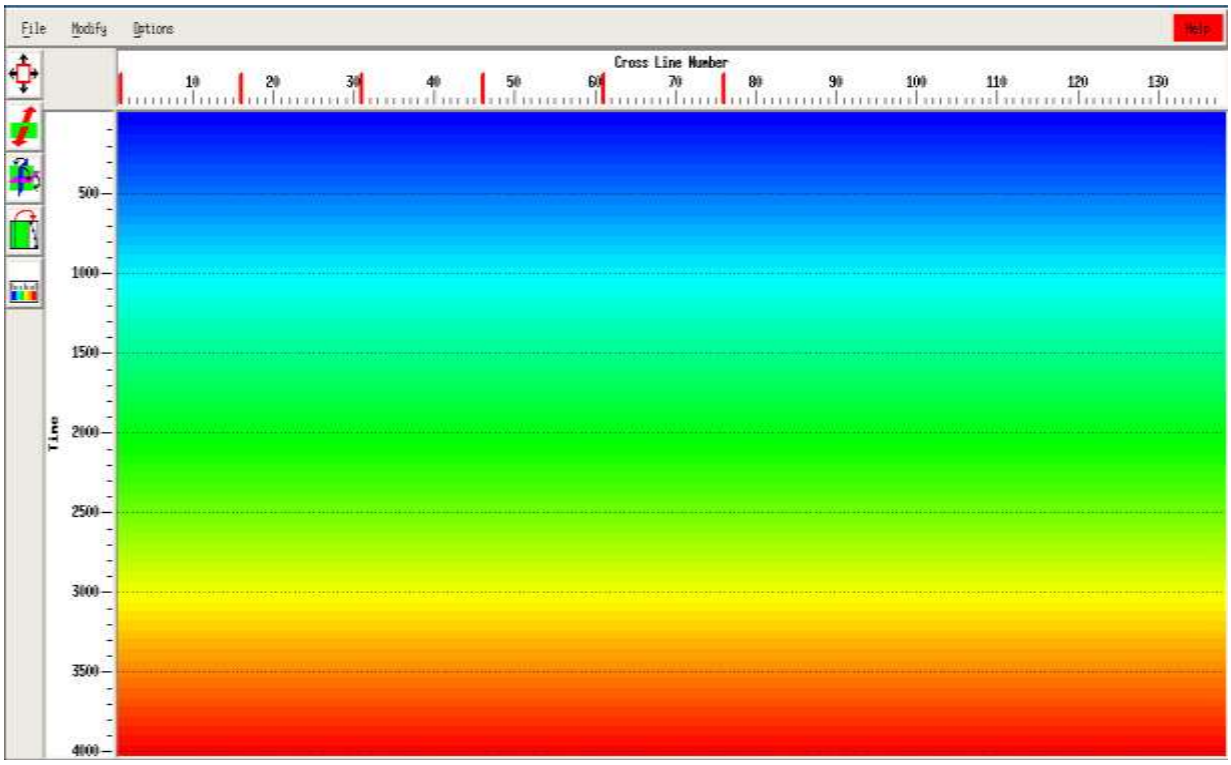

Figure 4.7: Velocity Field Obtained after 2nd Velocity Analysis

A refractor velocity wireframe diagram (Figure 4.8) was equally generated in different orientations for the SOKU area. The diagram basically shows the velocity field view over the area. This velocity field view is crucial in the build up to the much sought after comprehensive refraction statics solution.

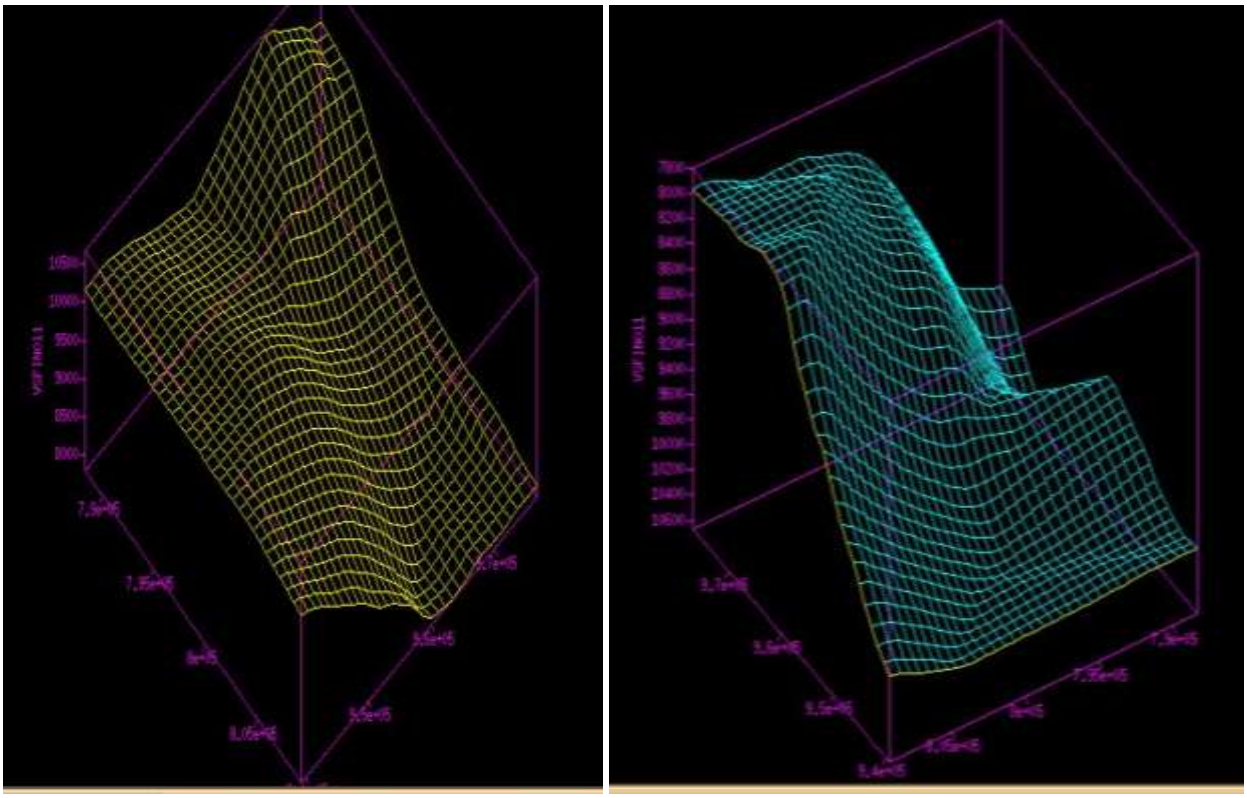

(a) (b)

Figure 4.8 Refractor velocity wireframe diagram

The obtained velocity field for the near-surface was equally generated in both In-line and X-line directions (Figure 4.9 and Figure 4. 10). The velocity trend obtained agrees with geology as velocities increased with increasing depths (Mares, 1984). This is an anticipated trend because increasing depths of burial would result into more compaction of sediments which would in turn increase velocities of seismic waves propagating at such zones or depths. The velocity fields over both the in-line and x-line directions are very similar and this is desirable for our target objective which is to adapt this near-surface velocity depth model to derive a refraction statics

solution that would completely solve the statics problem of SOKU for meaningful and accurate structural/stratigraphic interpretations.

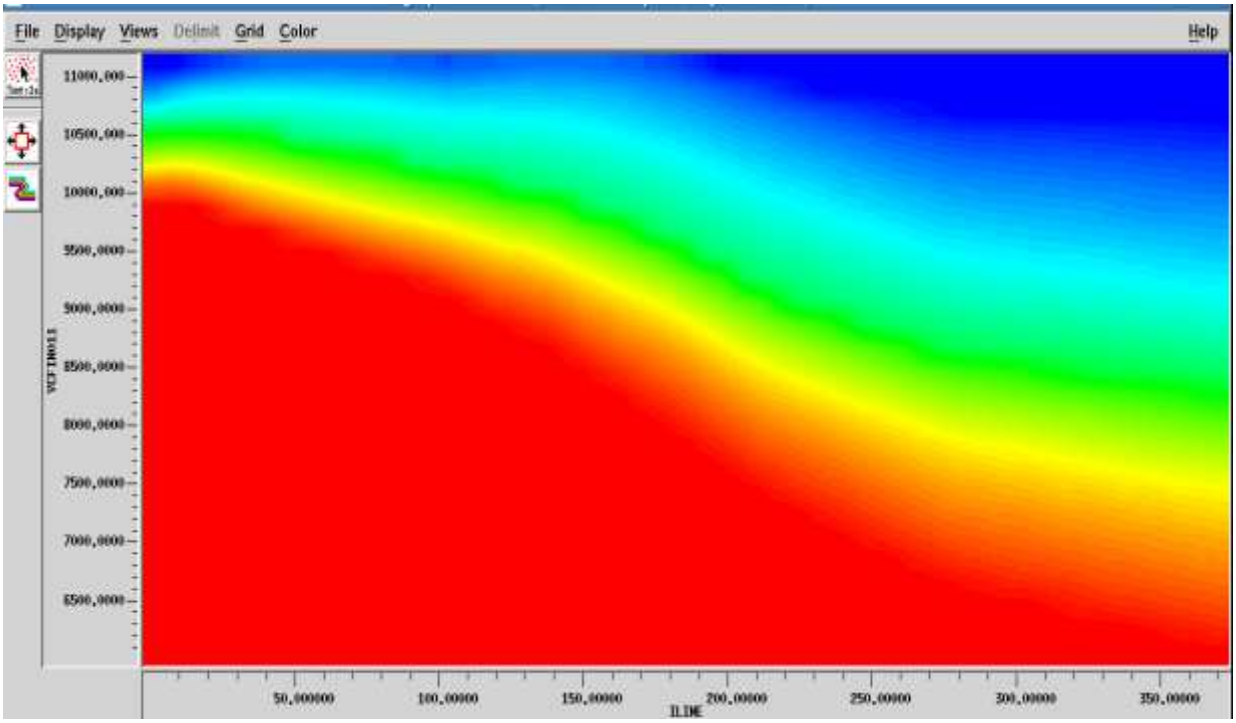

Figure 4.9: Velocity field in In-line Direction showing the various layers mapped

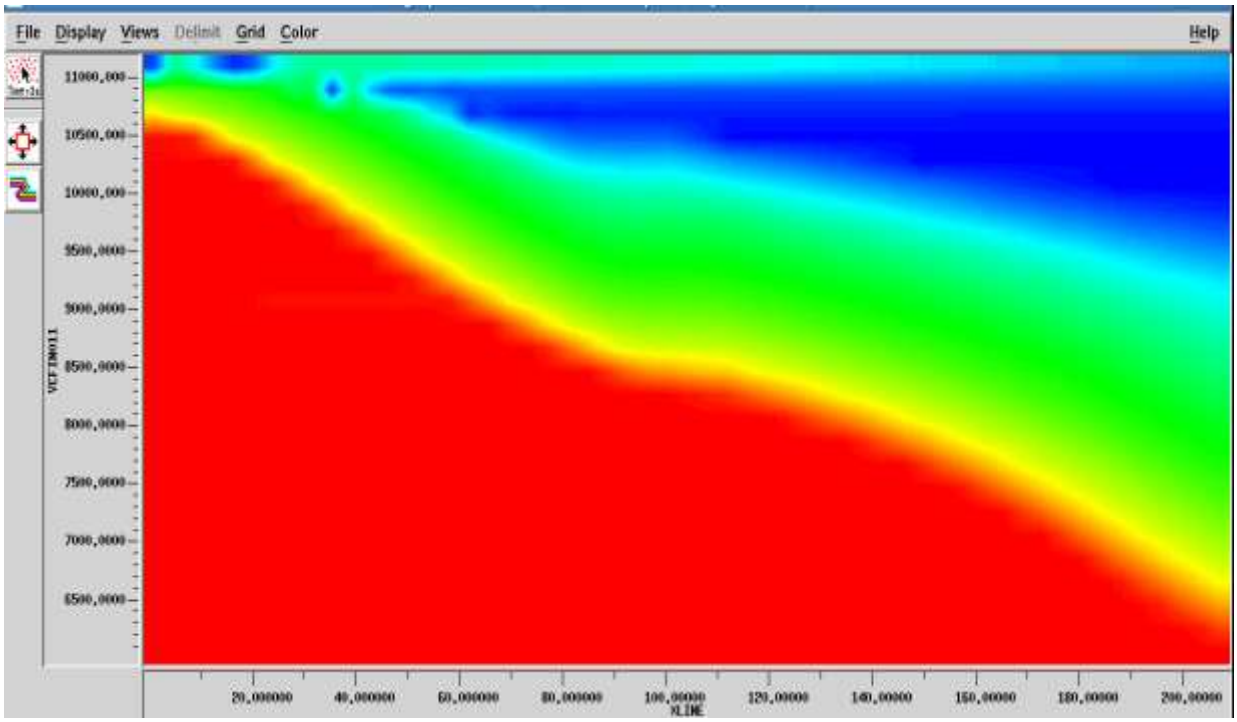

Figure 4.10: Velocity field in Cross-line (X-line) Direction showing the various layers mapped

Apart from the display of the velocity field in both the in-line and x-line directions, a generalized velocity field plot (Figure 4.11) over the SOKU area was obtained.

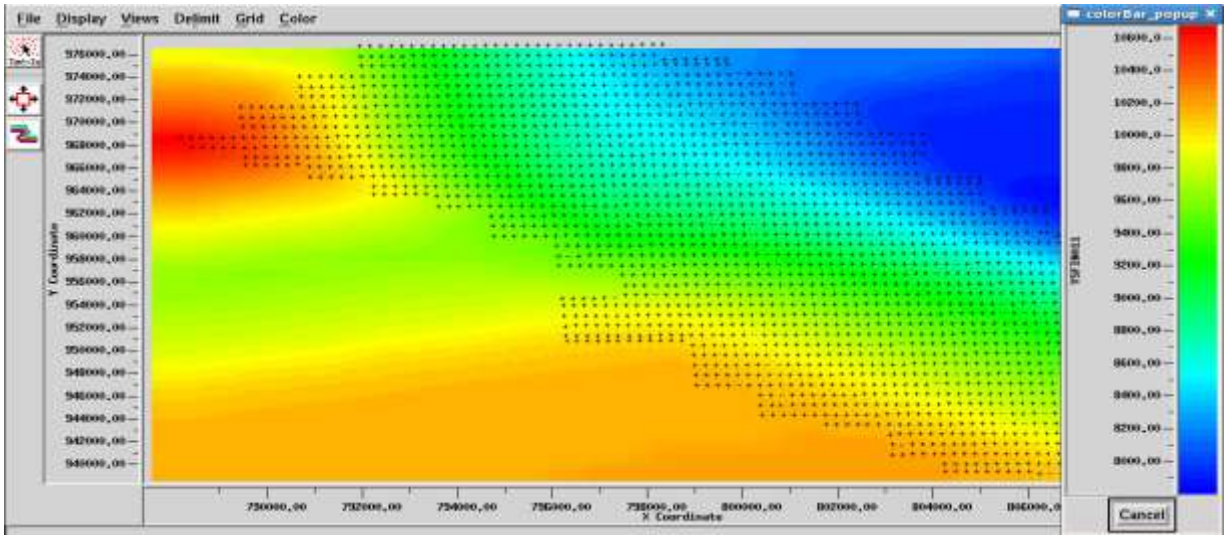

Figure 4.11: Generalized Velocity field over a part of the survey area showing the layers mapped

After successfully imaging the near-surface, the four (4) identified layers were modeled in terms of their velocity and thickness ranges in the form of a bar graph. This model is presented in Figure 4.12.

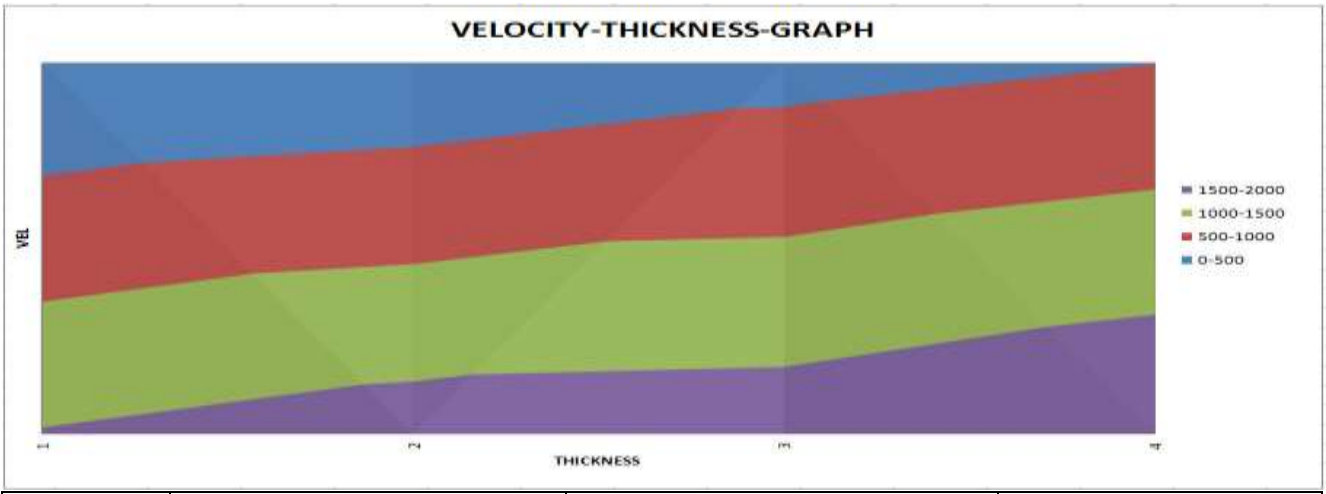

Bar Code	Annotation	Thickness (Depth) Range (m)	Velocity Range (m/s)
	Weathering Layer	3 – 18	520
	First Consolidated Layer	14 – 124	1614 – 1723
	Second Consolidated Layer	62 – 322	1708 – 1758
	Third Consolidated Layer	248 – 493	1950 – 1976

Figure 4.12: Velocity – Thickness Model with Appropriate Annotation

These values obtained were in close proximity with values obtained from a recent literature on near-surface characterization, imaging and velocity model building in the Niger Delta Basin (Opara *et al.*, 2017 and 2018). The velocity model of the near-surface was ideal. It increased progressively with increasing depth of burial. This trend is further highlighted by the graphs plotted for thickness versus velocity (Figure 4.13) and velocity versus thickness (Figure 4.14).

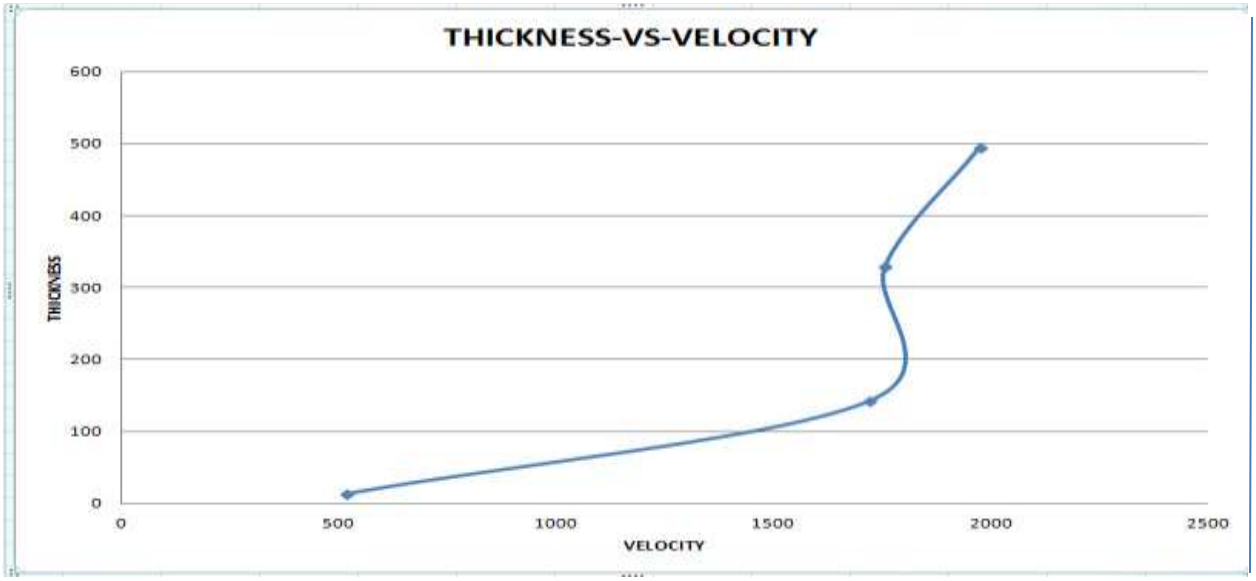

Figure 4.13: Thickness (m) Versus Velocity (m/s) Plot for the different layers over SOKU.

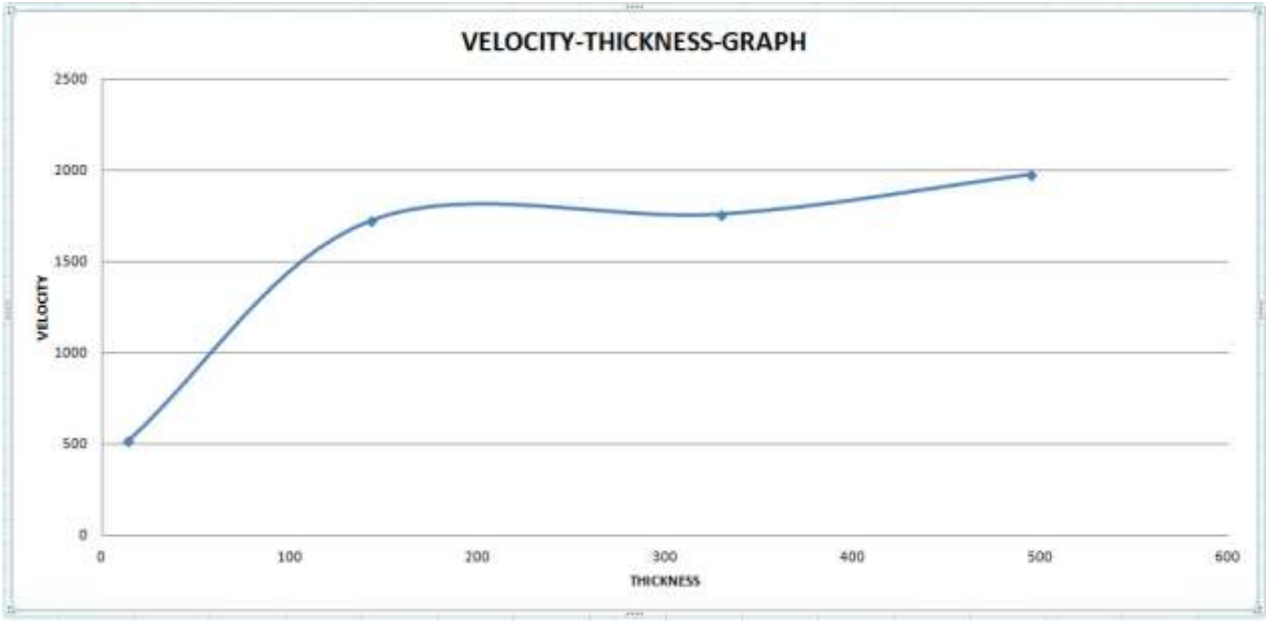

Figure 4.14: Velocity (m/s) – Thickness (m) graph showing mapped near-surface properties over SOKU.

A block representation of the imaged near-surface in terms of velocity and thickness ranges is summarized in Table 4.1.

Table 4.1: Velocity – Thickness (Depth) in In-line and Cross-line direction over SOKU

	In-line		**Cross-line**	
	Velocity (m/s)	**Thickness (m)**	**Velocity (m/s)**	**Thickness (m)**
Weathering Layer	520	5-14	520	3-18
1st Consolidated Layer	1614-1723	10-143	1568-1748	14-124
2nd Consolidated Layer	1708-1758	71-330	1736-1786	62-322
3rd Consolidated Layer	1950-1976	314-495	1923-1942	248-493

4.2 Adapting the Near-Surface Model to derive the Refraction Statics Solution

The near-surface model that was generated was used as input together with some field header information to derive a comprehensive refraction statics solution that would correct the statics problem of the SOKU prospect. The comprehensive statics solution comprised of the field statics, refraction statics and the residual statics. The field statics catered for the elevation statics (sometimes called datum statics) problem and a part of the short wave and long wave statics problem associated with the near-surface inhomogeneity situation of the SOKU area. The refraction statics took care of the problem of the Low Velocity Layer (LVL) and a part of both short wave and long wave statics, while the residual statics solved the remnant unresolved short wave and long wave statics problem that the field and refraction statics could not resolve. It was implemented twice on the dataset to achieve optimal result. It is insightful to note that the approach to refraction statics derivation and implementation differs from one processing software tool to the other. Slight differences in terminology thus exist, for some terms encountered during the processing on Promax™ and Vista™ platforms, for example Vista™

recognizes short wave and long wave statics whereas in Promax^{TM} both statics are embedded in refraction statics.

A set of solutions are now presented which when collectively combined together using appropriate flow commands would constitute the complete statics solution that addresses the statics problem already identified for SOKU. Figure 4.15 is the source elevation statics solution which is intended to resolve the uneven elevation problem.

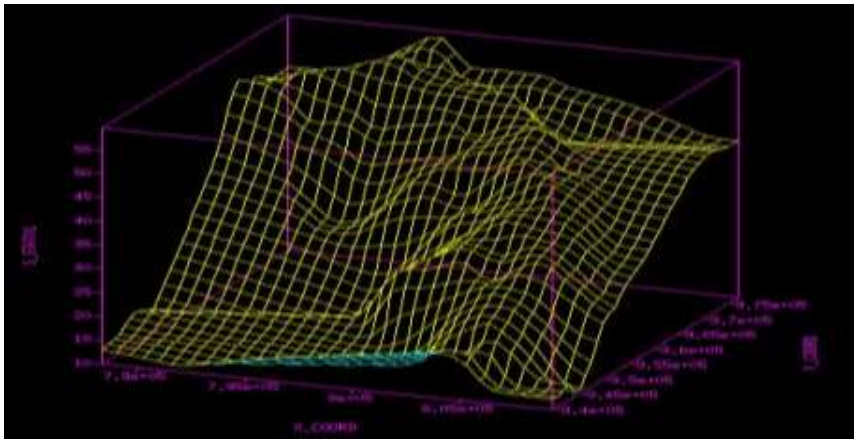

Figure 4.15: Source – Elevation Statics Solution

Figure 4.16 is a schematic diagram showing the Source – Refraction statics solution derived for the SOKU area. On close observation, it is noticed that the source and receivers are now being moved to the reference datum plane (the zero time mark) on the vertical axis. The objective here is for all the source and receivers to be at the same datum plane.

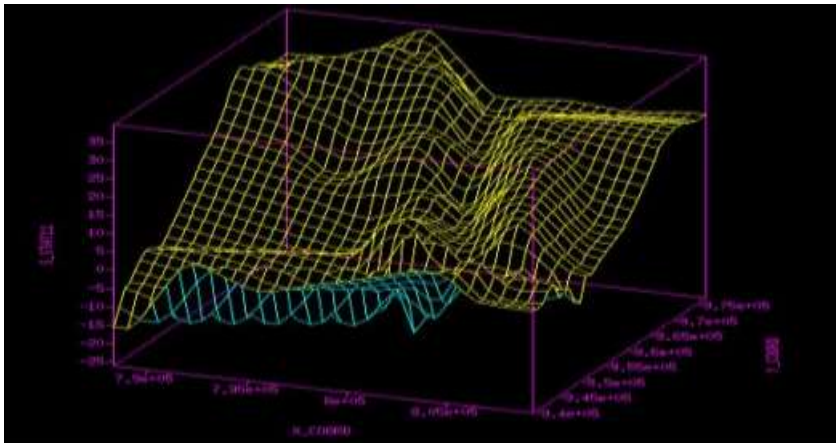

Figure 4.16: Source – Refraction Statics Solution

Figure 4.17 is a schematic of the source statics from the refraction statics which basically gives the source positioning and orientation across the prospect under investigation which must be corrected or moved to the reference datum.

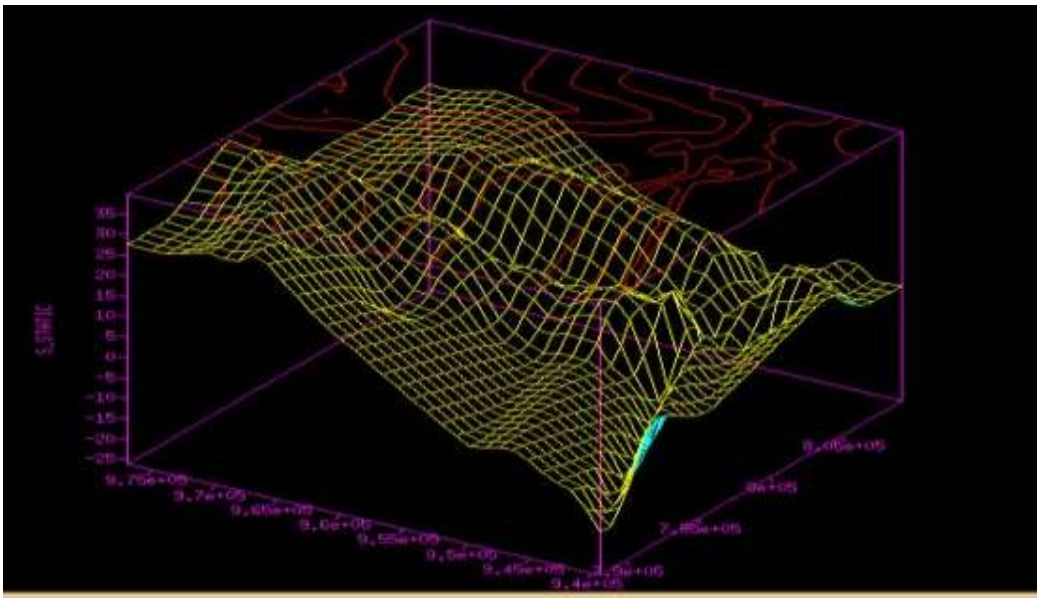

Figure 4.17: Source – Statics from Refraction Statics

The solutions so far derived were all adapted to build a complete refraction statics solution to final datum (Figure 4.18)

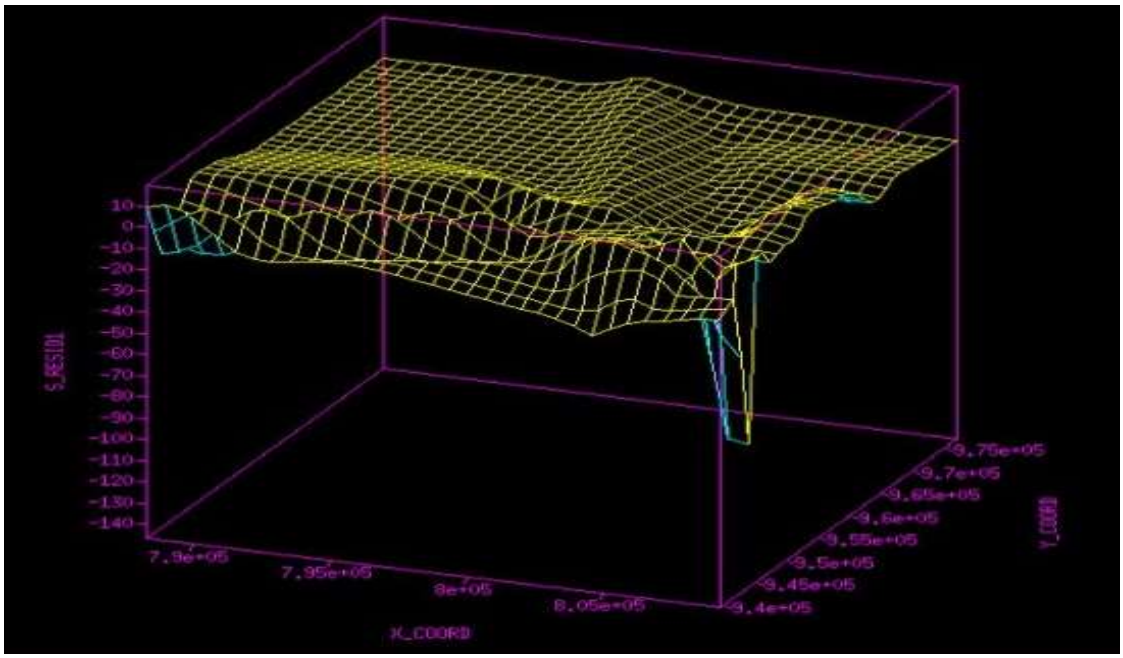

Figure 4.18: Refraction Statics Solution to Final Datum

It is very visible to see that sources and receivers are almost aligned now at the reference datum except for some trough like structures encountered at the edges of the grid. These anomalies account for unresolved short wave and long wave statics problems. These unresolved anomalies would subsequently be resolved (moved to the reference datum) when the first and second residual statics workflow would be applied, thereby enabling the source and receivers to be at a common datum plane which is the ultimate target.

4.3 Quantitative Field (Source and Receiver) Statics Results

The field statics derived and implemented corrected for the undulating, rugged and non-uniform topography of OML-23 SOKU. It was implemented to move source(s) and receiver(s) to a common datum. The operational domain for this component of the comprehensive statics solution was source (source statics) and receiver (receiver statics) based.

Tables 4.2 and 4.3 gives quantitative statics (time shift) values for the field statics component (source and receiver statics) derived and implemented for inline 79, showing the magnitude of statics in milliseconds (ms), at selected Source Index Number (SIN) points and receiver station locations respectively, along the chosen inline before statics application and after statics have been derived and applied.

Table 4.2: Quantitative values of the source statics components of the field statics solution before statics implementation and after statics have been derived and applied.

S/N	BEFORE		AFTER	
	SOURCE INDEX NUMBER	**SOURCE-STATICS (ms)**	**SOURCE INDEX NUMBER**	**SOURCE-STATICS (ms)**
1	22	38	22.1	31
2	24	34	24.4	29
3	41	29	40.6	23
4	118	32	117.8	32
5	139	32	139.4	30
6	159	34	159.5	28
7	320	11	320	15
8	374	23	374.1	23
9	390	17	390.3	18
10	433	15	432.7	11
11	472	13	472.1	11
12	515	15	514.6	7
13	594	5	594.1	6
14	626	13	625.7	2
15	679	4	679	1

Table 4.3: Quantitative values of the receiver statics components of the field statics solution before statics implementation and after statics have been derived and applied.

S/N	BEFORE		AFTER	
	RECEIVER STATION	**RECEIVER-STATICS (ms)**	**RECEIVER STATION**	**RECEIVER-STATICS(ms)**
1	118	50	118.3	35
2	159	36	158.6	22
3	181	52	180.7	52
4	211	25	210.9	27
5	235	47	235.1	40
6	362	22	361.9	40
7	430	52	430.3	39
8	475	21	474.6	23
9	533	19	532.9	20
10	978	35	978.8	24
11	1000	6	999.9	22
12	1016	33	1016	36
13	1135	30	1134.8	28
14	1258	22	1257.5	20
15	1408	26	1408.5	19

The statics values presented above show appreciable static shifts for the seismic traces for each source and receiver location at defined Source Index Number (SIN) locations and receiver stations respectively. These quantitative values are now modeled into receiver statics plots

(Figure 4.19) and source statics plots (Figure 4.20) to highlight at a quick glance the contribution of the source and receiver components of the field statics that was sought, derived and applied.

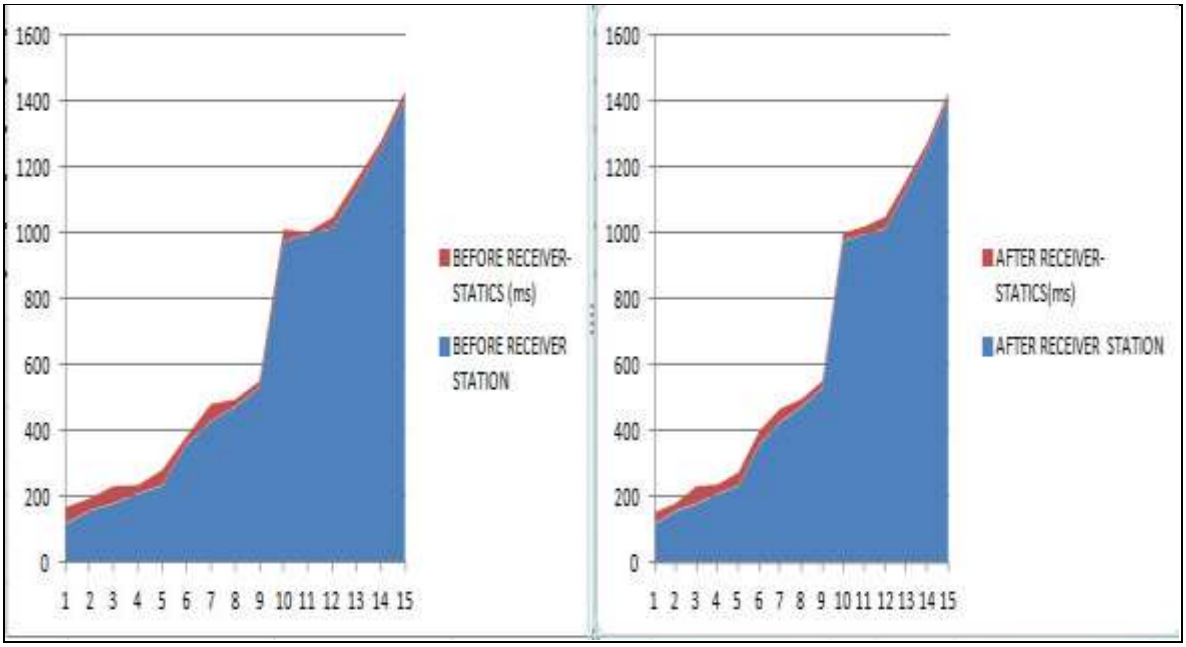

Figure 4.19: Receiver – statics plot of receiver statics values in (ms) versus receiver stations before and after application of the sought statics

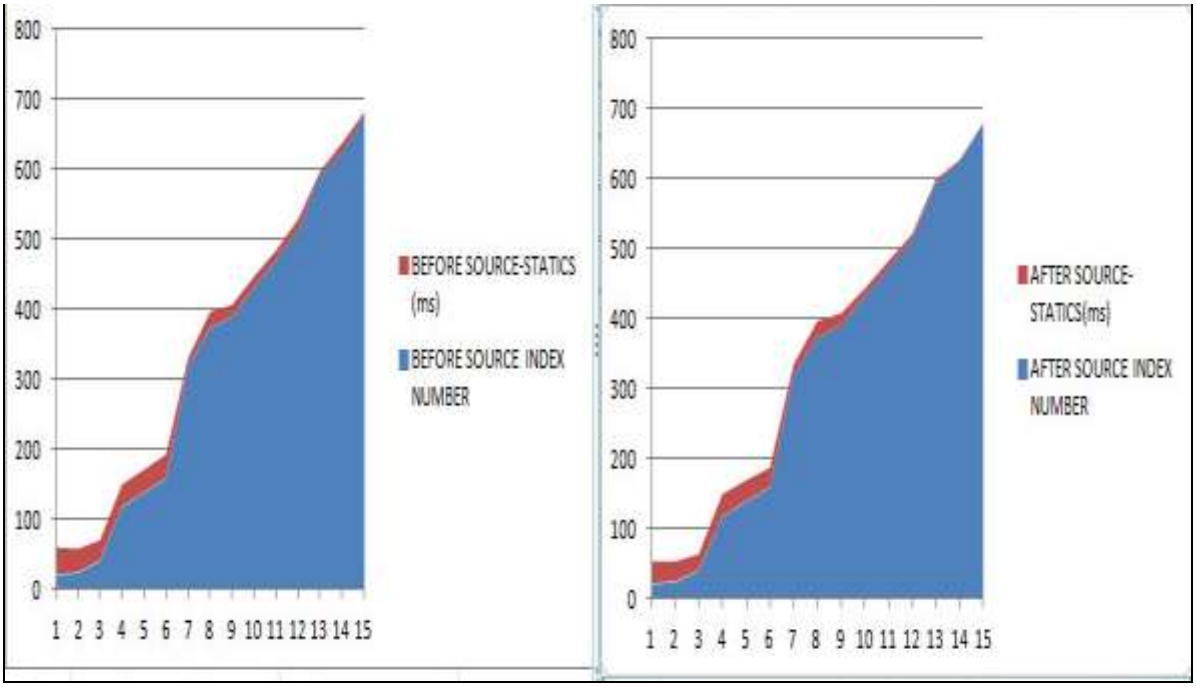

Figure 4.20: Source – statics plot of source statics values in (ms) versus Source Index Numbers (SIN) before and after application of the sought statics

After implementing field statics, refraction statics then 1st and 2nd residual statics were equally derived and applied to the SOKU dataset. The principle adopted to derive refraction statics relied on supplying the first break times of all traces along each FFID (field file identification) into VISTA and PROMAX modules to perform refraction statics. The software module then corrects for time in this operation and the corrected time(s) were in sync with those in the table earlier presented. The operational domain for refraction statics is also source and receiver based. The 1st and 2nd residual statics was implemented also to cater for effects (spatial short and long wavelength) along the common depth points (CDP). Unlike the previous two statics solution which are strictly source and receiver domain operational (based), the residual statics in addition to being operational in the source and receiver domain also incorporates the CDP (common depth point) domain. This bridges potential gaps in the build up to the comprehensive statics solution which the field and refraction statics components alone may not be able to resolve.

4.4 Application of the Derived Refraction Statics Solution on the Dataset

This section shows the results achieved after the derived refraction statics solution was applied. The results achieved are sequentially presented and clearly affirms the effectiveness of the derived and implemented refraction statics solution. The results presented here are grouped into three sub-sections; the first shows the effectiveness of the derived refraction statics solution on shot gathers, the second determines the effectiveness of the solution on a stacked seismic section and the final section determines the overall success of the derived solution on a migrated section of the data.

4.4.1 Derived Refraction Statics Solution applied to Seismic Shot Gathers

This section shows before and after refraction statics application results on seismic shot gathers in Field File Identification (FFID) configurations. The before and after result for each

FFID shot gather were placed side by side so that on close examination, the problem of the statics would be seen (on the before panel) and the same panel now corrected for the statics problem (on the after panel). The approach was basically to first display the seismic data in their respective shot gathers configuration in FFID before any form of processing and after the comprehensive refraction statics solution was applied to the data, they were again displayed in their respective shot gathers using the same FFID, as our primary focus was to mirror and compare the same shots in their gathers to demonstrate how the refraction statics solution derived and applied has solved the statics challenge for SOKU. Figure 4.21 shows before and after refraction statics displays for FFID's 629, 661, 668 and 693. On close observation, it is very evident that reflections were becoming more continuous and regular with better energy (amplitude) focus in after displays when the refraction statics solution was applied than in before displays with no refraction statics solution.

(a) FFID 629 - Before and After Refraction Statics (b) FFID 661- Before and After Refraction Statics

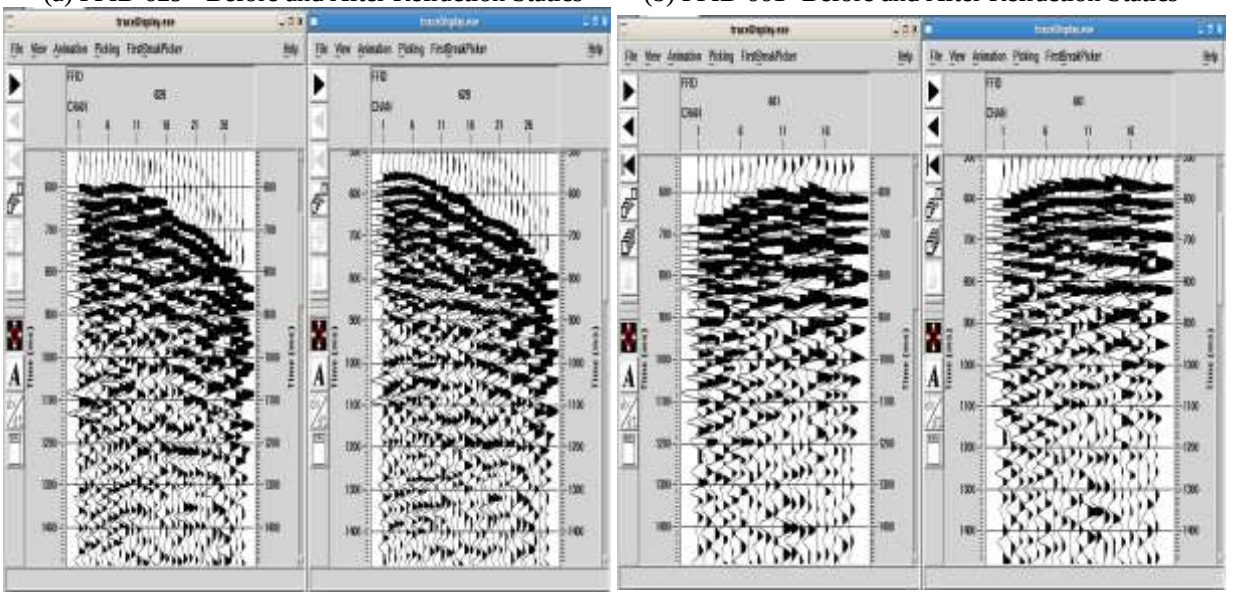

(c) FFID 668 - Before and After Refraction Statics (d) FFID 693- Before and After Refraction Statics

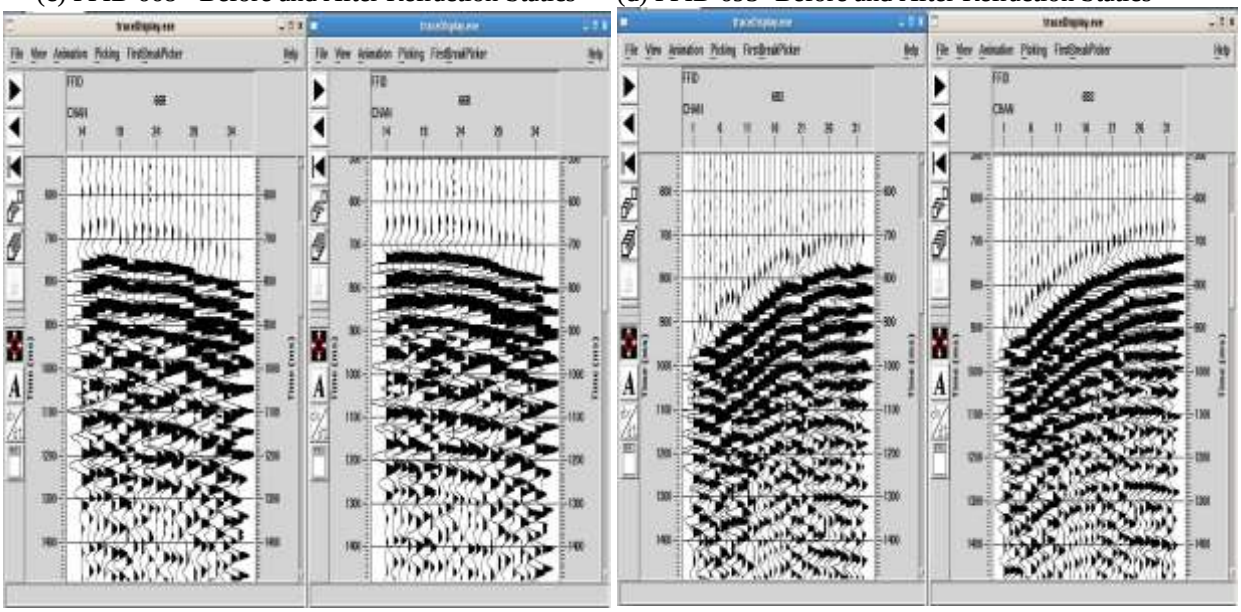

Figure 4.21: Derived refraction statics solution applied to shot gathers - FFID 629, FFID 661, FFID 668 and FFID 693

Similarly, Figure 4.22 and Figure 4.23 shows the before and after display of shot gathers in FFID's (733, 752, 758, 764, 793, 797) and (800, 853, 859) respectively. As earlier stated, on close examination of the shot gathers, it is observed that reflections are now properly moved out and aligned in their proper directions as it ought to. Failure to correct for these distortions in reflection patterns would eventual impede the success of other processing procedures like

stacking and migration and would ultimately lead to a false image of the subsurface structures that would be at variance with actual geology of the area (SOKU in this case).

(a) FFID 733 - Before and After Refraction Statics (b) FFID 752- Before and After Refraction Statics

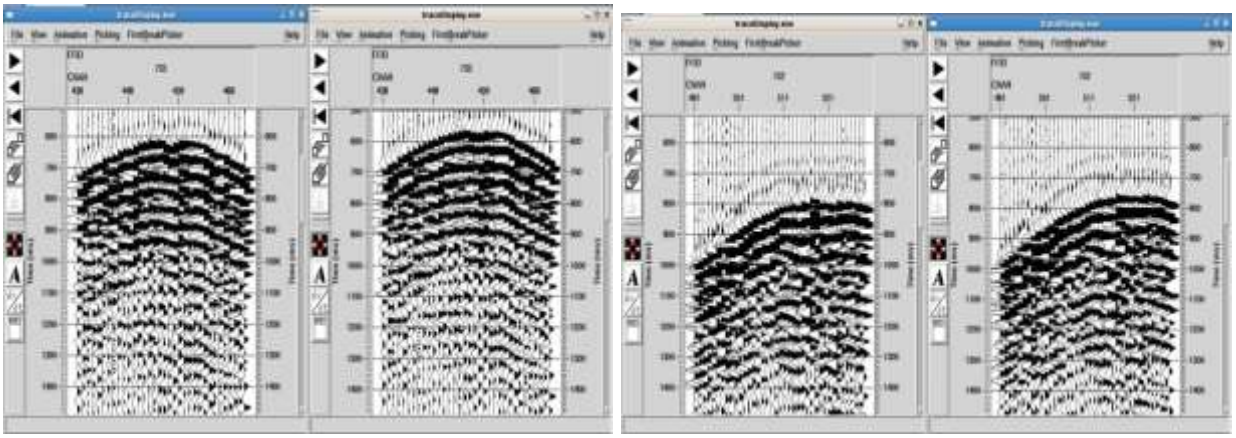

(c) FFID 758 - Before and After Refraction Statics (d) FFID 764- Before and After Refraction Statics

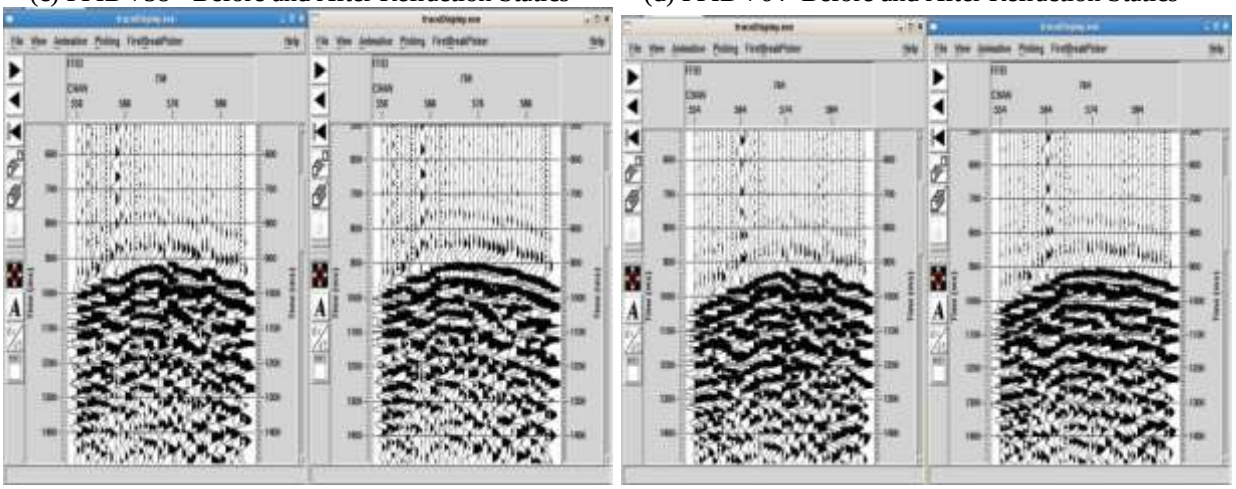

(e) FFID 793 - Before and After Refraction Statics (f) FFID 797- Before and After Refraction Statics

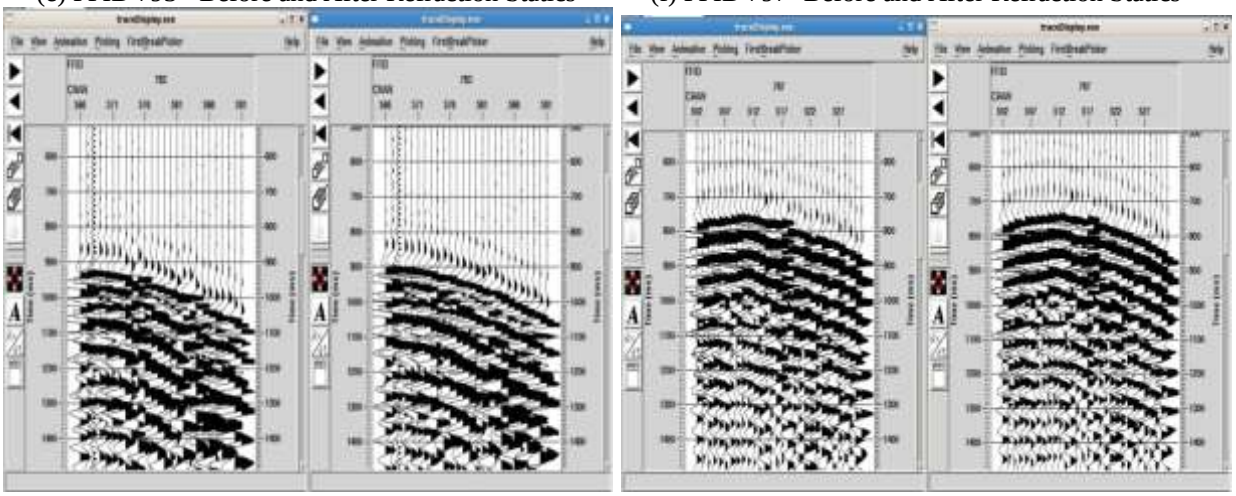

Figure 4.22: Derived statics solution applied to shot gathers - FFID 733, FFID 752, FFID 758, FFID 764, FFID 793 and FFID 797

(a) FFID 800 - Before and After Refraction Statics

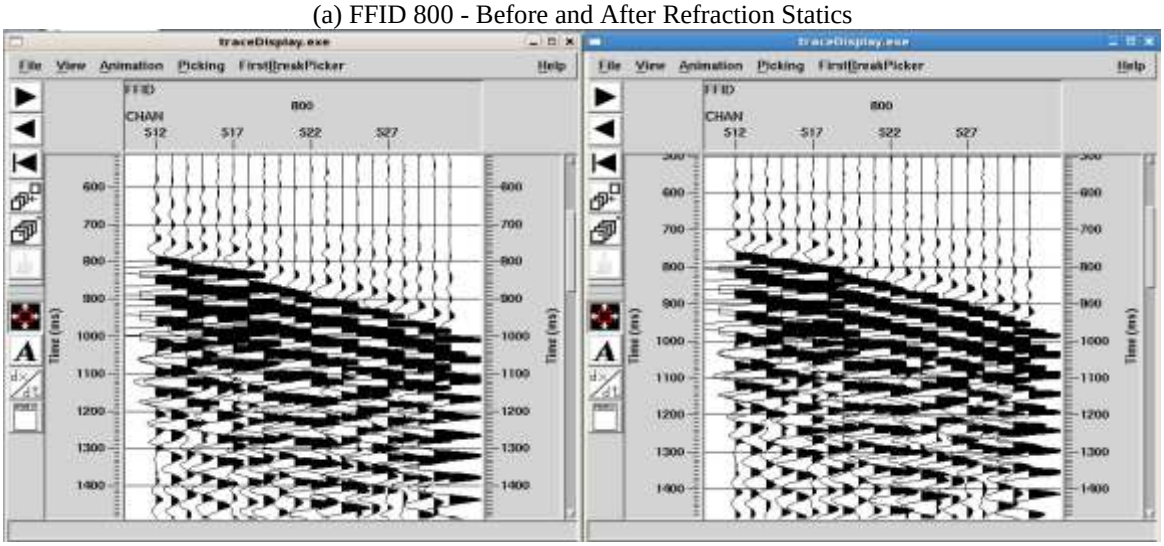

(b) FFID 853 - Before and After Refraction Statics

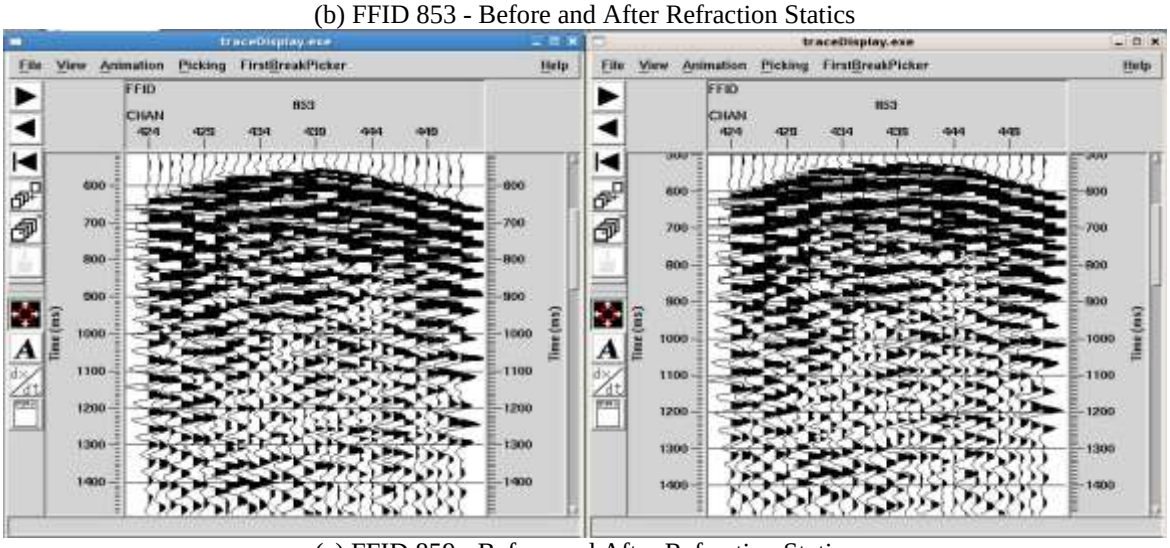

(c) FFID 859 - Before and After Refraction Statics

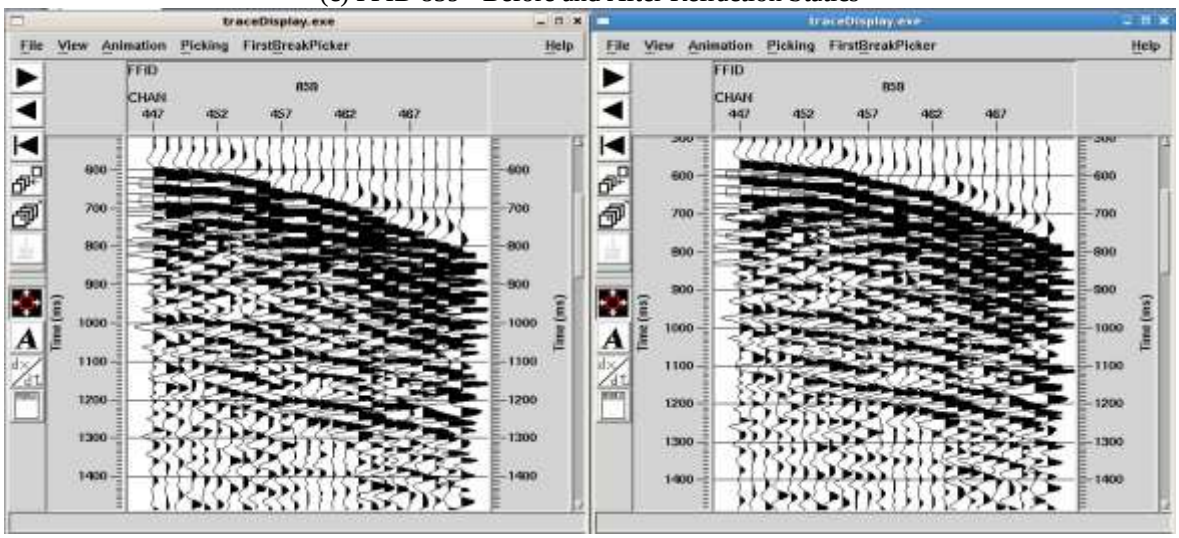

B

Figure 4.23: Derived statics solution applied to shot gathers - FFID 800, FFID 853 and FFID 859

Figure 4.24 now displays a collection of selected shots with included markers to show regions were the effect or impact of the application of the derived refraction statics solution is most visible.

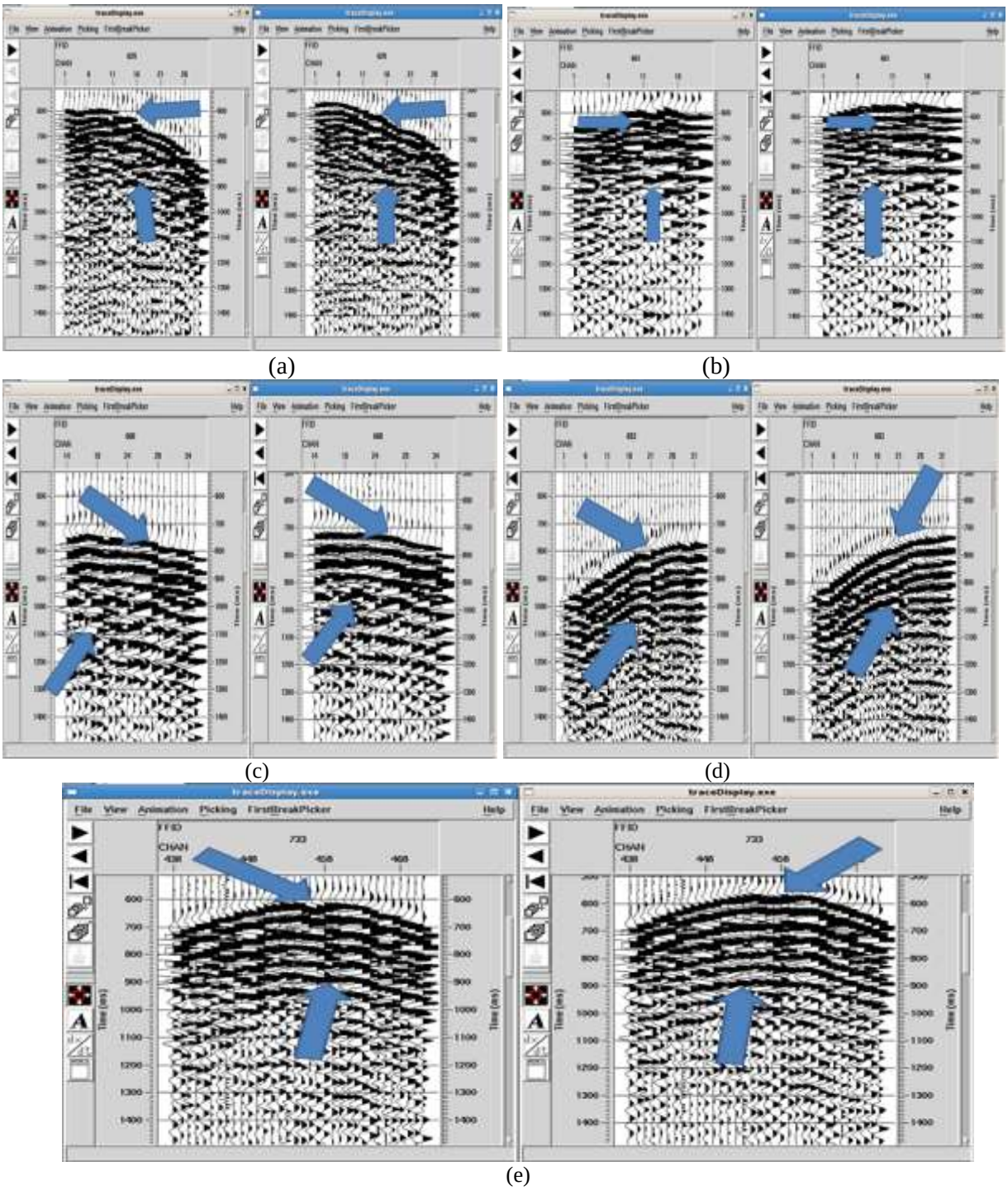

(a) (b) (c) (d) (e)

Figure 4.24: Selected collection of shots showing with markers (arrows) the resultant effect of the applied refraction statics solution derived on the shot gathers.

The quality of results achieved at this stage of the processing sequence was superior to those achieved by Opara *et al.*, 2017 and 2018, (Figure 4.25) when both outcomes were compared.

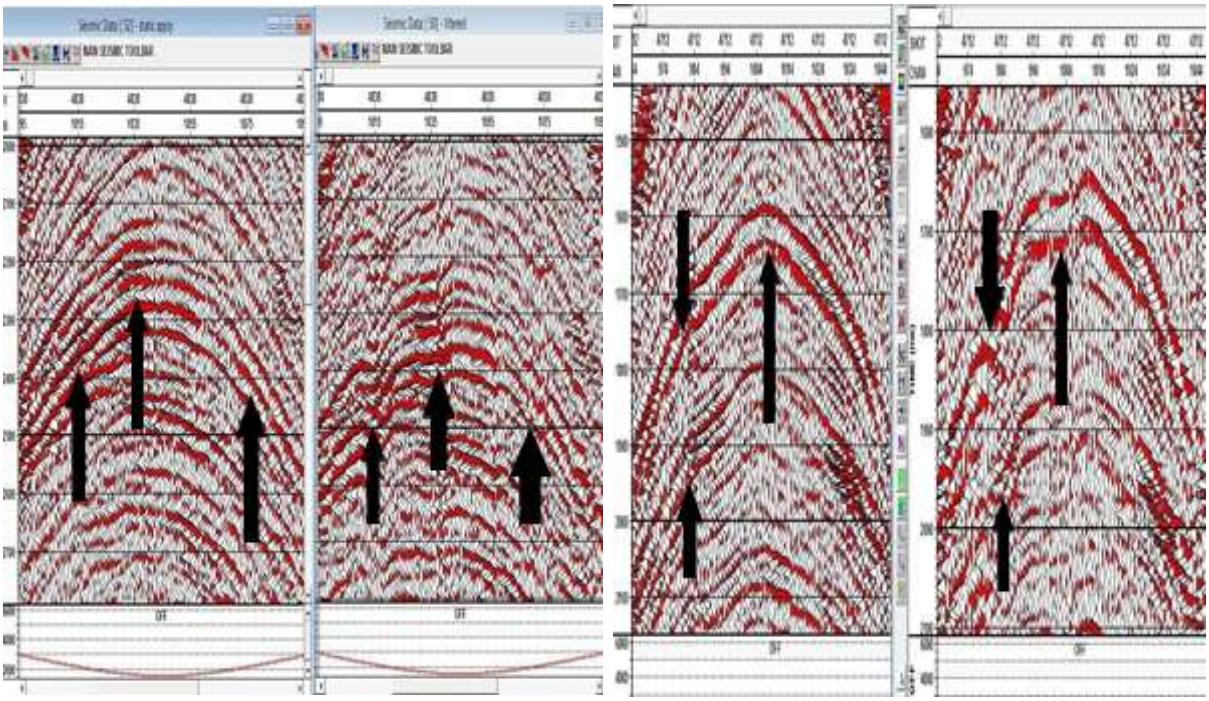

Figure 4.25: Juxtaposed view of partial statics corrected shot (left) and uncorrected shot (right) for shot gather 4838 and 4712 respectively showing the impact of their derived and implemented statics (From Opara et al., 2017 and 2018).

This superior result achieved at this processing stage of the present study is attributed to the more accurate and robust near-surface modeling algorithm we adopted (for the study) upon which the refraction statics solution was sought, derived and applied.

4.4.2 Derived Refraction Statics Solution applied to Stacked Section

After the demonstration of the effectiveness of the derived and applied refraction statics solution on the shot gathers, a further step was taken by stacking the data. Stacking is basically a data compression procedure. The approach adopted was the common midpoint (CMP) stack, which sums all offsets of a CMP gather into one block trace. To demonstrate the effectiveness of the derived refraction statics solution, we displayed a stacked CMP in a specific in-line direction

without any form of refraction statics correction applied and then we applied the derived refraction statics solution to the data and stacked. After stacking, the same in-line was equally extracted and displayed, to mirror the same events to see how the refraction statics solution has improved the alignment of reflection events and overall data quality of the stacked section. Figure 2.26 (a) shows a stacked section (in-line 79) without refraction statics, (b) shows the stacked section after the application of the derived refraction statics solution. The (c) part shows the stacked section after 1st residual statics and (d) the same stacked section after 2nd residual statics.

(a) Stacked Section without Refraction Statics (b) Stacked Section after Applying Refraction Statics

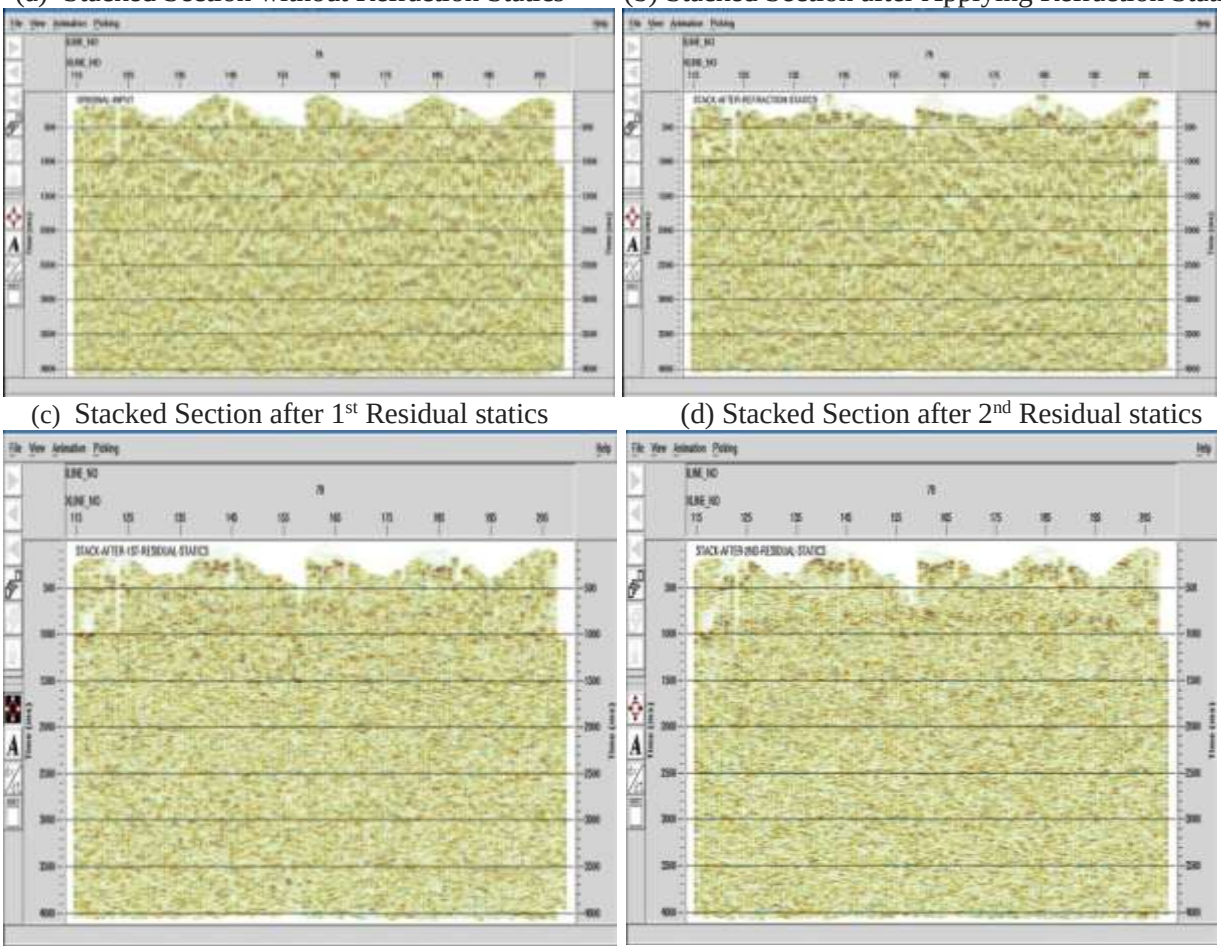

(c) Stacked Section after 1st Residual statics (d) Stacked Section after 2nd Residual statics

Figure 4.26: Selected slides showing stacked section without refraction statics (a), stacked section after the application of refraction statics (b), the stacked section after 1st residual statics (c) and the same stacked section after 2nd residual statics (d)

On first examination of Figure 4.26, the problems of refraction statics which have been resolved after the derived refraction statics solution was applied may not be easily seen by an inexperienced (novice) seismic data processor/interpreter. This now makes Figure 4.27 (a) and (b) more instructive as efforts have now been made to enlarge the already presented stacked section with annotations and markers inscribed to reveal areas were the stacked section has improved in its resolution as a result or consequence of the applied refraction statics solution as well as the 1st and 2nd residual statics corrections.

(a) Refraction statics problem is resolved as reflectors are moved backed to their actual positions

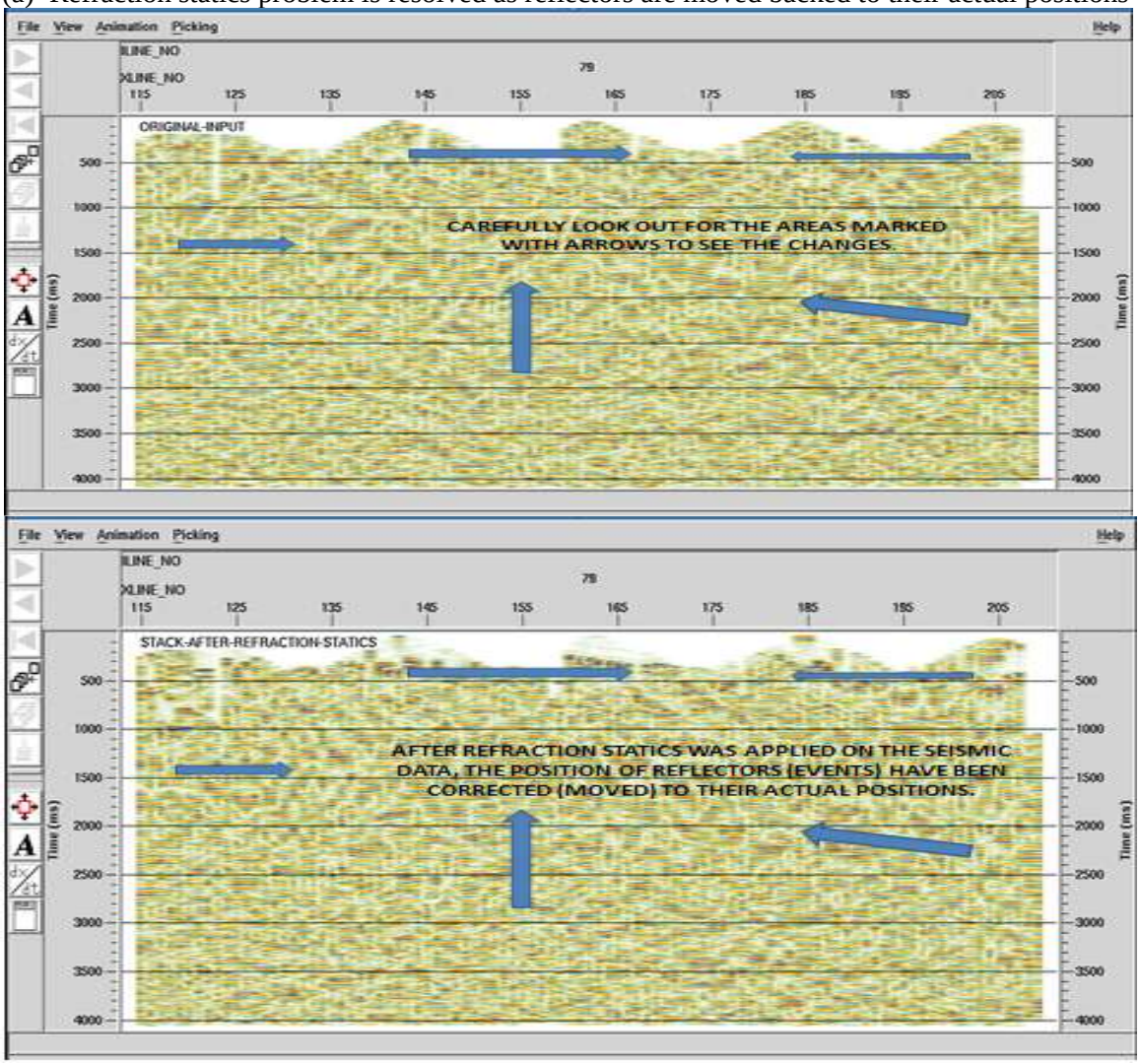

Figure 4.27: (a) Selected slides showing with marked arrows and annotation of the resultant effect of the applied refraction statics solution on the stacked seismic section.

(b) Remaining refraction statics problems are resolved with 1st and 2nd Residual Statics integrated into the refraction statics solution

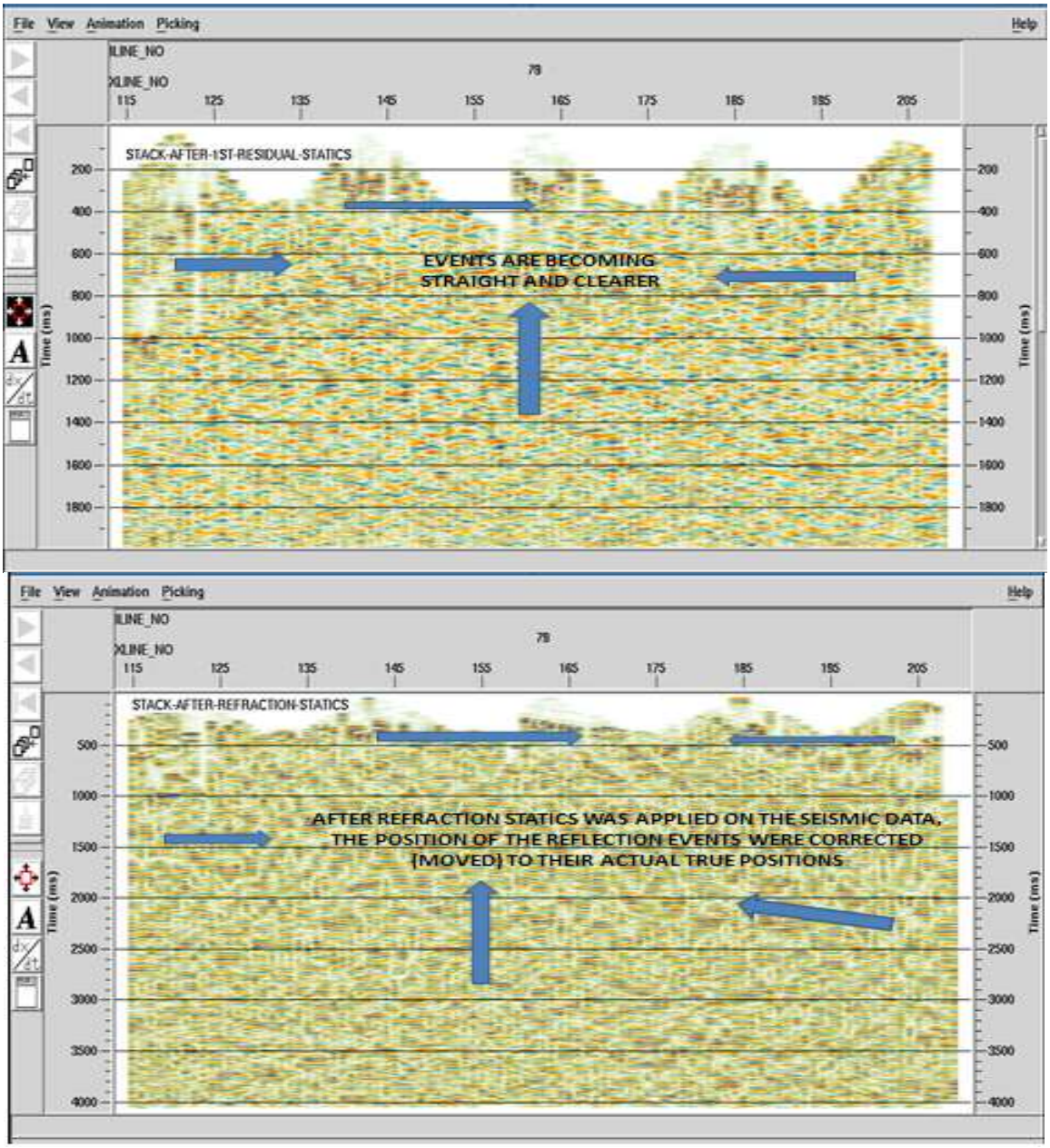

Figure 4.27(b): Selected slides showing with marked arrows and annotation of the resultant effect of 1st and 2nd residual statics correction added to the already applied refraction statics solution on the same stacked seismic section.

On close examination of the original input; the stacked section without refraction statics solution applied, spurious reflections or events at positions that are not true representation of the geology of the area being imaged are seen. After refraction statics was applied as seen on the

stack after refraction statics, events occurring at 500ms, 1500ms and 2000ms are seen to align properly and are exhibiting better continuity. This is a positive indication that the derived and applied refraction statics solution is the most appropriate for the SOKU prospect, and more importantly, that the solution is surface consistent. Similarly, on close examination of the section after 1st and 2nd residual statics correction (Figure 4.27 (b)), it is equally observed that events (reflectors/refractors) are more straight or continuous and certain portions of the stacked sections with strong pseudo amplitudes (energy) were tapered to their actual amplitudes, thus improving the reliability and integrity of the dataset. This type of stacked section is the most desirable (input data type) for QC checks and detailed interpretation.

Our conviction that the derived and applied refraction statics solution has tremendously improved the data quality and integrity of the stacked section is further supported in Figure 4.28 in which a final step which entailed decomposition of the stacked section into time frame displays of (0 – 1.5 seconds), (1.5 – 3 seconds) and (3 – 4 seconds) was extracted and displayed for this corrections to be made more visible in support of the assertion that the derived refraction statics solution as presented is the optimal solution to address the statics challenge for SOKU. The (a) part of Figure 4.25 represents the stacked section display before and after statics correction at time frame (0 – 1.5 seconds), the (b) part is the display for time frame (1.5 – 3 seconds) while the (c) part is for time frame (3 – 4 seconds)

(a) Stacked section before and after implementing refraction statics for time frame (0 - 1.5 seconds)

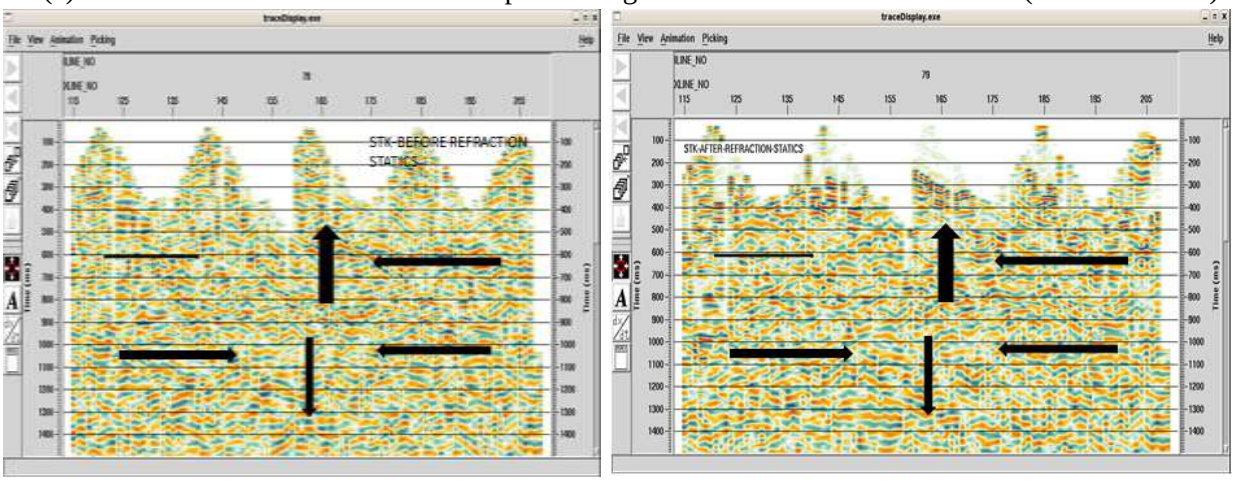

(b) Stacked section before and after implementing refraction statics for time frame (1.5 - 3 seconds)

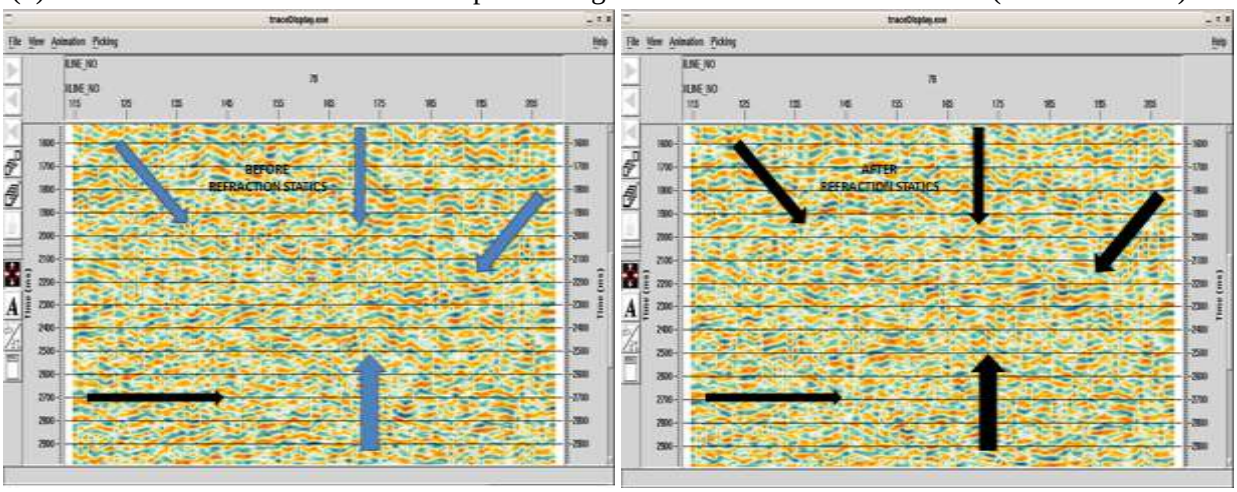

(c) Stacked section before and after implementing refraction statics for time frame (3 - 4 seconds)

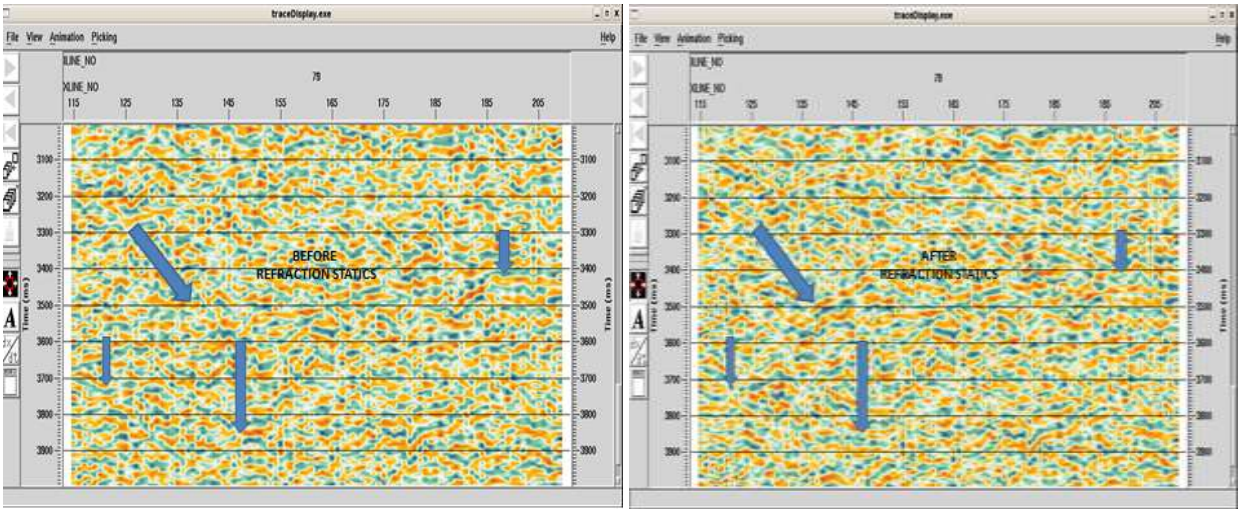

Figure 4.28: Decomposed/Time stretched slides of stacked section before and after application of refraction statics. Time frame of 0–1.5 seconds is shown in (a), Time frame 1.5–3.0 seconds in (b) and Time frame 3–4 seconds in (c). The effects of refraction static are now very evident and clearly visible.

4.3.3 Derived Refraction Statics Solution applied in Migrated Section

Migration of seismic data is a crucial (if not the most) important processing stage in the seismic data processing workflow, it is performed to move dipping events to their correct positions, collapse diffractions and increase the spatial resolution of the data being processed. Migration is a technology driven (dependent) procedure and could be achieved in time or depth domains. Computer power, time factor, resources and peculiarity of acquired datasets are key variables to consider when deploying a migration method/type. A time migration algorithm (an Explicit Finite Difference 3D Time Method, FX (Explicit) Type) was applied. This choice was guided by the processing power of our workstation, time, data specifications or peculiarity and the fact that time migration routines are relatively less complex to perform than depth migration routines.

The migration algorithm on Promax^{TM} used explicit F – XY spatially – variant extrapolators to perform time migration for the 3D seismic dataset. The migration caters for complex dips up to a maximum of 70 degrees. The migration used a vertical and spatially – variant interval velocity field in time, $V_{int}\ (x, y, t)$ as input. The deployed migration type is modern with a high degree of accuracy in achieving successes for time migration procedures. It solves the wave equation by applying spatially varying convolution operators in the F-X domain. Figure 4.29 is a time migrated stacked section of the area under consideration (in-line 79) without refraction statics implementation.

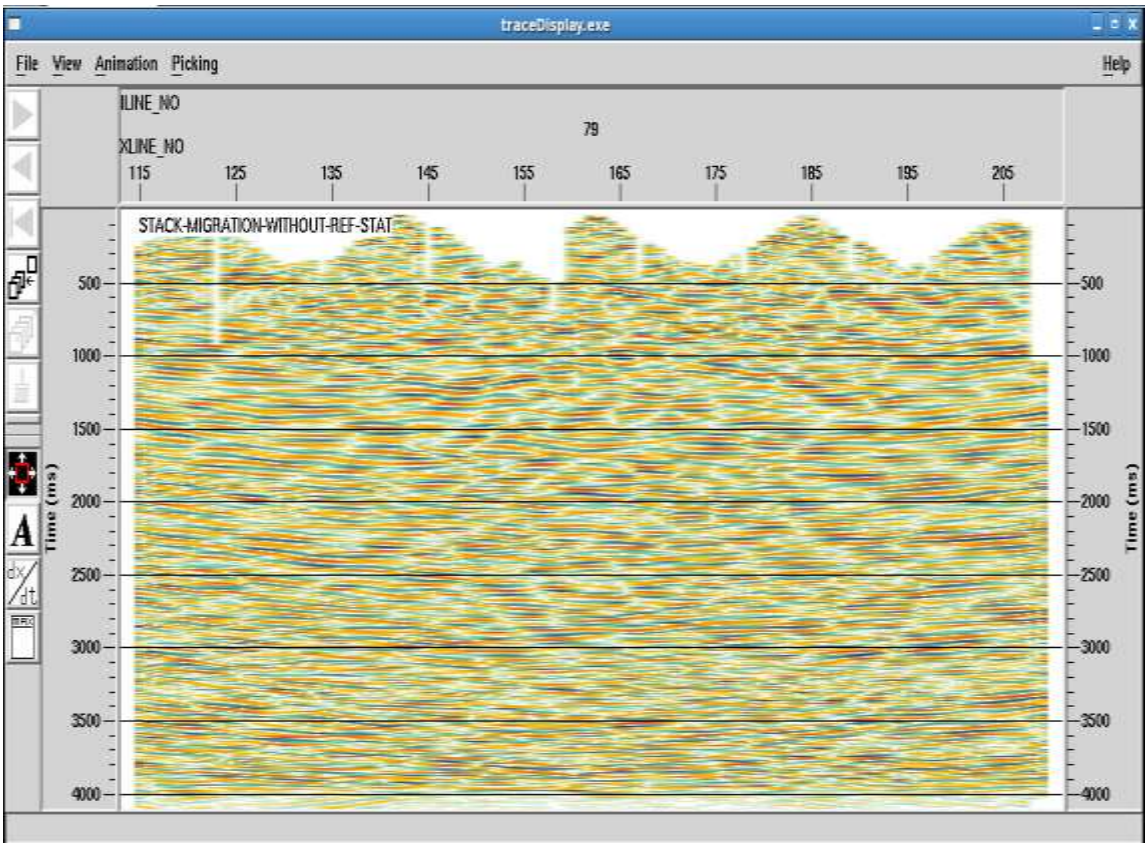

Figure 4.29: Migrated stacked seismic section without the application of refraction statics

Figure 4.30 is a time decomposed display of the migrated stacked section in intervals of 0 – 1 seconds, 1 – 2 seconds and 3 – 4 seconds for a clearer view of reflection events.

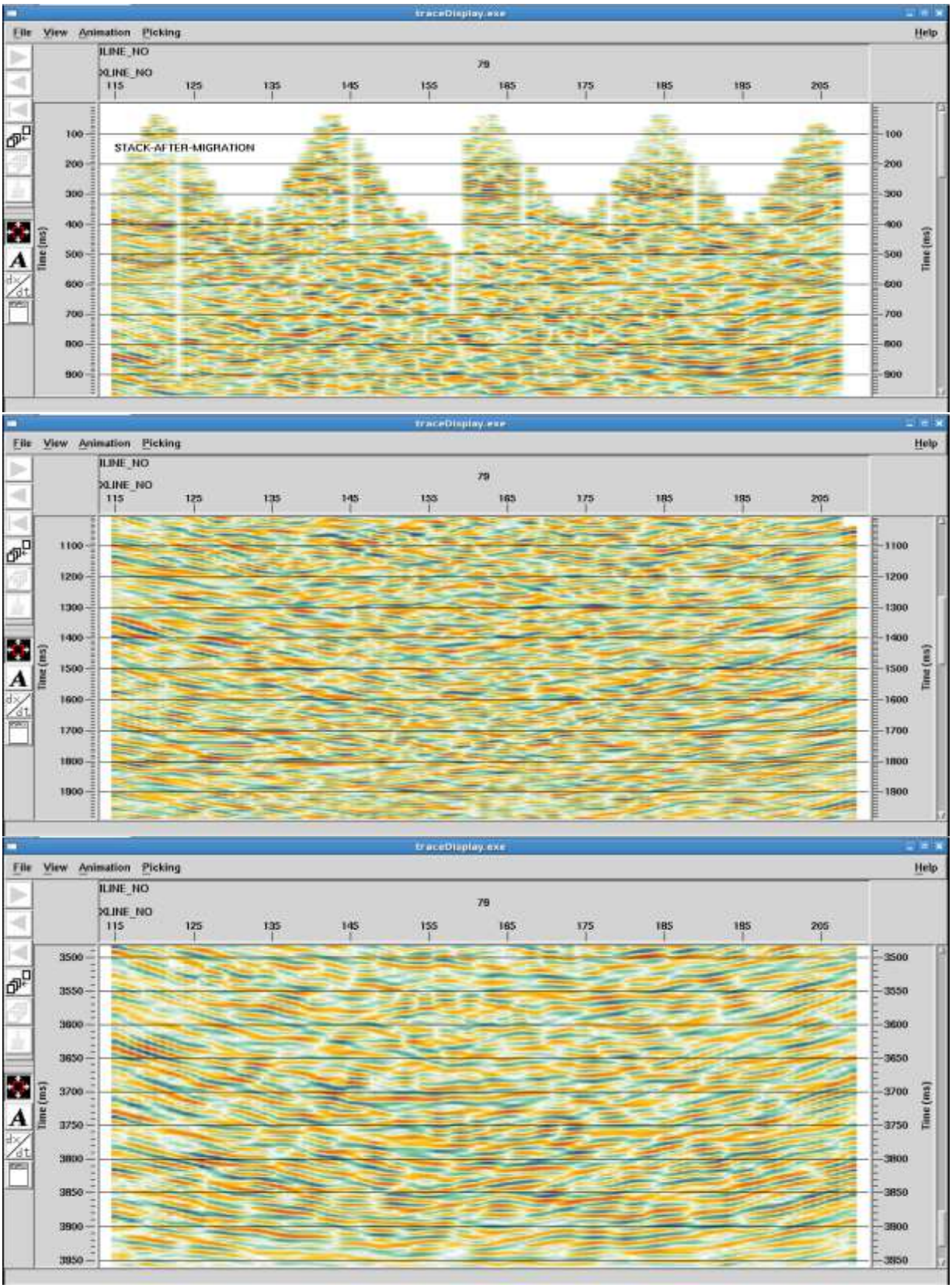

Figure 4.30: Stacked seismic section after migration decomposed into time frames to improve lateral and temporal resolution but without the application of refraction statics.

Figure 4.31 is also a time decomposed display of the same section within the same time interval but after the derived refraction statics solution was implemented then followed by migration.

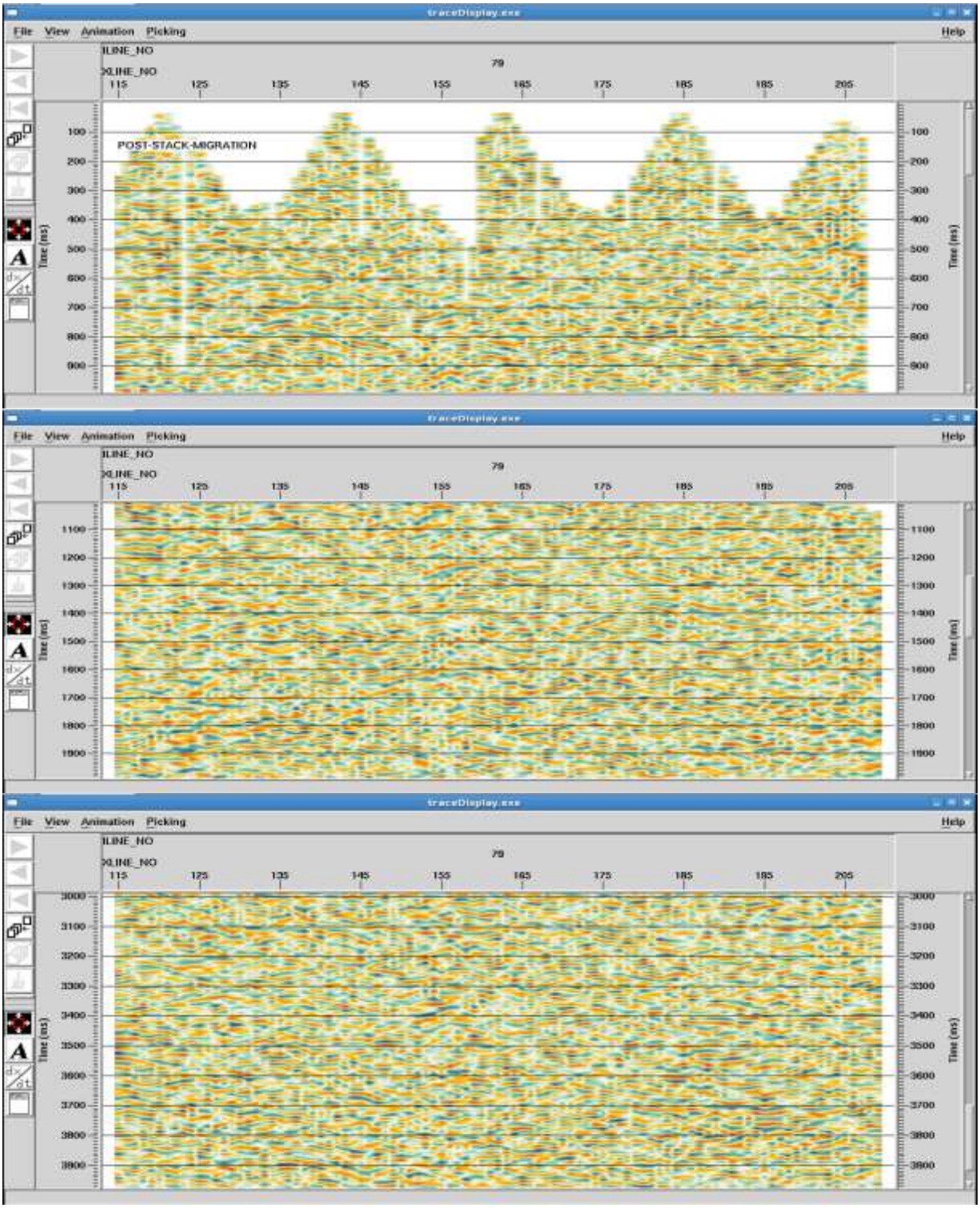

Figure 4.31: Stacked seismic section after migration decomposed into time frames to improve lateral and temporal resolution after the application of refraction statics

Upon close examination, it is observed that the imaging quality (spatial and temporal resolution, reflectors continuity and true amplitude display) has remarkably improved on the migrated stacked section (post migration display) after the refraction statics solution was applied. This equally, is an indication that the refraction statics solution derived for SOKU was optimal and has satisfactorily addressed the statics problem for the prospect. Figure 4.32 is a juxtaposed display of the before and after results achieved in the migration stage of the processing sequence to further buttress our present position.

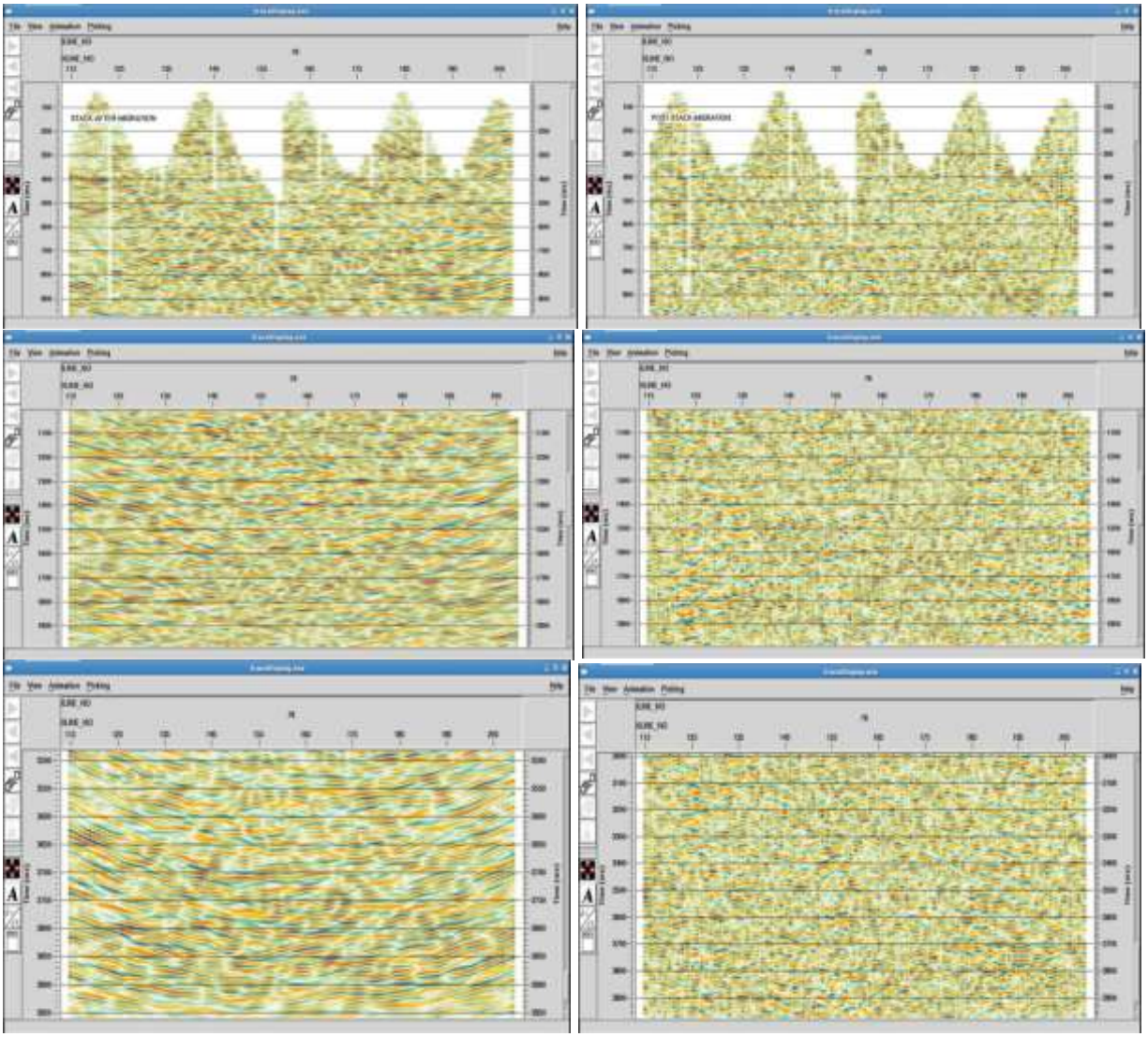

Figure 4.32: Migrated seismic sections before and after application of refraction static juxtaposed for easy assessment of the effectiveness of the derived and applied refraction statics solution.

CHAPTER FIVE

SUMMARY, CONCLUSION AND RECOMMENDATION

5.1 Summary

Statics correction involves basically a constant time shift of the seismic trace, as opposed to dynamic correction, which involves a set of time variable shifts. As with most seismic data processing steps, statics correction represents a slight simplification to physical reality. That notwithstanding, statics corrections have a dramatic effect on the final quality of the seismic section if derived and applied carefully as have been demonstrated for the SOKU dataset in this dissertation. Statics correction is important in the seismic processing sequence due to a number of reasons;

i) They place source and receiver at a common datum or plane.

ii) They ensure that reflection events on intersecting lines will be at the same time which tackles the problem of mis-ties of reflection events on the seismic section.

iii) They improve the quality of other key processing steps like velocity analysis, stacking and migration.

The effectiveness of applying a properly derived refraction statics solution (statics correction) in the overall 3D seismic data processing flow has been demonstrated in three key dimensions; on the seismic shot gathers, on a stacked section of the seismic section and finally on a migrated section of the data. It is pertinent to note that no one method in itself can solve the complete statics problem. In the pre-digital era of seismic data processing, field statics and datum statics were considered as complete solutions to resolve statics problems on seismic data. This view however, changed when refraction statics and residual statics programs evolved. The consensus point to be reiterated is that each method has its own place in adding to the complete statics

solution. In this study, we deployed all these approaches in arriving at the comprehensive solution which was applied in solving the statics problem of OML-23, SOKU. The field statics supplied the solution that resolved the elevation, near-surface inhomogeneity and a part of the long wavelength and short wavelength components of the statics problem, the refraction statics resolved bulk of the long wavelength and short wavelength component of the statics problem, while the residual statics addressed the remnant long and short wavelength components of the statics problem which the refraction statics alone could not resolve. It was by the iteration of these methods that the geological model of the subsurface was obtained which is strongly believed to be in close agreement with the actual geology of the SOKU area. It is only such valid geological model that can be interpreted for possible hydrocarbon accumulations with a high degree of accuracy.

5.2 Conclusion

The refractions extracted from a reflection survey (first-breaks) was inverted jointly with up-hole measurements using a special plugin and algorithm to image and characterize the uppermost 400 – 500 m (the near-surface) of the prospect (OML-23 SOKU), in terms of weathering and sub-weathering layer thicknesses and velocities. The obtained near-surface model was subsequently used to derive refraction statics solution for the SOKU dataset to address the identified statics problem of the area. The effectiveness of the derived refraction statics solution was evident as already demonstrated. The impact of the derived and applied refraction statics solution was first shown for shot gathers in their respective Field File Identification (FFID) arrays. Subsequently, it was demonstrated for the stacked section of the seismic data and finally on the migration result of the processing sequence affirming the effectiveness of the derived and applied refraction statics solution. The impact of the solution was remarkable and evident as reflection events were beginning to have greater

continuity and general flatness. Our conclusion therefore, is that, the refraction statics solution for the prospect (OML-23, SOKU) was derived to a reasonable high degree of accuracy. This position was supported by the before (without refraction statics applied) and after (with refraction statics applied) appearance of the shot gathers, final stacked section and the migrated sections. The derived and implemented refraction statics solution has therefore successfully solved the statics problem of SOKU as it corrected for apparent reflection times on the sections displayed. It has equally enhanced the continuity of reflection events and has reinforced the true amplitudes of the reflection events for a better energy focus.

5.3 Recommendation

The aim and target objectives of this dissertation have all be accomplished, however, it is necessary to note certain points which we wish to put forward as recommendations for those interested in this line of research. The recommendations are;

i) Travel-time inversion has an inherent non-uniqueness problem as is the case with all geophysical techniques, for this non-uniqueness problem to be minimal depends largely on the quality of the picked first arrivals and the degree of near-surface lateral velocity variations. Hence, caution should be applied in picking such arrivals to ensure accuracy and consistency, which by extension would result to a more realistic near-surface model.

ii) It is recommended that for a more thorough and exhaustive investigation of the subject matter, the tomographic/tomostatics near-surface modeling approach is implemented and compared with the approach we have deployed. The models obtained could complement each other when in agreement or could be averaged when they vary.

iii) Similarly, for the migration stage of our study, we recommend that a depth migration algorithm be deployed as more structural features, perhaps, would be revealed and it would be much easier to relate with depth than time if the end goal is for the interpretation and identification of potential reservoirs. This approach would however be more expensive and could take as long as 10 times more in seismic processing turnaround time to achieve.

5.4 Contribution to Knowledge

The dissertation has successfully solved the refraction statics (statics correction) problem of OML-23 SOKU. In the course of the study, we have arrived at some positions that we feel will become contributions to the pool of knowledge;

i) From available published literatures, this could be the first documented (pioneering) research on the subject of deriving a refraction statics solution, and applying same to seismic data up to the stacking and migration stages to demonstrate the effectiveness of the derived and applied statics solution in the Niger Delta Basin.

ii) An integrated (new hybrid) algorithm of iteratively combining both refracted arrival inversion with uphole measurements, have been deployed in this study, to build a very robust and more reliable near-surface model, which was subsequently used to derive and implement the statics.

iii) This study has successfully shown the impact and role of the derivation of refraction statics solution in enhancing the seismic imaging process, from shot gathers – stacked section – migrated section of datasets in this single but comprehensive study.

iv) Processing parameters, strategies and workflow have been carefully documented in the dissertation. These processing workflows would form a pool of resource that could be used for

future related work. Consequently, research journal articles (papers) on the successes achieved at the different stages of the dissertation have been published in reputable peer reviewed journals and now serve as reference materials for the global research community.

REFERENCES

Ahmad J., (2006), High-Resolution Seismic and Electrical Resistivity Tomography Techniques applied to image and characterize a buried channel, Thesis, University of Alberta, Canada.

Atul J., (2009), Accurate and Automatic Refraction Statics in Large 3D Seismic Datasets, Thesis, Department of Geological Sciences, University of Saskatchewen, Saskatoon.

Allen, J. R. L., (1965), Late Quaternary Niger Delta and adjacent areas; sedimentary environments and lithofacies, American Association of Petroleum Geologists (AAPG) Bulletin, (49): 547-600.

Alten, K., (2009), Statics correction in seismic surveys over complex topographies; Case study – Oichiental, Thesis of Wien University, Vienna – Austria.

Aster, R. C., Borchers, B. and Thurber, C. H., (2005), Parameter Estimation and Inverse Problems, e-Book by Elsevier, Academic Press.

Ajani, O. O., Fajemiroye, J.A. and Odumosu, O.A. (2013), Study of Near-surface Layer of Omerelu area using Low Velocity Layer (LVL) Method", *International Journal of Development and Sustainability*, 2(1): 131-139.

Bais, G., Bruno, P. G., Di Fiore, V. and Rapolla, A., (2003): Characterization of shallow volcano-clastic deposits by tuning ray seismic tomography: an application to the Naples urban area. *Journal of Applied Geophysics*, (52): 11-21.

Baker, G. S., (1999), Processing Near-surface Seismic Reflection Data: A Primer: Young, R.A., Series, Society of Exploration Geophysicists (SEG), Tulsa, Oklahoma.

Barry, K. M., (1967), Delay time and its application to refraction profile Interpretation in Seismic Refraction Prospecting, Society of Exploration Geophysicists (SEG), Tulsa, Oklahoma.

Becerra, C., Agudelo, W. and Guevara, S., (2009), Uncertainty Analysis in Statics Corrections Obtained by Tomographic Inversion: Application in a Mountainous Zone in Catatumbo (Colombia). The Leading Edge, 28(2): 212–215.

Beck, A., and Steinberg, J., (1986), Datum correction using transfer velocity map: Presentation at the 3rd Annual Summer Research Workshop of the Society of Exploration Geophysicists (SEG).

Beckett C., Brooks T., and Gregg P., (1995), Reducing 3D Seismic Turnaround; An Oil field Review.

Belfer, I. and Landa, E., (1996), Shallow velocity–depth model imaging by Refraction Tomography, Journal of Geophysical Prospecting (SEG) (44): 859-870.

Bergman, B., Tryggvason, A., and Juhlin, C., (2004), High resolution seismic travel-time tomography incorporating static corrections applied to a till-covered bed rock environment, Geophysics, (69): 1082-1090.

Bohm G., Accaino F., Rossi G. and Tinivella U., (2006), Tomographic joint inversion of first arrivals in a real case from Saudi Arabia, Madrid workshop on Near-surface 2005, Geophysical prospecting, (54): 667-680.

Boschetti, F., Dentithz, M.C. and List, R.D., (1996), Inversion of seismic refraction data using genetic algorithms, Geophysics, (61): 1715-1727.

Bridle, R., and Aramco, S., (2009), Delay-Time Refraction Methods applied to a 3D Seismic Block. The Leading Edge Publication, 28(2): 228–237.

Brouwer, J., and Helbig, K., (1998), Shallow High-resolution reflection seismic: Series Handbook of Geophysical Exploration (Seismic Exploration), Elsevier Publishing, (19).

Buker, F., Green, A.G., Horstmeyer, H., (1998), Shallow seismic reflection study of a glaciated valley. Geophysics, (63): 1395-1407.

Butler, D. K., (2005), Near-surface Geophysics: Publication of the Society of Exploration Geophysicist (SEG). Tulsa, Oklahoma.

Burger, P., Garotta R., and Granger, P. (1998), Improving resolution and seismic quality assurance through field pre-processing; The Leading Edge, (17): 1562-1569.

Chang, X., Liu, Y. K. and Wang, H., (2002), 3-D Tomography Static Correction, Geophysics, 67(4): 1275–1285.

Chun, J. H., and Jacewitz, C. A., (1981), The first arrival time surface and estimation of statics: A Presentation at the 51st Annual International Meeting of the Society of Exploration Geophysicist (SEG).

Coppens, F., (1985), First Arrival Picking on Common-Offset Trace Collections for Automatic Estimation of Static Corrections, Geophysics, 33(1): 1212–1231.

Cordier, J. P., (1985), Velocity in reflection seismology, Kluwer Academic publishers, The Netherlands.

Cox, M., (1999), Static Corrections for Seismic Reflection Surveys Handbook, Society of Exploration Geophysicists (SEG) Book Publication Series, Tulsa, Oklahoma.

Criss, D. E. and Cunningham, D., (2001), Turning-Ray Tomography for Statics Solution, Paper at EAGE 63rd Conference and Technical Exhibition-Amsterdam, The Netherlands, (11–15).

Deere J., (2009), Introduction to This Special Section—Statics, The Leading Edge, 28(2): 190–191.

Ditmar, P., Renopp, J., Kasig, R. and Makris, J., (1999), Interpretation of shallow refraction seismic data by reflection/refraction tomography. Geophysical Prospecting, (47): 871-901.

Dobrin, M. B. and Savit, C. H., (1988), Introduction to geophysical prospecting, 4th edition, McGraw publishers, New York, 876p.

Docherty, P., (1992), Solving for the thickness and velocity of the weathering layer using 2-D Refraction tomography. Geophysics, 57(10): 1307-1318.

Doust, H. and Omatsola, E., (1990), Niger-Delta: Divergent/Passive Margin Basins, AAPG Memoir 48, American Association of Petroleum Geologists (AAPG), Tulsa, (239-248).

Duan, Y. Q., (2006), Residual Static Corrections Based on Refraction Survey. OGP, 41(1): 32–35.

Dufour, J. and Lawton, D. C., (1994), Extension of delay time analysis for 3D seismic refraction statics, Consortium for Research in Elastic Wave Exploration Seismology – CREWES,

Research report, (6): 1-5.

Durotoye, B., (1975), Quaternary Sediments in Nigeria. Rockview Publications, Jos, (431-444).

Edge, A. B., and Laby, T. H., (1931), The principles and practice of geophysical prospecting: Cambridge University Press, (339-341).

El – Behairy, M. G., Hosney, H. M., Abdel Hady, Y. E. and Mehanee, S. A., (1997), Seismic refraction method to characterize engineering sites, Proceedings of the 12th annual meeting of the Egyptian Geophysical Society (EGS), (85-94).

Enikanselu, P.A., (2008), Geophysical Seismic Refraction and Uphole Survey Analysis of Weathered Layer Characteristics in the "Mono" Field, North Western Niger Delta, Nigeria, Proceedings of National Workshop on Geophysical Seismic Analysis, Delta State Nigeria, (1 – 7).

Enviroscan, (2009), Principles of Geophysics, Web address; http;//enviroscan.com/html/principles.html

Evans, B. J., (1997), A Handbook for seismic data acquisition in exploration, Geophysical monograph series, Published by the Society of Exploration Geophysicists (SEG), Tulsa.

Feroci, M., Orlando, L., Balia, R., Bosman, C., Cardarelli, E. and Deidda, G., (2000), Some considerations on shallow seismic reflection surveys, Journal of Applied Geophysics, (45): 127-139.

Franklin, A. G., (1981), Interpretation of uphole refraction surveys, Presented at the 51st Annual International Meeting of the Society of Exploration Geophysicists - SEG: (Abstract): Geophysics 1982, (47): 459

Gadallah, M. R. and Fisher, R. L., (2005), Applied Seismology, Geophysics reference book: Penn Hall Corporation, Tulsa – Oklahoma, USA.

Gardner, L.W., (1939), Seismograph prospecting: United States Patent 2153920; (Abstract), Geophysics, (4): 313.

Gholami, A., (2013), Residual Statics Estimation by Sparsity Maximization, Geophysics, 78(1): 11–19.

Global Geophysics Course Material, University College London (UCL), (2009), Sketch of a simple refraction model.

Hagedoorn, J. G., (1959), The plus-minus method of interpreting seismic refraction sections: *Geophysical Prospecting*, (7): 158 -182.

Han, X. L., Yang, C. C. and Ma, S. H., (2008), Static of Tomographic Inversion by First Breaks in Complex Areas. Journal of Progress in Geophysics, 23(2): 475–483.

Hampson, D., and Russell, B., (1984), First-break interpretation using generalized linear Inversion: *Journal of the Canadian Society of Exploration Geophysicist (CSEG)*, (20): 45-54.

Hao, J., Yang, R. J., and Wu, J., (2011), Processing of Static Correction Problems of Seismic Data in the Complex Surface, Journal of Complex Hydrocarbon Reservoirs, 4(3): 34–37.

Hatherly, P. J., Urosevic, M., and Lambourne, A. and Evans, B. J., (1994), A Simple Approach to calculating Refraction Statics Corrections. Geophysics, 59 (1): 156 –160.

Hawkins, L. V., (1961), The reciprocal method of routine shallow seismic refraction investigations, Geophysics, (26): 806-819.

He, L., Zhang, J., and Zhang, W., (2011), Tradeoffs in the near-surface seismic imaging solutions: SEG Technical Program Expanded Abstracts, (30): 4015-4019.

Henley, D. C., (2009), Ray path interferometry: Statics in Difficult Places. The Leading Edge, 28(2): 202–205.

Henley, D. C., (2012), Interferometric Application to Static Corrections, Geophysics, 77(1): 1–13.

Hospers, J. (1965), Gravity Field and the Structure of the Niger Delta, Nigeria Geological Society American Bulletin, (76): 407- 422.

Huang, M. Z., Feng, Z. Y. and Zhou, D. T., (2008), Directly Iterated Static Corrections Method in Offset Domain and Its Application. Journal of Progress in Exploration Geophysics, 31(1): 122–128.

Hui F., (2012), Comparism of Near-surface Seismic Velocity estimation methods with application to Onshore Peru and Offshore Malaysia, Thesis, University of Houston, USA.

Hunter, J. A. and Burns, R. A., (1990), Determination of over-burden *P*-wave velocities with a downhole 12-channel eel; Proceeding at the 60th Annual International Meeting of the Society of Exploration Geophysicists, Expanded Abstracts, (399-401).

Jing, X. L., (2003), Two Steps Solution Method for Big Residual Static Corrections, OGP, 38(1): 50-57.

Juhlin, C., Palm, H., Mullern, C. and Wallberg, B., (2002), Imaging of groundwater resources in glacial deposits using high-resolution reflection seismics, Sweden. Journal of Applied Geophysics, (51): 107-120.

Ke, B., Zhang, J. and Chen, B., (2007), Fast-Ray First Arrival Seismic Tomography and Its Application, Paper presented at the 77th Annual International Meeting, SEG and gazetted in the book of Expanded Abstracts.

Kearey, P. and Brooks, M., (1991), An introduction to geophysical exploration; Blackwell scientific publications incorporated, Oxford, UK. 296p.

Khan, K.A., (1994), An intelligent and efficient approach to picking first breaks: Proceedings at the 56th Meeting of the European Association of Exploration Geophysicists, (155).

Klett, T. R., Ahlbrandt, T. S., Schmoker, J. W., and Dolton, G. L., (1997), Ranking of the World's oil and gas provinces by known petroleum volumes: United States (US) Geological Survey Open- File Report, (97-463).

Knodel, K., Lange, G. and Voigt, H. J., (2007), Environmental Geology, Handbook of field methods and case studies, Springer Publishers, Berlin Heidelberg.

Knox, W. A., (1967), Multilayer near-surface refraction computations. Publication of the Society of Exploration Geophysicist (SEG), (197–216).

Kolawole, F., Okoro C., and Olaleye P., (2012), Downhole refraction survey in the Niger Delta Basin: A 3-layer model. ARPN Journal of Earth Sciences, 1(2) November 2012.

Krishnan, K. V. and Guha, R., (2002), Estimation of Statics from refraction data in seismic reflection records; Wiggle, (2).

Kulke, H., (1995), Nigeria in Regional Petroleum Geology of the World, Part II, Africa, America, Australia and Antarctica, Gebruder Borntraeger, Berlin, (143-172).

Kumar, T. K., (2005), 2D and 3D land seismic data acquisition and seismic data processing, a training report at Oil and Natural Gas Corporation (ONGC) in Chennai; Submitted as thesis to Department of Geophysics, Andhra University, Waltair, Visakhapatnam – India.

Laake, A., and Zaghloul, A., (2009), Estimation of static corrections from geologic and remote-sensing data. The Leading Edge, 28(2): 192–196.

Lankston, R. W., (1989), The seismic refraction method: a viable tool for mapping shallow targets into the 1990s: Geophysics, (54): 1535-1542.

Lankston, R. W., (1990): High resolution refraction seismic data acquisition and interpretation. In Ward, S. H. (Ed), *Geotechnical and Environmental Geophysics*, Volume 1, Society of Exploration Geophysicists, Investigations in Geophysics, (5): 45-73.

Lanz, E., Maurer, H. and Green, A.G., (1998), Refraction tomography over a buried waste disposal site, Geophysics, (63): 1414-1433.

Lawton, D. C., (1989), Computation of refraction static corrections using first-break travel time differences, Geophysics, (54): 1289 -1296.

Lawton, D. C., (1990), A nine-component refraction statics experiment, Proceedings at the 60th Annual International Meeting Society of Exploration Geophysicist (SEG), Expanded Abstracts, (1089-1092).

Li, P., Zhou, H. and Yan, Z., (2009a), Deformable Layer Tomostatics: 2D Examples in Western China, The Leading Edge, 28(2): 206–210.

Li, P., Feng, Z. and Li, Z., (2009b), Static Correction Technology and Applications in Complex areas of Western China. The Leading Edge, 28(2): 382–386.

Li, L., Chen, X. J. and Jing, X. L., (2011), Multiscale Inversion Algorithm for Seismic Residual Static Correction and Its Application, Xinjing Petroleum Geology Journal, 32(4): 402–405.

Li, Y., Sun, P., Yang, H., Zhang, D. and Zhou, J., (2007), Application of the FBTD converted wave static method in a sand dune area; First Break, (25).

Lin, B. X., Sun, J. M., Xu, Y. and Li, B., (2006), Discussion on several static correction methods. Petroleum Geophysics Series, 45(4): 367-372.

Lines, L.R. and Treitel, S., (1984), A review of least-squares inversion and its application to geophysical problems. Geophysical Prospecting, (32): 159-186.

Liu, J. K., Kuang, C. Y. and Gao, R., (2010), Data Processing Test and Research on the Deep Seismic Reflection Profile in Polymetallic Deposits Area: Taking an Example of Luzong Ore Concentrated Area, Acta Petrological Sinica Journal, 26(9): 2561–2576.

Liu, L. S., (1998), Constrained first-arrival pickup and first-break residual static correction, OGP, 33(5): 604–610.

Luo, Y. W., Yang, J., and Duan, W. X., (2010), Comparing between several static corrections Methods, Petroleum Instruments Series, 24(5): 41–43.

Macrides, C.G. and Dennis, L.P., (1994), 2D and 3D refraction statics via tomographic inversion with under-relaxation, First Break (12): 523-537.

Mares, S., (1984), AIntroduction to Applied Geophysics, Reidel D. Publishers, Dordrecht, Lancaster, 581p.

Mark, L., (1994), An implementation of 3-D seismic binning, A Consortium for Research in Elastic Wave Exploration Seismology (CREWES) Technical Paper, University of Calgary, Canada.

Marsden, D., (1993a). Statics corrections – a review, part I. The Leading Edge, 12(1): 43-49.

Marsden, D., (1993b). Statics corrections – a review, part II. The Leading Edge, 12(2): 115-120.

Marsden, D., (1993c). Statics corrections – a review, part III. The Leading Edge, 12(3): 210-216.

Marti, D., Carbonell, R., Tryggvason, A., Escuder, J. and Perez-Estaun, A., (2002), Mapping brittle fracture zones in three dimensions: high- resolution travel-time seismic tomography in a granitic pluton. Geophysical Journal International, (149): 95-105.

Menke, W., (1984), Geophysical Data Analysis: Discrete Inverse Theory, Revised Edition, New York Academic Press Incorporated.

Merki, P.J. (1970), Structural Geology of the Cenozoic Niger Delta (African Geology), University of Ibadan Press, Ibadan, (251-268).

Miller, K.C., Harder, S.H., Adams, D.C. and O'Donnel Jr., T., (1998), Integrating high-resolution refraction data into near-surface seismic reflection data processing and interpretation. Geophysics, 63: 1339-1347.

Morozov, I. B., and Jhajhria A., (2008), 3D Refraction Statics Integrated with Surface Consistent First-Break Picking, Iterative Inversion, and 3D Visualization, A proceeding at the 2008 CSPG/CSEG/CWLS Convention in Canada.

Olsen, K. B., (1989), A stable and flexible procedure for the inverse modeling of seismic first arrivals, Journal of Geophysical Prospecting, 7: 455-465.

Opara, C., Adizua, O. F. and Ebeniro, J. O. (2018), Application of static correction in the processing of 3D seismic data from onshore Niger Delta; *Universal Journal of Geoscience UJG*, 6(1): 1-7.

Opara, C., Adizua, O. F. and Ebeniro, J. O. (2017), Near-surface seismic velocity model building from first arrival travel-times – A case study from onshore , Niger – Delta; *Universal Journal of Physics and Application UJPA*, 12(1): 1-10.

Pan, H. X., Fang, W. B., and Wu, Y. S., (2003), An Improved Relative Refraction Statics Technique. Geophysical Prospecting for Petroleum, 42(2): 208–211.

Palmer, D., (1981), The Generalized Reciprocal Method of Seismic Refraction Interpretation. Society of Exploration Geophysicists (SEG) Geophysics online, (1–104).

Palmer, D., (1986), Refraction Seismics; Handbook of Geophysical Exploration, Volume 13: Geophysical Press, United States.

Ponnam, S., Navin, M., Sarvind, R., Sudhakar, M. and Dutta, N. M., (2013): Field Statics estimations: A case history from North Assam Shelf, Assam, India. A Technical paper presented at the 10th Biennial International Conference and Exposition – *SOCHI 2013*, (287-291).

Postma, G. W., (1955), Wave propagation in a stratified medium: Geophysics, 20: 780–806.

Press, F., (1966), Seismic velocities, in Clark, S. P., Jr., Ed., Handbook of physical constants: Geological Society of America Memoirs. 97: 195–218.

Pritchett, W. C., (1990), Acquiring better seismic data, A reference Geophysics book series, Published by Springer.

Pugin, A., and Pullan, S. E., (2000), First arrival alignment static corrections applied to Shallow seismic reflection data: Journal of Environmental and Engineering Geophysics (JEEG), 5: 7 – 15.

Qin, F., Cai, W., and Schuster, G.T., (1993), Inversion and imaging of refraction data, Proceedings at the 63rd Annual International Meeting of the Society Exploration Geophysicist (SEG), Expanded Abstracts, (613-615).

Raef, A., (2009), Land 3D-Seismic Data: Preprocessing Quality Control Utilizing Survey Design Specifications, Noise Properties, Normal Moveout, First Breaks, and Offset, *Journal of Earth Science*, 20(3): 640–648.

Rajasekaran, S. and McMechan, G. A., (1996), Tomographic estimation of the spatial distribution of statics. *GEOPHYSICS*, 61(4): 1198-1208

Ricker, N., (1977), Forms and laws of propagation of seismic wavelets, proceedings of the world petroleum congress – 1977, Geophysics Series, 18(1).

Ronen, J. and Claerbout J., (1985), Surface-Consistent Residual Statics Estimation by Stack-Power Maximization, *Geophysics*, 50(2): 2759–2767.

Roy, B. N., Chandra, V., Singh, S. S., Ramakrishna, G. S. and Guha, R., (2008), Improved imaging through Refraction Statics in a sand dune area: a case study, A paper presented at the Annual SPG Conference, Hyderabad 2008.

Roy, B. N., Singh, S. S., Guha, R., Sinha, K. K. and Pandey, U. S. D., (2010), Enhanced imaging through 3D volumetric refraction static in Rajasthan area: a case study, A paper presented at the 8th Biennial International Conference and Exposition on Petroleum Geophysics (Hyderabad 2010).

Russell, B. H., (1990), Statics correction – A tutorial; A scientific publication by Hampson-Russell software services limited in the *Recorder*, 14(3): 16-30.

Sabbione, J. I. and Velis, D., (2010): Automatic first – breaks picking: New strategies and algorithms. *GEOPHYSICS*, 75(4): 67-76.

Sadi, H. N. A., (1980), Seismic exploration, Birkhauser Verlag, Basel, Stuttgart, 250p.

Shell Processing Support (SPS) Format for Land 3-D Surveys, (2011), SOKU OML 23, 3D

Shell Producing Development Company (SPDC) Report, (2006), Environmental Impact Assessment (EIA) of SOKU (OML 23) 3D Seismic Survey, SPDC, Port Harcourt, Nigeria.

Sheriff, R. E., (1991), Encyclopedic Dictionary of Exploration Geophysics, Society of Exploration Geophysicists (SEG) Publication, 323p.

Sheriff, R. E. and Geldart, L. P., (1999), Exploration seismology, Cambridge university press (2nd edition), 592p.

Sheriff, R., (2002), Encyclopedic dictionary of applied geophysics: Society of Exploration Geophysicists (SEG) Publications, Seismology and Exploration Geophysics series.

Short, K.C. and Stauble, A.J., (1967), Outline of the Geology of Niger Delta. American Association of Petroleum Geologists Bulletin, 51: 761-779.

Simmons, J. L. and Backus, M. M., (1992), Linearized Tomographic Inversion of First-Arrival Times. *Geophysics*, 57(1): 1482–1492.

Sjoren, B., Ofsthus, A. and Sandberg, J., (1979), Seismic classification of rock mass qualities, Geophysical prospecting, 27: 10-40.

Stark, A., (2008), Seismic methods and applications, Brown Walker press, Boca Raton, Florida-USA.

Stefani, J. P., (1995), Turning – ray Tomography. *GEOPHYSICS*, 60(6): 1917-1929.

Stein, J. A., Langston, T., and Larson, S. E., (2009), A Successful Statics Methodology for land Data. The Leading Edge Publication, 28(2): 222–226.

Steeples, D. W., Miller, R. D., and Black, R. A., (1990), Static corrections from shallow reflection surveys: Geophysics, 55: 769 – 775.

Stone, D. G., (1995), Designing seismic surveys in two and three dimensions, Geophysical reference volume 5. A Publication of the Society of Exploration Geophysicist (SEG), Tulsa – Oklahoma, USA.

Taner, M.T., Lu, L., and Baysal, E., (1988), Unified method for 2D and 3D Refraction Statics with first break picking by supervised learning: 58th Annual International Meeting of the Society of Exploration Geophysicists (SEG), Expanded Abstracts, (772-774).

Taner, M. T., Wagner, D. E. and Baysal, E., (1998), A Unified Method for 2-D and 3-D Refraction Statics, Geophysics, 63: 260–274.

Telford, W. M., Geldart, L. P., Sheriff, R. E., and Keys, D. A. (1976), Textbook of Applied Geophysics, Cambridge University Press.

Uko E. D., Ekine A. S. and Ebeniro J. O. (1992), Weathering Structure of the East- Central Niger Delta, Nigeria. Geophysics, 57(9): 1228-1233.

Vossen, R. V. and Trampert, J., (2007), Full-Waveform Static Corrections Using Blind Channel Identification, *Geophysics*, 72(4): U55–U66.

Wang, S. D., (2005), Static Corrections of Complex Topography Based Wave Equation Datuming, *OGP*, 40(1): 31–34.

Wang, J. H., (1999), Thinking about the Normal Moveout Corrections and Static Corrections, *OGP*, 34: 18–26.

Wang, W., and Cheadle, S., (1995), Branch point analysis in refraction interpretation, CSEG National Convention, Expanded abstracts.

Whiteley, R. J., Holmes, W. H. and Dowle, R. D., (1990a), A new method for Downhole – Cross hole seismics for geotechnical investigation, Exploration Geophysics, 21: 83-89.

Whiteley, R. J., Fell, R. and MacGregor, J. P., (1990b), Vertical seismic shear wave profiling (VSSP) for engineering assessment of soils, Exploration Geophysics, 21: 45-52.

Wilson, W., (1994), Residual static estimation using the genetic algorithm. Geophysics, 59: 766 – 774.

Wong, J., Bregman, N., West, G. and Hurley, P., (1987), Cross-hole seismic scanning and Tomography, The Leading Edge, 6(1): 36-41.

Wu, K. F., Zhang, X. Q., and Zheng, G. Y., (2009), Review of Converted-Wave Statics Correction Method Based on Body-Wave. Chinese Journal of Engineering Geophysics, 6(6): 768–774.

Yan, X., Zhong, G. F. and Li, Q. Y., (2006), Stratal Carbonate Content Inversion Using Seismic Data and Its Applications to the Northern South China Sea. Journal of China University of Geosciences, 17(4): 320–325.

Yang, W. J., Duan, Y. Q. and Jiang, W. C., (2005), Tomographic Statics, Geophysical and Geochemical Exploration, 29(1): 41–43.

Yin, C., Xiong, X. J. and Zhang, B. L., (2004), The Study of Using the Fourth Accumulated Component in Residual Static Corrections, *Gas Industry Journal*, 24(12): 48–50.

Yilmaz, O., (1987), Seismic data processing, Society of Exploration Geophysicists (SEG), special processing manual, Tulsa, USA. 2027p.

Yilmaz, O., (2001), Seismic Data Analysis: Processing, Inversion, and Interpretation of data, Society of Exploration Geophysicists (SEG) Processing Reference Handbook, Tulsa, Oklahoma, USA.

Yordkayhun, S., Juhlin, C., Giese, R. and Cosma, C., (2007), Shallow Velocity–Depth Model using first arrival travel-time inversion at the CO_2SINK site, Ketzin, Germany;

Journal of Applied Geophysics (Publisher; ScienceDirect by Elsevier), 63: 68 -79.

Yordkayhun, S., Tryggvason, A. and Norden, B., (2009), 3D Seismic Travel-time Tomography Imaging of the Shallow Subsurface at the CO_2SINK Project Site, Ketzin, Germany. Geophysics, 74(1): G1–G15.

Zanzi, L., (1990), Inversion of refracted arrivals: a few problems: *Geophysical Prospecting*, 38: 339-364.

Zanzi, L., and Carlini, A., (1991), Refraction statics in the wavenumber domain, Geophysics, 56: 1661-1670.

Zhang, J. and Toksoz, M. N., (1998), Nonlinear refraction traveltime tomography. *GEOPHYSICS*, 63(5): 1726-1737.

Zhang, J., Zhao, B. and Zhou, H., (2009), Fast Ray Tomography with Optimal Relaxation Factor, Paper presented at the 79th Annual International Meeting of the Society of Exploration Geophysicists (SEG) gazetted in the book of Expanded Abstracts, (4044-4048).

Zhu, X., Sixta, D. P. and Angstman, B. G., (1992), Tomostatics; Turning – ray tomography + statics corrections. The Leading Edge, 11(12).

Zhu, X., Valasek, P. and Roy, B., (2008), Recent Applications of Turning-Ray Tomography, Geophysics, 73(5): VE243–VE254.

Zhu, X. S., Gao, R., Li, Q. S., Guan, Y., Lu, Z. and Wang, H., (2014), Static corrections methods in the processing of deep reflection seismic data, *Journal of Earth Science*, 25(2): 299–308.

Appendix

SOURCE INDEX FILE (SPS) (A Full Listing of Source Index File for Dynamite Shots)

```
H00 Sps format version num.      SPS003,13.10.10;
H01 Description of survey area   NIGERIA,XXXX,(SOKU,OML23);
H02 Date of survey               X.X.XXXX,X.X.XXXX;
H021Post-plot date of issue      00.00.XXXX;
H022Tape/disk identifier         3D-SOKU-10;
H03 Client                       XXXX XXXX;
H04 Geophysical contractor       XXXX/XXX Crew XXXX;
H05 Positioning contractor       XXXX/XXX Crew XXXX;
H06 Pos. proc. contractor        XXXX;
H07 Field computer system(s)     SN408 XL Software V6.1,SN408+Link,DOS disks;
H08 Coordinate location          Center of source and receiver patterns;
H09 Offset to coord. location    0.0m;
H10 Clock time w.r.t  GMT        +1;
H11 Swath No.                    Swath 11;
H12 Geodetic datum,-spheroid     Minna Datum,84,Clarke 1880,6378249.145,293.46500
H13 Spare                        ;
H14 Geodetic datum parameters    111.916 87.852 -114.499 -1.875-0.202-0.219-0.032
H15 Spare                        ;
H16 Spare                        ;
H17 Vertical datum description   Nigeria Lagos;
H18 Projection type              Transverse Mercator(t.m.);
H19 Projection zone              Nigeria Mid Belt;
H20 Description of grid units    Meter;
H201Factor to metres             1.00000000;
H220Long. of central meridian    0083000.000E;
H231Grid origin                  0040000.000N0083000.000E
H232Grid coord. at origin        0670553.98E      0.00N;
H241Scale factor                 0.9997500000;
H242Lat., long. scale factor     0040000.000N0083000.000E;
H256LAT., LONG. INITIAL LINE     0040000.000N 083000.000E0140000.000N0083000.000E
H257CIRCULAR BEARING OF H256     0000000.0000
H258QUADRANT BEARING OF H256     N000000.000S
H259ANGLE FROM SKEW              0000000.0000
H26 PM,DEFINITION OF CODES
H26 SA: SATELLITE PT. PM: PERMA NENT MARKER
H26 PROSPECT GRID ORIGIN         13374696(X:449924.4,Y:62754.8);
H26 SOURCE, RECEIVER DIGIT       4,4
H26 RCV,SRC LINE INCREMENT       350,400;
H26 RCV,SRC POINT INCREMENT      50,50;
H30 Project code and description SOKU OML 23,S3D;
H31 Line number format           Block(1:6),Strip(7:4),Line Number(12:5);
H400Type,model,polarity          1,SN408XL+Link,CM408,SEG;
H401Crew name,comment            1,XXXX/XXX Crew XXXX(Seismic 3);
H402Sample int.,record len.      1,2.00 MSEC, 8.00 SEC;
H403Number of channels           1,1440;
H404Tape type,format,density     1,IBM 3590 Cartridge, SEG-D 8058, 75742;
H405Filter_alias hz,db pnt,slope1,200 HZ, 3.00 DB, 84.00 DB/OCT;
H406Filter_notch hz,-3db points  1,Out, None;
H407Filter_low hz,db pnt,slope   1,Out, None;
H408Time delay FTB-SOD app Y/N   1,0.00 Msec, Not Applied;
H409Multi component recording    1,Z;
H410Aux. channel 1 contents      1,50Hz;
H411Aux. channel 2 contents      1,Uphole Time;
H412Aux. channel 3 contents      1,Confirmation TB;
H413Aux. channel 4 contents      1,TB;
H600Type,model,polarity          G1,Marsh,JFS-1,20DX,SEG;
H26 Type of Receiver points      G1,18 geophones in 2 strings in 4D;
H601Damp coeff,natural freq.     G1,0.7,10HZ;
H602Nunits,len(x),width(y)       G1,18,47.26m,00m;
H603Unit spacing x,y             G1,2.78m,00m;
H610Type,model,polarity          G2,Marsh,JFS-1,20DX,SEG;
H26 Type of Receiver points      G2,Bunched Geophone in 4D;
H611Damp coeff,natural freq.     G2,0.7,10HZ;
H612Nunits,len(x),width(y)       G2,18,00m,00m;
H613Unit spacing x,y             G2,00m,00m;
H620Type,model,polarity          H1,Hydrophone,MP24-13,SEG;
H26 Type of Receiver points      H1,single hydrophone in 4D;
H621Damp coeff,natural freq.     H1,None,10Hz;
H622Nunits,len(x),width(y)       H1,1,00m,00m;
```

```
H623Unit spacing x,y            H1,00m,00m;
H630Type,model,polarity         G3,Marsh,JFS-1,20DX,SEG;
H26 Type of Receiver points     G3,18 geophones in 2 strings in 3D;
H631Damp coeff,natural freq.    G3,0.7,10HZ;
H632Nunits,len(x),width(y)      G3,18,47.26m,00m;
H633Unit spacing x,y            G3,2.78m,00m;
H640Type,model,polarity         G4,Marsh,JFS-1,20DX,SEG;
H26 Type of Receiver points     G4,Bunched Geophone in 3D;
H641Damp coeff,natural freq.    G4,0.7,10HZ;
H642Nunits,len(x),width(y)      G4,18,00m,00m;
H643Unit spacing x,y            G4,00m,00m;
H650Type,model,polarity         H2,Hydrophone,MP24-13,SEG;
H26 Type of Receiver points     H2,single hydrophone in 3D;
H651Damp coeff,natural freq.    H2,None,10Hz;
H652Nunits,len(x),width(y)      H2,1,00m,00m;
H653Unit spacing x,y            H2,00m,00m;
H700Type,model,polarity         E1,Explosive,Seismex,SEG;
H26 Type of shot points         E1,30m single deep hole in 4D;
H701Size,vert. stk fold         E1,2000g,1;
H702Nunits,len(x),width(y)      E1,1,00m,00m;
H703Unit spacing x,y            E1,00m,00m;
H711Nom. shot depth,charge len. E1,42m,0.15m;
H712Nom. soil,drill method      E1,Clay Silt Sand;Flushing;
H713Weathering thickness        E1,1.5-7m;
H720Type,model,polarity         E2,Explosive,Seismex-1,SEG;
H26 Type of shot points         E2,5*6m linear pattern in 4D;
H721Size,vert. stk fold         E2,2000g,1;
H722Nunits,len(x),width(y)      E2,5,40m,00m;
H723Unit spacing x,y            E2,10m,00m;
H731Nom. shot depth,charge len. E2,6m,0.15m;
H732Nom. soil,drill method      E2,Clay Silt Sand;Flushing;
H733Weathering thickness        E2,1.5-7m;
H740Type,model,polarity         E3,Explosive,Seismex,SEG;
H26 Type of shot points         E3,5*3.5m linear pattern in 4D;
H741Size,vert. stk fold         E3,2000g,1;
H742Nunits,len(x),width(y)      E3,5,40m,00m;
H743Unit spacing x,y            E3,10m,00m;
H751Nom. shot depth,charge len. E3,3.5m,0.15m;
H752Nom. soil,drill method      E3,Clay Silt Sand;Thumping;
H753Weathering thickness        E3,1.5-7m;
H760Type,model,polarity         E4,Explosive,Seismex,SEG;
H26 Type of shot points         E4,5*3.5m circular pattern in 4D;
H761Size,vert. stk fold         E4,2000g,1;
H762Nunits,len(x),width(y)      E4,5,00m,00m;
H763Unit spacing x,y            E4,00m,00m;
H771Nom. shot depth,charge len. E4,3.5m,0.15m;
H772Nom. soil,drill method      E4,Clay Silt Sand;Thumping;
H773Weathering thickness        E4,1.5-7m;
H780Type,model,polarity         E5,Explosive,Seismex,SEG;
H26 Type of shot points         E5,5*6m circular pattern in 4D;
H781Size,vert. stk fold         E5,2000g,1;
H782Nunits,len(x),width(y)      E5,5,00m,00m;
H783Unit spacing x,y            E5,00m,00m;
H791Nom. shot depth,charge len. E5,6m,0.15m;
H792Nom. soil,drill method      E5,Clay Silt Sand;Flushing;
H753Weathering thickness        E5,1.5-7m;
H800Type,model,polarity         E6,Explosive,Seismex,SEG;
H26 Type of shot points         E6,42m single deep hole in 3D;
H801Size,vert. stk fold         E6,2000g,1;
H802Nunits,len(x),width(y)      E6,1,00m,00m;
H803Unit spacing x,y            E6,00m,00m;
H811Nom. shot depth,charge len. E6,42m,0.15m;
H812Nom. soil,drill method      E6,Clay Silt Sand;Flushing;
H813Weathering thickness        E6,1.5-7m;
H820Type,model,polarity         E7,Explosive,Seismex,SEG;
H26 Type of shot points         E7,5*6m linear pattern in 3D;
H821Size,vert. stk fold         E7,2000g,1;
H822Nunits,len(x),width(y)      E7,5,40m,00m;
H823Unit spacing x,y            E7,10m,00m;
H831Nom. shot depth,charge len. E7,6m,0.15m;
H832Nom. soil,drill method      E7,Clay Silt Sand;Flushing;
```

```
H833Weathering thickness        E7,1.5-7m;
H840Type,model,polarity         E8,Explosive,Seismex,SEG;
H26 Type of shot points         E8,5*3.5m linear pattern in 3D;
H841Size,vert. stk fold         E8,2000g,1;
H842Nunits,len(x),width(y)      E8,5,40m,00m;
H843Unit spacing x,y            E8,10m,00m;
H851Nom. shot depth,charge len. E8,3.5m,0.15m;
H852Nom. soil,drill method      E8,Clay Silt Sand;Thumping;
H853Weathering thickness        E8,1.5-7m;
H860Type,model,polarity         E9,Explosive,Seismex,SEG;
H26 Type of shot points         E9,5*3.5m circular pattern in 3D;
H861Size,vert. stk fold         E9,2000g,1;
H862Nunits,len(x),width(y)      E9,5,00m,00m;
H863Unit spacing x,y            E9,00m,00m;
H871Nom. shot depth,charge len. E9,3.5m,0.15m;
H872Nom. soil,drill method      E9,Clay Silt Sand;Thumping;
H873Weathering thickness        E9,1.5-7m;
H800Type,model,polarity         A1,Sleevegun,MK2,SEG;
H26 Type of Airgun              A1,Airgun shot,taken 12.5m eachside of peg in 4D
H881Size,vert. stk fold         A1,460 CU IN,1;
H882Nunits,len(x),width(y)      A1,5,40m,0m;
H886P-P Bar/m,Prim/Bubble       A1,22.2MPa.m,9.1;
H887Air Pressure PSI            A1,2000PSI;
H888NO. SUB ARRAYS,NOM DEPTH    A1,4,2.0M;
H880Type,model,polarity         A2,Sleevegun,MK2,SEG;
H26 Type of Airgun              A2,Airgun shot,taken at the peg position in 4D;
H891Size,vert. stk fold         A2,670 CU IN,1;
H892Nunits,len(x),width(y)      A2,5,40m,0m;
H896P-P Bar/m,Prim/Bubble       A2,35.1MPa.m,18.4;
H897Air Pressure PSI            A2,2000PSI;
H898NO. SUB ARRAYS,NOM DEPTH    A2,4,2.0M;
H900Type,model,polarity         A3,Sleevegun,MK2,SEG;
H26 Type of Airgun              A3,Airgun shot,taken 12.5m eachside of peg in 3D
H901Size,vert. stk fold         A3,460 CU IN,1;
H902Nunits,len(x),width(y)      A3,5,40m,0m;
H9036P-P Bar/m,Prim/Bubble      A3,22.2MPa.m,9.1;
H904Air Pressure PSI            A3,2000PSI;
H905NO. SUB ARRAYS,NOM DEPTH    A3,4,2.0M;
H910Type,model,polarity         A4,Sleevegun,MK2,SEG;
H26 Type of Airgun              A4,Airgun shot,taken at the peg position in 3D;
H911Size,vert. stk fold         A4,670 CU IN,1;
H912Nunits,len(x),width(y)      A4,5,40m,0m;
H913P-P Bar/m,Prim/Bubble       A4,35.1MPa.m,18.4;
H915Air Pressure PSI            A4,2000PSI;
H916NO. SUB ARRAYS,NOM DEPTH    A4,4,2.0M;
H990R,s,x file quality control  XXXXXXXXX,1830,XXXXXXX;
H991Co-ord. status final/prov   Final,XXXXXXXXX,2000,XXXXXX;
S2185                55981E1                  472474.4   83954.8      147114433
S2233                56761E1                  474424.4   85154.8      147114622
S2489                55961E1                  472424.4   91554.8      147114701
S2265                56241E1                  473124.4   85954.8      147114746
S2505                55961E1                  472424.4   91954.8      147114835
S2145                56201E1                  473024.4   82954.8      147114909
S2185                56021E1                  472574.4   83954.8      147114932
S2169                56181E1                  472974.4   83554.8      147115005
S2489                55981E1                  472474.4   91554.8      147115029
S2233                56701E1                  474274.4   85154.8      147115114
S2265                56261E1                  473174.4   85954.8      147115338
S2505                55981E1                  472474.4   91954.8      147115356
S2185                56041E1                  472624.4   83954.8      147115431
S2277                57561E1                  476424.4   86254.8      147115508
S2489                56001E1                  472524.4   91554.8      147115527
S2169                56401E1                  473524.4   83554.8      147120043
S2233                56601E1                  474024.4   85154.8      147121314
S2265                56281E1                  473224.4   85954.8      147121345
S2505                56021E1                  472574.4   91954.8      147121429
S2281                57541E1                  476374.4   86354.8      147121524
S2587                57241E1                  475624.4   94004.8      147121607
S2489                56021E1                  472574.4   91554.8      147121739
S2233                56541E1                  473874.4   85154.8      147121801
S2505                56041E1                  472624.4   91954.8      147124040
```

S2217	56361E1	473424.4	84754.8	147124252
S2201	55981E1	472474.4	84354.8	147124335
S2585	57221E1	475574.4	93954.8	147124411
S2489	56041E1	472624.4	91554.8	147124443
S2233	56521E1	473824.4	85154.8	147124526
S2265	56321E1	473324.4	85954.8	147124609
S2505	56061E1	472674.4	91954.8	147124626
S2217	56321E1	473324.4	84754.8	147124653
S2489	56061E1	472674.4	91554.8	147124758
S2265	56361E1	473424.4	85954.8	147130158
S2201	56021E1	472574.4	84354.8	147130244
S2163	56261E1	473174.4	83404.8	147130425
S2233	56261E1	473174.4	85154.8	147130542
S2489	56081E1	472724.4	91554.8	147130604
S2505	56081E1	472724.4	91954.8	147130713
S2219	57161E1	475424.4	84804.8	147130839
S2489	56101E1	472774.4	91554.8	147131152
S2233	56241E1	473124.4	85154.8	147131214
S2505	56101E1	472774.4	91954.8	147131353
S2215	57181E1	475474.4	84704.8	147131429
S2489	56121E1	472824.4	91554.8	147131504
S2265	56481E1	473724.4	85954.8	147131539
S2489	56141E1	472874.4	91554.8	147131655
S2265	56501E1	473774.4	85954.8	147131720
S2505	56121E1	472824.4	91954.8	147131741
S2489	56161E1	472924.4	91554.8	147131833
S2265	56561E1	473924.4	85954.8	147132110
S2489	56181E1	472974.4	91554.8	147132132
S2489	56201E1	473024.4	91554.8	147132545

SOURCE INDEX FILE (SPS) FOR AIRGUN SHOTS (A full listing for Air gun Shots)

```
H00 Sps format version num.     SPS003,13.10.10;
H01 Description of survey area  NIGERIA,XXXXX XXXXX,SOKU,OML23;
H02 Date of survey              XX.XX.XXXX,XX.XX.XXXX;
H021Post-plot date of issue     00.00.2010;
H022Tape/disk identifier        3D-SOKU-10;
H03 Client                      XXXXX XXXX;
H04 Geophysical contractor      XXXX/XXX Crew XXXX;
H05 Positioning contractor      XXXX/XXX Crew XXXX;
H06 Pos. proc. contractor       XXXX;
H07 Field computer system(s)    SN408 XL Software V6.1,SN408+Link,DOS disks;
H08 Coordinate location         Center of source and receiver patterns;
H09 Offset to coord. location   0.0m;
H10 Clock time w.r.t  GMT       +1;
H11 Swath No.                   Swath 11;
H12 Geodetic datum,-spheroid    Minna Datum,84,Clarke 1880,6378249.145,293.46500
H13 Spare                       ;
H14 Geodetic datum parameters   111.916 87.852 -114.499 -1.875-0.202-0.219-0.032
H15 Spare                       ;
H16 Spare                       ;
H17 Vertical datum description  Nigeria Lagos;
H18 Projection type             Transverse Mercator(t.m.);
H19 Projection zone             Nigeria Mid Belt;
H20 Description of grid units   Meter;
H201Factor to metres            1.00000000;
H220Long. of central meridian   0083000.000E;
H231Grid origin                 0040000.000N0083000.000E
H232Grid coord. at origin       0670553.98E      0.00N;
H241Scale factor                0.9997500000;
H242Lat., long. scale factor    0040000.000N0083000.000E;
H256LAT., LONG. INITIAL LINE    0040000.000N 083000.000E0140000.000N0083000.000E
H257CIRCULAR BEARING OF H256    0000000.0000
H258QUADRANT BEARING OF H256    N000000.000S
H259ANGLE FROM SKEW             0000000.0000
H26 PM,DEFINITION OF CODES
H26 SA: SATELLITE PT. PM: PERMA NENT MARKER
H26 PROSPECT GRID ORIGIN        13374696(X:449924.4,Y:62754.8);
H26 SOURCE, RECEIVER DIGIT      4,4
H26 RCV,SRC LINE INCREMENT      350,400;
H26 RCV,SRC POINT INCREMENT     50,50;
H30 Project code and description SOKU OML 23,S3D;
```

```
H31 Line number format          Block(1:6),Strip(7:4),Line Number(12:5);
H400Type,model,polarity         1,SN408XL+Link,CM408,SEG;
H401Crew name,comment           1,XXXX/XXX Crew XXXX(Seismic 3);
H402Sample int.,record len.     1,2.00 MSEC, 8.00 SEC;
H403Number of channels          1,1440;
H404Tape type,format,density    1,IBM 3590 Cartridge, SEG-D 8058, 75742;
H405Filter_alias hz,db pnt,slope1,200 HZ, 3.00 DB, 84.00 DB/OCT;
H406Filter_notch hz,-3db points 1,Out, None;
H407Filter_low hz,db pnt,slope  1,Out, None;
H408Time delay FTB-SOD app Y/N  1,0.00 Msec, Not Applied;
H409Multi component recording   1,Z;
H410Aux. channel 1 contents     1,50Hz;
H411Aux. channel 2 contents     1,Uphole Time;
H412Aux. channel 3 contents     1,Confirmation TB;
H413Aux. channel 4 contents     1,TB;
H600Type,model,polarity         G1,Marsh,JFS-1,20DX,SEG;
H26 Type of Receiver points     G1,18 geophones in 2 strings in 4D;
H601Damp coeff,natural freq.    G1,0.7,10HZ;
H602Nunits,len(x),width(y)      G1,18,47.26m,00m;
H603Unit spacing x,y            G1,2.78m,00m;
H610Type,model,polarity         G2,Marsh,JFS-1,20DX,SEG;
H26 Type of Receiver points     G2,Bunched Geophone in 4D;
H611Damp coeff,natural freq.    G2,0.7,10HZ;
H612Nunits,len(x),width(y)      G2,18,00m,00m;
H613Unit spacing x,y            G2,00m,00m;
H620Type,model,polarity         H1,Hydrophone,MP24-13,SEG;
H26 Type of Receiver points     H1,single hydrophone in 4D;
H621Damp coeff,natural freq.    H1,None,10Hz;
H622Nunits,len(x),width(y)      H1,1,00m,00m;
H623Unit spacing x,y            H1,00m,00m;
H630Type,model,polarity         G3,Marsh,JFS-1,20DX,SEG;
H26 Type of Receiver points     G3,18 geophones in 2 strings in 3D;
H631Damp coeff,natural freq.    G3,0.7,10HZ;
H632Nunits,len(x),width(y)      G3,18,47.26m,00m;
H633Unit spacing x,y            G3,2.78m,00m;
H640Type,model,polarity         G4,Marsh,JFS-1,20DX,SEG;
H26 Type of Receiver points     G4,Bunched Geophone in 3D;
H641Damp coeff,natural freq.    G4,0.7,10HZ;
H642Nunits,len(x),width(y)      G4,18,00m,00m;
H643Unit spacing x,y            G4,00m,00m;
H650Type,model,polarity         H2,Hydrophone,MP24-13,SEG;
H26 Type of Receiver points     H2,single hydrophone in 3D;
H651Damp coeff,natural freq.    H2,None,10Hz;
H652Nunits,len(x),width(y)      H2,1,00m,00m;
H653Unit spacing x,y            H2,00m,00m;
H700Type,model,polarity         E1,Explosive,Seismex,SEG;
H26 Type of shot points         E1,30m single deep hole in 4D;
H701Size,vert. stk fold         E1,2000g,1;
H702Nunits,len(x),width(y)      E1,1,00m,00m;
H703Unit spacing x,y            E1,00m,00m;
H711Nom. shot depth,charge len. E1,42m,0.15m;
H712Nom. soil,drill method      E1,Clay Silt Sand;Flushing;
H713Weathering thickness        E1,1.5-7m;
H720Type,model,polarity         E2,Explosive,Seismex-1,SEG;
H26 Type of shot points         E2,5*6m linear pattern in 4D;
H721Size,vert. stk fold         E2,2000g,1;
H722Nunits,len(x),width(y)      E2,5,40m,00m;
H723Unit spacing x,y            E2,10m,00m;
H731Nom. shot depth,charge len. E2,6m,0.15m;
H732Nom. soil,drill method      E2,Clay Silt Sand;Flushing;
H733Weathering thickness        E2,1.5-7m;
H740Type,model,polarity         E3,Explosive,Seismex,SEG;
H26 Type of shot points         E3,5*3.5m linear pattern in 4D;
H741Size,vert. stk fold         E3,2000g,1;
H742Nunits,len(x),width(y)      E3,5,40m,00m;
H743Unit spacing x,y            E3,10m,00m;
H751Nom. shot depth,charge len. E3,3.5m,0.15m;
H752Nom. soil,drill method      E3,Clay Silt Sand;Thumping;
H753Weathering thickness        E3,1.5-7m;
H760Type,model,polarity         E4,Explosive,Seismex,SEG;
H26 Type of shot points         E4,5*3.5m circular pattern in 4D;
```

```
H761Size,vert. stk fold         E4,2000g,1;
H762Nunits,len(x),width(y)      E4,5,00m,00m;
H763Unit spacing x,y            E4,00m,00m;
H771Nom. shot depth,charge len. E4,3.5m,0.15m;
H772Nom. soil,drill method      E4,Clay Silt Sand;Thumping;
H773Weathering thickness        E4,1.5-7m;
H780Type,model,polarity         E5,Explosive,Seismex,SEG;
H26 Type of shot points         E5,5*6m circular pattern in 4D;
H781Size,vert. stk fold         E5,2000g,1;
H782Nunits,len(x),width(y)      E5,5,00m,00m;
H783Unit spacing x,y            E5,00m,00m;
H791Nom. shot depth,charge len. E5,6m,0.15m;
H792Nom. soil,drill method      E5,Clay Silt Sand;Flushing;
H753Weathering thickness        E5,1.5-7m;
H800Type,model,polarity         E6,Explosive,Seismex,SEG;
H26 Type of shot points         E6,42m single deep hole in 3D;
H801Size,vert. stk fold         E6,2000g,1;
H802Nunits,len(x),width(y)      E6,1,00m,00m;
H803Unit spacing x,y            E6,00m,00m;
H811Nom. shot depth,charge len. E6,42m,0.15m;
H812Nom. soil,drill method      E6,Clay Silt Sand;Flushing;
H813Weathering thickness        E6,1.5-7m;
H820Type,model,polarity         E7,Explosive,Seismex,SEG;
H26 Type of shot points         E7,5*6m linear pattern in 3D;
H821Size,vert. stk fold         E7,2000g,1;
H822Nunits,len(x),width(y)      E7,5,40m,00m;
H823Unit spacing x,y            E7,10m,00m;
H831Nom. shot depth,charge len. E7,6m,0.15m;
H832Nom. soil,drill method      E7,Clay Silt Sand;Flushing;
H833Weathering thickness        E7,1.5-7m;
H840Type,model,polarity         E8,Explosive,Seismex,SEG;
H26 Type of shot points         E8,5*3.5m linear pattern in 3D;
H841Size,vert. stk fold         E8,2000g,1;
H842Nunits,len(x),width(y)      E8,5,40m,00m;
H843Unit spacing x,y            E8,10m,00m;
H851Nom. shot depth,charge len. E8,3.5m,0.15m;
H852Nom. soil,drill method      E8,Clay Silt Sand;Thumping;
H853Weathering thickness        E8,1.5-7m;
H860Type,model,polarity         E9,Explosive,Seismex,SEG;
H26 Type of shot points         E9,5*3.5m circular pattern in 3D;
H861Size,vert. stk fold         E9,2000g,1;
H862Nunits,len(x),width(y)      E9,5,00m,00m;
H863Unit spacing x,y            E9,00m,00m;
H871Nom. shot depth,charge len. E9,3.5m,0.15m;
H872Nom. soil,drill method      E9,Clay Silt Sand;Thumping;
H873Weathering thickness        E9,1.5-7m;
H800Type,model,polarity         A1,Sleevegun,MK2,SEG;
H26 Type of Airgun              A1,Airgun shot,taken 12.5m eachside of peg in 4D
H881Size,vert. stk fold         A1,460 CU IN,1;
H882Nunits,len(x),width(y)      A1,5,40m,0m;
H886P-P Bar/m,Prim/Bubble       A1,22.2MPa.m,9.1;
H887Air Pressure PSI            A1,2000PSI;
H888NO. SUB ARRAYS,NOM DEPTH    A1,4,2.0M;
H880Type,model,polarity         A2,Sleevegun,MK2,SEG;
H26 Type of Airgun              A2,Airgun shot,taken at the peg position in 4D;
H891Size,vert. stk fold         A2,670 CU IN,1;
H892Nunits,len(x),width(y)      A2,5,40m,0m;
H896P-P Bar/m,Prim/Bubble       A2,35.1MPa.m,18.4;
H897Air Pressure PSI            A2,2000PSI;
H898NO. SUB ARRAYS,NOM DEPTH    A2,4,2.0M;
H900Type,model,polarity         A3,Sleevegun,MK2,SEG;
H26 Type of Airgun              A3,Airgun shot,taken 12.5m eachside of peg in 3D
H901Size,vert. stk fold         A3,460 CU IN,1;
H902Nunits,len(x),width(y)      A3,5,40m,0m;
H9036P-P Bar/m,Prim/Bubble      A3,22.2MPa.m,9.1;
H904Air Pressure PSI            A3,2000PSI;
H905NO. SUB ARRAYS,NOM DEPTH    A3,4,2.0M;
H910Type,model,polarity         A4,Sleevegun,MK2,SEG;
H26 Type of Airgun              A4,Airgun shot,taken at the peg position in 3D;
H911Size,vert. stk fold         A4,670 CU IN,1;
H912Nunits,len(x),width(y)      A4,5,40m,0m;
```

```
H913P-P Bar/m,Prim/Bubble       A4,35.1MPa.m,18.4;
H915Air Pressure PSI            A4,2000PSI;
H916NO. SUB ARRAYS,NOM DEPTH    A4,4,2.0M;
H990R,s,x file quality control  XXXXXXXXX,1830,XXXXXX;
H991Co-ord. status final/prov   Final,XXXXXXXXX,2000,XXXXXX;
S2333                57281A1                  475724.4   87654.8      147094813
S2333                57282A1                  475724.4   87654.8      147094917
S2333                57301A1                  475774.4   87654.8      147094957
S2333                57302A1                  475774.4   87654.8      147095028
S2457                57321A1                  475824.4   90754.8      147102206
S2457                57322A1                  475824.4   90754.8      147102259
S2457                57301A1                  475774.4   90754.8      147102326
S2457                57302A1                  475774.4   90754.8      147102453
S2457                57303A1                  475774.4   90754.8      147102528
S2457                57281A1                  475724.4   90754.8      147102553
S2457                57282A1                  475724.4   90754.8      147102617
S2457                57261A1                  475674.4   90754.8      147102643
S2457                57262A1                  475674.4   90754.8      147102708
S2457                57241A1                  475624.4   90754.8      147102734
S2457                57242A1                  475624.4   90754.8      147102759
S2457                57221A1                  475574.4   90754.8      147102824
S2457                57222A1                  475574.4   90754.8      147102849
S2457                57201A1                  475524.4   90754.8      147102915
S2457                57202A1                  475524.4   90754.8      147102941
S2457                57181A1                  475474.4   90754.8      147103006
S2457                57182A1                  475474.4   90754.8      147103213
S2457                57161A1                  475424.4   90754.8      147103244
S2457                57162A1                  475424.4   90754.8      147103309
S2457                57141A1                  475374.4   90754.8      147103335
S2457                57142A1                  475374.4   90754.8      147103401
S2457                57121A1                  475324.4   90754.8      147103427
S2457                57122A1                  475324.4   90754.8      147103616
S2457                57101A1                  475274.4   90754.8      147103654
S2457                57102A1                  475274.4   90754.8      147103717
S2457                57081A1                  475224.4   90754.8      147103739
S2457                57082A1                  475224.4   90754.8      147103802
S2457                57061A1                  475174.4   90754.8      147103825
S2457                57062A1                  475174.4   90754.8      147103849
S2457                57041A1                  475124.4   90754.8      147103912
S2457                57042A1                  475124.4   90754.8      147103935
S2457                57021A1                  475074.4   90754.8      147103957
S2457                57022A1                  475074.4   90754.8      147104021
S2457                57001A1                  475024.4   90754.8      147104044
S2457                57002A1                  475024.4   90754.8      147104107
S2457                56981A1                  474974.4   90754.8      147104130
S2457                56982A1                  474974.4   90754.8      147104153
S2457                56961A1                  474924.4   90754.8      147104217
S2457                56962A1                  474924.4   90754.8      147104240
S2457                56941A1                  474874.4   90754.8      147104303
S2457                56942A1                  474874.4   90754.8      147104325
S2457                56921A1                  474824.4   90754.8      147104349
S2457                56922A1                  474824.4   90754.8      147104412
S2457                56901A1                  474774.4   90754.8      147104434
S2457                56902A1                  474774.4   90754.8      147104457
S2457                56881A1                  474724.4   90754.8      147104519
S2457                56882A1                  474724.4   90754.8      147104541
S2457                56861A1                  474674.4   90754.8      147104603
S2457                56862A1                  474674.4   90754.8      147104625
S2457                56841A1                  474624.4   90754.8      147104646
S2457                56842A1                  474624.4   90754.8      147104708
S2457                56821A1                  474574.4   90754.8      147104729
S2457                56822A1                  474574.4   90754.8      147104751
S2457                56801A1                  474524.4   90754.8      147104812
S2457                56802A1                  474524.4   90754.8      147104833
S2457                56781A1                  474474.4   90754.8      147104853
S2457                56782A1                  474474.4   90754.8      147104915
S2457                56761A1                  474424.4   90754.8      147104936
S2457                56762A1                  474424.4   90754.8      147104957
S2457                56741A1                  474374.4   90754.8      147105547
S2457                56742A1                  474374.4   90754.8      147110318
S2457                56721A1                  474324.4   90754.8      147110451
```

S2457	56722A1	474324.4	90754.8	147110534
S2457	56701A1	474274.4	90754.8	147110600
S2457	56702A1	474274.4	90754.8	147113455
S2457	56681A1	474224.4	90754.8	147113530
S2457	56682A1	474224.4	90754.8	147113601
S2457	56661A1	474174.4	90754.8	147113631
S2457	56662A1	474174.4	90754.8	147113700
S2465	56801A1	474524.4	90954.8	147120106
S2465	56802A1	474524.4	90954.8	147120132
S2459	56801A1	474524.4	90804.8	147122313
S2459	56802A1	474524.4	90804.8	147122404
S2459	56821A1	474574.4	90804.8	147122430
S2459	56822A1	474574.4	90804.8	147122501
S2459	56841A1	474624.4	90804.8	147122531
S2459	56842A1	474624.4	90804.8	147122557
S2459	56861A1	474674.4	90804.8	147122625
S2459	56862A1	474674.4	90804.8	147122654
S2459	56881A1	474724.4	90804.8	147122720
S2459	56882A1	474724.4	90804.8	147122748
S2459	56901A1	474774.4	90804.8	147122813
S2459	56902A1	474774.4	90804.8	147122839
S2459	56921A1	474824.4	90804.8	147122904
S2459	56922A1	474824.4	90804.8	147122930
S2459	56941A1	474874.4	90804.8	147122956
S2459	56942A1	474874.4	90804.8	147123023
S2459	56961A1	474924.4	90804.8	147123123
S2459	56962A1	474924.4	90804.8	147123255
S2459	57221A1	475574.4	90804.8	147124824
S2459	57222A1	475574.4	90804.8	147124853
S2459	57201A1	475524.4	90804.8	147124918
S2459	57202A1	475524.4	90804.8	147124945
S2459	57181A1	475474.4	90804.8	147125006
S2459	57182A1	475474.4	90804.8	147125030
S2459	57161A1	475424.4	90804.8	147125058
S2459	57162A1	475424.4	90804.8	147125117
S2459	57141A1	475374.4	90804.8	147125139
S2459	57142A1	475374.4	90804.8	147125158
S2459	57121A1	475324.4	90804.8	147125217
S2459	57122A1	475324.4	90804.8	147125247
S2459	57101A1	475274.4	90804.8	147125316
S2459	57102A1	475274.4	90804.8	147125338
S2459	57081A1	475224.4	90804.8	147125426
S2459	57082A1	475224.4	90804.8	147125919
S2459	57061A1	475174.4	90804.8	147125943
S2459	57062A1	475174.4	90804.8	147130011
S2459	57041A1	475124.4	90804.8	147130033
S2459	57042A1	475124.4	90804.8	147130100

Receiver File (SPS) for selected Shots (Geophone and Hydrophone)
(A full listing is too large and extensive to fully display)

```
H000SPS format version num.     SPS001,05.06.12;
H010Description of survey area  <untitled>,,N/A,N/A;
H020Date of survey              XX.XX.XX,XX.XX.XX;
H021Post-plot date of issue     XX.XX.XX;
H022Tape/disk identifier        N/A;
H030Client                      N/A;
H040Geophysical contractor      N/A,N/A;
H050Positioning contractor      N/A;
H060Pos. proc. contractor       N/A;
H070Field computer system(s)    N/A,N/A,N/A;
H080Coordinate location         N/A;
H090Offset to coord. location   N/A,N/A;
H100Clock time w.r.t. GMT       N/A;
H110Spare                       N/A;
H120Geodetic datum,-spheroid    N/A,N/A,N/A,N/A;
H130Spare                       N/A;
H140Geodetic datum parameters   N/A,N/A,N/A,N/A,N/A,N/A,N/A;
H150Spare                       N/A;
H160Spare                       N/A;
H170Vertical datum description  N/A,N/A,N/A,N/A;
H180Projection type             N/A;
```

```
H190Projection zone             N/A,N/A;
H200Description of grid units   Metres;
H201Factor to metre             1.00000000;
H210Lat. of standard parallel(s);
H220Long. of central meridian   ;
H231Grid origin                 ;
H232Grid coord. at origin       ;
H241Scale factor                ;
H242Lat., long. scale factor    ;
H256Lat., long. initial line    ;
H257Circular bearing of H256    ;
H258Quadrant bearing of H256    ;
H259Angle from skew             ;
H300Project code and description;
H310Line number format          ;
H400Type,Model,Polarity         ;
H401Crew name,Comment           ;
H402Sample int.,Record Len.     1,0.000000,N/A;
H403Number of channels          1,1;
H404Tape type,format,density    ;
H405Filter_alias Hz,dB pnt,slope;
H406Filter_notch Hz,-3dB points ;
H407Filter_low Hz,dB pnt,slope  ;
H408Time delay FTB-SOD app Y/N  ;
H409Multi component recording   ;
H410Aux. channel 1 contents     ;
H411Aux. channel 2 contents     ;
H412Aux. channel 3 contents     ;
H413Aux. channel 4 contents     ;
H414Spare                       ;
H415Spare                       ;
H416Spare                       ;
H417Spare                       ;
H418Spare                       ;
H419Spare                       ;
H600Type,model,polarity         G1,geophone 1;
H601Damp coeff,natural freq.    ;
H602Nunits,len(X),width(Y)      ;
H603Unit spacing X,Y            ;
H604Spare                       ;
H605Spare                       ;
H606Spare                       ;
H607Spare                       ;
H608Spare                       ;
H609Spare                       ;
H700Type,model,polarity         A1,air gun 1;
H701Size,vert. stk fold         ;
H702Nunits,len(X),width(Y)      ;
H703Unit spacing X,Y            ;
H716P-P bar m,prim/bubble       ;
H717Air pressure psi            ;
H718No. sub arrays,Nom depth    ;
H719Spare                       ;
H720Type,model,polarity         E1,explosive 1;
H721Size,vert. stk fold         ;
H722Nunits,len(X),width(Y)      ;
H723Unit spacing X,Y            ;
H620Type,model,polarity         EI;
H621Damp coeff,natural freq.    ;
H622Nunits,len(X),width(Y)      ;
H623Unit spacing X,Y            ;
H624Spare                       ;
H625Spare                       ;
H626Spare                       ;
H627Spare                       ;
H628Spare                       ;
H629Spare                       ;
R5645               667.51G1                  473649.4   62729.8
R5645               668.51G1                  473649.4   62779.8
R5645               669.51G1                  473649.4   62829.8
R5645               670.51G1                  473649.4   62879.8
```

R5645	671.51G1	473649.4	62929.8
R5645	672.51G1	473649.4	62979.8
R5645	673.51G1	473649.4	63029.8
R5645	674.51G1	473649.4	63079.8
R5645	675.51G1	473649.4	63129.8
R5645	676.51G1	473649.4	63179.8
R5645	677.51G1	473649.4	63229.8
R5645	678.51G1	473649.4	63279.8
R5645	679.51G1	473649.4	63329.8
R5645	680.51G1	473649.4	63379.8
R5645	681.51G1	473649.4	63429.8
R5645	682.51G1	473649.4	63479.8
R5645	683.51G1	473649.4	63529.8
R5645	684.51G1	473649.4	63579.8
R5645	685.51G1	473649.4	63629.8
R5645	686.51G1	473649.4	63679.8
R5645	687.51G1	473649.4	63729.8
R5645	688.51G1	473649.4	63779.8
R5645	689.51G1	473649.4	63829.8
R5645	690.51G1	473649.4	63879.8
R5645	691.51G1	473649.4	63929.8
R5645	692.51G1	473649.4	63979.8
R5645	693.51G1	473649.4	64029.8
R5645	694.51G1	473649.4	64079.8
R5645	695.51G1	473649.4	64129.8
R5645	696.51G1	473649.4	64179.8
R5645	697.51G1	473649.4	64229.8
R5645	698.51G1	473649.4	64279.8
R5645	699.51G1	473649.4	64329.8
R5645	700.51G1	473649.4	64379.8
R5645	701.51G1	473649.4	64429.8
R5645	702.51G1	473649.4	64479.8
R5645	703.51G1	473649.4	64529.8
R5645	704.51G1	473649.4	64579.8
R5645	705.51G1	473649.4	64629.8
R5645	706.51G1	473649.4	64679.8
R5645	707.51G1	473649.4	64729.8
R5645	708.51G1	473649.4	64779.8
R5645	709.51G1	473649.4	64829.8
R5645	710.51G1	473649.4	64879.8
R5645	711.51G1	473649.4	64929.8
R5645	712.51G1	473649.4	64979.8
R5645	713.51G1	473649.4	65029.8
R5645	714.51G1	473649.4	65079.8
R5645	715.51G1	473649.4	65129.8
R5645	716.51G1	473649.4	65179.8
R5645	717.51G1	473649.4	65229.8
R5645	718.51G1	473649.4	65279.8
R5645	719.51G1	473649.4	65329.8
R5645	720.51G1	473649.4	65379.8
R5645	721.51G1	473649.4	65429.8
R5645	722.51G1	473649.4	65479.8
R5645	723.51G1	473649.4	65529.8
R5645	724.51G1	473649.4	65579.8
R5645	725.51G1	473649.4	65629.8
R5645	726.51G1	473649.4	65679.8
R5645	727.51G1	473649.4	65729.8
R5645	728.51G1	473649.4	65779.8
R5645	729.51G1	473649.4	65829.8
R5645	730.51G1	473649.4	65879.8
R5645	731.51G1	473649.4	65929.8
R5645	732.51G1	473649.4	65979.8
R5645	733.51G1	473649.4	66029.8
R5645	734.51G1	473649.4	66079.8
R5645	735.51G1	473649.4	66129.8
R5645	736.51G1	473649.4	66179.8
R5645	737.51G1	473649.4	66229.8
R5645	738.51G1	473649.4	66279.8
R5645	739.51G1	473649.4	66329.8
R5645	740.51G1	473649.4	66379.8
R5645	741.51G1	473649.4	66429.8

R5645	742.51G1	473649.4	66479.8
R5645	743.51G1	473649.4	66529.8
R5645	744.51G1	473649.4	66579.8
R5645	745.51G1	473649.4	66629.8
R5645	746.51G1	473649.4	66679.8
R5645	747.51G1	473649.4	66729.8
R5645	748.51G1	473649.4	66779.8
R5645	749.51G1	473649.4	66829.8
R5645	750.51G1	473649.4	66879.8
R5645	751.51G1	473649.4	66929.8
R5645	752.51G1	473649.4	66979.8
R5645	753.51G1	473649.4	67029.8
R5645	754.51G1	473649.4	67079.8
R5645	755.51G1	473649.4	67129.8
R5645	756.51G1	473649.4	67179.8
R5645	757.51G1	473649.4	67229.8
R5645	758.51G1	473649.4	67279.8
R5645	759.51G1	473649.4	67329.8
R5645	760.51G1	473649.4	67379.8
R5645	761.51G1	473649.4	67429.8
R5645	762.51G1	473649.4	67479.8
R5645	763.51G1	473649.4	67529.8
R5645	764.51G1	473649.4	67579.8
R5645	765.51G1	473649.4	67629.8
R5645	766.51G1	473649.4	67679.8
R5645	767.51G1	473649.4	67729.8
R5645	768.51G1	473649.4	67779.8
R5645	769.51G1	473649.4	67829.8
R5645	770.51G1	473649.4	67879.8
R5645	771.51G1	473649.4	67929.8
R5645	772.51G1	473649.4	67979.8
R5645	773.51G1	473649.4	68029.8
R5645	774.51G1	473649.4	68079.8
R5645	775.51G1	473649.4	68129.8
R5645	776.51G1	473649.4	68179.8
R5645	777.51G1	473649.4	68229.8
R5645	778.51G1	473649.4	68279.8
R5645	779.51G1	473649.4	68329.8
R5645	780.51G1	473649.4	68379.8
R5645	781.51G1	473649.4	68429.8
R5645	782.51G1	473649.4	68479.8
R5645	783.51G1	473649.4	68529.8
R5645	784.51G1	473649.4	68579.8
R5645	785.51G1	473649.4	68629.8
R5645	786.51G1	473649.4	68679.8
R5645	787.51G1	473649.4	68729.8
R5645	788.51G1	473649.4	68779.8
R5645	789.51G1	473649.4	68829.8
R5645	790.51G1	473649.4	68879.8
R5645	791.51G1	473649.4	68929.8
R5645	792.51G1	473649.4	68979.8
R5645	793.51G1	473649.4	69029.8
R5645	794.51G1	473649.4	69079.8
R5645	795.51G1	473649.4	69129.8
R5645	796.51G1	473649.4	69179.8
R5645	797.51G1	473649.4	69229.8
R5645	798.51G1	473649.4	69279.8
R5645	799.51G1	473649.4	69329.8
R5645	800.51G1	473649.4	69379.8
R5645	801.51G1	473649.4	69429.8
R5645	802.51G1	473649.4	69479.8
R5645	803.51G1	473649.4	69529.8
R5645	804.51G1	473649.4	69579.8
R5645	805.51G1	473649.4	69629.8
R5645	806.51G1	473649.4	69679.8
R5645	807.51G1	473649.4	69729.8
R5645	808.51G1	473649.4	69779.8
R5645	809.51G1	473649.4	69829.8
R5645	810.51G1	473649.4	69879.8
R5645	811.51G1	473649.4	69929.8
R5645	812.51G1	473649.4	69979.8

R5645	813.51G1	473649.4	70029.8
R5645	814.51G1	473649.4	70079.8
R5645	815.51G1	473649.4	70129.8
R5645	816.51G1	473649.4	70179.8
R5645	817.51G1	473649.4	70229.8
R5645	818.51G1	473649.4	70279.8
R5645	819.51G1	473649.4	70329.8
R5645	820.51G1	473649.4	70379.8
R5645	821.51G1	473649.4	70429.8
R5645	822.51G1	473649.4	70479.8
R5645	823.51G1	473649.4	70529.8
R5645	824.51G1	473649.4	70579.8
R5645	825.51G1	473649.4	70629.8
R5645	826.51G1	473649.4	70679.8
R5645	827.51G1	473649.4	70729.8
R5645	828.51G1	473649.4	70779.8
R5645	829.51G1	473649.4	70829.8
R5645	830.51G1	473649.4	70879.8
R5645	831.51G1	473649.4	70929.8
R5645	832.51G1	473649.4	70979.8
R5645	833.51G1	473649.4	71029.8
R5645	834.51G1	473649.4	71079.8
R5645	835.51G1	473649.4	71129.8
R5645	836.51G1	473649.4	71179.8
R5645	837.51G1	473649.4	71229.8
R5645	838.51G1	473649.4	71279.8
R5645	839.51G1	473649.4	71329.8
R5645	840.51G1	473649.4	71379.8
R5645	841.51G1	473649.4	71429.8
R5645	842.51G1	473649.4	71479.8
R5645	843.51G1	473649.4	71529.8
R5645	844.51G1	473649.4	71579.8
R5645	845.51G1	473649.4	71629.8
R5645	846.51G1	473649.4	71679.8
R5645	847.51G1	473649.4	71729.8
R5645	848.51G1	473649.4	71779.8
R5645	849.51G1	473649.4	71829.8
R5645	850.51G1	473649.4	71879.8
R5645	851.51G1	473649.4	71929.8
R5645	852.51G1	473649.4	71979.8
R5645	853.51G1	473649.4	72029.8
R5645	854.51G1	473649.4	72079.8
R5645	855.51G1	473649.4	72129.8
R5645	856.51G1	473649.4	72179.8
R5645	857.51G1	473649.4	72229.8
R5645	858.51G1	473649.4	72279.8
R5645	859.51G1	473649.4	72329.8
R5645	860.51G1	473649.4	72379.8
R5645	861.51G1	473649.4	72429.8
R5645	862.51G1	473649.4	72479.8
R5645	863.51G1	473649.4	72529.8
R5645	864.51G1	473649.4	72579.8
R5645	865.51G1	473649.4	72629.8
R5645	866.51G1	473649.4	72679.8
R5645	867.51G1	473649.4	72729.8
R5645	868.51G1	473649.4	72779.8
R5645	869.51G1	473649.4	72829.8
R5645	870.51G1	473649.4	72879.8
R5645	871.51G1	473649.4	72929.8
R5645	872.51G1	473649.4	72979.8
R5645	873.51G1	473649.4	73029.8
R5645	874.51G1	473649.4	73079.8
R5645	875.51G1	473649.4	73129.8
R5645	876.51G1	473649.4	73179.8
R5645	877.51G1	473649.4	73229.8
R5645	878.51G1	473649.4	73279.8
R5645	879.51G1	473649.4	73329.8
R5645	880.51G1	473649.4	73379.8
R5645	881.51G1	473649.4	73429.8
R5645	882.51G1	473649.4	73479.8
R5645	883.51G1	473649.4	73529.8

R5645	884.51G1	473649.4	73579.8
R5645	885.51G1	473649.4	73629.8
R5645	886.51G1	473649.4	73679.8
R5645	887.51G1	473649.4	73729.8
R5645	888.51G1	473649.4	73779.8
R5645	889.51G1	473649.4	73829.8
R5645	890.51G1	473649.4	73879.8
R5645	891.51G1	473649.4	73929.8
R5645	892.51G1	473649.4	73979.8
R5645	893.51G1	473649.4	74029.8
R5645	894.51G1	473649.4	74079.8
R5645	895.51G1	473649.4	74129.8
R5645	896.51G1	473649.4	74179.8
R5645	897.51G1	473649.4	74229.8
R5645	898.51G1	473649.4	74279.8
R5645	899.51G1	473649.4	74329.8
R5645	900.51G1	473649.4	74379.8
R5645	901.51G1	473649.4	74429.8
R5645	902.51G1	473649.4	74479.8
R5645	903.51G1	473649.4	74529.8
R5645	904.51G1	473649.4	74579.8
R5645	905.51G1	473649.4	74629.8
R5645	906.51G1	473649.4	74679.8
R5645	907.51G1	473649.4	74729.8
R5645	908.51G1	473649.4	74779.8
R5645	909.51G1	473649.4	74829.8
R5645	910.51G1	473649.4	74879.8
R5645	911.51G1	473649.4	74929.8
R5645	912.51G1	473649.4	74979.8
R5645	913.51G1	473649.4	75029.8
R5645	914.51G1	473649.4	75079.8
R5645	915.51G1	473649.4	75129.8
R5645	916.51G1	473649.4	75179.8
R5645	917.51G1	473649.4	75229.8
R5645	918.51G1	473649.4	75279.8
R5645	919.51G1	473649.4	75329.8
R5645	920.51G1	473649.4	75379.8
R5645	921.51G1	473649.4	75429.8
R5645	922.51G1	473649.4	75479.8
R5645	923.51G1	473649.4	75529.8
R5645	924.51G1	473649.4	75579.8
R5645	925.51G1	473649.4	75629.8
R5645	926.51G1	473649.4	75679.8
R5645	927.51G1	473649.4	75729.8
R5645	928.51G1	473649.4	75779.8
R5645	929.51G1	473649.4	75829.8
R5645	930.51G1	473649.4	75879.8
R5645	931.51G1	473649.4	75929.8
R5645	932.51G1	473649.4	75979.8
R5645	933.51G1	473649.4	76029.8
R5645	934.51G1	473649.4	76079.8
R5645	935.51G1	473649.4	76129.8
R5645	936.51G1	473649.4	76179.8
R5645	937.51G1	473649.4	76229.8
R5645	938.51G1	473649.4	76279.8
R5645	939.51G1	473649.4	76329.8
R5645	940.51G1	473649.4	76379.8
R5645	941.51G1	473649.4	76429.8
R5645	942.51G1	473649.4	76479.8
R5645	943.51G1	473649.4	76529.8
R5645	944.51G1	473649.4	76579.8
R5645	945.51G1	473649.4	76629.8
R5645	946.51G1	473649.4	76679.8
R5645	947.51G1	473649.4	76729.8
R5645	948.51G1	473649.4	76779.8
R5645	949.51G1	473649.4	76829.8
R5645	950.51G1	473649.4	76879.8
R5645	951.51G1	473649.4	76929.8
R5645	952.51G1	473649.4	76979.8
R5645	953.51G1	473649.4	77029.8
R5645	954.51G1	473649.4	77079.8